THEORETICAL INVESTIGATION OF STRUCTURAL AND ELECTRONIC PROPERTIES OF SOME TRANSITION METAL ANSA COMPLEXES

BAZI GEÇİŞ METALİ ANSA KOMPLEKSLERİNİN YAPISAL VE ELEKTRONİK ÖZELLİKLERİNİN KURAMSAL İNCELENMESİ

DİLEK YÜKSEL

Prof. Dr. FATMA SEVİN DÜZ
Supervisor

Submitted to Institute of Graduate Studies in Science
of Hacettepe University as a partial fulfillment
to the requirements for the award of the degree of
DOCTOR OF PHILOSOPHY
in
CHEMISTRY

2013

This study named "**Theoretical Investigation of Structural and Electronic Properties of Some Transition Metal Ansa Complexes**" by **DİLEK YÜKSEL** has been accepted as a thesis for the degree of **DOCTOR OF PHILOSOPHY IN CHEMISTRY** by the below mentioned examining committee members.

Head
Prof. Dr. Lemi TÜRKER

Supervisor
Prof. Dr. Fatma SEVİN DÜZ

Member
Prof. Dr. Nurcan KARACAN

Member
Prof. Dr. Metin ZORA

Member
Prof. Dr. Vildan ADAR

This thesis has been approved as a thesis for the degree of **DOCTOR OF PHILOSOPHY IN CHEMISTRY** by the Board of Directors of the Institute of Graduate Studies in Science of Hacettepe University.

Prof.Dr. Fatma SEVİN DÜZ
Director of the Institute of
Graduate Studies in Science

To my family

ETHICS

In this thesis study, prepared in accordance with the spelling rules of Institute of Graduate Studies in Science of Hacettepe University,

I declare that

- all the information and documents have been obtained in the base of the academic rules
- all audio-visual and written information and results have been presented according to the rules of scientific ethics
- in case of using others works, related studies have been cited in accordance with the scientific standards
- all cited studies have been fully referenced
- I did not do any distortion in the data set
- and any part of this thesis has not been presented as another thesis study at this or any other university.

21/01/2013

Dilek YÜKSEL

ABSTRACT

THEORETICAL INVESTIGATION OF STRUCTURAL AND ELECTRONIC PROPERTIES OF SOME TRANSITION METAL ANSA COMPLEXES

DİLEK YÜKSEL

Doctor of Philosophy, Department of Chemistry

Supervisor: Prof. Dr. FATMA SEVİN DÜZ

January 2013, 167 pages

Ansa metallocenes have attracted some catalytic and synthetic interest due to their impressive reactivity and stability, which can be quite different from that of their non-*ansa*-bridged counterparts, metallocenes. In addition, the ring-strained *ansa* metallocenes are able to produce stable metallopolymers via ring opening polymerization (ROP), and the properties of these metallopolymers can be determined via changing the *ansa* bridging group or the transition metal in the structure of the *ansa* metallocene monomer. For these reasons, design and synthesis of strained *ansa* metallocenes become more and more important for organometallic chemistry, nanotechnology and materials sciences.

In this thesis, the influences of changing the transition metal and/or the *ansa* bridging element, on the structural and electronic properties of Group 4-9 *ansa* metallocenes having Group 13-16 elements in the *ansa* bridge were investigated by means of DFT calculations.

In the first part of the study, bond distances, bond angles, electronic spectra and NMR spectra of 29 known *ansa* metallocene structures taken from the literature, were computed by using different DFT methods, and the computational results were compared with the experimental results. It was found that B3P86 functional performs well in reproducing the geometric and the spectroscopic experimental data of the selected *ansa* metallocenes, and B3LYP displays large deviations from experimental values.

In the second part of the study, geometric and electronic properties of 216 model *ansa* metallocenes along with their 18 parent metallocenes, were predicted

computationally at B3P86 level. Characteristic angles (α, β, δ, θ) and distances (Cp-M, M-E, C_{ipso}-E, C_{ipso}-M) were determined. In addition, frontier molecular orbital properties, dipole moments, charge distributions on the transition metal centers, electronic spectra and ^{13}C NMR chemical shifts were also computed.

According to the computational results, among *ansa* metallocenes of the same transition metal, the tilt angle α is the highest for Group 16 bridged *ansa* metallocenes and the lowest for Group 13 bridged structures. Greatest tilt angles belong to the *ansa* metallocenes having 2nd period bridging elements. In general, *ansa* bridge formation and the periodic effects increasing α, cause a decrease in HOMO-LUMO gaps and therefore a bathochromic shift in the lowest energy absorbance wavelengths of *ansa* metallocenes with respect to their parent metallocenes. In Groups 4-6 *ansa* metallocenes, as a trend, a downfield shift in the *ipso* carbon ^{13}C NMR signal was observed with respect to the high field carbon signals of the parent metallocenes, where in Groups 7-9, *ansa* metallocene formation leads upfield shifts.

Keywords: Strained metallocenophanes, *Ansa* metallocenes, Tilt angle, Frontier molecular orbitals, DFT, GIAO, TD-DFT, M06, B3LYP, B3PW91, B3P86, Def2-TZVP.

ÖZET

BAZI GEÇİŞ METALİ ANSA KOMPLEKSLERİNİN YAPISAL VE ELEKTRONİK ÖZELLİKLERİNİN KURAMSAL İNCELENMESİ

DİLEK YÜKSEL

Doktora, Kimya Bölümü

Tez Danışmanı: Prof. Dr. FATMA SEVİN DÜZ

Ocak 2013, 167 sayfa

Ansa metalosenler, *ansa* köprüsü taşımayan muadilleri olan metalosenlere göre oldukça dikkat çekici farklılıklar gösterebilen reaktivite ve kararlılıkları nedeniyle, katalitik kimya ve sentez açısından ilgi toplamaktadırlar. Ayrıca, halka gerginliğine sahip *ansa* metalosenler halka açılması polimerizasyonu yoluyla kararlı metalopolimerler oluşturabilirler. Bu metalopolimerlerin özellikleri yapıdaki *ansa* köprüsü ya da metal atomu değiştirilerek belirlenebilir. Bu nedenlerden dolayı, gergin halkalı *ansa* metalosenlerin tasarım ve sentezi organometalik kimya, nanoteknoloji ve malzeme bilimi açısından gün geçtikçe artan bir önem kazanmaktadır.

Bu tezde, metal ve/veya köprü atomlarının değiştirilmesinin, *ansa* köprüsünde Grup 13-16 elementleri bulunan Grup 4-9 *ansa* metalosenlerinin yapısal ve elektronik özellikleri üzerindeki etkisi, DFT hesaplamaları vasıtasıyla araştırılmıştır.

Çalışmanın ilk aşamasında, literatürden seçilmiş ve yapıları bilinen 29 *ansa* metalosene ait bağ uzunlukları, bağ açıları, elektronik spektrumlar ve ^{13}C NMR spektrumları, farklı DFT yöntemleri kullanılarak hesaplanmış, sonuçlar deneysel verilerle karşılaştırılmıştır. Seçilen *ansa* metalosenlere ait geometrik ve spektroskopik verilerin hesaplanmasında B3P86 metodunun en iyi performansı gösterdiği bulunmuştur. B3LYP metodu deneysel verilerden büyük sapmalar göstermiştir.

Çalışmanın ikinci aşamasında, temel alınan 18 metalosenle birlikte 216 model *ansa* metalosenin geometrik ve elektronik özellikleri, B3P86 seviyesinde hesaplanmıştır. Karakteristik açılar (α, β, δ, θ) ve uzunluklar (Cp-M, M-E, C_{ipso}-E, C_{ipso}-M) saptanmıştır. Bunlara ek olarak, tüm yapıların sınır moleküler orbital

özellikleri, dipol momentleri, geçiş metali üzerindeki yük dağılımları, elektronik spektrumları ve ^{13}C NMR spektrumları da hesaplanmıştır.

Hesaplama sonuçlarına göre, aynı geçiş metalinin *ansa* metalosenleri arasında bükülme açısı, α, *ansa* köprüsünde Grup 16 elementi içeren yapılar için en yüksek, Grup 13 elementi içeren yapılar için ise en düşük değerlere sahiptir. Tüm yapılar içinde en büyük bükülme açıları *ansa* köprüsünde 2. Periyod elementleri bulunan *ansa* metalosenlere aittir. Genel olarak, *ansa* köprüsü oluşumu ve α değerini artıran periyodik etkiler, HOMO-LUMO aralığında azalmaya ve bu yüzden de *ansa* metalosenlerin düşük enerjili absorbans dalga boylarında, temel alınan metalosenlere göre kırmızıya kaymaya neden olmaktadır. Grup 4-6 *ansa* metalosenlerinde, ^{13}C NMR δ C_{ipso} sinyalleri, temel alınan metalosenin yüksek alan sinyaline göre düşük alana kayma eğilimindedir. Grup 7-9 *ansa* metalosenlerinde ise *ansa* köprü oluşumu yüksek alana kaymaya yol açmaktadır.

Anahtar Kelimeler: Gergin metalosenofanlar, *Ansa* metalosenler, Bükülme açısı, Sınır moleküler orbitalleri, DFT, GIAO, TD-DFT, M06, B3LYP, B3PW91, B3P86, Def2-TZVP.

ACKNOWLEDGEMENTS

This thesis would not have been possible without the support of many people.

First of all I would like to thank my advisor, Prof. Dr. Fatma SEVİN DÜZ, who offered guidance, encouragement, patience and all. I appreciate the time and energy she reserved for this study.

I also want to thank my thesis progress committee members, Prof. Dr. Nurcan KARACAN and Prof. Dr. Metin ZORA for their priceless advices at each step of this thesis.

I am indebted to my colleagues in the department, especially to Tuğba ARİFİOĞLU and Dilek IŞIK TAŞGIN for their support.

Lastly but not least, fond acknowledgement should go to my family and numerous friends who endured this long process with me, always offering support and love.

CONTENTS

Page

SYMBOLS AND ABBREVIATIONS

Symbols

α	Tilt Angle
β	$Cp_{centroid}$ - C_{ipso} - E Angle
δ	$Cp_{centroid}$ - M - $Cp_{centroid}$ Angle
θ	C_{ipso} - E - C_{ipso} Angle
η	Hardness
μ	Chemical Potential

Abbreviations

B3LYP	Becke 3-term Functional with Lee-Yang-Parr Exchange Correlations
B3P86	Becke 3-term Functional with Perdew 86 Exchange Correlations
B3PW91	Becke 3-term Functional with Perdew-Wang 91 Exchange Correlations
Cp	Cyclopentadienyl ring
$Cp_{centroid}$	Centroid of the cyclopentadienyl ring
C_{ipso}	The carbon atom of cyclopentadienyl ring attached to the bridging atom
Def2-TZVP	Definition 2 Triple-Zeta Valence Polarization
DFT	Density Functional Theory
E	Bridging element on the *ansa* bridge
HOMO	Highest Occupied Molecular Orbital
LUMO	Lowest Unoccupied Molecular Orbital
M	The transition metal in the metallocene or *ansa* metallocene structure
ROP	Ring Opening Polymerization

1. INTRODUCTION

1.1. General Information

1.1.1. Transition Metal *ansa* Complexes

Transition metal *ansa* complexes are organometallic ring systems composed of a transition metal center and two aromatic π-hydrocarbon ligands (η^5-cyclopentadienyl, η^6-phenyl or η^7-tropylium) bridged by an *ansa* chain.

The Latin prefix "*ansa*", meaning "handle", has been previously used in nomenclature of organic aromatic rings connected at both para ends by a chain of at least ten carbon atoms long, so that the bridging chain stay on one side of the aromatic ring like a handle. The term was first used in organometallic chemistry to define a titanocene complex with an interannular ethylene bridge by Brintzinger and co-workers in 1979 [1].

According to the type of the π-hydrocarbon ligands, and the number of the atoms in the *ansa* bridge, there are a number of possible structures for *ansa* complexes, which can be classified mainly in three groups:

i. *ansa* Metallocenes
ii. *ansa* Metalloarenes
iii. *ansa* Complexes with mixed π-hydrocarbon ligands

1.1.1.1. *Ansa* Metallocenes

In the case of both π-hydrocarbon ligands are the same and η^5-C_5H_4, the *ansa* complex is called as *ansa* metallocene or [n]metallocenophane. Representative structures for *ansa* metallocenes containing 1 and 2 atoms in the *ansa* bridge is shown in Figure 1.

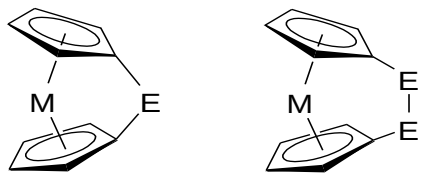

Figure 1. [1] and [2]metallocenophanes

E denotes here the *ansa* bridging element or group, and [n] is the number of the atoms in the *ansa* chain.

1.1.1.2. *Ansa* Metalloarenes

In the case of both π-hydrocarbon ligands are the same and different from cycyclopentadienyl, the *ansa* complexes are called as *ansa* bis(arene) complexes or [n]metalloarenophanes. Representative structures for *ansa* bis(phenyl) complexes containing 1 and 2 atoms in the *ansa* bridge is shown in Figure 2.

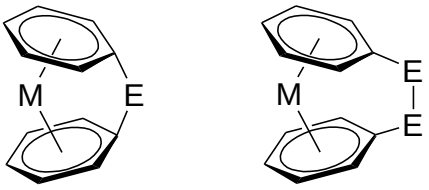

Figure 2. [1] and [2]metalloarenophane structures

1.1.1.3. *Ansa* Complexes with mixed π-hydrocarbon ligands

There are also *ansa* bridged complexes with mixed π-hydrocarbon ligands such as in the following examples with general formula [M(η^5-C_5H_4)E(η^6-C_6H_5)] and [M(η^5-C_5H_4)E(η^7-C_7H_6)].

For these complexes a generic name can not be applied, but each complex has its unique name according to the transition metal in the structure. For example, the titanium complexes with the general formula, [Ti(η^5-C_5H_4)E(η^7-C_7H_6)], are called as [n]troticenophanes and the chromium complexes with the general formula, [Cr(η^5-C_5H_4)E(η^7-C_7H_6)], are called as [n]trochrocenophanes, etc. [2].

1.1.2. Characteristic Properties of *ansa* Metallocenes

In Figure 3, a representative structure for a [1]metallocenophane is shown, where two η^5-cyclopentadienyl (Cp) rings are π-bonded to a transition metal center (M) and a single *ansa* bridging element (E) is σ-bonded to the cyclopentadienyl rings at *ipso* carbon atoms (C_{ipso}). L^1 and L^2 are generic ligands and may or may not be present depending on the coordination number of M. R_x is any atom or group that is attached to E.

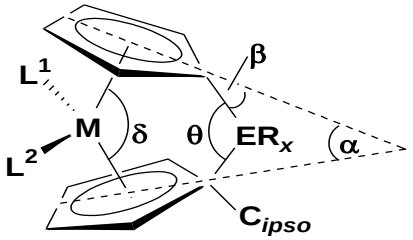

Figure 3. Geometric parameters for a [1]metallocenophane structure

Introduction of an *ansa* bridge to a metallocene structure leads some important changes in the geometry of the metallocene. The two cyclopentadienyl rings are tilted towards the *ansa* bridge in an eclipsed conformation, which constrains the motion of the rings greatly. The degree of ring tilt is expressed by the tilt angle, α. Other characteristic angles, used in defining the bent *ansa* metallocene geometry are β, δ and θ, as seen in Figure 3.

Besides the ring tilt, the distance between the metal and the two *ipso* carbon atoms of the Cp ring decreases and the bond angles of the *ipso* carbons are distorted as a result of *ansa* bridge formation. Furthermore, for some metallocenes, *ansa* bridging results in a strained ring structure. The amount of the ring strain of an *ansa* metallocene depends on several parameters, which will be discussed later.

These geometric changes and restrictions, also effect the electronic structure and the reactivity of the metallocenes [3]. For strained *ansa* metallocenes, due to the increased reactivity at C_{ipso}-E and Cp-M bonds, insertion reactions into Cp-M bond [2, 4] or ring opening polymerization reactions via the cleavage of the C_{ipso}-E bonds [2 and references therein], has been reported. For other *ansa* metallocenes,

on the other hand, an increased stability of the metallocene against above mentioned reactions has been observed [2, 3].

All these properties of *ansa* bridged metallocenes, which called as "*ansa* effect" by Shapiro [5], can be characterized via some certain structural and electronic parameters listed below.

1.1.2.1. Structural Parameters

1.1.2.1.1. Characteristic Angles

The angles α, β, δ, θ shown in Figure 3, are the characteristic angles for an *ansa* metallocene.

α is the dihedral angle between the mean planes of two cyclopentadienyl rings, β denotes the $Cp_{centroid}$ – C_{ipso} – E angle, θ is C_{ipso} – E – C_{ipso} angle and δ is $Cp_{centroid}$ – M – $Cp_{centroid}$ angle [2].

Among these, the tilt angle α is an especially important characteristics for the strained *ansa* metallocenes, because it can be used as a measure of ring strain on the *ansa* metallocene ring. Higher α values pointed out higher ring tilt and higher distortion from normal metallocene geometry. Along with other geometric parameters, greater α values indicate possible ring strain on the *ansa* metallocene ring [2, 6, 7].

α can be established via X-ray crystallography or for a model molecule, can be calculated computationally.

1.1.2.1.2. Characteristic Distances

The distances used in the characterization of an *ansa* metallocene geometry are:

i. Cp-M: the distance between the centroid of the cyclopentadienyl ring and the metal center.
ii. C_{ipso}-M: the distance between the *ansa* bridging carbon of the cyclopentadienyl ring and the metal center.

iii. C_{ipso}-E: the distance between the *ansa* bridging carbon of the cyclopentadienyl ring and the bridging element.
iv. M-E: the distance between the metal center and the bridging element.

An increase in Cp-M bond distance via *ansa* cyclization indicates the weakening of the Cp-M bond, and therefore, the presence of a ring strain. Also, an increase in Cp-M bond decreases the steric hinderence on the transition metal center, opens more coordination space and makes it more reactive. If there is a decrease in Cp-M bond distance via *ansa* cyclization, the stability of the *ansa* metallocene increases. Similarly, high C_{ipso}-E values indicate the instability of the *ansa* metallocene on that bond [2, 5, 8, 9].

1.1.2.1.3. NMR Spectra

Determinig the ^{13}C NMR chemical shifts on the *ipso* carbon atoms of the cyclopentadienyl rings is also an useful tool in characterization of an *ansa* metallocene, since *ansa* bridge formation causes upfield or downfield shifts in the signals of *ipso* carbons, according to the nature of the bridging group.

Upfield shift in the *ipso* carbon signals of [1]ferrocenophanes via *ansa* bridge formation with main group elements has been reported in several articles [2, 4, 10, 11], where downfield shift is observed in *ansa* bridging of [1]ruthenocenophane with zirconium [2].

1.1.2.2. Electronic Parameters

1.1.2.2.1. Charge Distribution

Charge distribution on the metal center of an *ansa* metallocene gives information about the reactivity of it in nucleophilic or electrophilic reactions.

The reactivity is enhanced when the metallocene shows high positive or negative charges on the transition metal center. Higher positive charges increases the

feasibility of a nucleophilic attack [8], where negatively charged metal centers are identified as most suitable for electrophilic attack.

1.1.2.2.2. Dipole Moments

Estimation of the dipole moment and the polarizability of an *ansa* metallocene is important, because it provides data on the electron density distribution of a molecule.

The d electron configuration of the metal is the most important factor on the geometrical structure of metallocenes [3].

1.1.2.2.3. Frontier Molecular Orbitals

According to the type of the reaction, that *ansa* metallocene expected to undergo, the HOMO or the LUMO energy levels of *ansa* metallocene molecule become importance.

For example, in the activation reaction of metallocenes with an alkyllithium compound, Wölfler and co-workers showed that the activation is enhanced, when there is a small gap between the HOMO of MeLi and the LUMO of the metallocene [8].

1.1.2.2.4. Electronic Spectra

Metallocenes show high energy absorbtion bands in the UV region due to the π-π* transitions between the cyclopentadienyl ring orbitals and low energy absorbtion bands in the visible region due to the ligand-to-metal charge transfer (LMCT) transitions between the metals d orbitals and the ligand orbitals [12].

In characterisation of *ansa* metallocenes, inspection of electronic spectra is also important. Upon the addition of *ansa* bridge, a change in the intensity and the wavelength of the lowest energy absorbtion band has been reported for *ansa* metallocene structures. For example, for [1]ferrocenophanes, increasing tilt angles are accompanied with a red shift and increase in the intensity of the lowest energy absorbtion band of the *ansa* ferrocene structures [2, 13].

1.1.3. Synthesis of *ansa* Metallocenes

There are two commonly used synthetic methods that yielding *ansa* metallocenes, which are referred to as the dilithiation route (i) and the fly-trap route (ii) [2] as seen in Scheme 1.

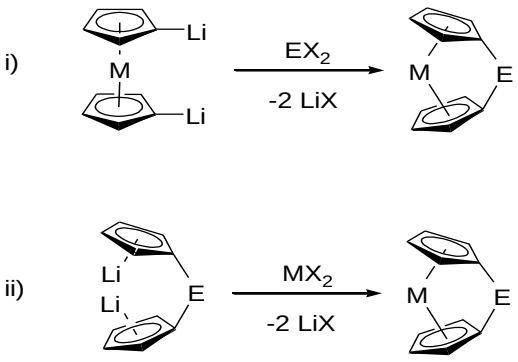

Scheme 1. Two main pathways to synthesize [1]metallocenophanes. Dilithiation route (i) and flytrap route (ii).

In the route (i), the metallocene is dilithiated with an alkyl-lithium reagent like *n*BuLi and a base like tmeda (N,N,N',N'-tetramethylethylenediamine) in an organic solvent. In the second step, a salt metathesis reaction takes place between dilithiometallocene(tmeda) and dihalide salt of the bridging element.

In the route (ii) salt metathesis reaction takes place between an appropriate bridged $(\eta^5\text{-}C_5H_4)_2$ dianionic linker and transition metal dihalides.

Because of polycondensation and other side reactions that take place during the fly-trap synthesis, the dilithiation route (i) is said to be more preferable with higher reaction yields [2].

1.1.4. Ring Opening Polymerization of Srained *ansa* Metallocenes

Strained *ansa* metallocenes can produce polymeric products via ring opening polymerization (ROP) reaction as seen in Scheme 2.

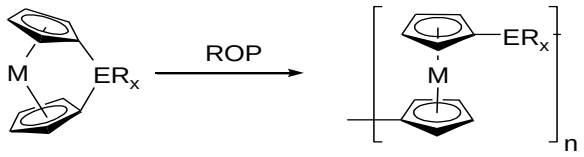

Scheme 2. Ring Opening Polymerization of an *ansa* Metallocene

After Foucher and co-workers reported that strained ferrocenophanes undergo ROP to yield high molecular weight polyferrocenes in 1992 [14], the researchs on ROP of strained *ansa* metallocenes has attracted a great interest and the area of materials science and technology associated with the ring-opened polymers has proved a rapid development [6, 15, 16, 17].

The chance of defining the structure of polyolefin or metallopolymer products via just changing the *ansa* bridge or the transition metal center, encouraged the researchers to investigate the synthesis of strained *ansa* metallocenes for ROP [2].

Especially the chemistry of strained [1]ferrocenophanes is deeply explored by Ian Manners and co-workers [2]. Some polyferrocenylsilanes produced via thermal or anionic ROP of [1]ferrocenophanes are found applications in industry [18,19].

Investigations on non-ferrocene strained *ansa* metallocenes, however, are limited with a few reports on the synthesis and ring opening polymerization reactions of ruthenocenophanes [20, 21], rhenocenophanes [22] and cobaltocenophanes [23-26].

1.2. RESEARCH OBJECTIVES

Ansa metallocenes are utilized in many kinds of reactions and transformations. The principal application of Group 4 and 5 *ansa* complexes is their uses as catalyst precursors in olefin polymerization [27]. The uses as reagents in organic synthesis [28], in the dehydrocoupling of hydrosilanes to form polysilanes [29], in enantioselective hydrogenations, hydrosilations, in alcoholysis of silanes and other conversions are also of importance [30].

Among Group 7 and 8 [1]metallocenophanes, especially the ones possessing ring strain, can undergo ring opening polymerisations (ROP) [2, 6].

To date, [1]ferrocenophanes are the most well characterized *ansa* metallocenes in the literature. [1]ferrocenophanes with B, Al, Ga, Si, Ge, P, As, S and Se elements in the *ansa* bridge are known [2, 6 and references therein].

[1]metallocenophanes of Ti, Zr, Hf, V, Nb, Ta, Cr, Mo, W, Re and Ru transition metals has been also reported mostly with Group 14 elements C and Si in bridging positions [2, 6, 27].

To the best of our knowledge, [1]metallocenophanes with second period elements N and O in the *ansa* bridge and [1]metallocenophanes of Mn, Tc, Os, Co, Rh and Ir are not known. Some examples of [2]cobaltocenophanes has been synthesized and used in ROP by Ian Manners and co-workers [24, 26].

In all the above examples, it has been indicated that the electronic properties and, therefore, the reactivity of the *ansa* metallocene is directly related to the structural properties of the *ansa* metallocene, and even slight changes in the type of the transition metal or the bridging element could be very influential.

For these reasons, the investigations on the design of *ansa* metallocene complexes is important.

In this work, it was aimed to design and computationally characterize [1]metallocenophane structures for the use of possible future applications.

It was also intended to investigate the trends in structural and electronic properties of *ansa* metallocenes against variations in the transition metal center and the *ansa*

bridging element.

Another purpose of this study was to investigate the general trends in structural and electronic properties of *ansa* metallocenes throughout the periodic table.

With this in mind, firstly, transition metals and *ansa* bridging elements, that will be the building blocks of the *ansa* metallocene, were selected considering the applications and structures in the literature, as mentioned above (Figure 4).

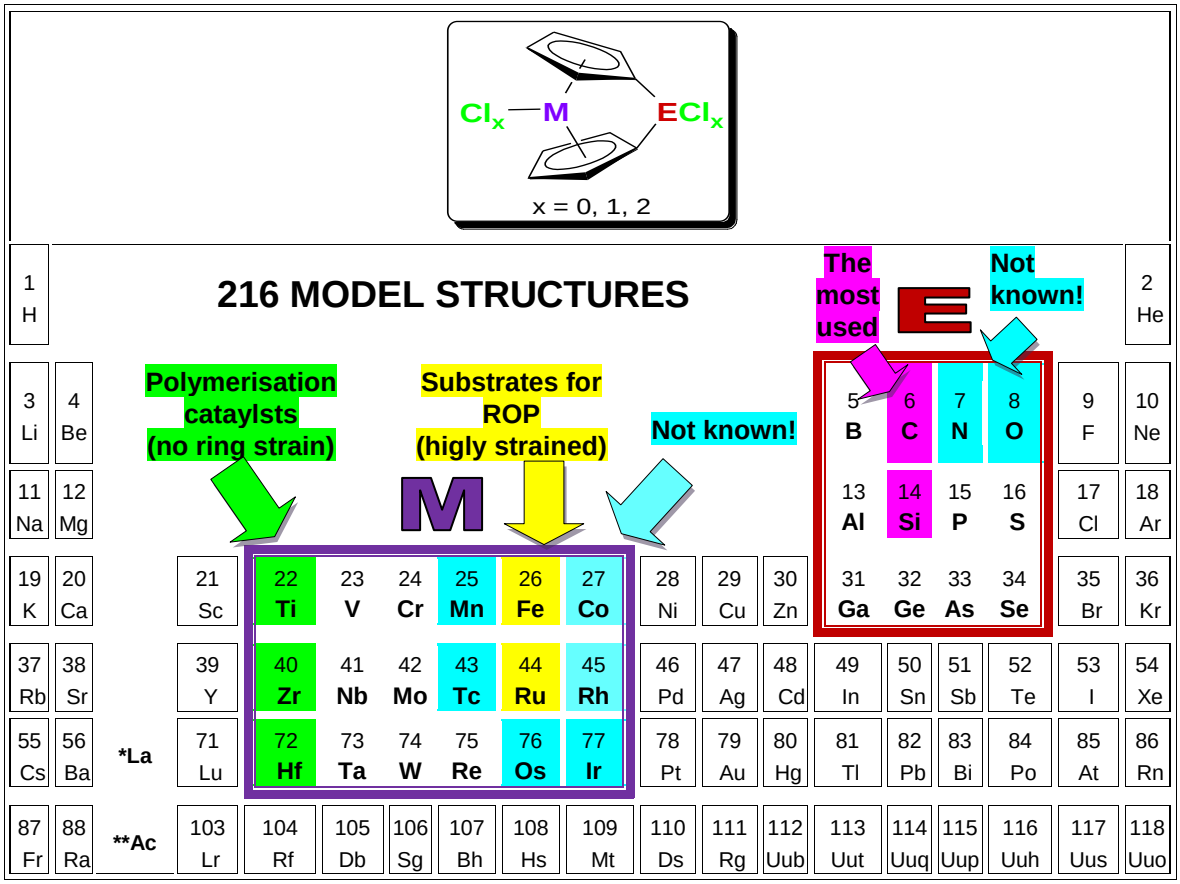

Figure 4. Selected transition metals and bridging elements

Secondly, with selected transition metals and the bridge elements, the structural models were constructed.

[1]metallocenophanes investigated in this thesis, were constructed according to three main structural models, namely model A, model B and model C, depending

on the number of ligands attached to the transition metal center (M), as shown in Figure 5.

In the structural Model A, [1]metallocenophanes were derived from parallel ring metallocenes of Group 8 (Fe, Ru, Os) and Group 9 (Co, Rh, Ir) transition metals.

The ring tilt caused by the *ansa* bridge is highest in this group and therefore the A-

type *ansa* derivatives are most likely to possess ring strain and they are potential substrates for ring opening polymerization (ROP) reactions.

The structural Model B was derived from the bent metallocenes of Group 7 (Mn, Tc, Re) transition metals, coordinated to a single ligand.

In the structural Model C, [1]metallocenophanes were derived from bent metallocenes of Group 4 (Ti, Zr, Hf), Group 5 (V, Nb, Ta) and and Group 6 (Cr, Mo, W) transition metals, each carrying two ligands beside the two cyclopentadienyl rings.

Each structural model was also classified into three sub-groups according to the number of ligands attached to the bridging atom (E) as 1, 2 and 3.

A1, B1, ad C1 type metallocenophanes do not possess any ligand at the bridging element, where A2, B2 and C2 type molecules have one and the A3, B3 and C3 type molecules have two ligands at the bridging element, E.

Chloride was used as a general ligand for both transition metals and bridging groups, when necessary to complete the coordination number.

So 216 model [1]metallocenophane structures were derived under nine geometric frames.

Although there are many [1]metallocenophane structures characterised experimentally in literature similar to our model structures, except for the five structures, [Fe{(η^5-$C_5H_4)_2SiCl_2$}], [Fe{(η^5-$C_5H_4)_2GeCl_2$}], [Fe{(η^5-$C_5H_4)_2PCl$}], [Fe{(η^5-$C_5H_4)_2S$}], [Fe{(η^5-$C_5H_4)_2Se$}], to the best of our knowledge, the model geometries are novel.

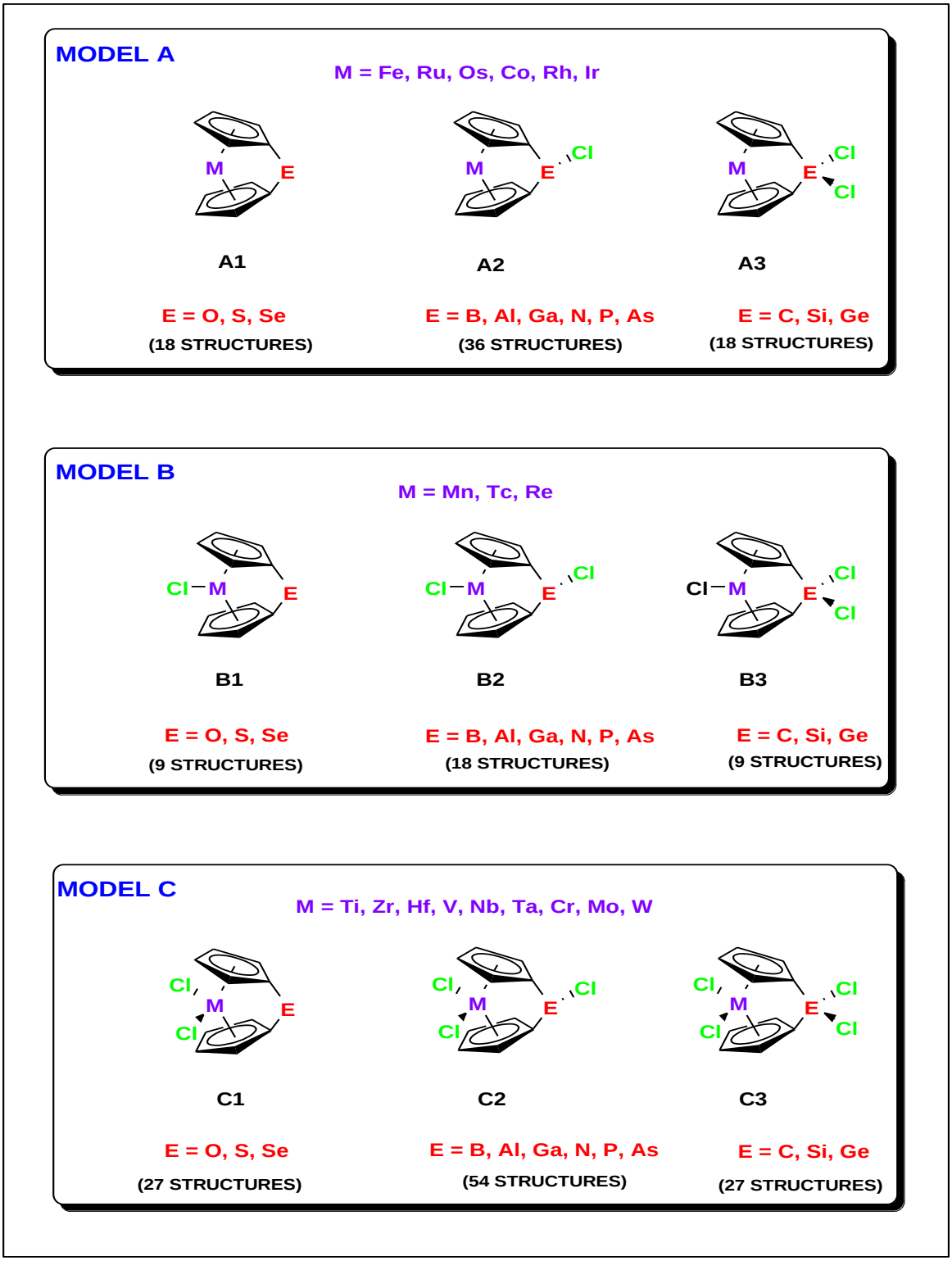

Figure 5. Model Molecules

2. COMPUTATIONAL DETAILS

2.1. DFT Methods and Software

All calculations presented in this work were performed with the Gaussian 09 Revision C.01 [31] molecular modeling software using density functional theory (DFT) [32-34] methods, which can predict successful geometries, relative energies, and vibrational frequencies for transition metal complexes [35].

DFT functionals used in this thesis are:

i) B3P86: Becke's three-parameter hybrid exchange functional and the gradient corrections of Perdew, along with his 1981 local correlation functional [36, 37],

ii) B3LYP: Becke's three-parameter hybrid exchange functional and the correlation functional of Lee, Yang, and Parr, which includes both local and non-local terms [36, 38],

iii) B3PW91: Becke's three-parameter hybrid exchange functional and Perdew and Wang's 1991 gradient-corrected correlation functional [36, 39],

iv) and Truhlar's meta hybrid functional M06 [40].

Ahlrichs polarized triple-ζ quality basis set, def2-TZVP [41] was used for the computation of H, and the 2nd, the 3rd and the 4th period elements (B, C, N, O, Al, Si, P, S, Cl, Ti, V, Cr, Mn, Fe, Co, Ga, Ge, As).

For the 5th and the 6th period transition metals (Zr, Hf, Nb, Ta, Mo, W, Tc, Re, Ru, Os, Rh, Ir) effective core potentials (ECPs) for def2-TZVP basis set was applied [42]. This basis set combinations was found to be in good agreement with the experimental results in describing metal–carbon bonds for organometallic compounds in many cases [43, 44].

All geometries were fully optimized and the optimized geometries were also subjected to full frequency analyses at the same level of optimization to verify the nature of the stationary points. Equilibrium geometries were characterized by the

absence of imaginary frequencies in the reaction coordinate.

Besides the Mulliken charges [45], NBO charges on the transition metals were also determined [46]. Natural atomic orbital and natural bond orbital (NBO) analyses were made with Gaussian NBO Version 3.1.

The time-dependent density functional theory (TDDFT) [47] approach was used for the calculation of the vertical excitation energies in the UV-vis region.

NMR chemical shifts were computed by using Gauge-Independent Atomic Orbital (GIAO) method [48]. The ^{13}C NMR chemical shifts were referenced to TMS (GIAO magnetic shielding tensors for ^{13}C (178.2 ppm (M06),184.6 ppm (B3LYP), 187.6 ppm (B3PW91) and 187.8 ppm (B3P86)) these values are related to the GIAO isotropic magnetic susceptibility. Absolute chemical shifts computed with GIAO method were correlated to δ(TMS) values by computing the absolute chemical shift for TMS at the same level and taking the difference between that value and the absolute shift computed for the nucleus in question [49].

2.2. Determination of Geometric Properties

The geometrical parameters were determined using GaussView 5.0 and Mercury 3.0.1 visualization programs (Figures 6 and 7).

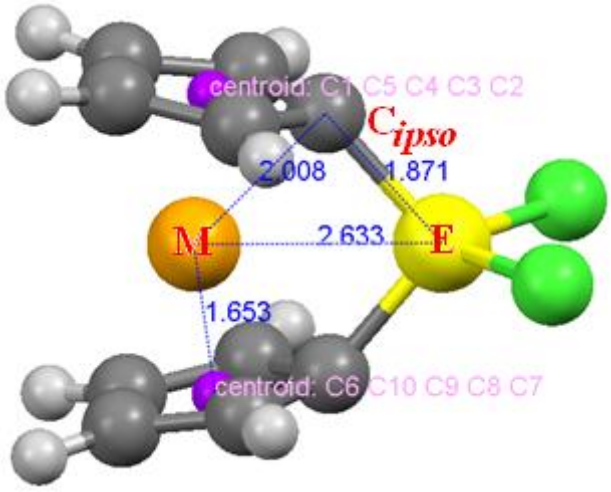

Figure 6. Determination of distances

Determination of the referred distances of a [1]metallocenophane is seen in Figure 6. The cyclopentadienyl ligand mean centroids were computed from the mean values of related C atoms.

The characteristic angles of a representative [1]metallocenophane is seen in Figure 7. The cyclopentadienyl ligand mean planes were computed from the mean values of related C atoms similarly to that of centroids.
The angle α is the angle between the mean planes and the angle β is supplementary angle of $Cp_{centroid}$-C_{ipso}-E angle and calculated from that value.

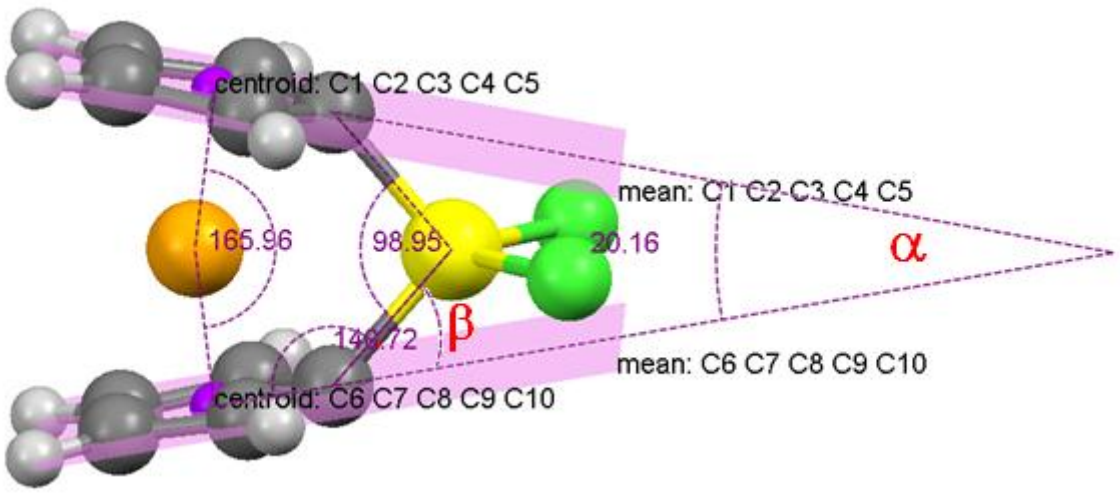

Figure 7. Determination of angles

2.3. Calculations of Frontier Molecular Orbital Properties

Electronegativity (X), chemical potential (μ) and hardness (η) are electronic properties that characterize the reactivity of a chemical system [50]. The values are defined as:

$$X = -\mu = \tfrac{1}{2}(I + A) \quad \text{and} \quad \eta = \tfrac{1}{2}(I - A)$$

where I and A are the ionization potential and electron affinity of any chemical system, atom, ion, molecule, or radical.

According to the Koopmans' theorem [51] the frontier orbital energies can be given by the formula:

$$-\varepsilon_{HOMO} = I \qquad \text{and} \quad -\varepsilon_{LUMO} = A$$

So the electronegativity, chemical potential and the hardness become:

$$X = -\tfrac{1}{2}(\varepsilon_{HOMO} + \varepsilon_{LUMO}) = \mu \qquad \text{and} \qquad \eta = \tfrac{1}{2}(\varepsilon_{LUMO} - \varepsilon_{HOMO})$$

As can be seen in Figure 8 hard molecules have a large HOMO-LUMO gap, and soft molecules have a small HOMO-LUMO gap.

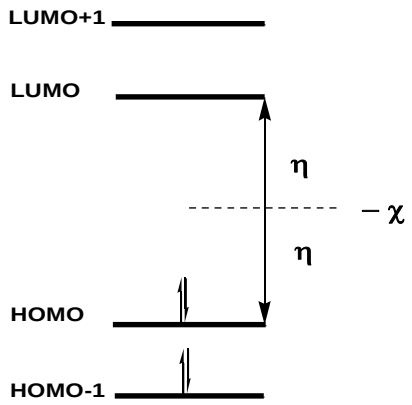

Figure 8. Hardness and electronegativity

3. RESULTS AND DISCUSSION

3.1. Properties of Known *ansa* Metallocenes

In the literature, there are numerous *ansa* metallocene structures known that have been synthesized, and characterized by means of X-ray diffraction.

In Table 1, structural and spectroscopic parameters of some experimentally characterized [1] and [2]metallocenophane structures (**1**-**29** in Figure 9) are given.

Table 1. Structural and spectroscopic data for some reference [1] and [2]metallocenophane structures

Structure	α (°)	β (°)	δ (°)	θ (°)	M-E (Å)	Cp-M (Å)	C_{ipso}-M (Å)	C_{ipso}-E (Å)	λ_{max} (nm)	δC_{ipso} (ppm)	Ref.
1	31.0	29.0	156.9	89.0	2.794	-[a]	1.954	1.807	504	14.3	[13]
2	26.4	30.0	160.0	86.0	2.906	-[a]	1.960	-[a]	500	5.6	[13]
3	31.4	35.3	155.9	102.0	2.559	1.634	1.989	1.623	498	44.2	[11]
4	26.9	32.3	155.2	90.7	2.774	1.630	1.979	1.849	-[a]	18.7	[52]
5	19.2	40.7	166.5	101.0	2.588	-[a]	2.007	1.850	470	36.1	[53]
6	19.4	39.5	166.0	98.0	2.655	1.639	2.014	1.871	-[a]	33.8	[54]
7	20.8	37.0	164.7	95.7	2.690	-[a]	2.001	1.851	478	33.5	[55, 56]
8	21.0	37.4	164.7	96.2	2.691	1.641	2.003	1.880	-[a]	32.2	[57, 58]
9	19.1	40.0	167.3	99.2	2.636	1.650	2.014	-[a]	-[a]	31.0	[56,59]
10	19.0	35.9	165.3	91.7	2.804	1.630	2.001	1.977	486	31.0	[60]
11	21.0	35.9	164.9	91.5	2.994	1.807	2.149	2.200	363	31.8	[21]
12	26.0	10.9	160.8	-[a]	2.925	1.629	1.965	1.518	454	90.4	[61]
13	33.6	12.6	157.0	-[a]	3.010	1.794	1.982	1.596	346	89.2	[61]
14	27.1	16.6	158.0	-[a]	2.966	1.717	1.979	1.512	486	-[a]	[62]
15	50.5	22.4	134.5	94.7	2.831	1.777	2.117	1.530	-[a]	52.7	[63]
16	53.1	20.9	131.3	95.7	2.892	1.853	2.175	1.542	-[a]	31.0	[22]
17	38.5	-[a]	143.3	-[a]	-[a]	1.780	2.160	1.530	506	-[a]	[64]
18	63.7	17.1	122.6	91.4	3.331	2.192	2.464	1.827	-[a]	110.8	[65]
19	65.8	16.3	121.3	96.8	3.042	2.044	2.329	1.519	593	115.5	[66]
20	65.8	16.8	121.5	97.2	3.042	2.057	2.337	1.530	-[a]	119.3	[67]
21	59.7	17.6	126.0	93.2	3.360	2.199	2.479	1.880	470	114.3	[68]
22	55.1	24.7	126.5	100	3.280	2.179	2.526	1.850	-[a]	-[a]	[69]
23	63.3	16.4	124.4	94.4	2.993	1.965	2.256	1.518	-[a]	-[a]	[70]
24	53.1	22.9	133.1	94.8	3.159	2.079	2.362	1.879	-[a]	70.2	[71]
25	54.8	21.2	131.9	93.3	3.187	2.084	2.360	1.876	-[a]	72.4	[71]
26	67.1	17.2	113.4	99.9	3.199	2.181	2.509	1.518	-[a]	142.7	[72]
27	50.4	21.3	138.2	91.0	3.124	1.961	2.251	1.866	-[a]	45.3	[73]
28	45.7	1.1	141.9	-[a]	3.235	1.936	2.213	1.532	-[a]	106.8	[74]
29	50.9	3.4	136.7	-[a]	3.318	1.961	2.198	1.527	-[a]	105.7	[73]

[a] The value is not reported

In order to determine the most suitable DFT functional to use for the computations of model *ansa* metallocenes in this thesis study, trial computations on these 29 known structures were made. In these computations, three popular DFT methods,

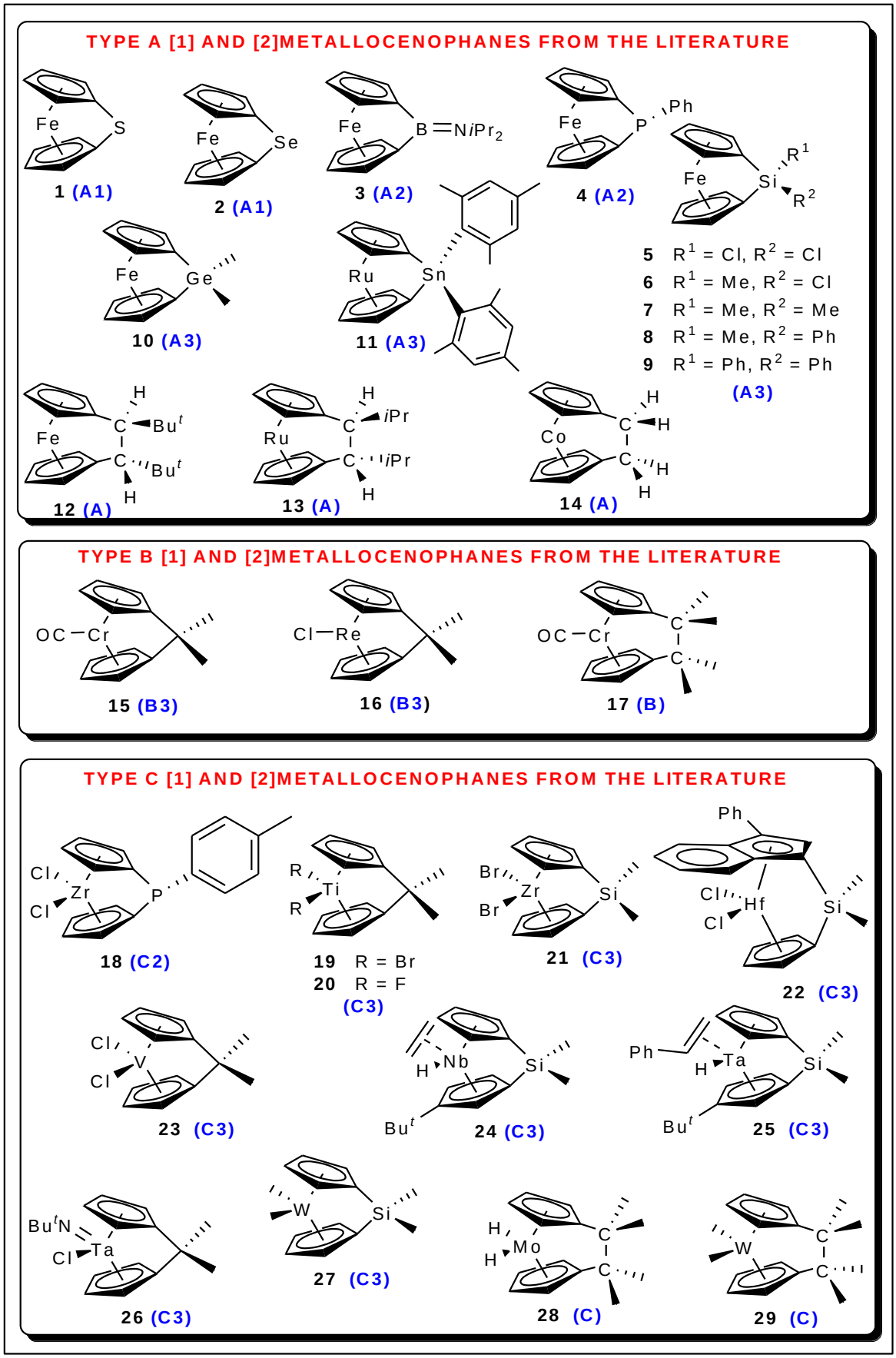

Figure 9. Some reference metallocenophane structures from the literature

B3LYP, B3PW91, B3P86 and the new DFT functional M06 was used in combination with the Ahlrich's Def2-TZVP basis set and related Effective Core Potentials (ECPs) were employed, for 5th and 6th period transition metals.
Mean absolute deviation (MAD) and mean signed deviation (MSD) values of DFT results from experimental data were calculated.

3.1.1. Comparison of Experimental and DFT Bond Angles

DFT and experimental values for the angles α, β, δ, θ are listed in Tables 2-5 and the mean absolute deviation (MAD) and the mean signed deviation (MSD) values of each DFT method from the corresponding experimental value are shown in Figures 10-13.

3.1.1.1. Tilt Angle α

In predicting α, the most precise method is found to be M06, with 0.7° MAD and 0.3°MSD, which is followed by B3P86 with 0.9° MAD and 0.6° MSD. B3LYP is the worst method of all with more than twice MAD and MSD values when compared with other three methods.

3.1.1.2. The Angle β

Computations on the angle β showed that the most precise method is found to be M06, with 0.8° MAD and -0.2° MSD, which is followed by B3P86 with 0.8° MAD and -0.6° MSD. The largest deviation from the experiment is shown for B3LYP with 1.5° MAD and -1.5° MSD.

3.1.1.3. The Angle δ

In predicting δ, the most precise method is found to be B3P86 and B3PW91, with 0.8° MAD and 0.4° MSD, which is followed by M06 with 0.8° MAD and 0.6° MSD. Again the largest deviations recieved again from the B3LYP results with 1.0° MAD and -0.5° MSD.

3.1.1.4. The Angle θ

For the computation of θ, the best density functional is found as B3P86. MAD value of this functional is 0.9° and MSD is -0.3°.

Table 2. Calculated α angles versus experimental value (°)

Structure	EXP	M06	B3LYP	B3PW91	B3P86
1	31.0	31.9	34.5	32.3	32.3
2	26.4	26.8	29.5	27.5	27.5
3	31.4	31.6	34.5	31.9	31.9
4	26.9	26.8	29.7	27.4	27.4
5	19.2	19.4	23.0	20.0	20.1
6	19.4	19.7	23.3	20.5	20.6
7	20.8	19.8	23.4	20.8	20.8
8	21.0	19.2	23.0	20.3	20.3
9	19.1	18.8	22.7	19.9	19.9
10	19.0	18.7	21.8	19.6	19.6
11	21.0	20.7	23.0	20.5	20.5
12	26.0	26.0	27.6	25.9	25.9
13	33.6	32.9	33.6	31.5	31.6
14	27.1	27.5	29.4	27.5	27.5
15	50.5	49.8	51.4	49.8	49.7
16	53.1	54.4	55.3	54.5	54.5
17	38.5	38.8	39.7	38.4	38.3
18	63.7	64.0	65.4	64.5	64.3
19	65.8	66.1	67.9	66.7	66.5
20	65.8	65.6	67.9	66.8	66.6
21	59.7	60.0	61.3	60.1	60.0
22	55.1	61.5	64.2	62.6	62.2
23	63.3	62.6	64.2	63.0	62.8
24	53.1	53.3	55.6	53.7	53.5
25	54.8	54.1	56.4	54.7	54.5
26	67.1	68.1	69.5	68.6	68.4
27	50.4	51.2	52.6	51.3	51.2
28	45.7	45.7	46.4	45.3	45.2
29	50.9	51.6	52.5	51.9	51.6

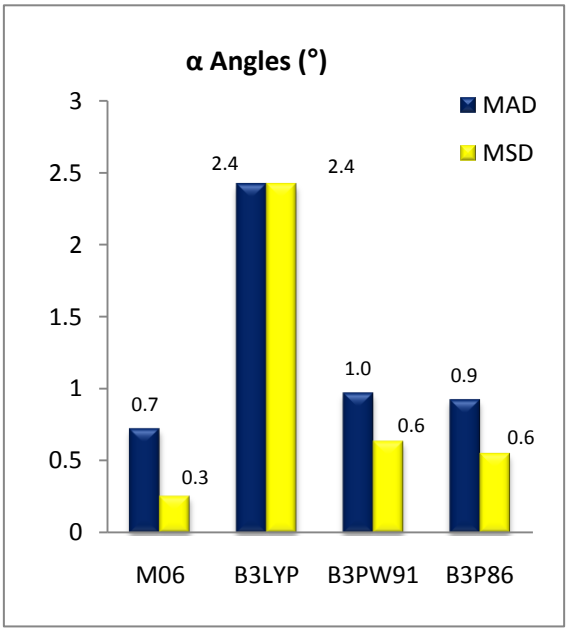

Figure 10. Deviation of DFT methods from experiment in α (degrees)

Table 3. β Angles (°)

Structure	EXP	M06	B3LYP	B3PW91	B3P86
1	29.0	28.0	27.0	27.8	27.9
2	30.0	29.6	28.3	29.1	29.2
3	35.3	35.5	33.9	35.2	35.2
4	32.3	32.2	30.7	31.9	31.9
5	40.7	40.0	37.7	39.4	39.4
6	39.5	39.0	36.6	38.1	38.1
7	37.0	37.9	35.6	37.0	36.9
8	37.4	38.8	36.2	37.7	37.7
9	40.0	39.4	36.6	38.2	38.3
10	35.9	37.0	35.0	36.1	36.1
11	35.9	35.9	33.8	35.3	35.4
12	10.9	10.5	9.31	10.1	10.2
13	12.6	12.2	11.1	12.1	12.2
14	16.6	14.7	13.6	14.3	14.5
15	22.4	22.8	22.1	22.6	22.8
16	20.9	21.7	21.2	21.6	21.7
18	17.1	14.9	14.7	15.1	15.1
19	16.3	16.5	15.7	16.0	16.2
20	16.8	16.9	15.8	16.1	16.3
21	17.6	18.0	17.2	17.7	17.8
22	24.7	20.4	19.7	20.0	20.1
23	16.4	17.2	16.5	16.7	16.9
24	22.9	22.7	21.4	22.4	22.4
25	21.2	22.0	20.8	21.7	21.8
26	17.2	16.8	16.1	16.3	16.4
27	21.3	21.1	20.2	20.7	20.8
28	1.1	0.7	0.7	0.9	1.0
29	3.4	3.3	3.9	3.95	3.6

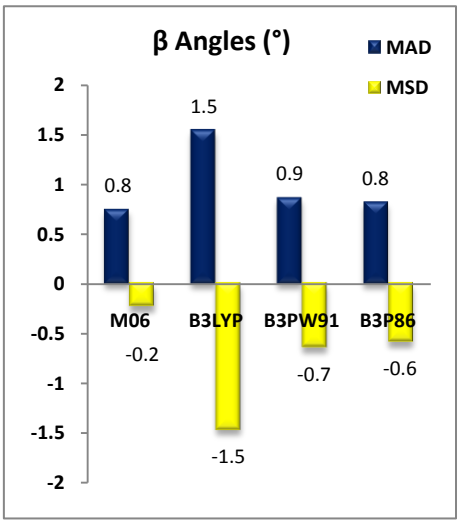

Figure 11. Deviation of DFT methods from experiment in β (degrees)

Table 4. δ Angles (°)

Structure	EXP	M06	B3LYP	B3PW91	B3P86
1	156.9	157.1	156.3	157.2	157.2
2	160.0	160.7	159.5	160.4	160.4
3	155.9	156.5	155.4	156.7	156.7
4	155.2	160.7	159.4	160.6	160.5
5	166.5	166.2	164.5	166.1	166.1
6	166.0	165.8	164.0	165.5	165.4
7	164.7	165.5	163.7	165.1	165.0
8	164.7	166.0	164.0	165.5	165.5
9	167.3	166.3	164.3	165.8	165.8
10	165.3	165.8	164.3	165.4	165.4
11	164.9	164.9	163.8	165.1	165.0
12	160.8	162.0	161.6	162.4	162.4
13	157.0	158.4	158.4	159.3	159.2
14	158.0	157.9	157.2	158.2	158.2
15	134.5	135.5	134.4	135.3	135.4
16	131.3	132.5	131.9	132.4	132.4
17	143.3	143.9	143.1	144.0	144.0
18	122.6	122.2	121.3	121.9	122.0
19	121.3	121.7	120.7	121.3	121.3
20	121.5	121.8	120.8	121.0	121.1
21	126.0	125.9	124.7	125.6	125.6
22	126.5	127.2	126.1	126.7	126.7
23	124.4	125.8	124.4	125.0	125.1
24	133.1	133.7	132.5	133.5	133.6
25	131.9	132.4	130.9	131.9	131.9
26	113.4	113.1	111.2	112.2	112.4
27	138.2	138.7	137.5	138.2	138.3
28	141.9	142.1	141.5	142.4	142.4
29	136.7	137.2	136.4	136.8	136.9

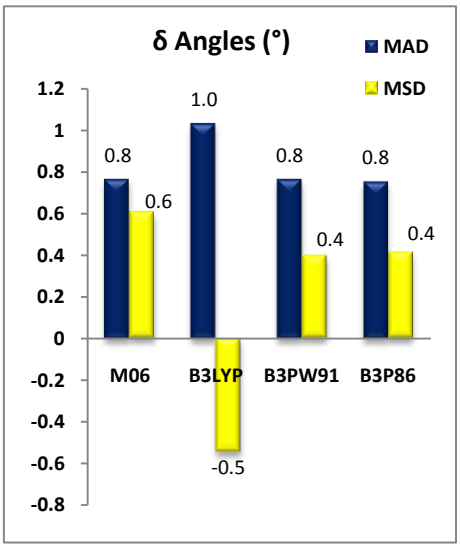

Figure 12. Deviation of DFT methods from experiment in δ (degrees)

Table 5. θ Angles (°)

Structure	EXP	M06	B3LYP	B3PW91	B3P86
1	89.0	88.1	88.8	88.4	88.4
2	86.0	86.1	86.1	85.8	85.9
3	102.0	103.0	103.0	103.0	103.0
4	90.7	90.2	90.3	90.3	90.2
5	101.0	99.7	98.6	99.1	99.1
6	98.0	97.9	96.8	97.1	97.1
7	95.7	96.1	95.0	95.2	95.1
8	96.2	97.3	95.9	96.1	96.2
9	99.2	98.0	96.4	96.8	96.8
10	91.7	92.8	92.0	92.0	92.0
11	91.5	92.1	90.4	90.9	91.1
15	94.7	95.1	95.7	94.9	95.1
16	95.7	97.2	97.3	96.6	96.8
18	91.4	90.2	90.8	90.6	90.7
19	96.8	97.4	97.8	97.2	97.3
20	97.2	98.1	98.5	97.9	98.0
21	93.2	94.4	94.4	94.1	94.2
22	100.0	95.2	95.2	95.0	95.0
23	94.4	95.5	96.0	95.2	95.3
24	94.8	95.3	94.9	94.8	94.9
25	93.3	94.8	94.4	94.2	94.3
26	99.9	100.0	100.0	99.7	99.8
27	91.0	91.4	91.3	90.9	91.0

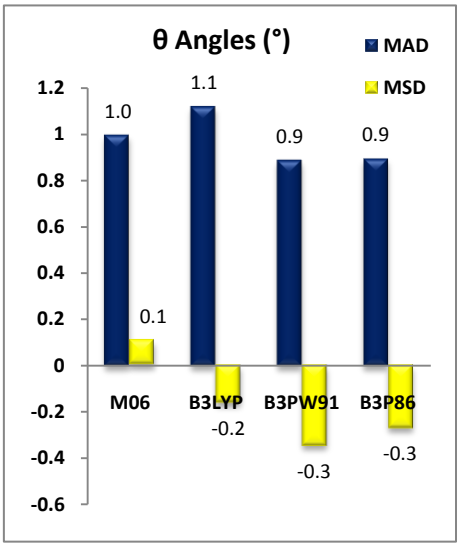

Figure 13. Deviation of DFT methods from experiment in θ (degrees)

3.1.1.5. Overall Deviation in Angles

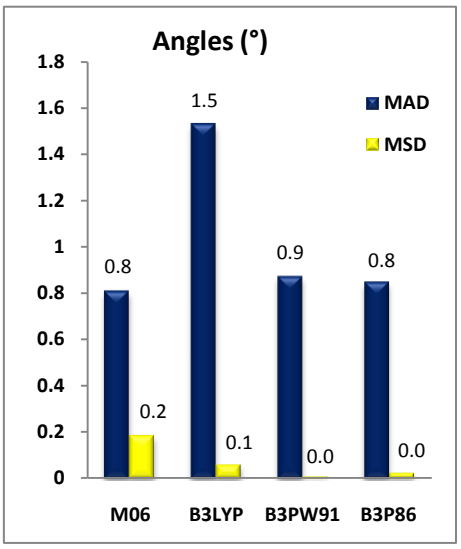

Figure 14. Overall Deviation in Angles (degrees)

When the means of MAD and MSD values were calculated from the results of angles, it is found that the best performing DFT functional was B3P86. As seen in Figure 14, the deviations from experiment are 0.8 (MAD). When the MSD is considered it was seen that the value of it is nearly zero.

3.1.2. Comparison of Experimental and DFT Bond Lengths

Experimental and DFT Cp-M, C_{ipso}-M, C_{ipso}-E and M-E distances are listed in Tables 6-9 and in Figures 15-18 the mean absolute deviation (MAD) and the mean signed deviation (MSD) values of each DFT method is shown.

3.1.2.1. M-E

In predicting M-E distances, the most precise method is found to be B3P86, with 0.0019 Å MAD and 0.002 Å MSD, which is followed by M06 with 0.0021 Å MAD and 0.009 Å MSD. B3LYP has 0.0036 Å MAD and 0.031 Å MSD and B3PW91 0.0034 Å MAD and -0.008 Å MSD.

3.1.2.2. Cp-M

For Cp-M distances, again the most precise method is found to be B3P86, with 0.012 Å MAD and 0.010 Å MSD, which is followed by with B3PW91 0.015 Å MAD and 0.014 Å MSD. B3LYP has 0.047 Å both for MAD and MSD values. Deviations for M06 functionals are 0.024 Å and 0.022 Å for MAD and MSD, respectively.

3.1.2.3. C_{ipso}-M

The deviations of DFT functionals in measuring C_{ipso}-M distances are 0.017 Å MAD and 0.005 Å MSD for M06, 0.031 Å MAD and 0.03 Å MSD for B3LYP, 0.019 Å MAD and 0.012 Å MSD for B3PW91 and 0.018 Å MAD and 0.008 Å MSD for B3P86. According to these results M06 is better than the other functional.

3.1.2.4. C_{ipso}-E

When the experimental and DFT results for C_{ipso}-E distances are compared, following MAD and MSD values are found. For M06, 0.014 Å MAD and 0.003 Å MSD, for B3LYP, 0.019 Å MAD and 0.014 Å MSD, for B3PW91, 0.015 Å MAD and 0.008 Å MSD and for B3P86, 0.013 Å MAD and 0.005 Å MSD. B3P86 is best performing functional.

Table 6. M-E Distance (Å)

Structure	EXP	M06	B3LYP	B3PW91	B3P86
1	2.794	2.810	2.825	2.807	2.804
2	2.906	2.894	2.923	2.901	2.897
3	2.559	2.524	2.552	2.533	2.528
4	2.774	2.788	2.814	2.790	2.787
5	2.588	2.619	2.667	2.634	2.630
6	2.655	2.659	2.708	2.679	2.676
7	2.690	2.701	2.750	2.274	2.721
8	2.691	2.677	2.733	2.704	2.699
9	2.636	2.662	2.721	2.690	2.685
10	2.804	2.79	2.836	2.810	2.806
11	2.994	2.984	3.040	3.004	2.995
12	2.925	2.924	2.956	2.936	2.930
13	3.010	2.933	2.965	2.943	2.938
14	2.966	2.935	2.974	2.955	2.950
15	2.831	2.801	2.832	2.814	2.808
16	2.892	2.845	2.873	2.858	2.853
18	3.331	3.387	3.414	3.388	3.382
19	3.042	3.027	3.061	3.045	3.039
20	3.042	3.024	3.059	3.047	3.041
21	3.360	3.349	3.394	3.371	3.364
22	3.280	3.288	3.337	3.314	3.307
23	2.993	2.956	2.995	2.980	2.973
24	3.159	3.148	3.194	3.163	3.158
25	3.187	3.176	3.224	3.196	3.189
26	3.199	3.201	3.259	3.229	3.221
27	3.124	3.113	3.153	3.136	3.129
28	3.235	3.229	3.261	3.237	3.230
29	3.318	3.301	3.337	3.319	3.311

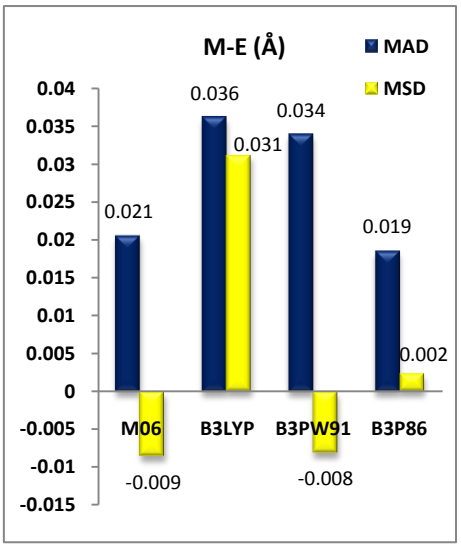

Figure 15. Deviation of DFT methods from experiment in M-E (Å)

Table 7. Cp-M Distance (Å)

Structure	EXP	M06	B3LYP	B3PW91	B3P86
3	1.634	1.639	1.681	1.645	1.643
4	1.630	1.642	1.683	1.648	1.646
6	1.639	1.649	1.689	1.654	1.651
8	1.641	1.648	1.688	1.654	1.651
9	1.650	1.648	1.687	1.653	1.651
10	1.630	1.648	1.688	1.654	1.651
11	1.807	1.817	1.836	1.802	1.801
12	1.629	1.632	1.667	1.634	1.632
13	1.794	1.81	1.830	1.795	1.794
14	1.717	1.725	1.770	1.732	1.728
15	1.777	1.766	1.813	1.773	1.770
16	1.853	1.862	1.890	1.861	1.860
17	1.780	2.153	1.832	1.791	1.789
18	2.192	2.21	2.253	2.223	2.219
19	2.044	2.047	2.093	2.063	2.058
20	2.057	2.055	2.107	2.081	2.075
21	2.199	2.217	2.258	2.228	2.223
22	2.179	2.204	2.247	2.220	2.215
23	1.965	1.953	2.002	1.970	1.964
24	2.079	2.083	2.123	2.087	2.083
25	2.084	2.087	2.129	2.093	2.090
26	2.181	2.197	2.253	2.215	2.210
27	1.961	1.973	2.010	1.980	1.977
28	1.936	1.934	1.961	1.929	1.928
29	1.961	1.969	2.002	1.972	1.971

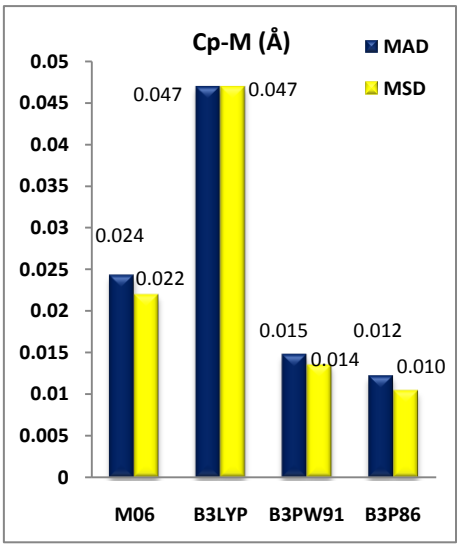

Figure 16. Deviation of DFT methods from experiment in Cp-M (Å)

Table 8. C_{ipso}-M Distance (Å)

Structure	EXP	M06	B3LYP	B3PW91	B3P86
1	1.954	1.964	1.985	1.965	1.964
2	1.960	1.981	2.002	1.982	1.981
3	1.989	1.980	1.999	1.982	1.980
4	1.979	1.983	2.003	1.985	1.982
5	2.007	2.000	2.027	2.011	2.008
6	2.014	2.010	2.028	2.012	2.009
7	2.001	2.011	2.029	2.013	2.010
8	2.003	2.013	2.030	2.014	2.011
9	2.014	2.014	2.030	2.014	2.012
10	2.001	2.007	2.000	2.040	2.022
11	2.149	2.152	2.158	2.141	2.140
12	1.965	1.959	1.979	1.962	1.959
13	1.982	2.077	2.089	2.072	2.070
14	1.979	2.074	2.106	2.085	2.082
15	2.117	2.099	2.131	2.107	2.104
16	2.175	2.164	2.187	2.168	2.166
17	2.160	2.132	2.167	2.139	2.137
18	2.464	2.472	2.506	2.483	2.479
19	2.329	2.324	2.356	2.336	2.332
20	2.337	2.330	2.363	2.347	2.343
21	2.479	2.490	2.525	2.502	2.498
22	2.526	2.479	2.519	2.497	2.491
23	2.256	2.238	2.276	2.254	2.249
24	2.362	2.355	2.383	2.358	2.355
25	2.360	2.363	2.396	2.371	2.368
26	2.509	2.512	2.564	2.530	2.526
27	2.251	2.248	2.277	2.258	2.255
28	2.213	2.206	2.229	2.205	2.203
29	2.198	2.234	2.261	2.239	2.239

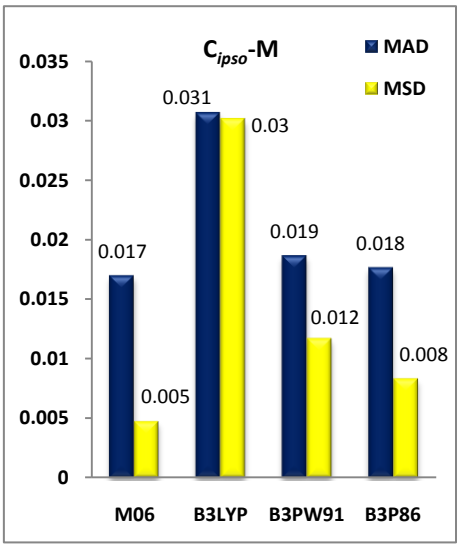

Figure 17. Deviation of DFT methods from experiment in C_{ipso}-M (Å)

Table 9. C_{ipso}-E Distance (Å)

Structure	EXP	M06	B3LYP	B3PW91	B3P86
3	1.623	1.605	1.614	1.611	1.608
4	1.849	1.877	1.884	1.875	1.872
5	1.850	1.868	1.879	1.874	1.871
6	1.871	1.884	1.895	1.890	1.886
7	1.851	1.903	1.914	1.909	1.905
8	1.880	1.898	1.910	1.904	1.900
10	1.977	1.981	1.996	1.985	1.981
11	2.200	2.196	2.214	2.200	2.194
12	1.518	1.524	1.534	1.529	1.526
13	1.596	1.526	1.538	1.533	1.530
14	1.512	1.504	1.514	1.509	1.506
15	1.530	1.525	1.537	1.531	1.529
16	1.542	1.535	1.547	1.540	1.538
17	1.530	1.523	1.534	1.528	1.525
18	1.827	1.849	1.856	1.848	1.845
19	1.519	1.518	1.529	1.524	1.521
20	1.530	1.520	1.531	1.525	1.523
21	1.880	1.880	1.891	1.887	1.883
22	1.850	1.882	1.890	1.887	1.883
23	1.518	1.516	1.528	1.522	1.519
24	1.879	1.884	1.894	1.890	1.886
25	1.876	1.884	1.893	1.889	1.886
26	1.518	1.522	1.533	1.527	1.524
27	1.866	1.870	1.881	1.876	1.873
28	1.532	1.528	1.539	1.533	1.530
29	1.527	1.523	1.534	1.528	1.525

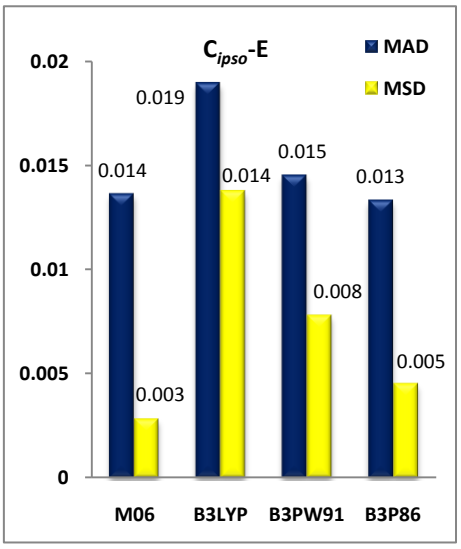

Figure 18. Deviation of DFT methods from experiment in C_{ipso}-E (Å)

3.1.2.5. Overall Deviation in Distances

When the means of MAD and MSD values were calculated for the computed angles, the best performing DFT functional was found to be B3P86 with 0.015 MAD Å and 0.006 Å MSD, as seen in Figure 19.

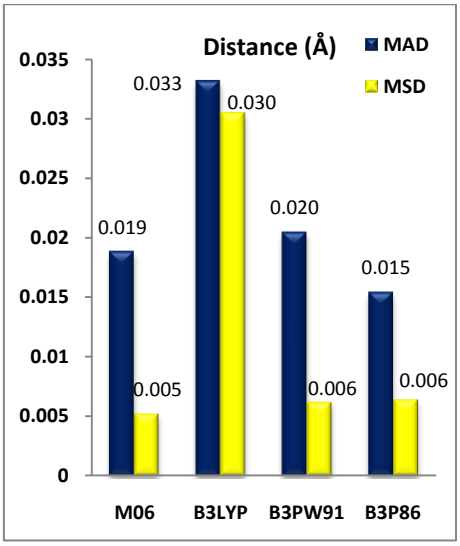

Figure 19. Overall Deviation in Distances (Å)

3.1.3. Comparison of Experimental and DFT ^{13}C NMR Chemical Shifts

In comparing DFT and experimental NMR chemical shifts, ^{13}C NMR δ C_{ipso} Shifts were taken in the consideration, because these values are important characteristics for *ansa* compounds.

When the four functionals were compared according to the mean deviations from experimental values, it was seen that the deviations for B3P86 and B3PW91 were close to each other and these functionals perform better than the other two functionals M06 and B3LYP as seen in Figure 20 and Table 10.

The lowest deviations belong to B3PW91 functional with 5.7 ppm MAD and 5.4 ppm MSD.

Table 10. ^{13}C NMR δ C_{ipso} Shifts (ppm)

Structure	EXP	M06	B3LYP	B3PW91	B3P86
1	14.3	14.5	29.3	27.5	27.5
2	5.6	9.7	26.7	24.7	24.7
3	44.2	28.4	43.7	41.9	42.1
4	18.7	11.1	30.1	28.2	28.4
5	36.1	27.4	44.8	42.8	43.2
6	33.8	20.4	39.9	38.2	38.7
7	33.5	19.2	37.8	36.4	36.9
8	32.2	17.6	37.4	36.0	36.5
9	31.0	17.1	36.4	35.1	35.6
10	31.0	18.5	38.5	36.5	36.9
11	31.8	35.8	41.5	38.3	38.2
12	90.4	90.2	98.9	96.4	96.7
13	89.2	88.5	95.1	92.5	92.5
15	52.7	61.3	65.6	60.8	60.9
16	31.0	33.9	39.0	36.9	37.2
18	110.8	114.0	115.1	112.8	112.8
19	115.5	119.8	120.6	119.7	119.7
20	119.3	125.0	124.9	124.2	124.3
21	114.3	115.6	114.7	112.5	112.6
24	70.2	75.9	78.4	73.7	73.9
25	72.4	79.8	82.2	77.9	77.9
26	142.7	149.5	155.5	152.7	152.8
27	45.3	51.6	55.6	50.9	51.0
28	106.8	109.0	113.8	109.1	109.1
29	105.7	106.9	112.8	108.2	108.1

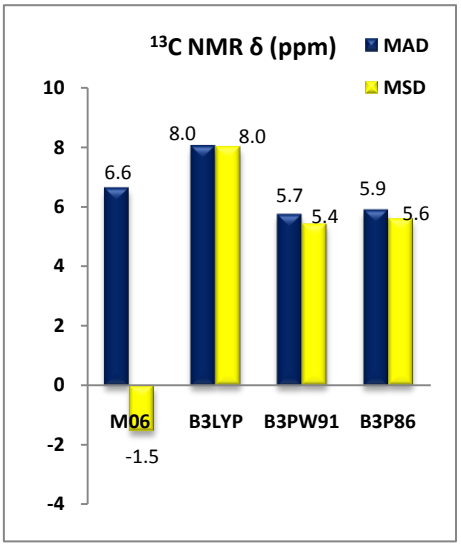

Figure 20. Deviation in ^{13}C NMR δ C_{ipso} Shifts (ppm)

3.1.4. Comparison of Experimental and DFT Electronic Spectra

Comparison of computational electronic spectra with experimental electronic spectra is difficult, because of the solvent effects, and other factors that can not be applied on the gas phase DFT computations. However, a general trend in the changes on higher or lower energy absorbance bands can be achieved. With this purpose we have compared the lowest energy absorbance wavelengths. The results are listed in Table 11 and mean deviations are shown in Figure 21.

Table 11. UV-Vis λ_{max} Values (nm)

Structure	EXP	M06	B3LYP	B3PW91	B3P86
1	504	620	547	502	500
2	500	609	538	495	493
3	498	615	540	497	494
4	497	610	540	498	495
5	470	577	513	473	470
7	478	588	522	481	478
10	486	594	525	485	481
11	363	389	372	346	346
12	454	545	486	452	450
13	346	386	370	344	344
14	486	708	637	580	575
17	506	350	343	334	333
19	593	541	559	547	546
21	470	379	385	378	377

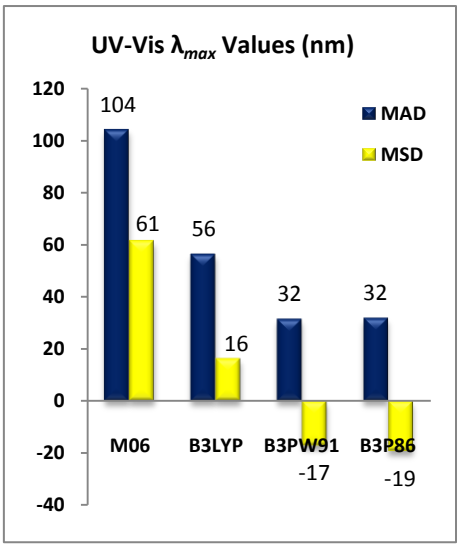

Figure 21. Deviation in UV-Vis λ_{max} Values (nm)

Although the M06 functional has proved good results in predicting bond lengths of angles, the deviations in predicting absorbance wavelengths are much higher than the other three functionals.

Similar to the results in NMR computations, best results were obtained with B3PW91 and B3P86 with nearly same MAD and MSD values.

Especially for *ansa* ferrocenes, very close absorbtion λ_{max} values were achieved with B3P86 and B3PW91.

In summary, for the structural computations M06 and B3P86, and for the spectroscopic computations, B3PW91 and B3P86 functionals displayed smallest mean deviations from the experiment and B3LYP showed large deviations in both cases.

According to these results, it was decided to conduct the computations of the model *ansa* metallocenes in this thesis at B3P86 level of theory, which has proven good results in both structural and electronic computations.

3.2. Computational Characterization of Model *ansa* Metallocenes

3.2.1. Group 4

In Figure 22, model *ansa* metallocenes of Group 4 transition metals are seen.

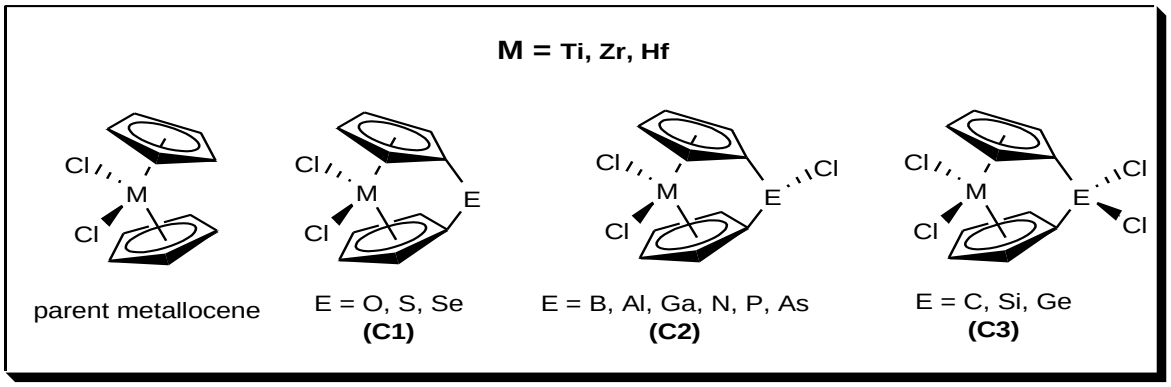

Figure 22. Parent metallocene and [1]metallocenophane structures of Group 4

3.2.1.1. Structural Parameters

Among the eight structural parameters, α, δ, Cp-M and C_{ipso}-M are found both in *ansa* complexes and their unbridged parent metallocenes, therefore evaluating these values may give important clues about the *ansa* bridge contribution to the structural properties of a metallocene. Higher α and lower δ values indicate higly bent structures.

Unlike α, δ, Cp-M and C_{ipso}-M, β, θ, M-E and C_{ipso}-E are defined only for bridged metallocenes and directly related to the bridging group. Evaluating these values is important for structural characterization of *ansa* metallocenes.

3.2.1.1.1. Tilt Angles (α)

The geometry of Group 4 parent metallocenes, $[Ti\{(\eta^5\text{-}C_5H_5)_2\}Cl_2]$, $[Zr\{(\eta^5\text{-}C_5H_5)_2\}Cl_2]$ and $[Hf\{(\eta^5\text{-}C_5H_5)_2\}Cl_2]$ are already bent with α values 50.4°, 52.8° and 52.9°, respectively. Addition of *ansa* bridge further increases these values in an

amount depending the type of the bridging element as seen in Figure 23.

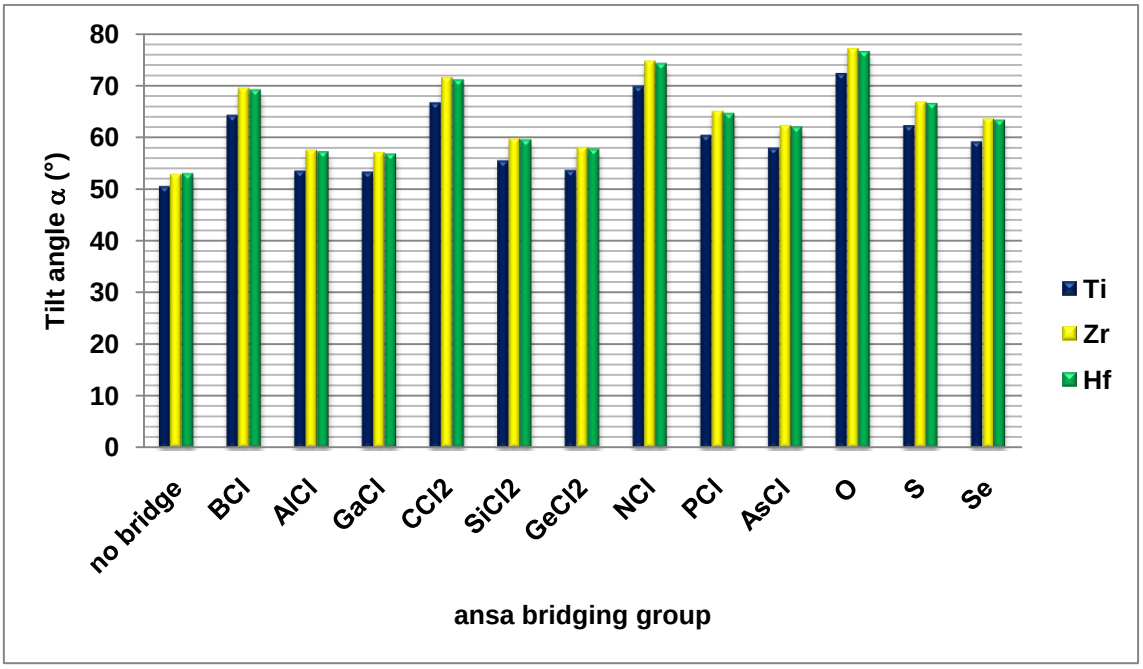

Figure 23. Tilt angle (α) values of group 4 [1]metallocenophanes with different *ansa* bridges

Among Group 4 [1]metallocenophanes, the highest α value (77.0°) belongs to the oxygen bridged *ansa* zirconocene, [Zr{(η^5-C_5H_4)$_2$O}Cl_2], which is 24.2° more tilted with respect to its parent metallocene. The lowest value for α (53.2°) is that of gallium-bridged species [Ti{(η^5-C_5H_4)$_2$GaCl}Cl_2], which exhibits only 2.8° more ring tilt than non-bridged titanocenedichloride.

Second row bridging elements (B, C, N, O) increases α by 13.7-24.2°, the third row elements (Al, Si, P, S) by 3.0-13.9° and the fourth row elements (Ga, Ge, Se) cause an increase by 2.8-10.6°.

In general, α values of Group 4 *ansa* Metallocenes for

- Zr >Hf >Ti
- 2nd row bridging elements >> 3rd row > 4th row and
- the same period of E Group 16 > Group15> Group 14> Group 13.

In Figure 24, the effect of changing the α on the calculated relative energy of the group 4 metallocenes is shown.

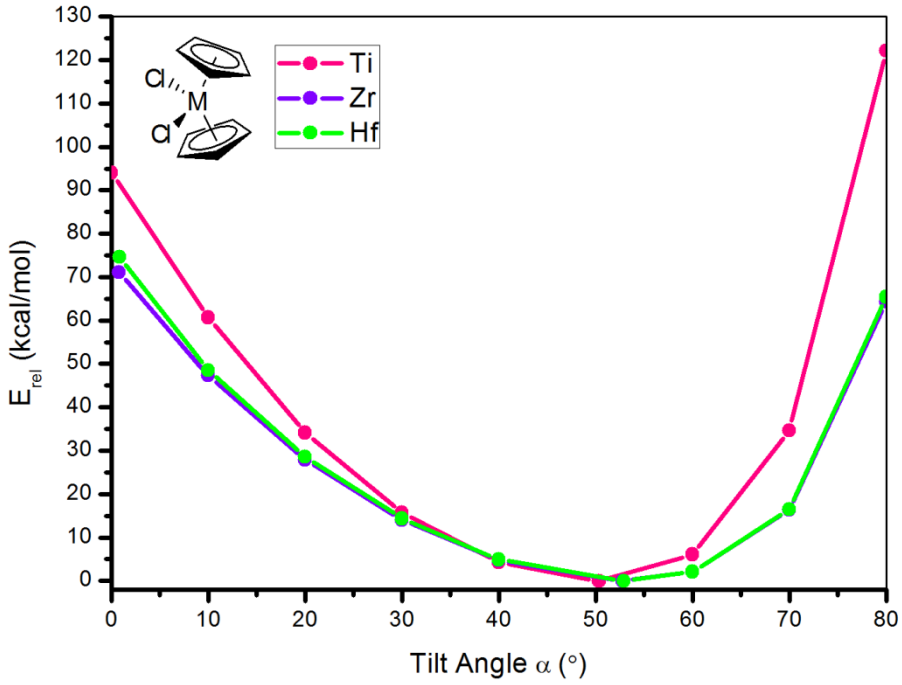

Figure 24. Tilt angle α relative energy relationship in group 4 metallocenes

In Group 4, since the parent metallocene geometries are already bent, it is difficult to achieve a strained *ansa* metallocene via ring tilting. Tilting up to about 50°, decreases the relative energy of the metallocene. Between 50-60°, for Ti 6 kcal/mol and for Zr and Hf metallocenes about 2 kcal/mol increase in energy is observed. Between 60-70°, the rise in energy become significant and reaches up to 29 kcal/mol for Ti and about 15 kcal/mol for Zr and Hf. Increasing α beyond 70° causes a sharp increase in total energies of all three metallocenes.

According to these results, Group 4 *ansa* metallocenes having greater tilt angles than 70° are expected to possess ring strain. Those structures are [Ti{(η^5-$C_5H_4)_2O$}Cl_2] (72.2°), [Zr{(η^5-$C_5H_4)_2CCl_2$}Cl_2] (70.9°), [Zr{(η^5-$C_5H_4)_2NCl$}Cl_2] (74.6°), [Zr{(η^5-$C_5H_4)_2O$}Cl_2] (77°), [Hf{(η^5-$C_5H_4)_2CCl_2$}Cl_2] (70.9°), [Hf{(η^5-$C_5H_4)_2NCl$}Cl_2] (74.1°) and [Hf{(η^5-$C_5H_4)_2O$}Cl_2] (76.4°).

δ angle trends are just the opposite of α. Largest values belong to the parent metallocenes, 131.8°, 129.4° and 129.1° for [Ti{(η^5-C_5H_5)$_2$}Cl_2], [Zr{(η^5-C_5H_5)$_2$}Cl_2] and [Hf{(η^5-C_5H_5)$_2$}Cl_2], respectively, and the smallest values belong to their most tilted (oxygen bridged) counterparts, 116.6°, 110.6° and 110.4°, respectively.

In Group 4 *ansa* metallocenes, β angles lie in the range 13.3-27.6°, 12.3-26° and 12.5-26.1° for Ti, Zr and Hf complexes, respectively. The smallest β value (12.3°) belongs to [Zr{(η^5-C_5H_4)$_2$S}Cl_2], where the largest value is 27.6° and belongs to [Ti{(η^5-C_5H_4)$_2$BCl}Cl_2].

θ values ranges from 84° ([Ti{(η^5-C_5H_4)$_2$Se}Cl_2]) to 111.2° ([Hf{(η^5-C_5H_4)$_2$BCl}Cl_2]). More detailed data can be found in Tables A1-A4 in Appendix A.

3.2.1.1.2. Metal Cyclopentadienyl Ring Distances (Cp-M)

The distance between the transition metal center and the centroid of the cyclopentadienyl ligand, Cp-M, in Group 4 metallocenes [Ti{(η^5-C_5H_4)$_2$}Cl_2], [Zr{(η^5-C_5H_4)$_2$}Cl_2] and [Hf{(η^5-C_5H_4)$_2$}Cl_2] are 2.072 Å, 2.225 Å and 2.225 Å, respectively.

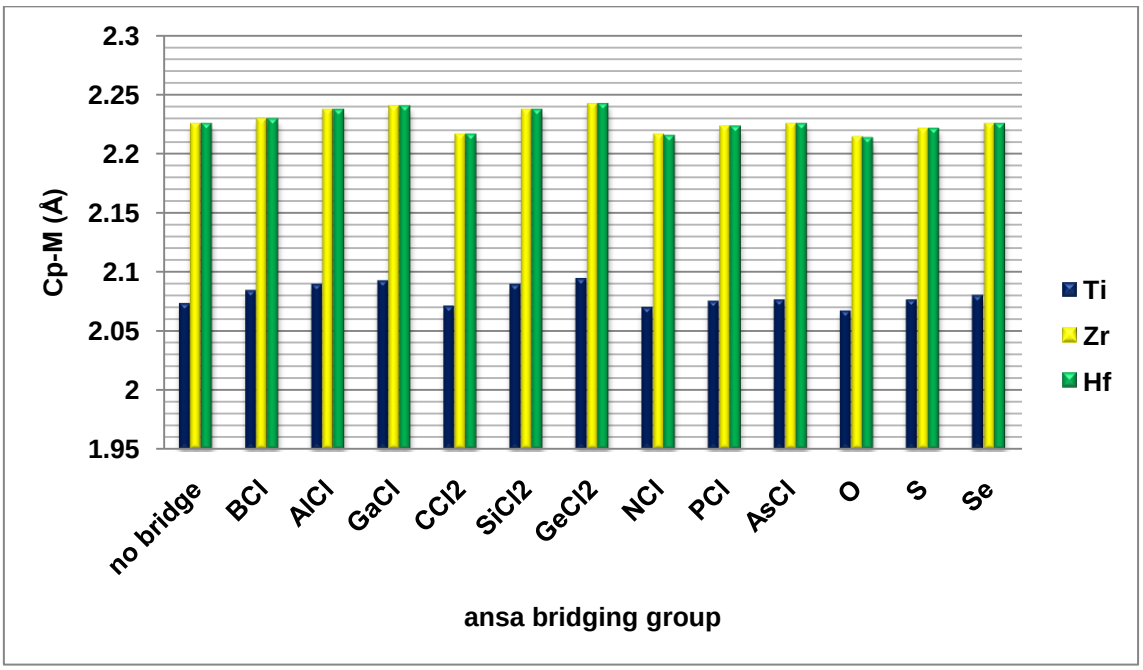

Figure 25. Cp-M Distances

The effects increasing Cp-M, also weakens the metal cyclopentadienyl bond and is a sign of the present ring strain in the molecule.

Among Group 4 *ansa* metallocenes, bridging by Group 13 elements (Al, Ga) and Group 14 elements (Si, Ge) increases Cp-M the most, 2nd period bridges decreases Cp-M, as seen in Figure 25. The highest Cp-M distances are those of Ga and Ge bridged structures. Lowest Cp-M values belong to C, N and O bridged structures.

Cp-M, C_{ipso}-M, C_{ipso}-E and M-E distances of Group 4 *ansa* metallocenes can be found in Appendix A in Tables A4-A8.

3.2.1.1.3. δ C_{ipso} ^{13}C NMR TMS Chemical Shifts

Calculated ^{13}C NMR chemical shifts (ppm) of cyclopentadienyl carbon atoms and corresponding C-M distances (Å) (in parantheses) of parent metallocenes are as follows. For [Ti{(η^5-$C_5H_5)_2$}Cl_2] five doublets at δ 108.4 (2.370), 116.1 (2.383), 122.7 (2.396), 124 (2.406), 140.3 (2.416); for [Zr{(η^5-$C_5H_5)_2$}Cl_2] δ 107 (2.507), 114.6 (2.514), 120.1 (2.530), 120.3 (2.542), 134.4 (2.547) and for [Hf{(η^5-$C_5H_5)_2$}Cl_2] δ 106.1 (2.509), 114.6 (2.516), 118.9 (2.541), 119.3 (2.530), 133.3 (2.546). Also, signals shift downfield as C-M distances increase.

In Group 4 *ansa* metallocenes, in general, C_{ipso} ^{13}C NMR chemical shifts are found to be shifted towards lower magnetic fields with respect to the highest field signal of parent metallocenes. This effect is the most obvious in the O and N bridged structures of Ti, Zr and Hf. (Figure 26, Table A9 in Appendix A). The most tilted structure of the group, [Zr{(η^5-$C_5H_4)_2$O}Cl_2] have a chemical shift value of 144.2 ppm, where its parent metallocene have 114. 4 ppm δ C_{ipso} ^{13}C NMR TMS chemical shift value.

Only for sulfur and selenium bridged *ansa* titanocenes, *ipso* carbon signals show an upfield shift with 106.5 ppm and 105.1 ppm, respectively.

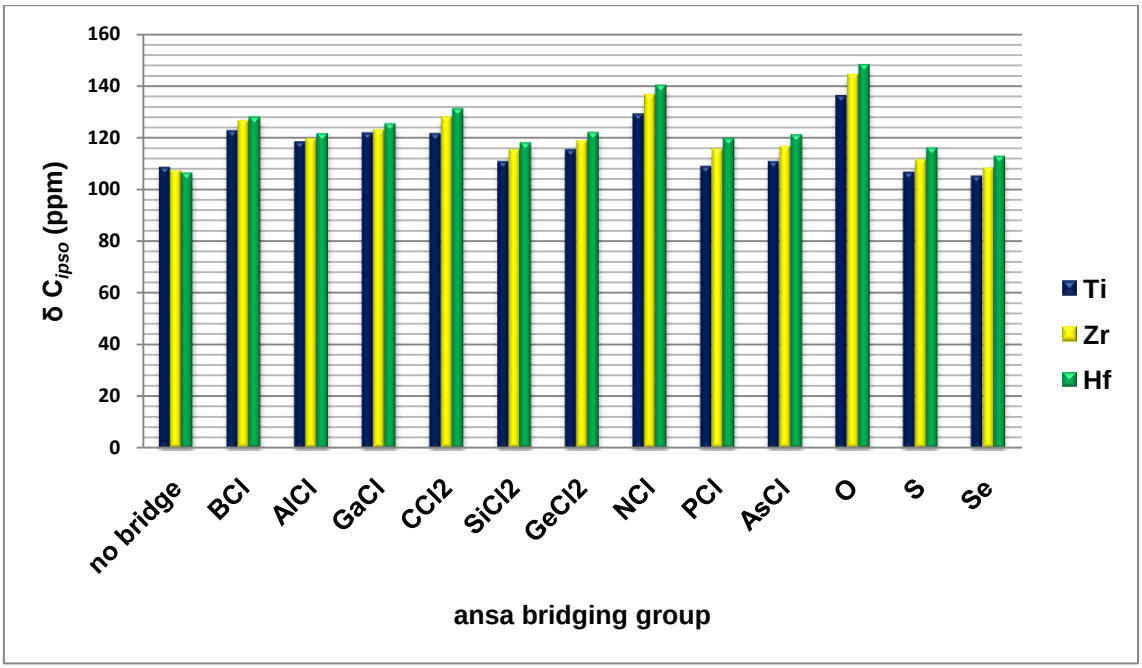

Figure 26. C_{ipso} ^{13}C NMR δ values of group 4 [1]metallocenophanes with different *ansa* bridges

3.2.1.2. Electronic Parameters

3.2.1.2.1. NPA Charges on Metal

NPA analyses indicate an appreciable negative charge of -0.416 on Ti, where Zr (0.756) and Hf (0.923) centers of corresponding parent metallocenes are positively charged (Figure 27, Table A12).

For *ansa* titanocenes, it was seen that *ansa* bridging with C, N, S and Se increased the charge on Ti, where bridging with other elements decreased the charge on Ti further, making it more nucleophilic.

For *ansa* zirconocenes and *ansa* hafnocenes, on the other hand, *ansa* bridge formation with Al, Ga, Si, and Ge decreased the charge on metal where bridging with other elements increased it. The metal center of these complexes are identified as most suitable for electrophilic attack in Group 4 *ansa* metallocenes.

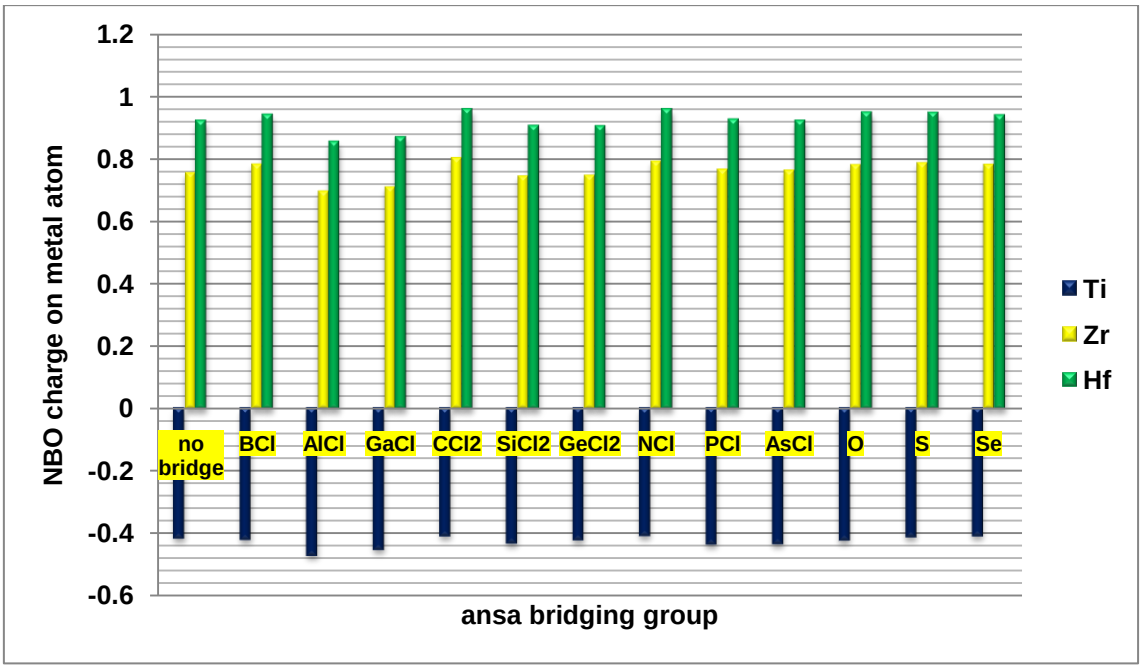

Figure 27. NBO charges on metal atom of group 4 [1]metallocenophanes with different *ansa* bridges

3.2.1.2.2. Dipole Moments

Dipole moments for the non-bridged parent metallocene structures of Ti, Zr, and Hf are 5.19, 4.73, and 4.55 D, respectively (See Table A10 in Appendix A). Introduction of *ansa* bridge in the structure generally decreases the dipole moment of the parent metallocene. The effect is greatest for Group 14 (C, Si and Ge) bridged structures. For example dipole moment of $[Hf\{(\eta^5\text{-}C_5H_4)_2GeCl_2\}Cl_2]$ species is 0.85 D.

3.2.1.2.3. Frontier Molecular Orbitals

As seen in Figure 28, in Group 4 metallocenes, there is a slight decrease in HOMO-LUMO energy gap.

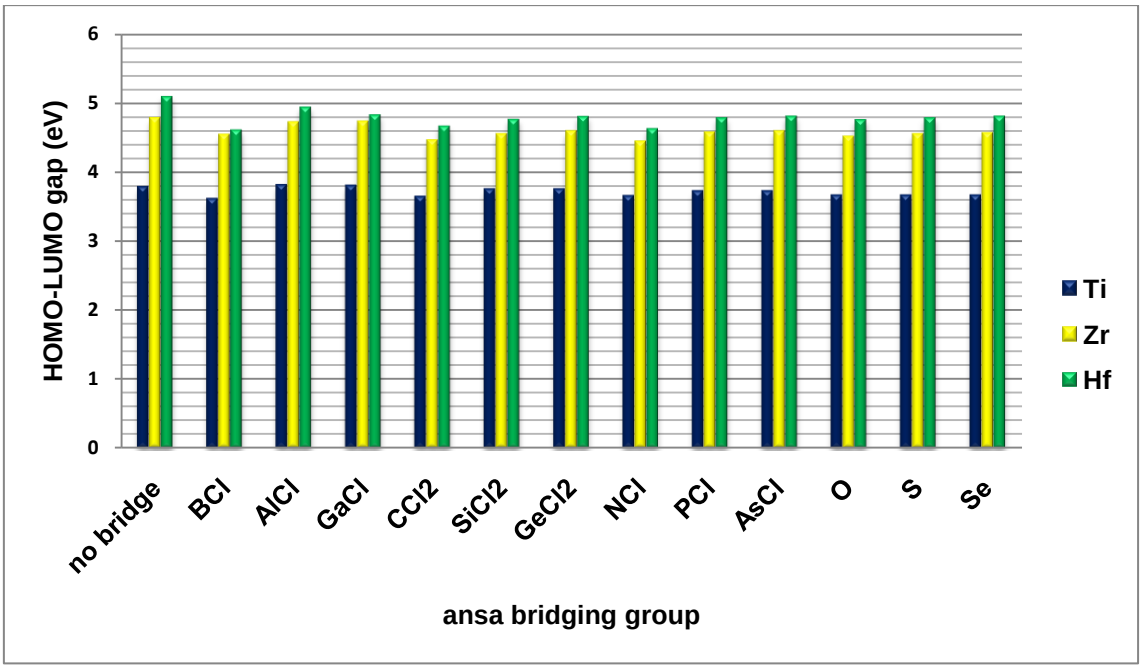

Figure 28. HOMO-LUMO gaps of group 4 [1]metallocenophanes with different *ansa* bridges

3.2.1.2.4. Absolute Hardness (η)

Absolute hardness values of Group 4 *ansa* metallocenes are listed in Table A18. Parallel to the decreasing HOMO-LUMO energy gaps, formation of *ansa* bridge makes Group 4 metallocenes softer indicating higher reactivity.

3.2.1.2.5. Chemical Potential (μ)

Chemical potentials, of metallocenes decreases significantly via *ansa* bridge formation. Especially for *ansa* titanocenes. Lowest value (-5.62) is observed for $[Ti\{(\eta^5\text{-}C_5H_4)_2GeCl_2\}Cl_2]$ (Figure 29, Table A17).

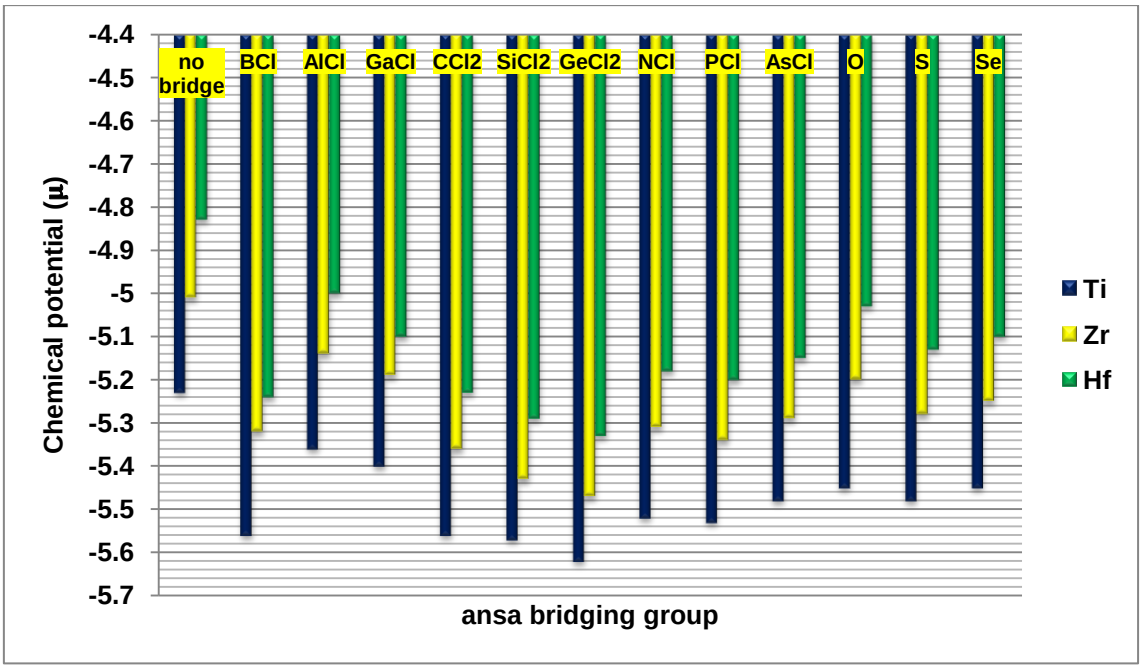

Figure 29. Chemical potential (μ) values of group 4 [1]metallocenophanes with different *ansa* bridges

3.2.1.2.6. Electronic Spectra

Computational electronic spectra of *ansa* titanocenes, *ansa* zirconocenes and *ansa* hafnocenes are given in Figures 30-32.

The highest energy absorbtion bands of parent mettallocenes, corresponding to the LMCT transitions between Cp and M orbitals were observed at 278, 208 and 192 nm for Ti, Zr and Hf non-bridged metallocenes respectively.

Formation of *ansa* bridge cause a red-shift in these bands. In addition, via *ansa* bridging lowest energy bands become more intense, which is especially obvious for $[Ti\{(\eta^5\text{-}C_5H_4)_2GeCl_2\}Cl_2]$.

In general, smaller bridge atoms result higher red-shifts in the values of λ_{max}.

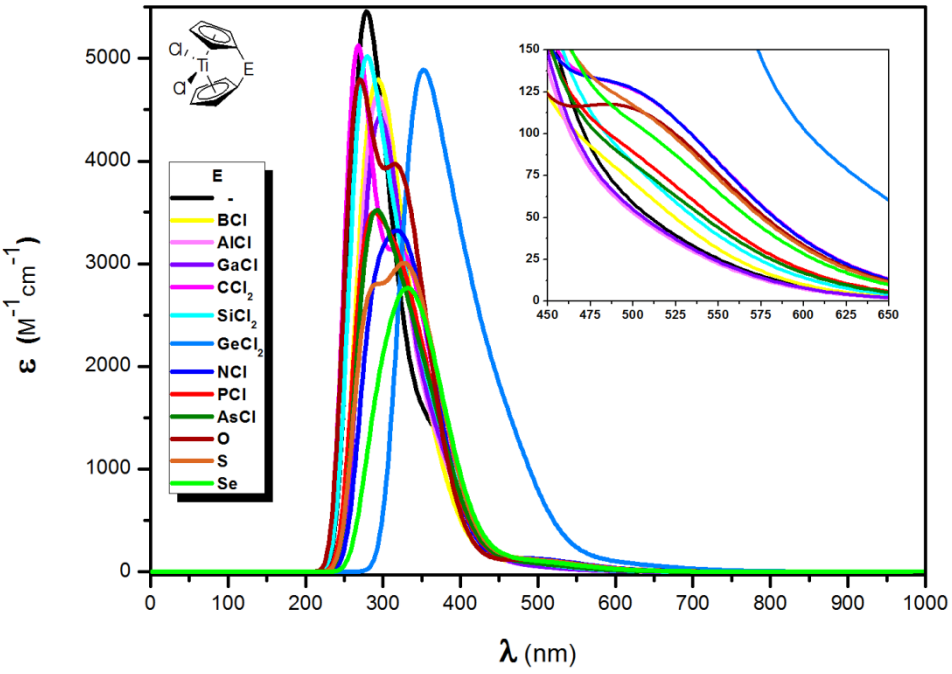

Figure 30. Change in electronic spectra of [1]titanocenophanes with changing *ansa* bridge

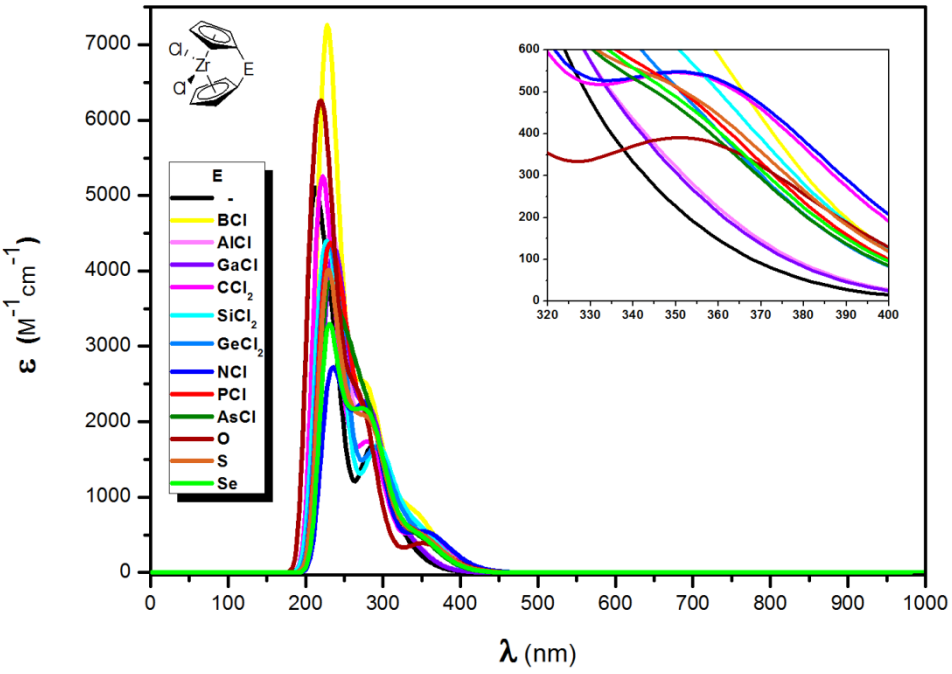

Figure 31. Change in electronic spectra of [1]zirconocenophanes with changing *ansa* bridge

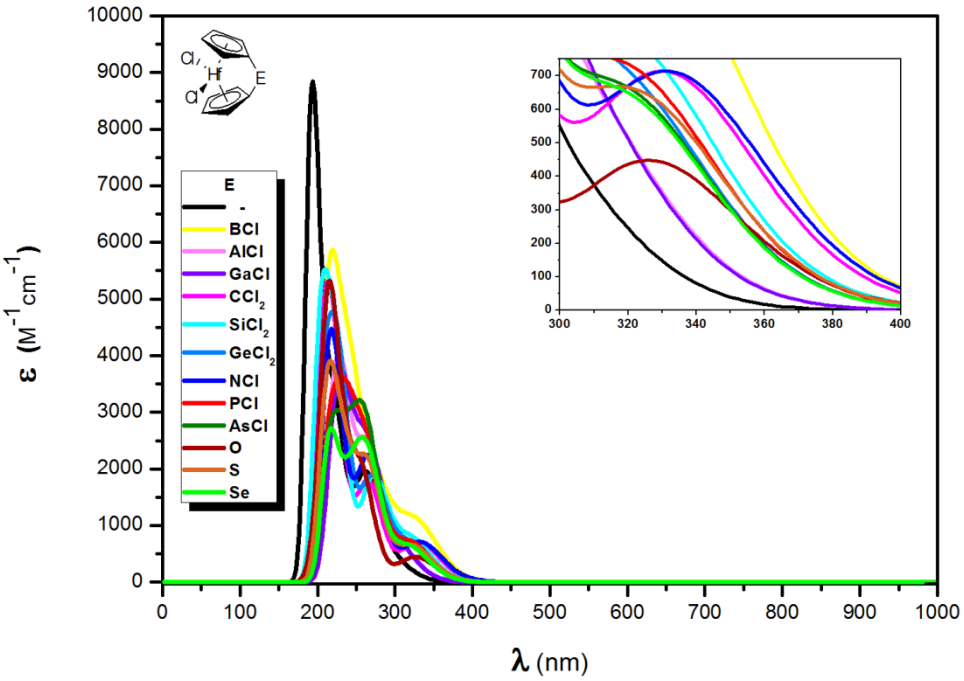

Figure 32. Change in electronic spectra of [1]hafnocenophanes with changing *ansa* bridge

3.2.2 Group 5

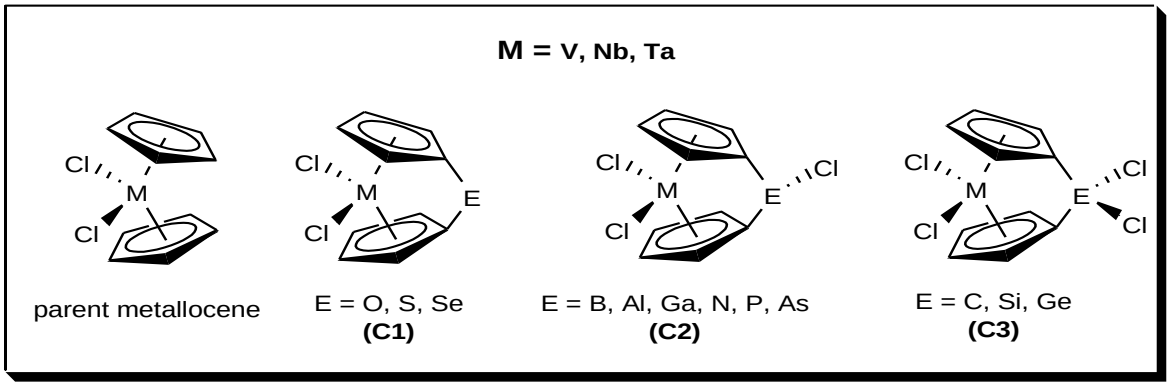

Figure 33. Parent metallocene and [1]metallocenophane structures of Group 5

3.2.2.1. Structural Parameters

3.2.2.1.1. Tilt Angles (α)

Likewise the Group 4 parent metallocenes, Group 5 metallocenes [V{(η^5-$C_5H_5)_2$}Cl_2], [Nb{(η^5-$C_5H_5)_2$}Cl_2] and [Ta{(η^5-$C_5H_5)_2$}Cl_2] are bent with smaller α values as 45.0°, 48.9° and 50.3°, respectively. As can be seen in Figure 34,

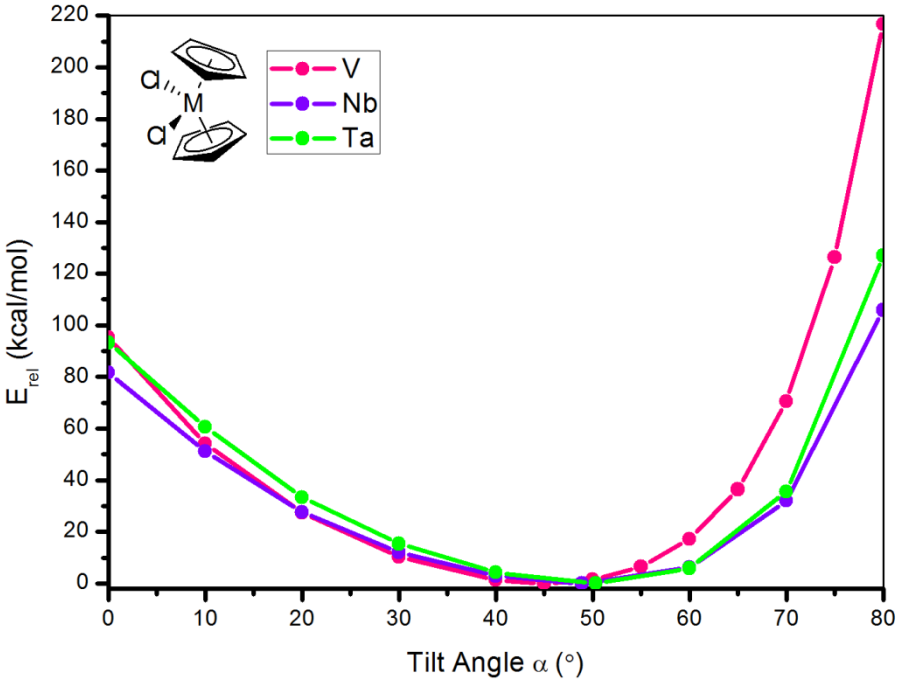

Figure 34. Tilt angle relative energy relationship in group 5 metallocenes

significant increases in relative energy via bending starts at 60° and at 70°, increases in energy values are 70 kcal/mol for V and about 35 kcal/mol for Nb and Ta.

For α values greater than 70°, structures are expected to be ring-strained. As seen in Figure 35, those structures are [Nb{(η^5-C_5H_4)$_2$NCl}Cl_2] (70.6°), [Nb{(η^5-C_5H_4)O}Cl_2] (73.3°), [Ta{(η^5-C_5H_4)$_2$NCl}Cl_2] (70.6°) and [Ta{(η^5-C_5H_4)$_2$O}Cl_2] (73.1°).

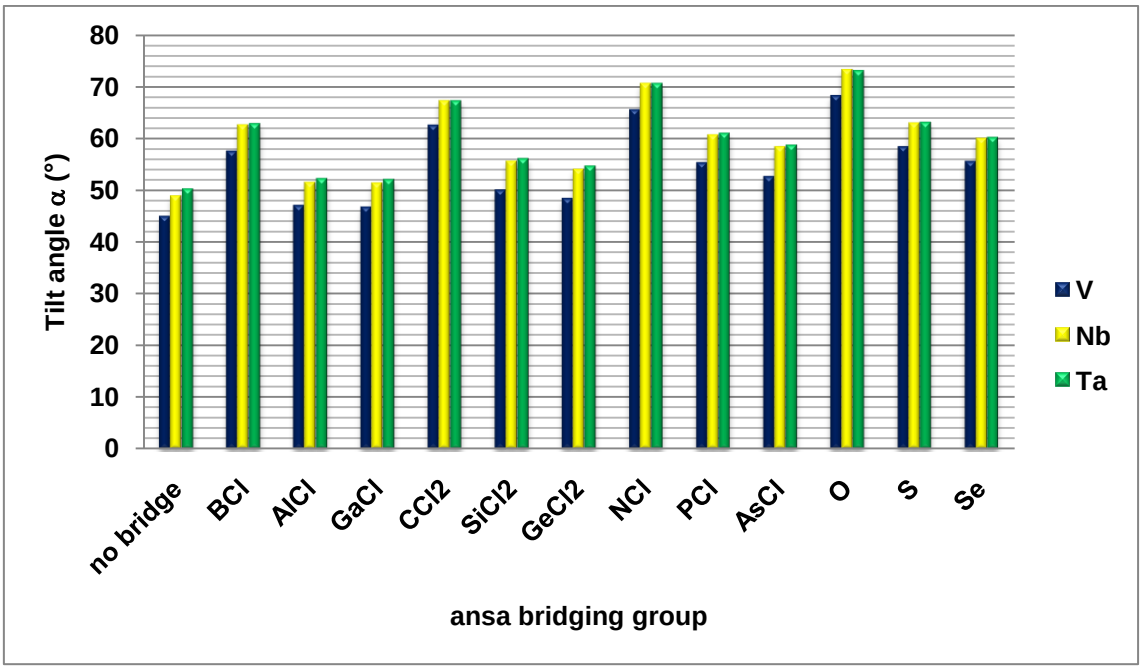

Figure 35. Tilt angle (α) values of group 5 [1]metallocenophanes with different *ansa* bridges

3.2.2.1.2. Metal Cyclopentadienyl Ring Distances (Cp-M)

In Group 5 *ansa* metallocenes, bridging by Group 13 elements (Al, Ga) and Group 14 elements (Si, Ge) increases Cp-M, as seen in Figure 36. The highest Cp-M distances are those of Ga and Ge bridged structures. Lowest Cp-M values belong to C, N and O bridged structures, similarly with Group 4 *ansa* metallocenes.

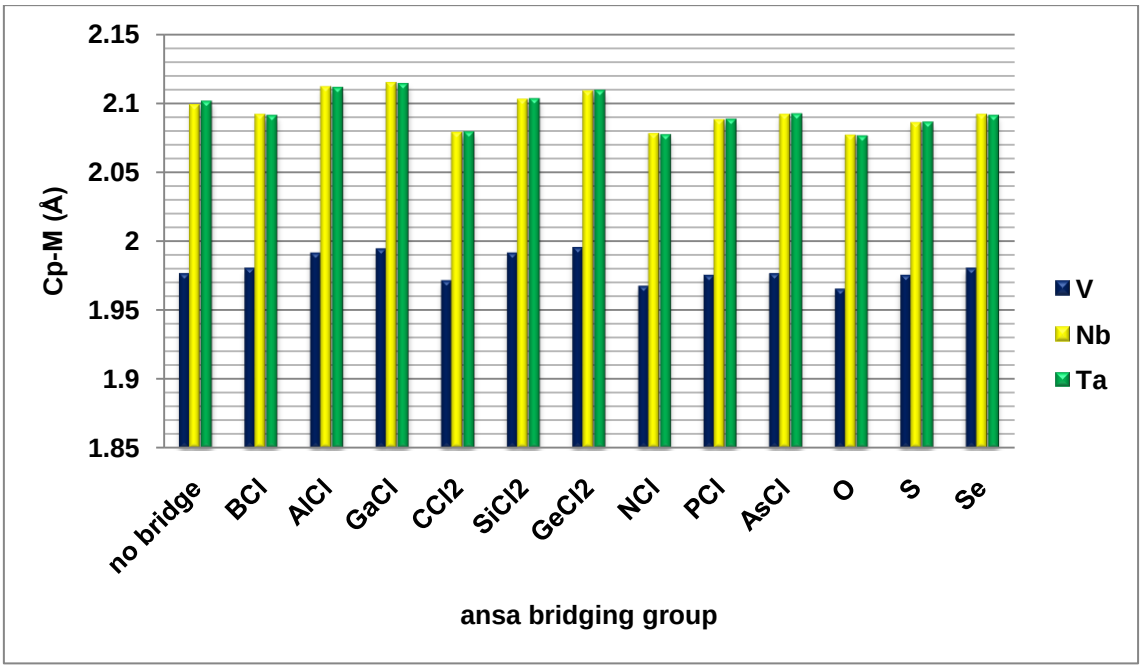

Figure 36. Cp-M Distances

3.2.2.1.3. δ C_{ipso} ^{13}C NMR TMS Chemical Shifts

In Figure 37 and in Table A9 in Appendix A, δ ^{13}C NMR chemical shifts for Group 5 *ansa* metallocenes and that of parents metallocenes are seen and^{13}C NMR

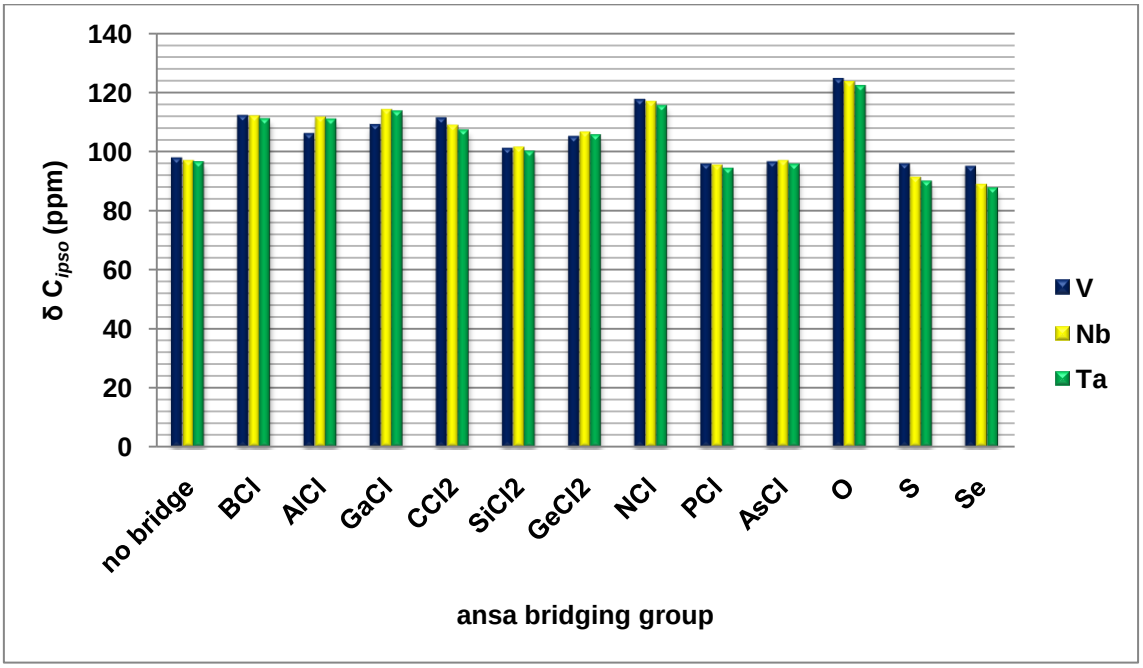

Figure 37. C_{ipso} ^{13}C NMR δ values of group 5 [1]metallocenophanes with different *ansa* bridges

chemical shifts (ppm) of cyclopentadienyl carbon atoms and corresponding C-M distances (Å) (in parantheses) of parent metallocenes are as follows. For [V{(η^5-$C_5H_5)_2$}Cl_2] δ 97.7 (2.316), 108.1 (2.311), 118.3 (2.301), 127.8 (2.295), 135.0 (2.337); for [Nb{(η^5-$C_5H_5)_2$}Cl_2] δ 96.9 (2.409), 100.3 (2.388), 109.6 (2.377), 127.9 (2.449), 134.47 (2.472) and for [Ta{(η^5-$C_5H_5)_2$}Cl_2] δ 96.3 (2.420), 99.0 (2.385), 106.9 (2.382), 123.8 (2.442), 134.9 (2.477).

In Group 5, *ansa* bridging effects the cyclopentadienyl δ ^{13}C NMR chemical shifts in two ways. For P (95.6 ppm), As (96.3 ppm), S (95.7 ppm) and Se (94.84 ppm) bridged compounds upfield shift is observed, where the other molecules show downfield shifts.

In the most tilted structure of the group, [Nb{(η^5-$C_5H_4)_2$O}Cl_2] has a chemical shift value of 123.6 ppm, where its parent metallocene has 107.9 ppm δ C_{ipso} ^{13}C NMR TMS chemical shift value.

3.2.2.2. Electronic Parameters

3.2.2.2.1. NPA Charges on Metal

The transition metal on the parent metallocene and *ansa* metallocenes of V are negatively charged, where the metal center in Nb complexes are nearly neutral and Ta complexes are positively charged. In general *ansa* bridge formation decreases the charges of V complexes and except with Al, Ga, Si and Ge, *ansa* bridging increases the charges on metal in both Nb and Ta complexes.

3.2.2.2.2. Dipole Moments

Dipole moments for the non-bridged parent metallocene structures of V, Nb, and Ta are 6.88, 6.41, and 5.96 D, respectively (See Table A10 in Appendix A). Introduction of *ansa* bridge in the structure generally decreases the dipole moment of the parent metallocene.

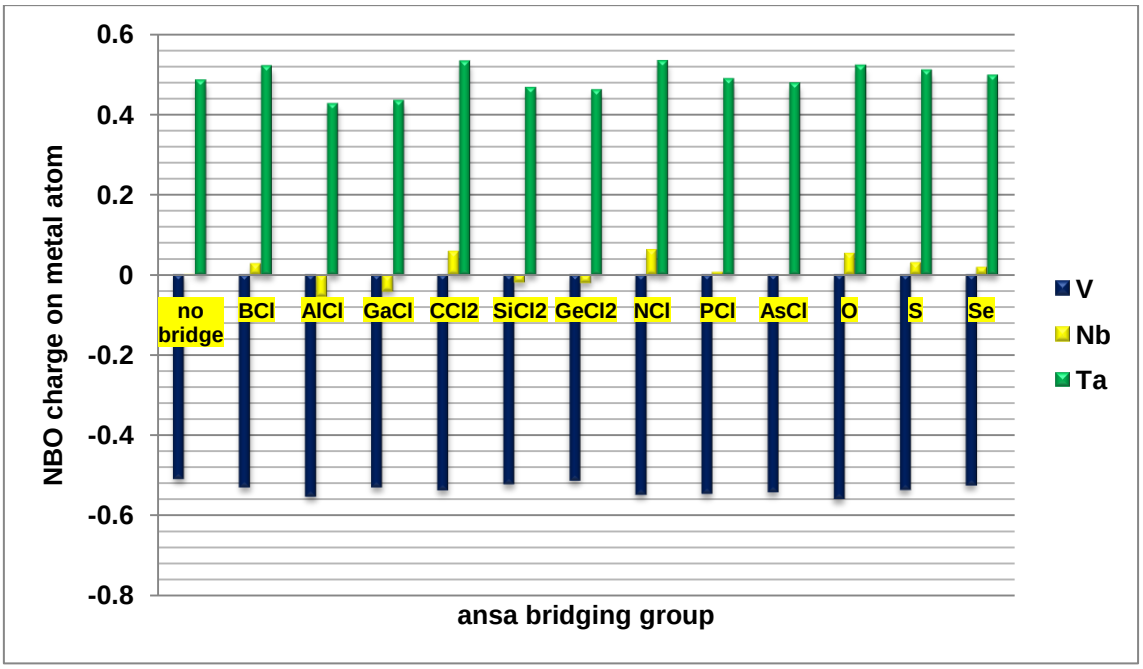

Figure 38. NBO charges on metal atom of group 5 [1]metallocenophanes with different *ansa* bridges

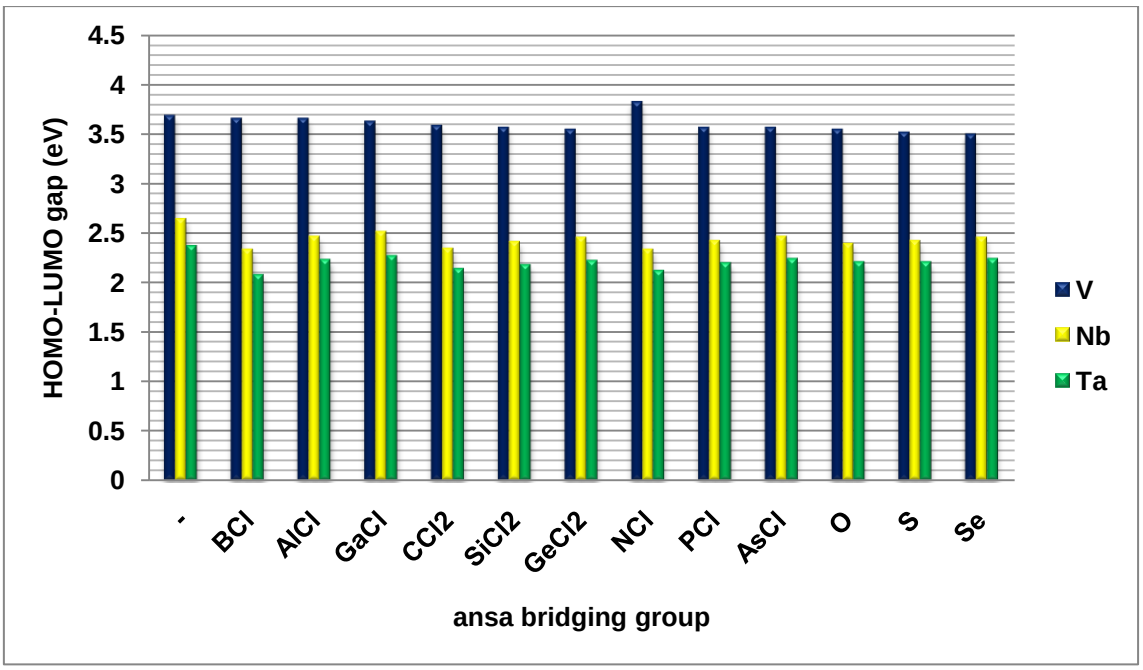

Figure 39. HOMO-LUMO gaps of group 5 [1]metallocenophanes with different *ansa* bridges

3.2.2.2.3. Frontier Molecular Orbitals

As seen in Figure 39, in Group 5 metallocenes, *ansa* bridging causes a decrease in HOMO-LUMO energy gap, except for the structure [V{(η^5-$C_5H_4)_2$NCl}Cl_2].

3.2.2.2.4. Absolute Hardness (η)

Absolute hardness values are half of the energy value of HOMO-LUMO gap. So *ansa* bridging makes the structures softer, again except for the structure [V{(η^5-$C_5H_4)_2$NCl}Cl_2], which is a harder molecule than its parent metallocene.

3.2.2.2.5. Chemical Potential (μ)

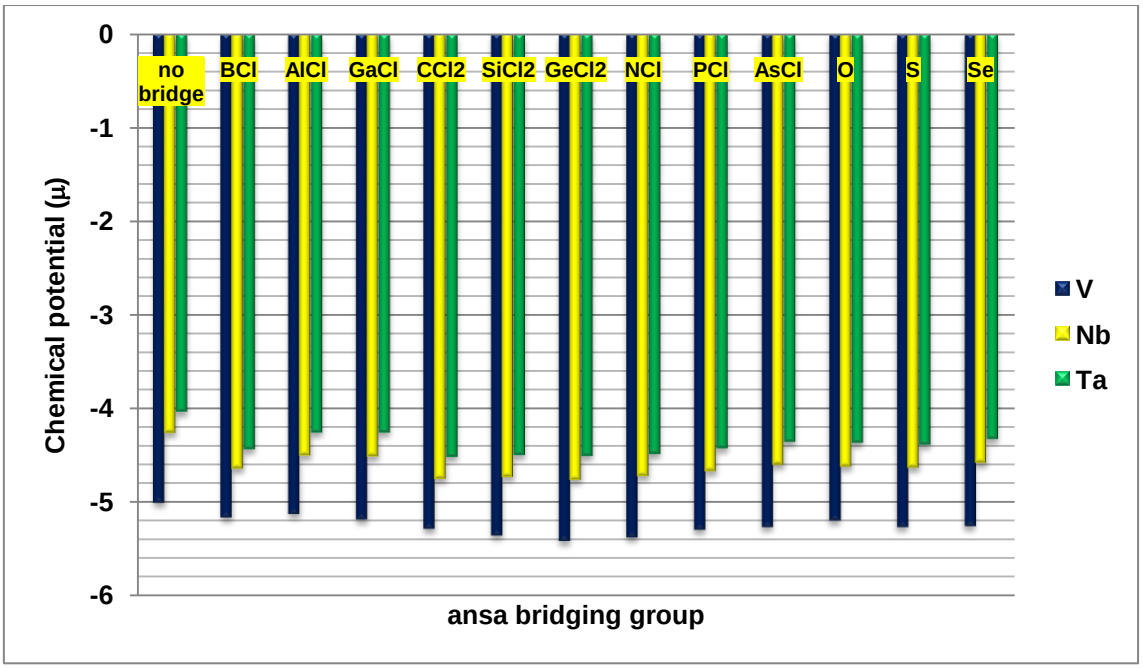

Figure 40. Chemical potential (μ) values of group 5 [1]metallocenophanes with different *ansa* bridges

Similar to Group 4 *ansa* metallocenes, chemical potentials of Group 5 metallocenes decreases via *ansa* bridge formation as seen in Figure 40. Lowest value (-5.42) is observed for [V{(η^5-$C_5H_4)_2$$GeCl_2$}$Cl_2$].

3.2.2.2.6. Electronic Spectra

Computational electronic spectra of *ansa* vanadocene, *ansa* niobocene and *ansa* tantalocene are given in Figures 41-43.

The highest energy absorbtion bands of parent mettallocenes, corresponding to the LMCT transitions between Cp and M orbitals were observed at 372, 274 and 291 nm for V, Nb and Ta non-bridged metallocenes, respectively.

Generally, formation of *ansa* bridge cause a red-shift accompanied with increase in intensity in these bands. Again, smaller bridge atoms result higher red-shifts in the values of λ_{max}. Highest λ_{max} value belongs to $[V\{(\eta^5\text{-}C_5H_4)_2Se\}Cl_2]$ (537 nm).

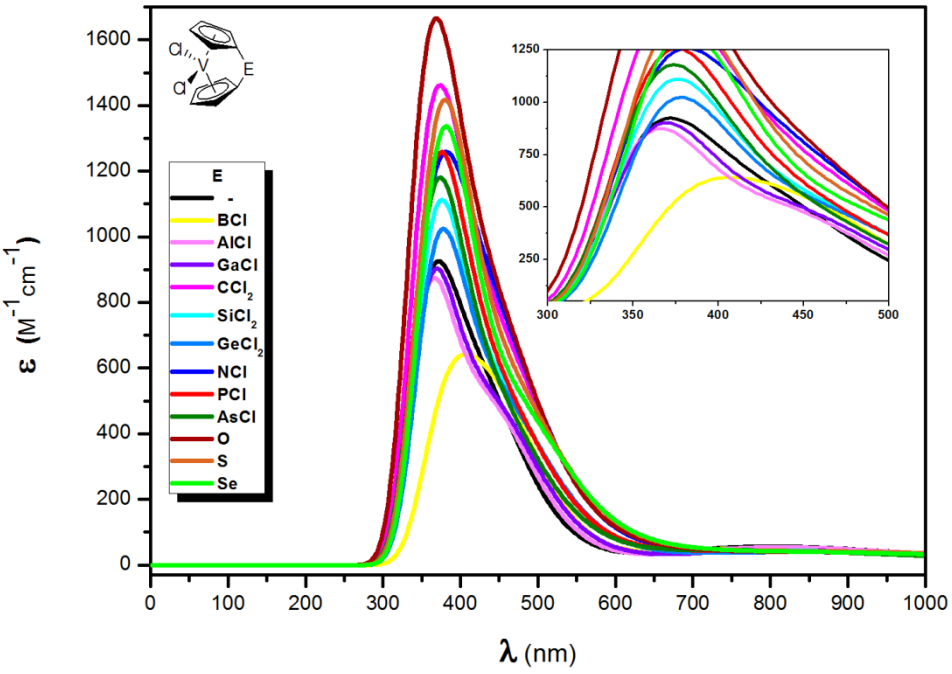

Figure 41. Change in electronic spectra of [1]vanadocenophanes with changing *ansa* bridge

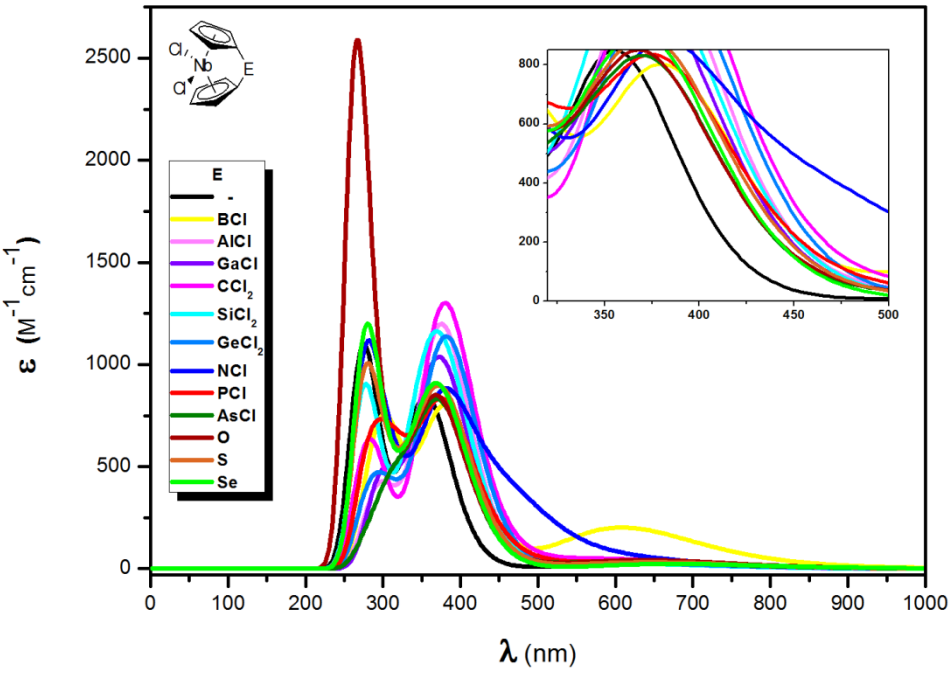

Figure 42. Change in electronic spectra of [1]niobocenophanes with changing *ansa* bridge

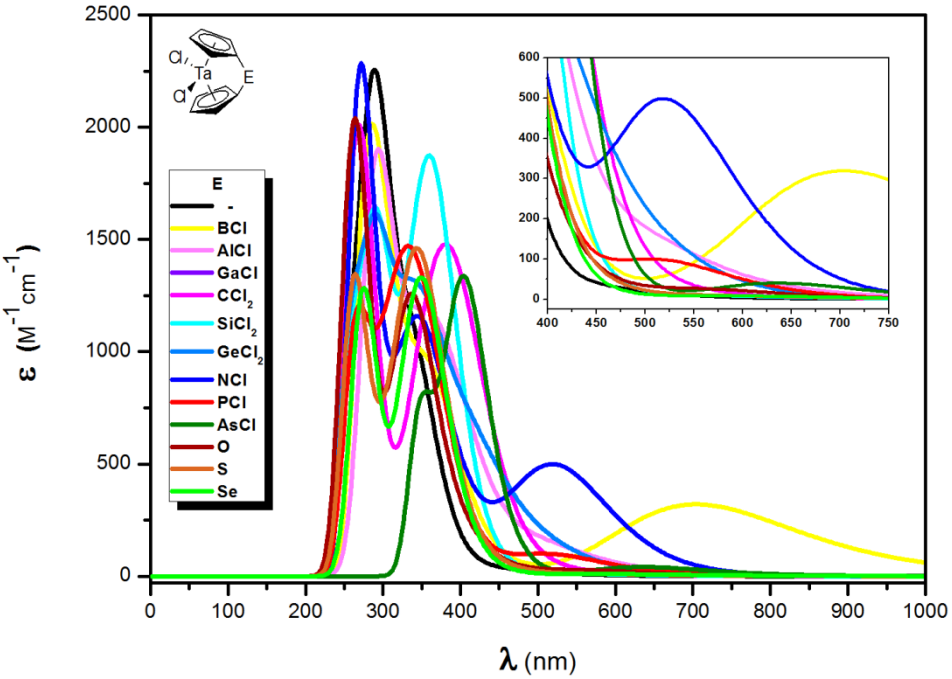

Figure 43. Change in electronic spectra of [1]tantalocenophanes with changing *ansa* bridge

3.2.3. Group 6

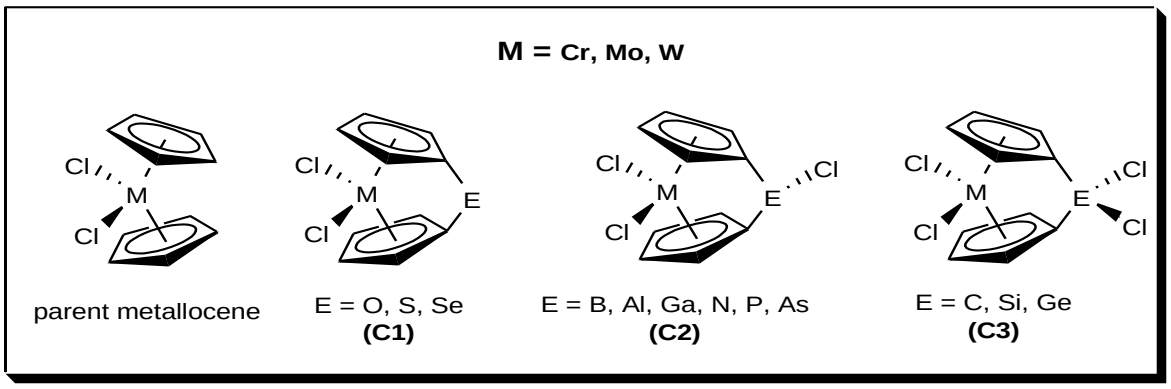

Figure 44. Parent metallocene and [1]metallocenophane structures of Group 6

3.2.3.1. Structural Parameters

3.2.3.1.1. Tilt Angles (α)

Group 6 metallocenes $[Cr\{(\eta^5\text{-}C_5H_5)_2\}Cl_2]$, $[Mo\{(\eta^5\text{-}C_5H_5)_2\}Cl_2]$ and $[W\{(\eta^5\text{-}C_5H_5)_2\}Cl_2]$ are also bent with smaller α values than that of Group 4 and Group 5 metallocenes, as 41.1°, 49.6° and 51.1°, respectively. As can be seen in Figure 45, significant increases in relative energy via bending starts at 60° and at 70°, increases in energy values are 87 kcal/mol for Cr and about 61 kcal/mol for Mo and 49 kcal/mol for W.

For α values greater than 70°, structures are expected to be ring-strained. As seen in Figure 46, those structures are $[Mo\{(\eta^5\text{-}C_5H_4)O\}Cl_2]$ (70.1°) and $[W\{(\eta^5\text{-}C_5H_4)_2O\}Cl_2]$ (70.8°), although in Group 6, the highest tilted structure is $[Cr\{(\eta^5\text{-}C_5H_4)O\}Cl_2]$ (α = 64.4°), which is 23.3° more tilted than chromocene dichloride.

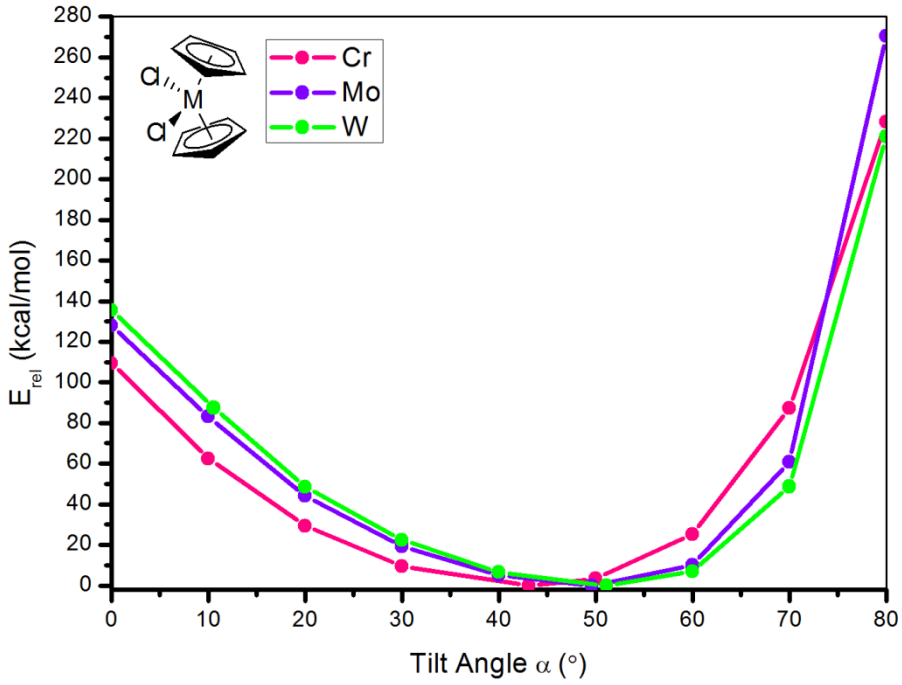

Figure 45. Tilt angle relative energy relationship in group 6 metallocenes

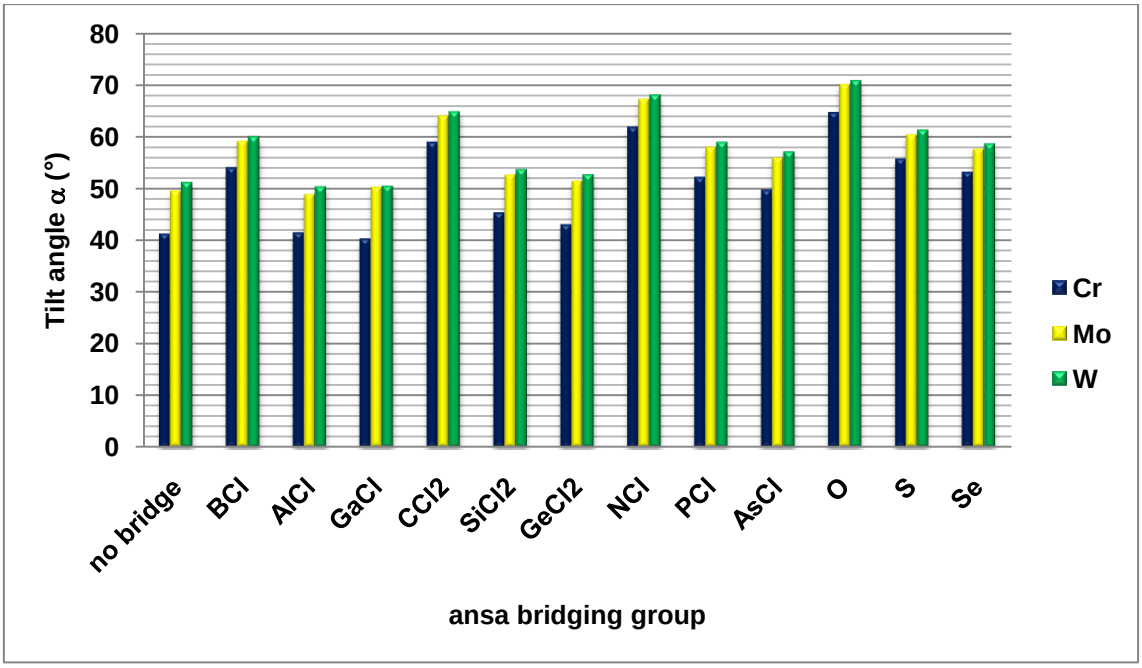

Figure 46. Tilt angle (α) values of group 6 [1]metallocenophanes with different *ansa* bridges

3.2.3.1.2. Metal Cyclopentadienyl Ring Distances (Cp-M)

In Group 6 *ansa* metallocenes, bridging by Group 13 elements (Al, Ga) and Group 14 elements (Si, Ge) increases Cp-M, as seen in Figure 47. The highest Cp-M distances are those of Ga and Ge bridged structures. Lowest Cp-M values belong to C, N and O bridged structures, similarly with Group 4 *ansa* metallocenes. So, the effects incresing α decreases Cp-M and with these results, there is no appreciable ring strain suggested in this group, either.

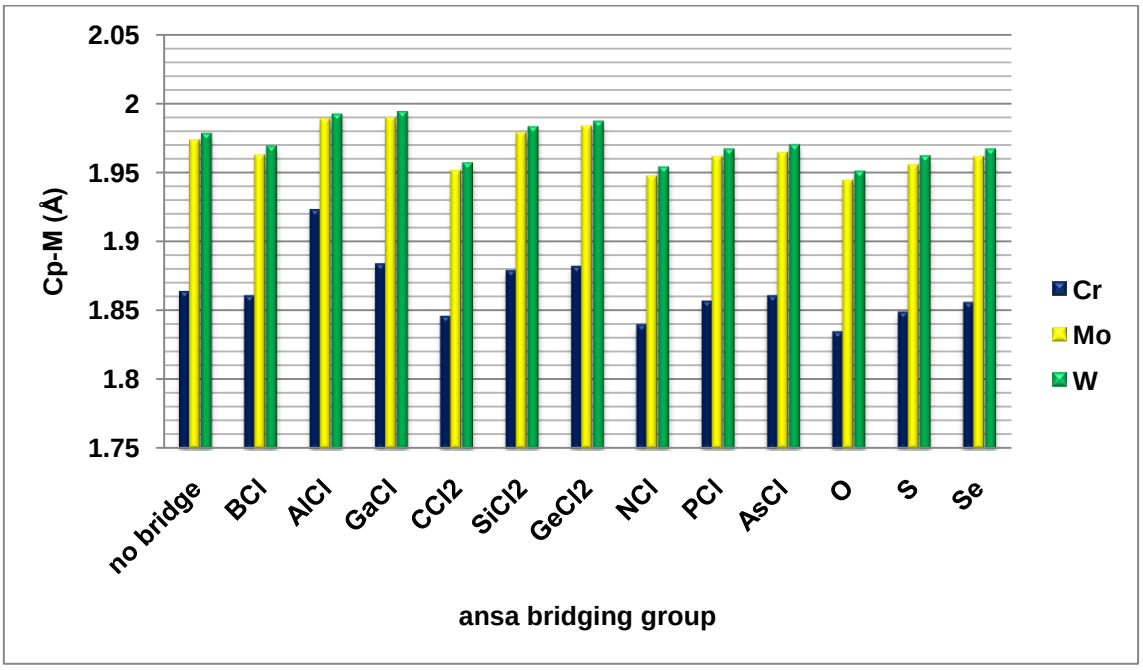

Figure 47. Cp-M Distances

3.2.3.1.3. δ C_{ipso} ^{13}C NMR TMS Chemical Shifts

In Figure 48 and in Table A9 in Appendix A, δ ^{13}C NMR chemical shifts for Group 6 *ansa* metallocenes and that of parents metallocenes are seen and ^{13}C NMR chemical shifts (ppm) of cyclopentadienyl carbon atoms and corresponding C-M distances (Å) (in parantheses) of parent metallocenes are as follows. For [Cr{(η^5-$C_5H_5)_2$}Cl_2] δ 83.5 (2.261), 99.56 (2.213), 103.7 (2.218), 129.4 (2.273), 136.3 (2.180); for [Mo{(η^5-$C_5H_5)_2$}Cl_2] δ 82.5 (2.2.277), 82.6 (2.290), 95.2 (2.244), 129.8 (2.369), 132.5 (2.381) and for [W{(η^5-$C_5H_5)_2$}Cl_2] there are only three peaks, two quartets and a doublet as δ 110.0 (q, 2.509), 114.6 (d, 2.516), 118.9 (q, 2.541).

In the most tilted structure of the group, $[W\{(\eta^5\text{-}C_5H_4)_2O\}Cl_2]$ have a chemical shift value of 123.6 ppm, where its parent metallocene have 90.6 ppm δ C_{ipso} ^{13}C NMR TMS chemical shift value.

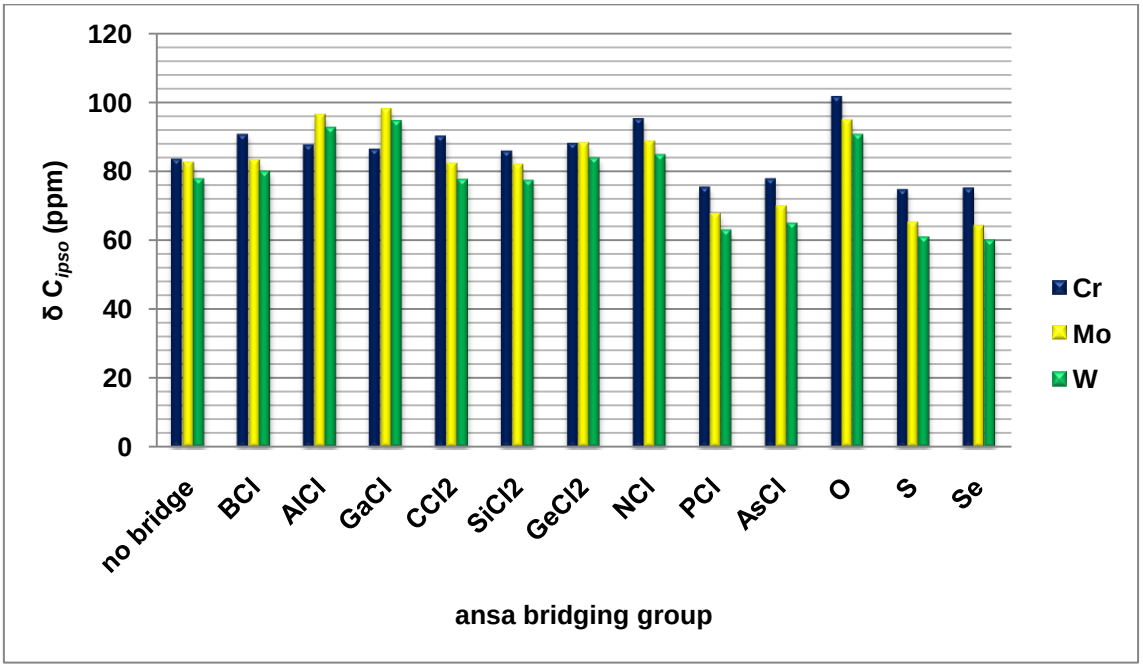

Figure 48. C_{ipso} ^{13}C NMR δ values of group 6 [1]metallocenophanes with different *ansa* bridges

3.2.3.2. Electronic Parameters

3.2.3.2.1. NPA Charges on Metal

The transition metal on the parent metallocene and *ansa* metallocenes of Cr and Mo are negatively charged, where W complexes are positively charged. Bridge formation dos not effect much the charges on the metals in Group 6 complexes (Figure 49).

3.2.3.2.2. Dipole Moments

Dipole moments for the non-bridged parent metallocene structures of Cr, Mo, and W are 7.71, 6.9, and 6.44 D, respectively (See Table A10 in Appendix A). Dipole moments of *ansa* bridged complexes are generallysmallerthan that of the parent metallocene.

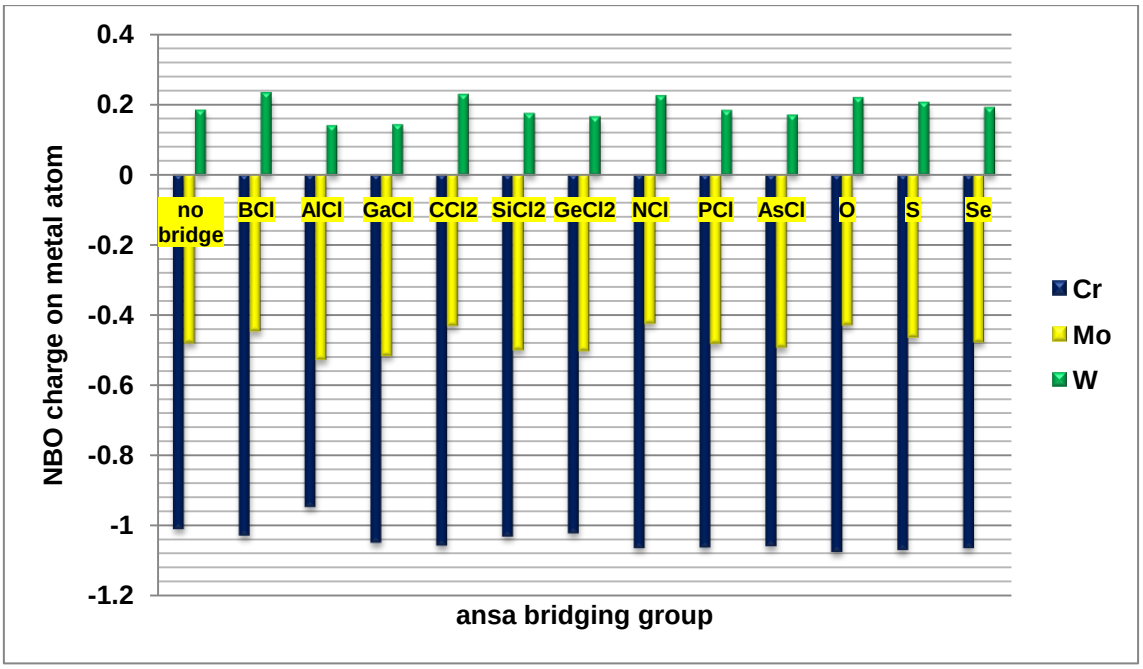

Figure 49. NBO charges on metal atom of group 6 [1]metallocenophanes with different *ansa* bridges

3.2.3.2.3. Frontier Molecular Orbitals

As can be seen in Figure 50, HOMO-LUMO energy differences in *ansa* metallocenes of Group 6 are in general greater than the corresponding

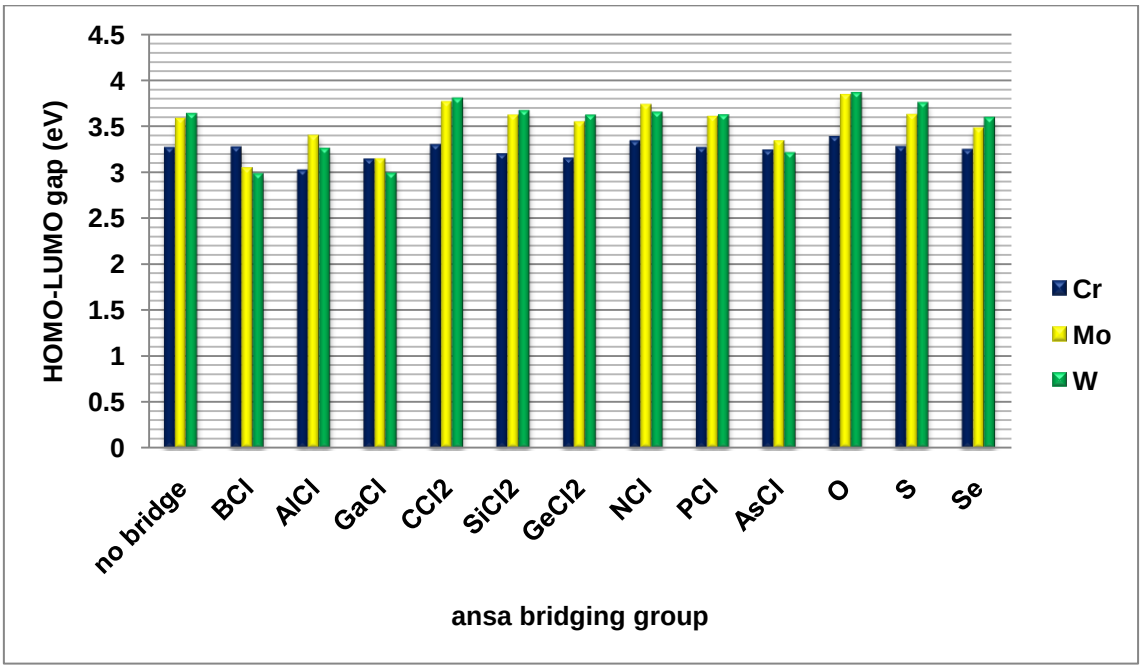

Figure 50. HOMO-LUMO gaps of group 6 [1]metallocenophanes with different *ansa* bridges

metallocene. *Ansa* bridging decreases the energies of both the HOMO and the LUMO.

3.2.3.2.4. Absolute Hardness (η)

Hardest molecules in Group 6 are the *ansa* metallocenes of 2nd period elements. For example hardnesses of oxygen bridged complexes of Cr, Mo and W are 1.69, 1.92 and 1.93, respectively.

See Table A18 in Appendix A, for the complete list of hardness values.

3.2.3.2.5. Chemical Potential (μ)

For all complexes of Group 6 *ansa* metallocenes, have lower chemical potentials than the parent metallocenes, as seen in Figure 51.

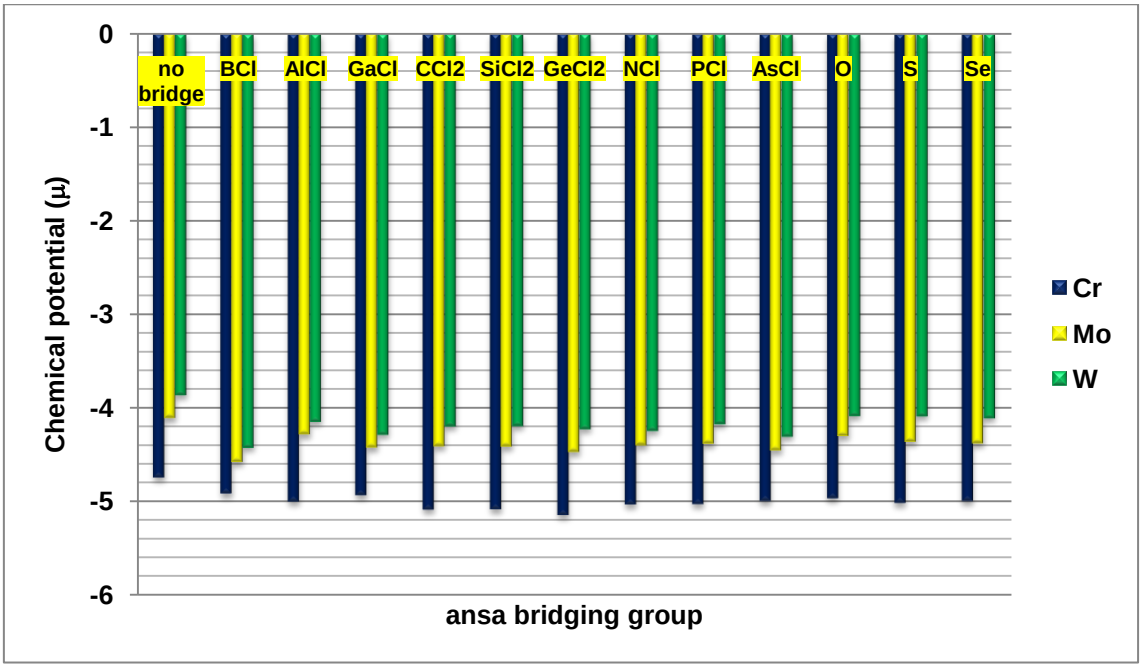

Figure 51. Chemical potential (μ) values of group 6 [1]metallocenophanes with different *ansa* bridges

Lowest value (-5.15) is observed for $[Cr\{(\eta^5\text{-}C_5H_4)_2GeCl_2\}Cl_2]$ and the highest value belongs to tungstenocene dichloride (-3.86). All *ansa* tungstenocenes have lower chemical potentials than the parent metallocene, suggesting that *ansa*

bridge formation increased the stability of complexes in this group.

3.2.3.2.6. Electronic Spectra

Computational electronic spectra of *ansa* chromocenes, *ansa* molybdocenes and *ansa* tungstenocenes are given in Figures 52-54.

The highest energy absorbtion bands of parent mettallocenes, corresponding to the LMCT transitions between Cp and M orbitals were observed at 326, 242 and 250 nm for Cr, Mo and W non-bridged metallocenes respectively. Intensity of these bands is highest for W and lowest for Cr complex.

Formation of *ansa* bridge cause a red-shift in these bands. In addition, via *ansa* bridging lowest energy bands become more intense, especially for [Cr{(η^5-$C_5H_4)_2O$}Cl_2], [Mo{(η^5-$C_5H_4)_2PCl$}Cl_2] and [Cr{(η^5-$C_5H_4)_2NCl$}Cl_2].

In general, smaller bridge atoms result higher red-shifts in the values of λ_{max}.

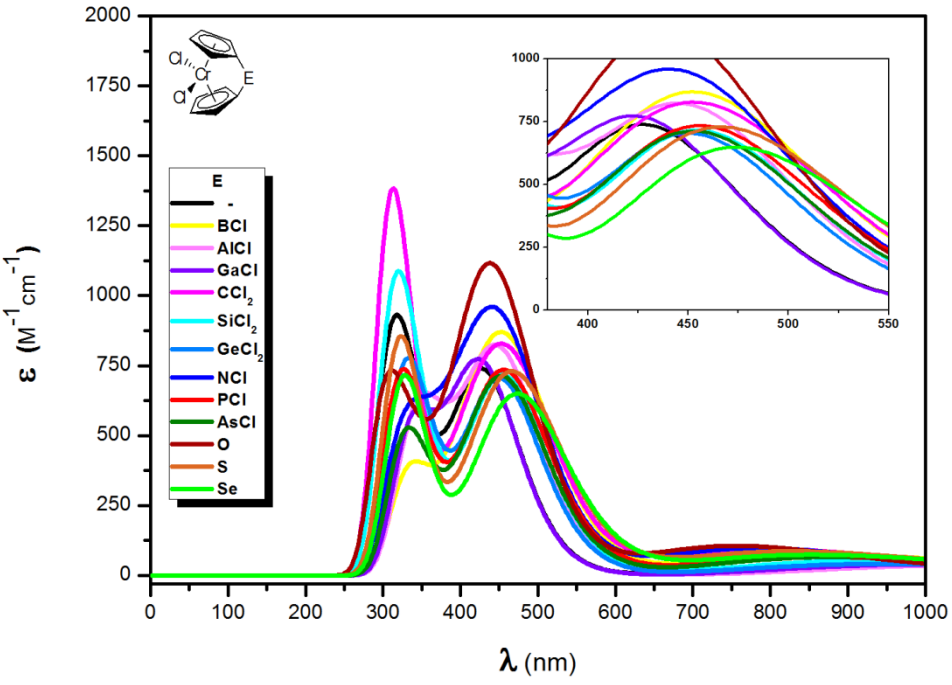

Figure 52. Change in electronic spectra of [1]chromocenophanes with changing *ansa* bridge

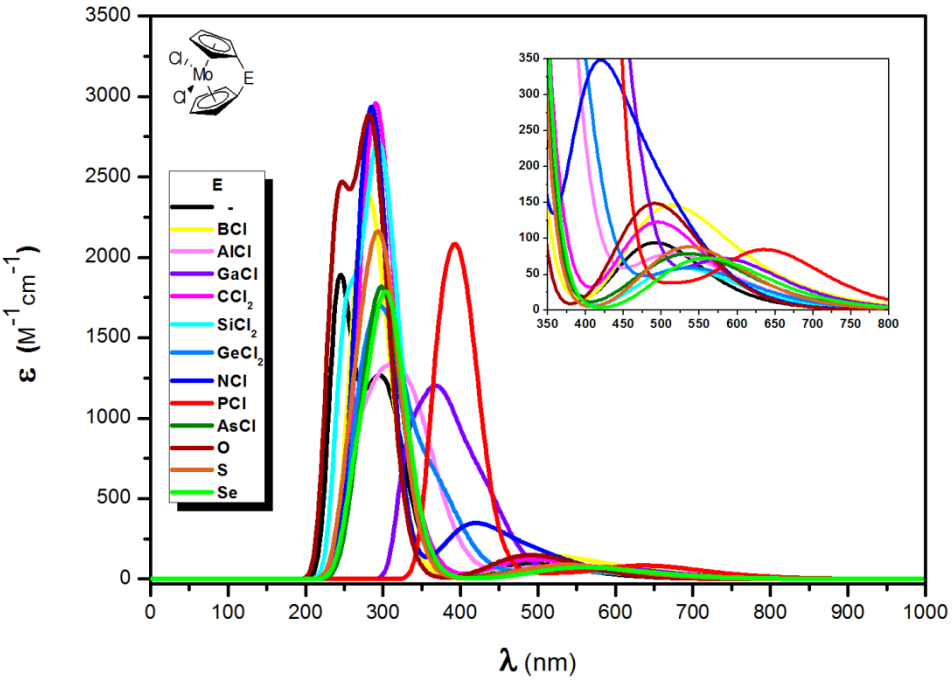

Figure 53. Change in electronic spectra of [1]molibdocenophanes with changing *ansa* bridge

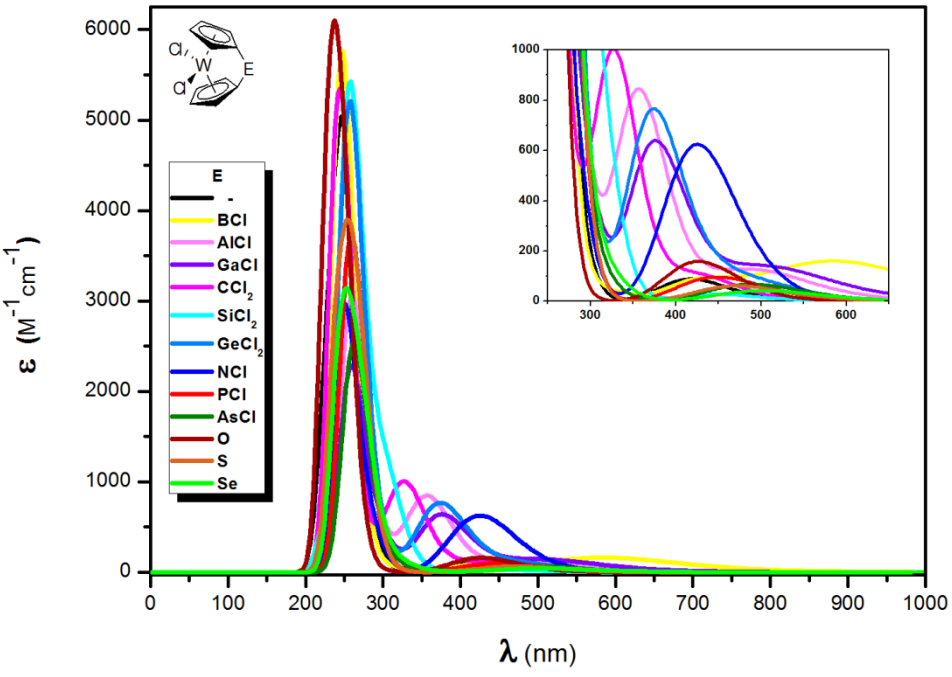

Figure 54. Change in electronic spectra of [1]tungstenocenophanes with changing *ansa* bridge

3.2.4. Group 7

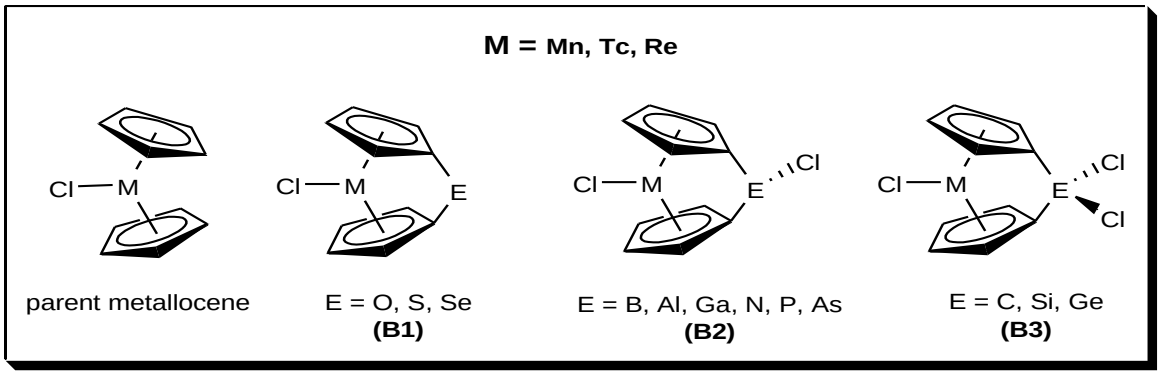

Figure 55. Parent metallocene and [1]metallocenophane structures of Group 7

3.2.4.1. Structural Parameters

3.2.4.1.1. Tilt Angles (α)

Tilt angles of Group 7 parent metallocenes Mn{(η^5-$C_5H_5)_2$}Cl], [Tc{(η^5-$C_5H_5)_2$}Cl] and [Re{(η^5-$C_5H_5)_2$}Cl] are 31.1°, 38.2° and 38.9°, respectively (See Appendix A, Table A1). As can be seen, these values are smaller than α values of Group 4, 5 and 6 parent metallocenes, therefore it is thought that smaller tilt angles would produce higher ring strains in this grup than previous groups.

Indeed, relative energy versus increasing tilt angle calculations (Figure 56) showed that by 60° tilting, energy of manganocene chloride reached to a value 54.6 kcal/mol, which is about ten times higher than that of corresponding titanocene dichloride.

Periodic trends for α is similar to previous groups. α values are highest for Tc, and lowest for Mn complexes, and the most tilted structure is [Re{(η^5-$C_5H_4)_2$O}Cl] with 21.5° net ring tilt (α=60.4°).

Variation of tilt angle with respect to changing bridges is seen in Figure 57.

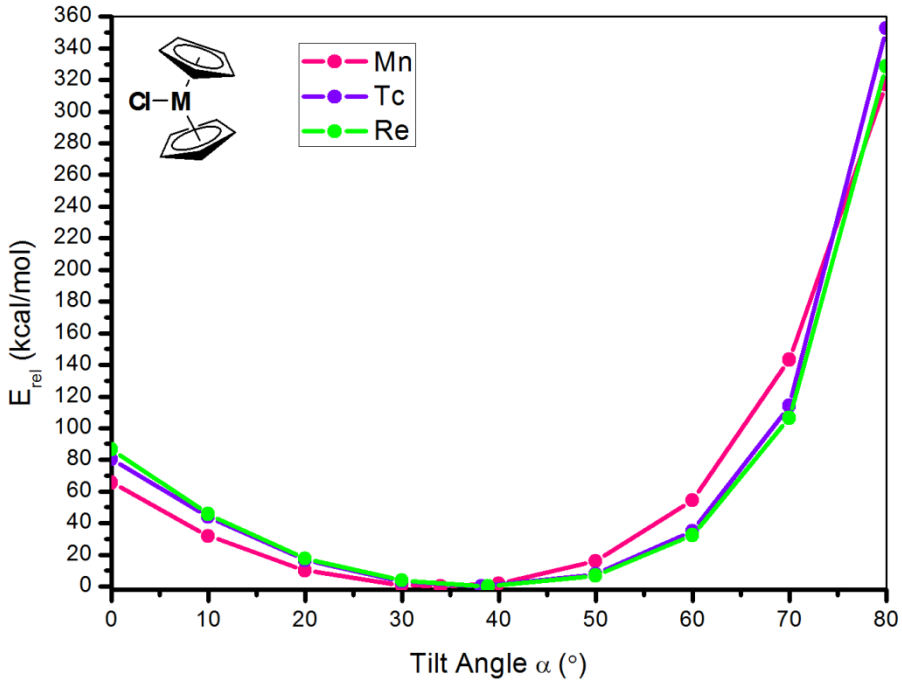

Figure 56. Tilt angle relative energy relationship in group 7 metallocenes

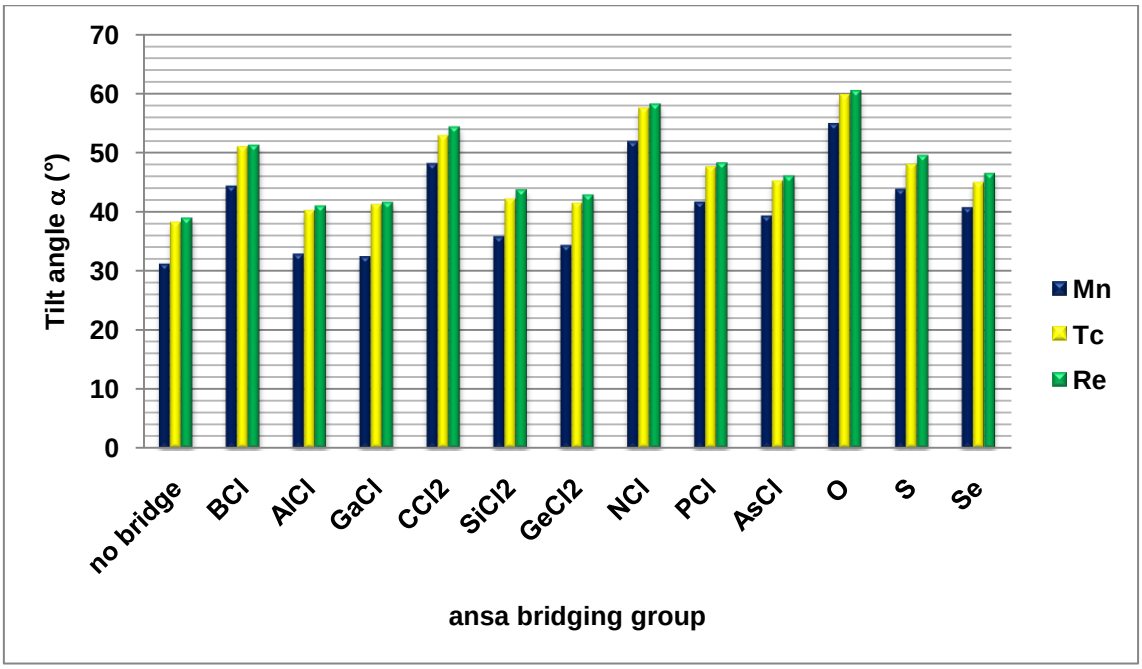

Figure 57. Tilt angle (α) values of group 7 [1]metallocenophanes with different *ansa* bridges

3.2.4.1.2. Metal Cyclopentadienyl Ring Distances (Cp-M)

Cp-M distances in Group 7 decreases via *ansa* formation except for Al, Ga, Si and Ge bridged compounds, as seen in figure 58.

These bridges have a weakening effect on Cp-M bond.

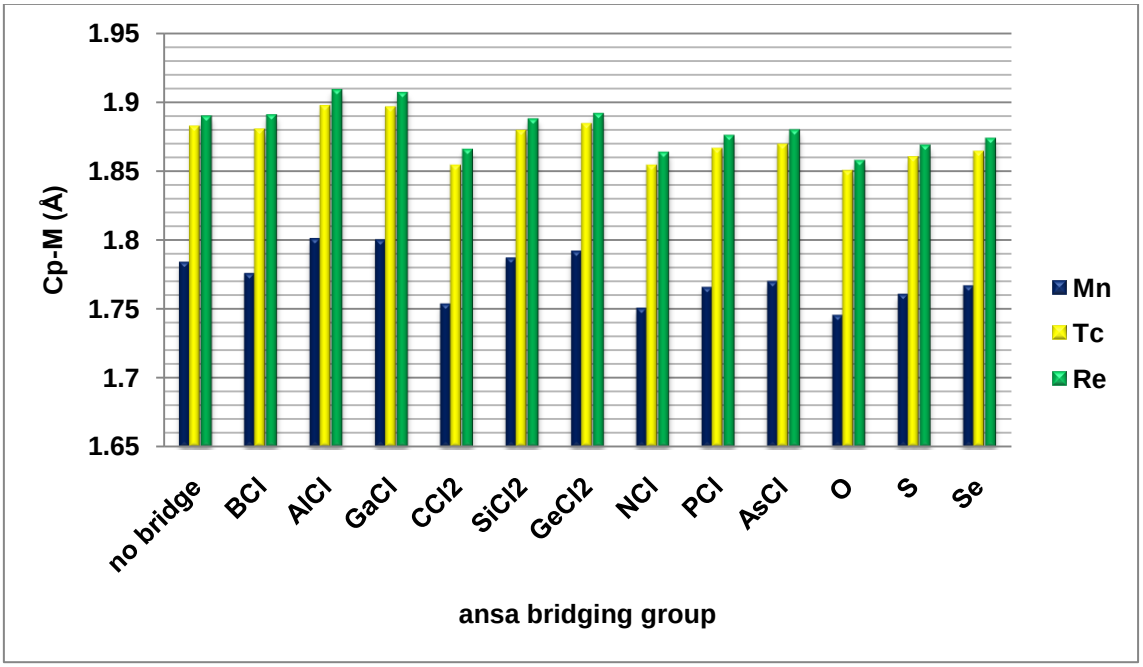

Figure 58. Cp-M Distances

3.2.4.1.3. δ C_{ipso} ^{13}C NMR TMS Chemical Shifts

^{13}C NMR chemical shifts (ppm) of cyclopentadienyl carbon atoms and corresponding C-M distances (Å) (in parantheses) of parent metallocenes are as follows. For $[Mn\{(\eta^5\text{-}C_5H_5)_2\}Cl_2]$ δ 70.8 (2.132), 83.6 (2.216), 85.6 (2.162), 113 (2.15), 115 (2.152); for $[Tc\{(\eta^5\text{-}C_5H_5)_2\}Cl_2]$ δ 76.6 (2.264), 77.7 (2.188), 128 (2.280) and for $[Re\{(\eta^5\text{-}C_5H_5)_2\}Cl_2]$ δ 70.5 (2.5194), 70.7 (2.194), 71.6 (2.271), 71.6 (2.272), 121 (2.292).

In Group 7, except Group 13 bridged Tc and Re complexes, all complexes exhibit upfield shift in C_{ipso} signal.Highest field signal belongs to sulfur and Se bridged complexes, as seen in Figure 59.

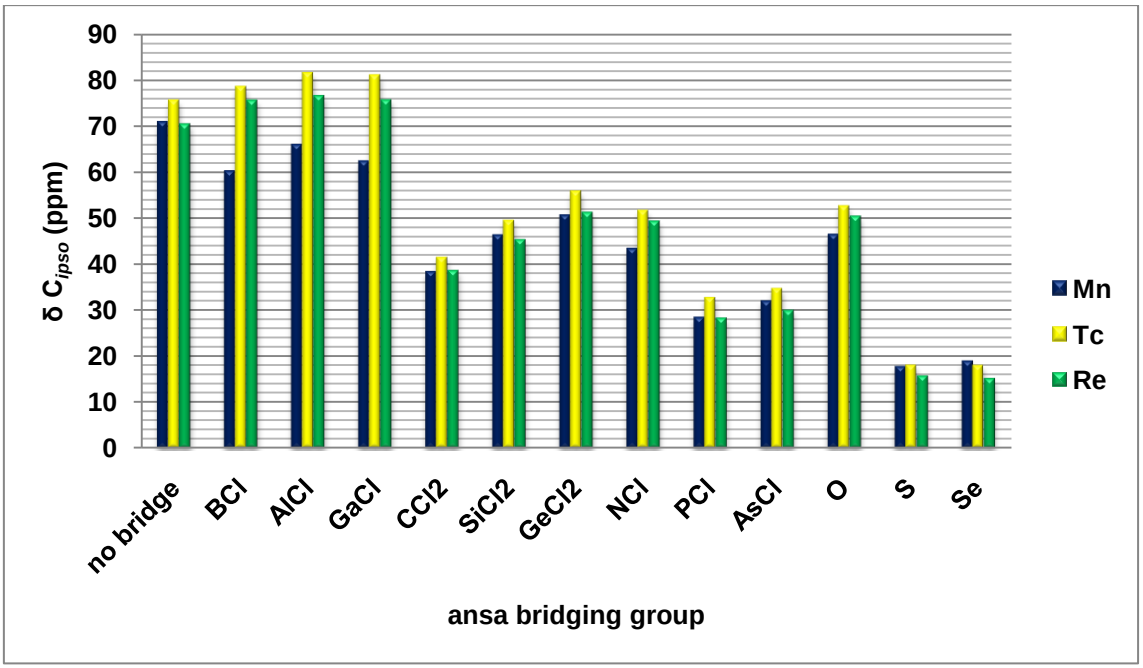

Figure 59. C_{ipso} ^{13}C NMR δ values of group 7 [1]metallocenophanes with different *ansa* bridges

3.2.4.2. Electronic Parameters

3.2.4.2.1. NPA Charges on Metal

NPA analyses indicate an appreciable negative charge on Mn (-0.404), Tc (-0.534) and Re (-0.047). (Figure 60, Table A12).

C, N, and O *ansa* bridges cause an increase in metal charge, where other bridging elements further decrease the charge on the metal.

3.2.4.2.2. Dipole Moments

As in the previous groups dipole moments of the metallocenes of these group, are higher than that of corresponding *ansa* complex. *Ansa* bridge formation decrease the polarizability of the parent metallocene.

3.2.4.2.3. Frontier Molecular Orbitals

Energy gap between HOMO and LUMO of *ansa* metallocenes are seen in Figure 61.

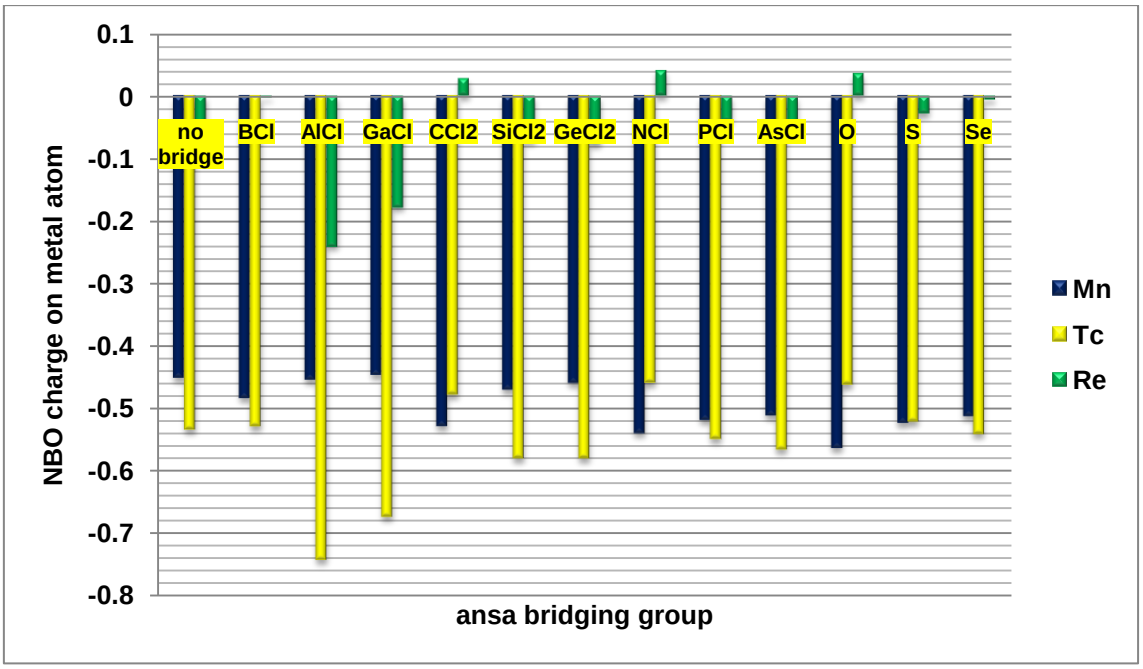

Figure 60. NBO charges on metal atom of group 7 [1]metallocenophanes with different *ansa* bridges

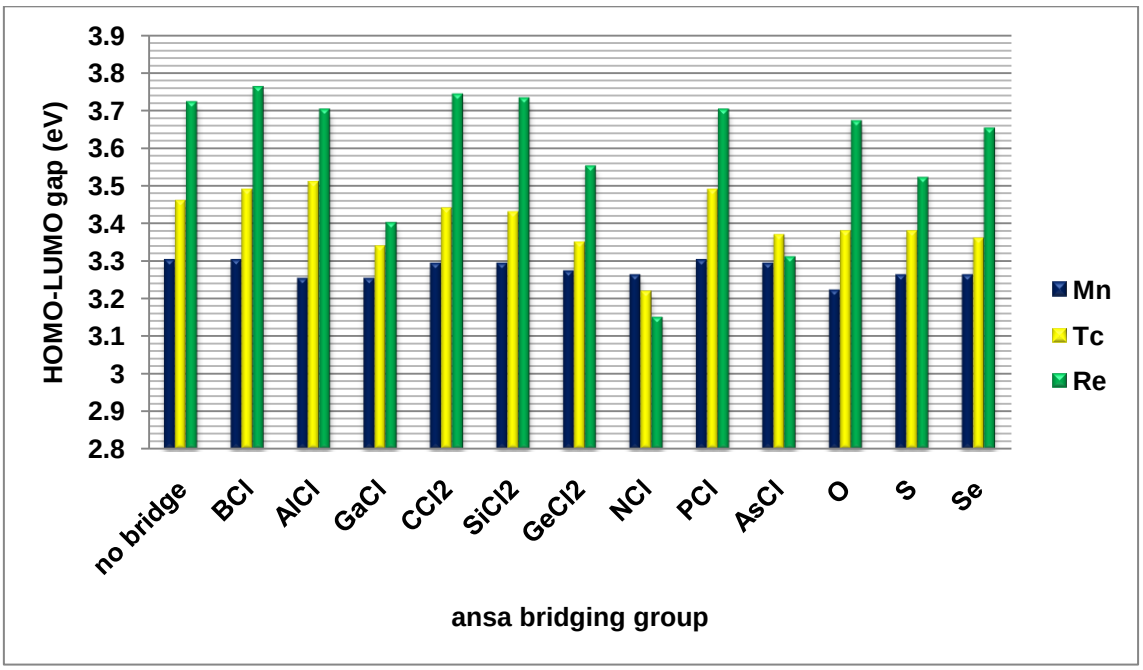

Figure 61. HOMO-LUMO gaps of group 7 [1]metallocenophanes with different *ansa* bridges

There is an appreciable decrease in HOMO-LUMO gap of Nitrogen, Gallium and Arsenic bridged compounds of Tc and Re.

3.2.4.2.4. Absolute Hardness (η)

Absolute hardnesse of compounds are decreased via *ansa* bridge formation in Group 7 as seen in Table A18 in Appendix A.

3.2.4.2.5. Chemical Potential (μ)

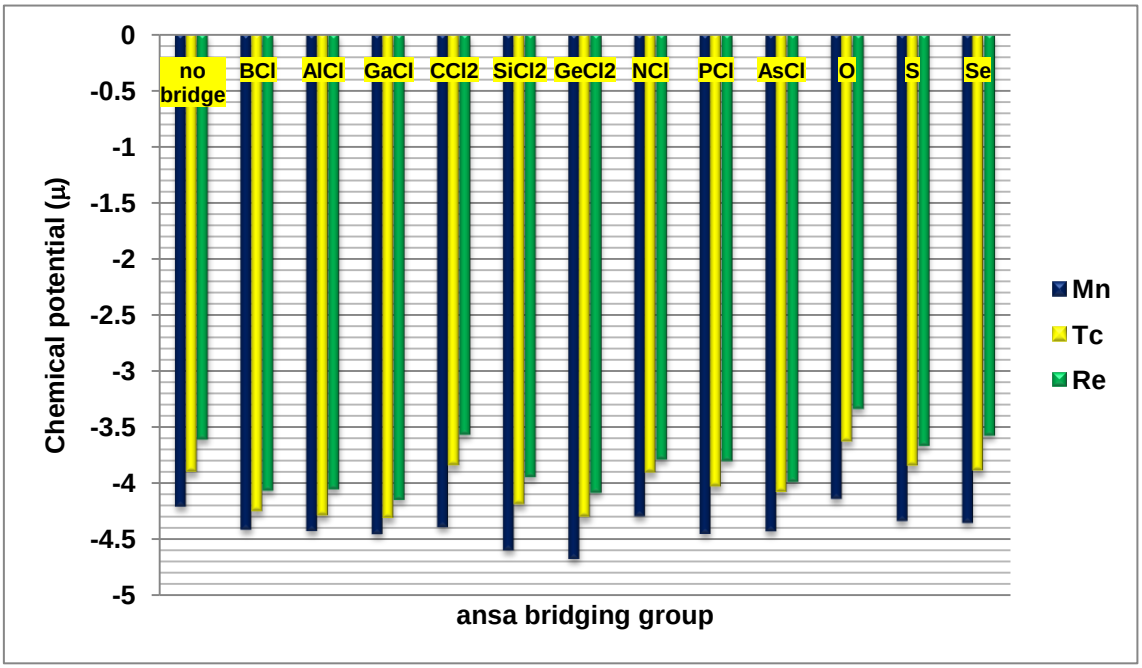

Figure 62. Chemical potential (μ) values of group 7 [1]metallocenophanes with different *ansa* bridges

Chemical potentials of parent metallocenes decreases via *ansa* formation, which increases the stability of *ansa* complexes.

3.2.4.2.6. Electronic Spectra

Electronic spectra for Group 7 *ansa* metallocenes are seen in Figures 63-65.

LMCT transitions between Cp and M orbitals were observed at 260, 229 and 235 nm for Mn, Tc and Re non-bridged metallocenes respectively.

Formation of *ansa* bridge results in decrease of the intensity of these bands,

where low energy d-d transition bands become more intense. Exceptions are Si bridged manganocene compound, and C, N and O bridged Tc complexes. The intensity of higher energy bands are as high as that of the parent metallocene.

Also, C, N and O bridged complexes depict higher red-shifts in their region of λ_{max}.

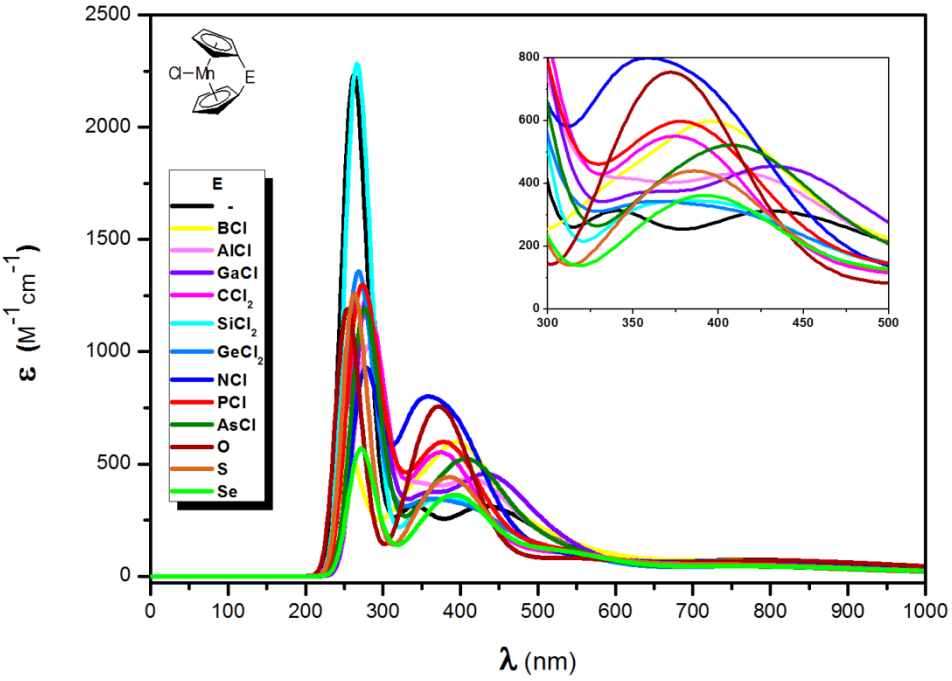

Figure 63. Change in electronic spectra of [1]manganocenophanes with changing *ansa* bridge

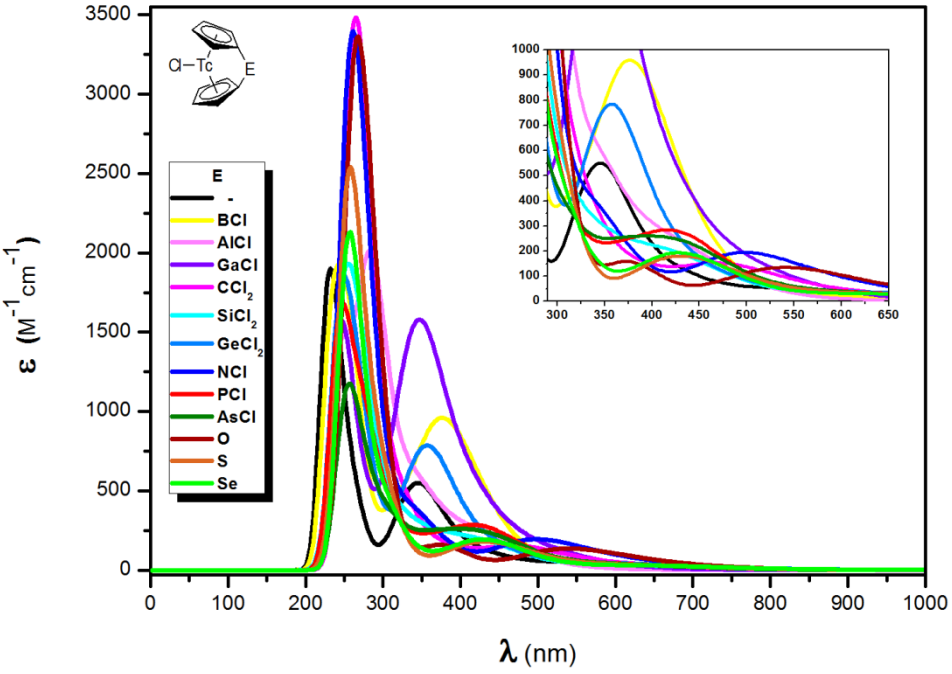

Figure 64. Change in electronic spectra of [1]technetocenophanes with changing *ansa* bridge

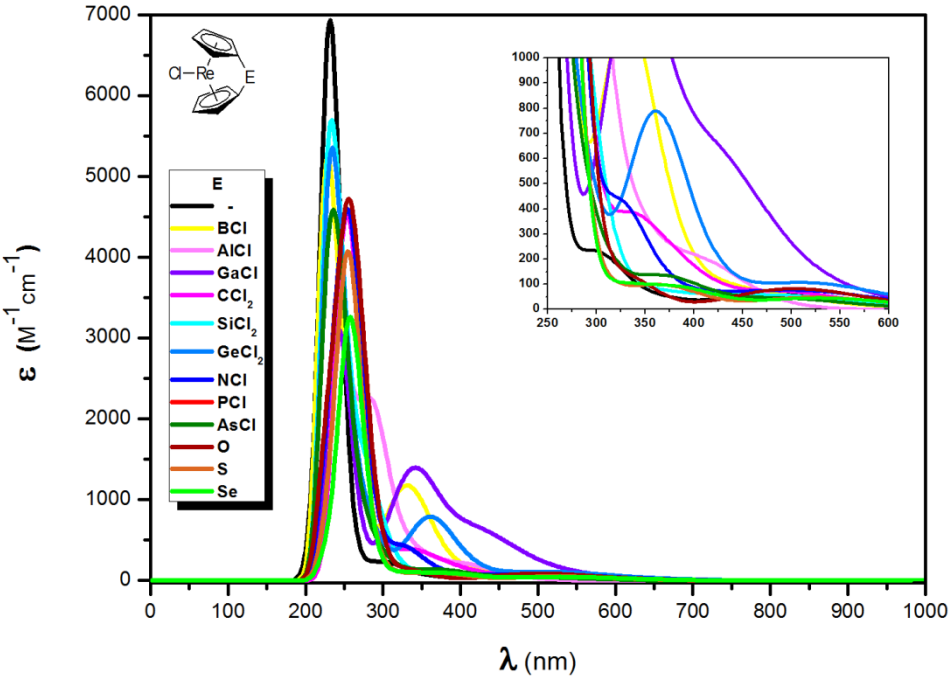

Figure 65. Change in electronic spectra of [1]rhenocenophanes with changing *ansa* bridge

3.2.5. Group 8

Unlike the metallocenes of Group 4, 5, 6, and 7, Group 8 metallocenes are in a parallel ring geometry (α=0), as seen in Figure 66.

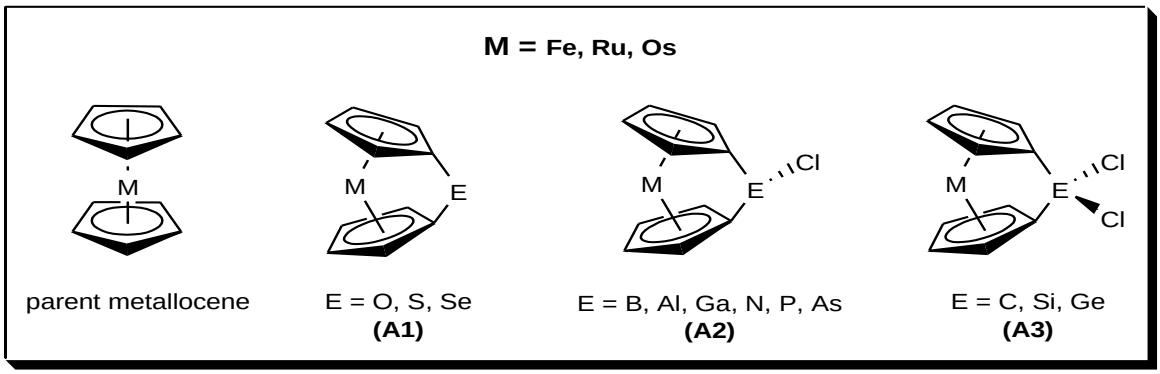

Figure 66. Parent metallocene and [1]metallocenophane structures of Group 8

3.2.5.1. Structural Parameters

3.2.5.1.1. Tilt Angles (α)

Because of zero tilt angle of the parent metallocene, any ring tilted structure is thought to increase the relative energy of metallocene, which may cause a ring strain. However, there are other factors, previously discussed, such as Cp-M distances and β angles, that can balance the increased energy via ring tilt.

According to the previous results of this work, for bent metallocenes of Group 4-7 transition metals, desired tilt angle to produce a strained ring is above 50°.

The change in energy upon tilting of Group 8 metallocenes is seen in Figure 67. For parallel ring Group 8 metallocenes, however, by 30° bending, Ferrocene, Ruthenocene and Osmocene structures gain 26.5 kcal/mol, 27.7 kcal/mol and 29.4 kcal/mol energy, respectively. Thermal ROP of [1]ferrocenophane and [1]ruthenocenophane structures with tilt angles about 30° has been reported [2].

In Figure 68, the effects of the metal and the bridging group on α is seen. In general, *ansa* ferrocenes have the smallest, and *ansa* ruthenocenes have the

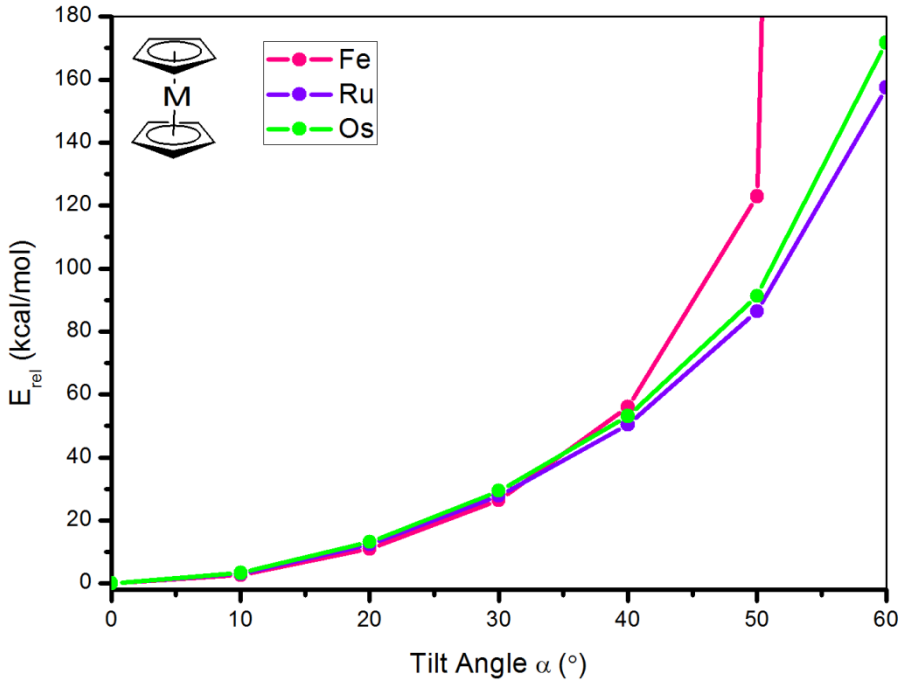

Figure 67. Tilt angle relative energy relationship in group 8 metallocenes

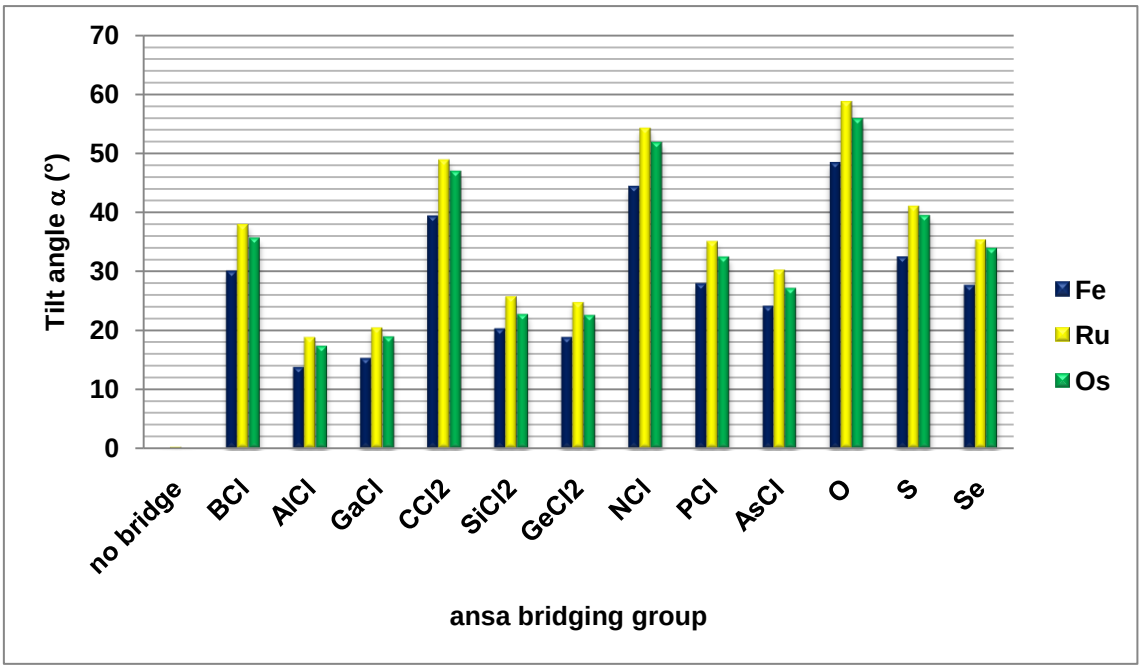

Figure 68. Tilt angle (α) values of group 8 [1]metallocenophanes with different *ansa* bridges

highest α values. α is highest for Group 16 and 2nd period bridging elements.

In Group 8, the most tilted structure is [Ru{(η^5-$C_5H_4)_2$O}] (α=58.7°) and the least tilted one is [Fe{(η^5-$C_5H_4)_2$AlCl}] (α=13.7°).

3.2.5.1.2. Metal Cyclopentadienyl Ring Distances (Cp-M)

Cp-M distances in Group 8 metallocenes [Fe{(η^5-$C_5H_5)_2$}], [Ru{(η^5-$C_5H_5)_2$}] and [Os{(η^5-$C_5H_5)_2$}] are 1.658 Å, 1.810 Å and 1.826 Å, respectively.

For all *ansa* ferrocenes, Cp-M distances are shorter than that of ferrocene (Table A5, Figure 69). In [Fe{(η^5-$C_5H_4)_2$S}], the bond is shortest (1.645 Å).

For *ansa* ruthenocenes, Cp-M distances decreases via *ansa* bridge formation except with B, Al, Ga and O bridged *ansa* ruthenocenes. They have longer Cp-M bonds than ruthenocene.

For *ansa* osmocenes, Cp-M distances decreases via *ansa* bridge formation with two exceptions. Al and Ga bridged *ansa* osmocenes have longer Cp-M bonds than osmocene.

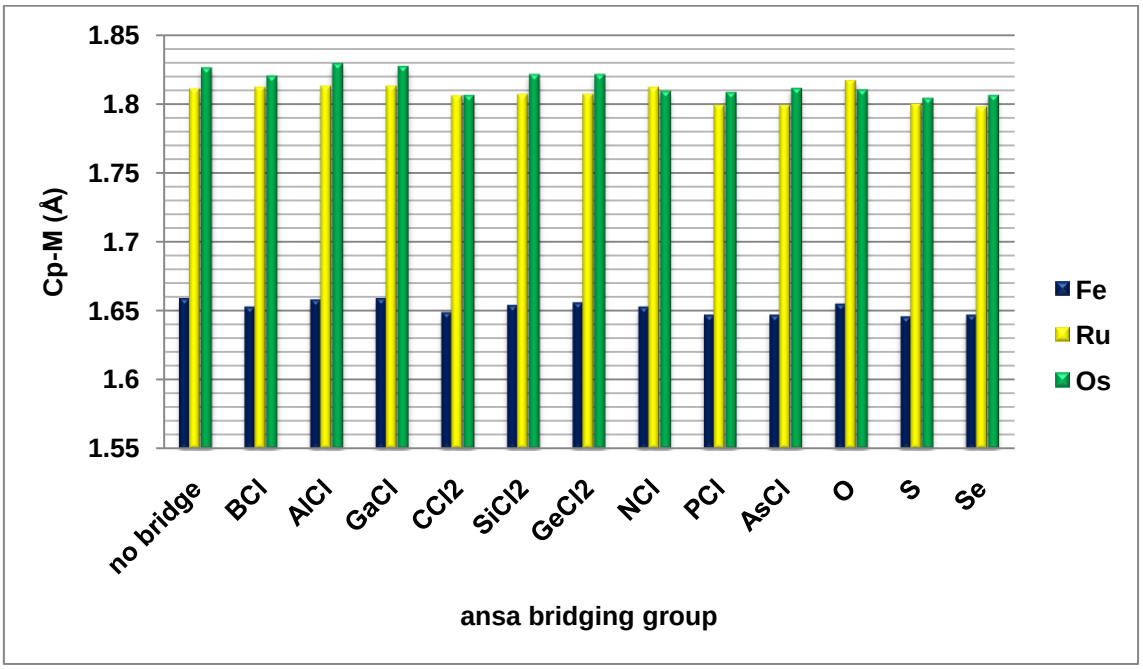

Figure 69. Cp-M Distances

3.2.5.1.3. δ C_{ipso} ^{13}C NMR TMS Chemical Shifts

Cyclopentadienyl carbons on ferrocene have a multiplet at 72.1 ppm, that of ruthenocene at 74.4 ppm and osmocene at 69.6 ppm.

Group 8 *ansa* metallocenes have characteristic C_{ipso} ^{13}C NMR shifts, which are shifted upfield with respect to yhe parent metallocenes, as seen in Figure 70.

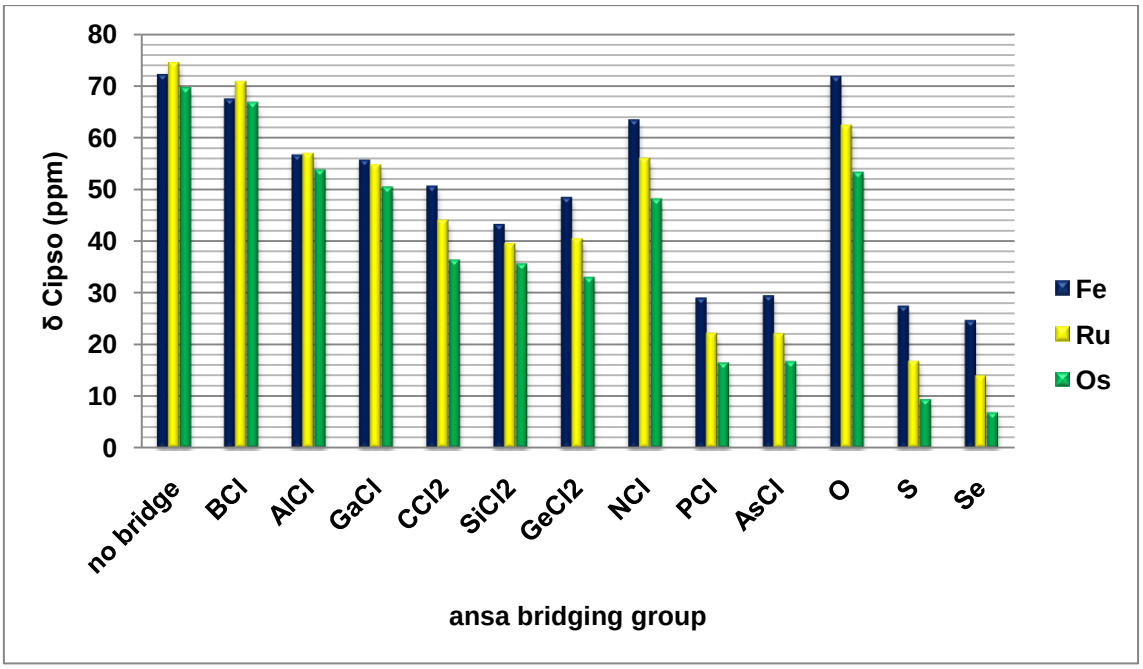

Figure 70. C_{ipso} ^{13}C NMR δ values of group 8 [1]metallocenophanes with different *ansa* bridges

Even the *ipso* carbons of the oxygen bridged ferrocene species has a higher magnetic shielding value (71.7 ppm) with respect to ferrocene.

3.2.5.2. Electronic Parameters

3.2.5.2.1. NPA Charges on Metal

The change in NPA charges with different bridging groups are seen in Figure 71. Fe and Ru complexes are negatively charged, where Os complexes have smaller positive or negative charges on metal atom.

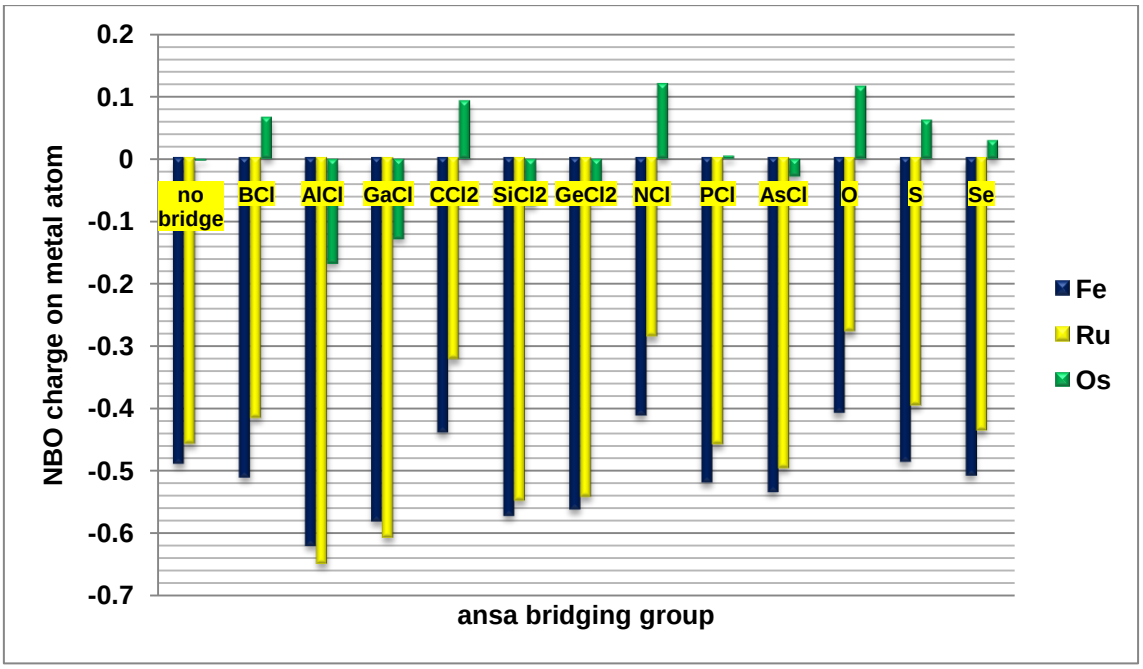

Figure 71. NBO charges on metal atom of group 8 [1]metallocenophanes with different *ansa* bridges

Bridging with Al, Ga, Si and Ge decreases the charge on metal atom.

3.2.5.2.2. Dipole Moments

Eclipsed metallocene structures of Group 8 metallocenes have zero dipole moments.*Ansa* bridging increases the polarizability of molecule. Highest dipole moments are attributed to Ge bridged Fe (4.39 D), Ru (4.06 D) and Os (4.12 D) complexes

3.2.5.2.3. Frontier Molecular Orbitals

Ansa bridging decreases the energies of HOMO and LUMO orbitals. HOMO-LUMO gap is also decreased in *ansa* metallocenes (Figure 72).

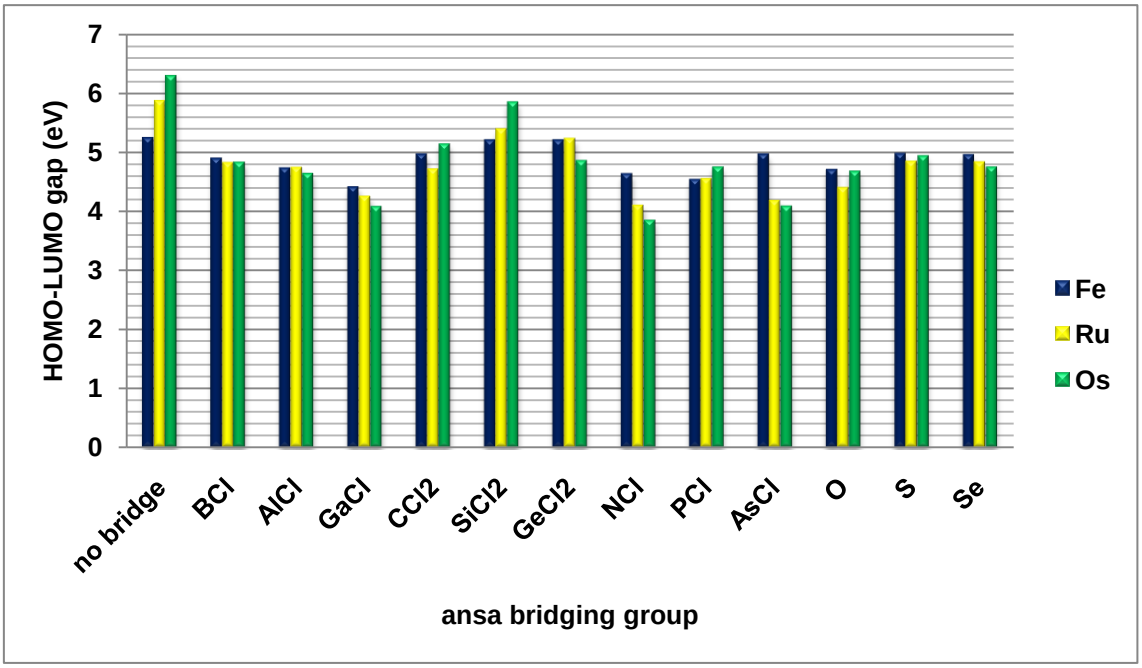

Figure 72. HOMO-LUMO gaps of group 8 [1]metallocenophanes with different *ansa* bridges

3.2.5.2.4. Absolute Hardness (η)

Group 8 metallocenes have higher hardness values than the rest of Group 4-9 metallocenes (Table A18). *Ansa* bridge formation decreases their hardness and increases their reactivity.

3.2.5.2.5. Chemical Potential (μ)

Chemical potentials of Group 8 metallocenes are low and decreased via *ansa* ring formation (Figure 73, Table A17).

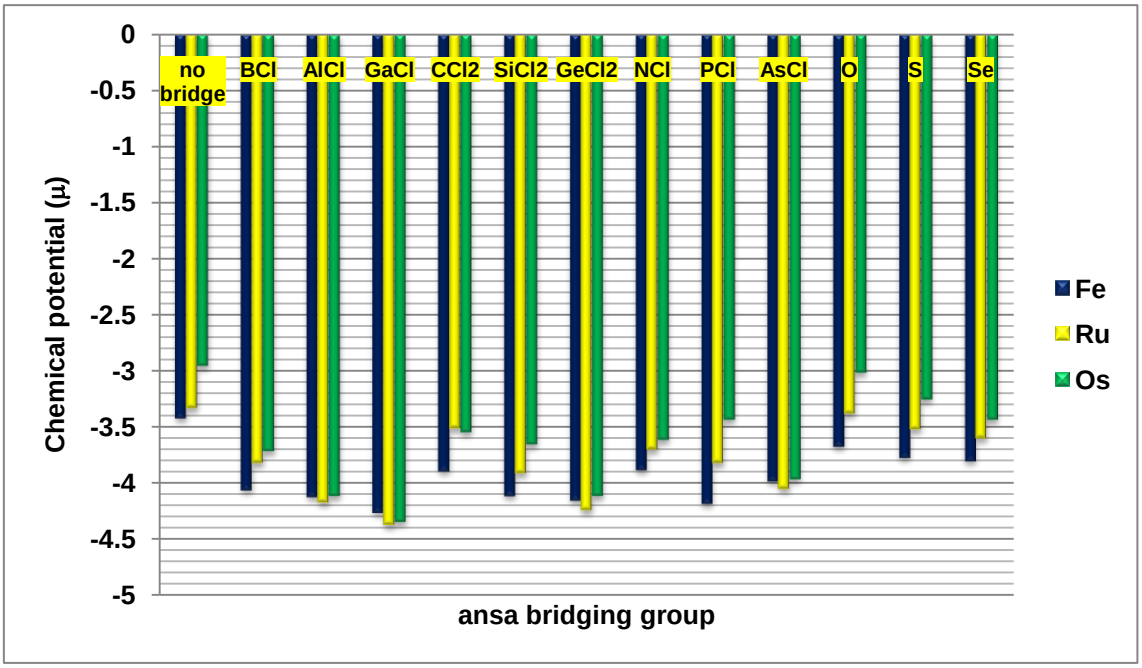

Figure 73. Chemical potential (μ) values of group 8 [1]metallocenophanes with different *ansa* bridges

3.2.5.2.6. Electronic Spectra

Electronic spectra of Group 8 *ansa* metallocenes are given in Figures 74-76. The *ansa* effect on electronic spectrum of a metallocene is clearly shown in the spectrum of Ferrocene (Figure 74), which posses a single high energy absorbtion band at 216 nm (Ɛ= 2500 $M^{-1}cm^{-1}$).

Ansa ferrocenes, on the other hand, posses additional lower energy bands between 300-700 nm, corresponding to d-d transitions. Furthermore, as α of the *ansa* compound increses, a red-shift at these lower energy bands occurs, with increased intensity of the band.

Decreasing order of α for 2nd period bridged *ansa* ferrocenes are as follows O (48.2°) > N (44.2°) > C (39.2°) > B(29.9°).

Related λ_{max} values are O (536 nm) > N (525 nm) > C (511 nm) > B(474 nm). Similar trends are also seen in the spectrum of Ruthenium and osmium compounds.

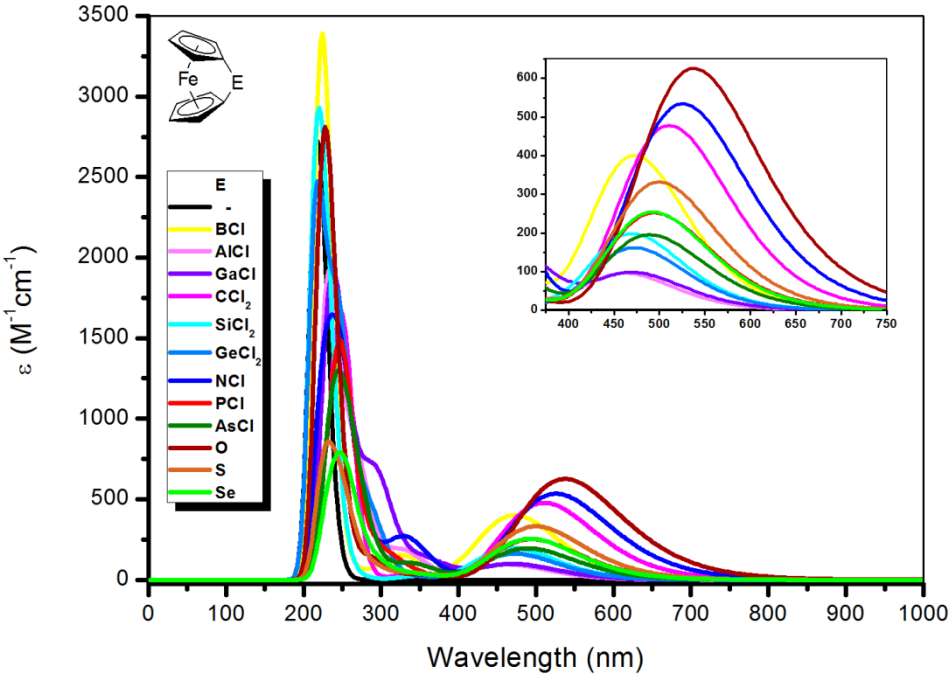

Figure 74. Change in electronic spectra of [1]ferrocenophanes with changing *ansa* bridge

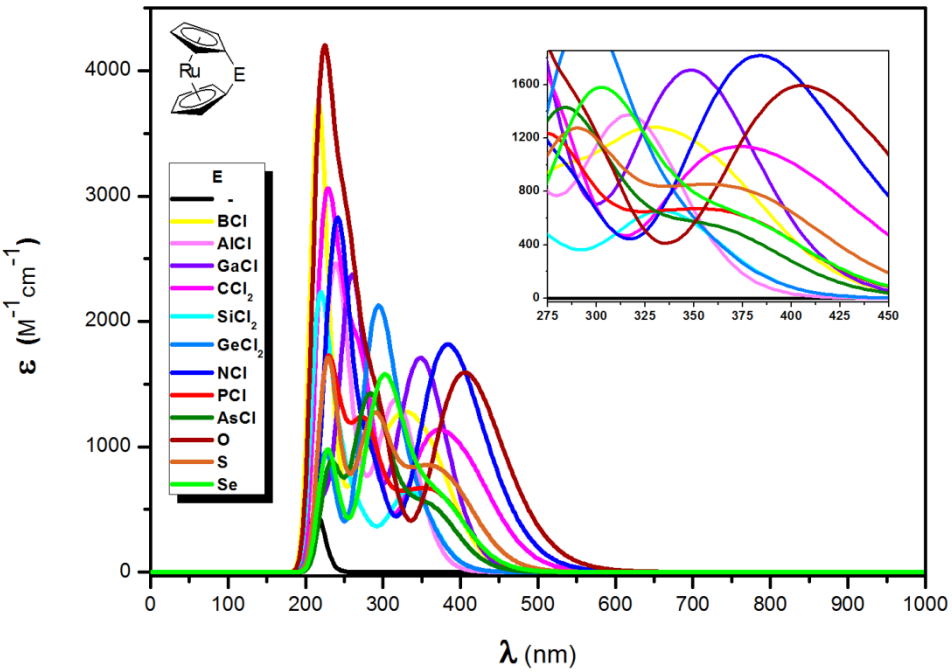

Figure 75. Change in electronic spectra of [1]ruthenocenophanes with changing *ansa* bridge

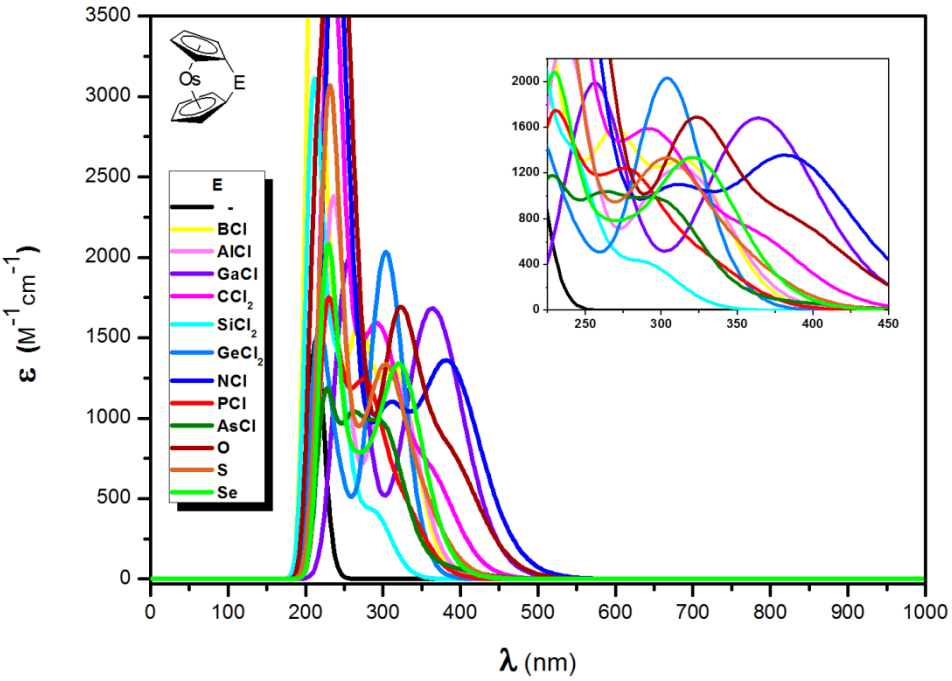

Figure 76. Change in electronic spectra of [1]osmocenophanes with changing *ansa* bridge

3.2.6 Group 9

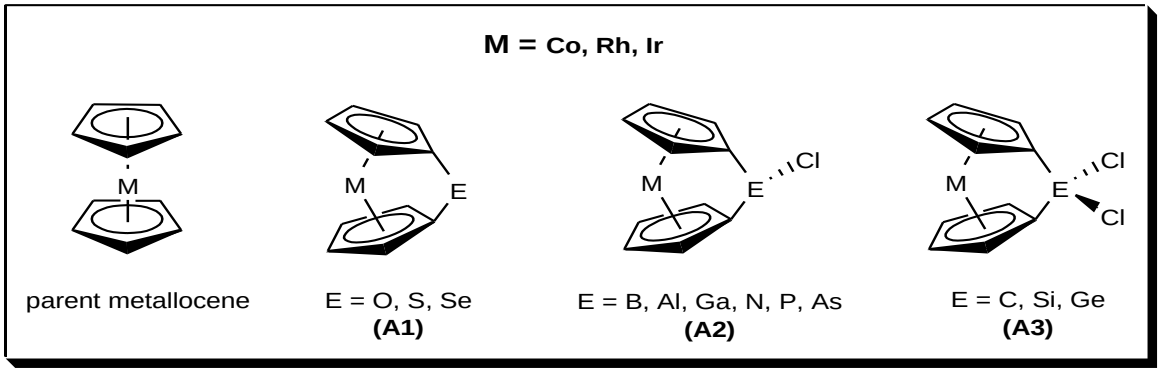

Figure 77. Parent metallocene and [1]metallocenophane structures of Group 9

3.2.6.1. Structural Parameters

3.2.6.1.1. Tilt Angles (α)

Like Group 8 metallocenes, Group 9 metallocenes also posses parallel ring structures and *ansa* bridge formation in these structures suggest a ring strained *ansa* metallocene. As seen in Figure 78, Group 9 metallocenes reach 30 kcal/mol energy level by 40° ring tilt.

At 40° relative energy of cobaltocene, rhodocene and iridocene are 38.6 kcal/mol, 28.5 kcal/mol and 31.4 kcal/mol, respectively. As seen in Figure 79, Group 9 *ansa* metallocenes reach extremely high tilt angles, for example in [Rh{(η^5-$C_5H_4)_2O$}] complex, α=80.6°. Nevertheless, ring strain may not be so high, because β angle of this complex is very low (8.96°).

3.2.6.1.2. Metal Cyclopentadienyl Ring Distances (Cp-M)

Cp-M distances in Group 9 metallocenes [Co{(η^5-$C_5H_5)_2$}], [Rh{(η^5-$C_5H_5)_2$}] and [Ir{(η^5-$C_5H_5)_2$}] are 1.748 Å, 1.919 Å and 1.937 Å, respectively.

Cp-M distances of B, C, N and O bridged *ansa* cobaltocenes are higher, others are lower than that of cobaltocene and Cp-M distances of Si, Ge and Se bridged *ansa* ruthenocenes are lower, others are higher than that of ruthenocene. For Ir,

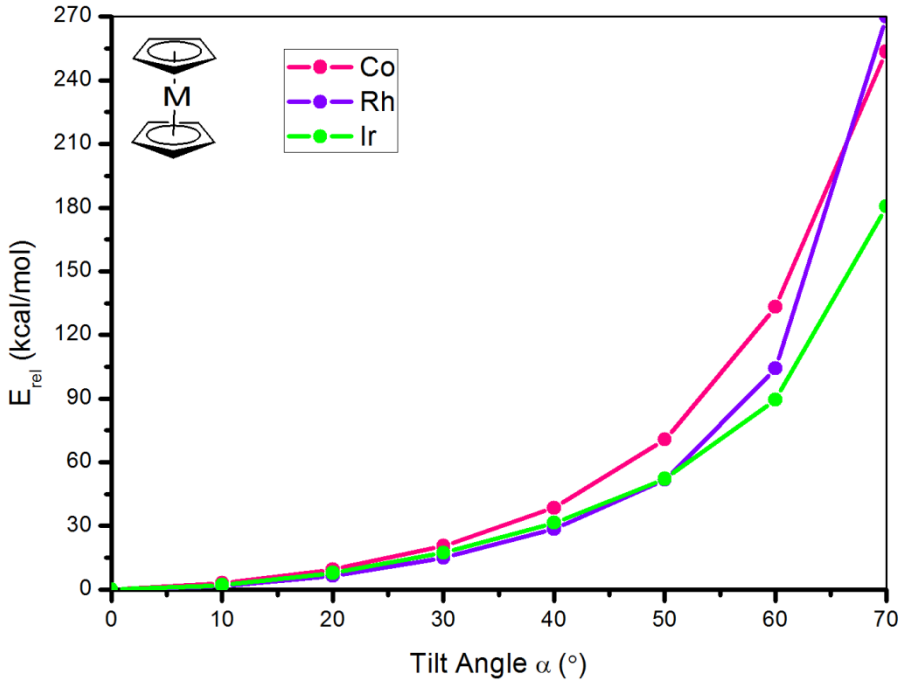

Figure 78. Tilt angle relative energy relationship in group 9 metallocenes

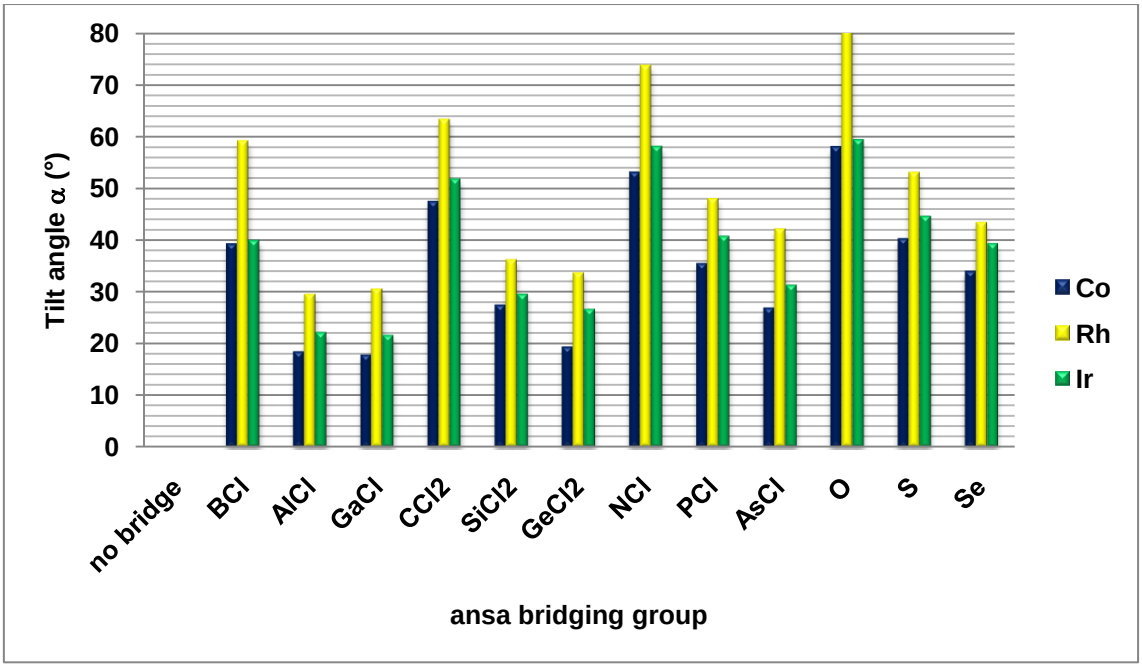

Figure 79. Tilt angle (α) values of group 9 [1]metallocenophanes with different *ansa* bridges

ansa complexation decreases Cp-M distances, as seen in Figure 80.

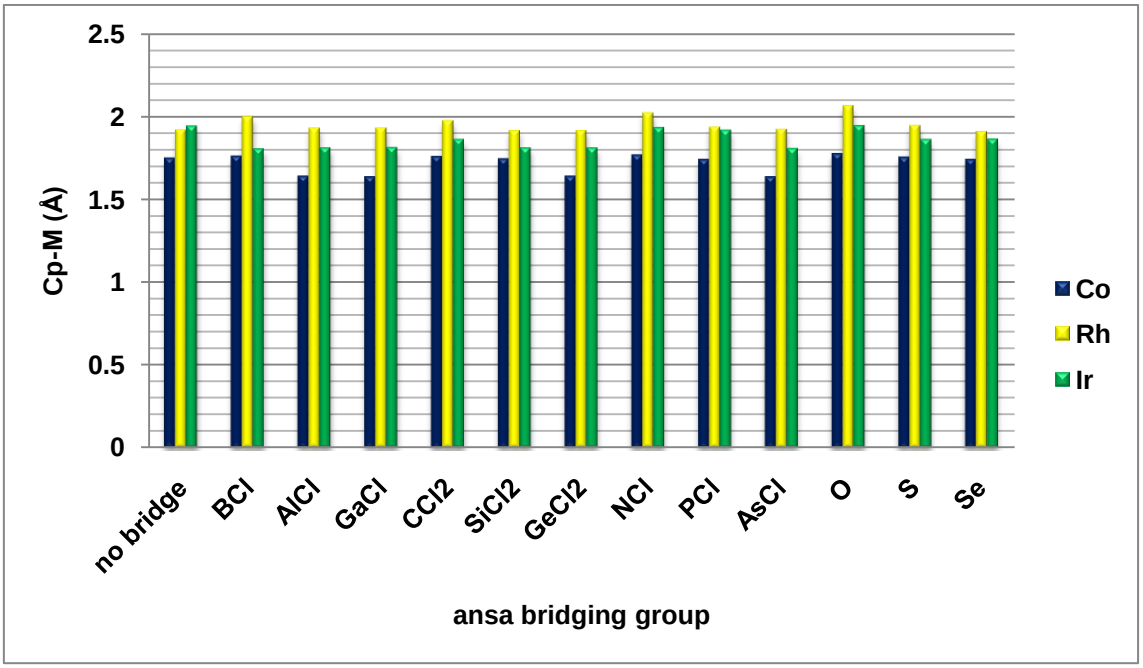

Figure 80. Cp-M Distances

3.2.6.1.3. δ C_{ipso} ^{13}C NMR TMS Chemical Shifts

^{13}C NMR chemical shifts (ppm) of cyclopentadienyl carbon atoms and corresponding C-M distances (Å) (in parantheses) of parent metallocenes are as follows. For [Co{(η^5-$C_5H_5)_2$}] δ 78.6 (2.090), 79.5 (2.097), 86.7 (2.136), 88.4 (2.143), 92.7 (2.153); for [Rh{(η^5-$C_5H_5)_2$}] δ 82.1 (2.231), 82.3 (2.234), 87 (2.277), 87.9 (2.283), 92.4 (2.313) and for [Ir{(η^5-$C_5H_5)_2$}] δ 73.7 (2.228), 76 (2.195), 83.2 (2.338), 84.2 (2.183), 86 (2.470).

Formation of *ansa* compounds, in Group 9, in general shifts C_{ipso} NMR values to higher fields as seen in Figure 81.

3.2.6.2. Electronic Parameters

3.2.6.2.1. NPA Charges on Metal

Charge distrubituon on Group 9 *ansa* metallocenes are is seen in Figure 82.

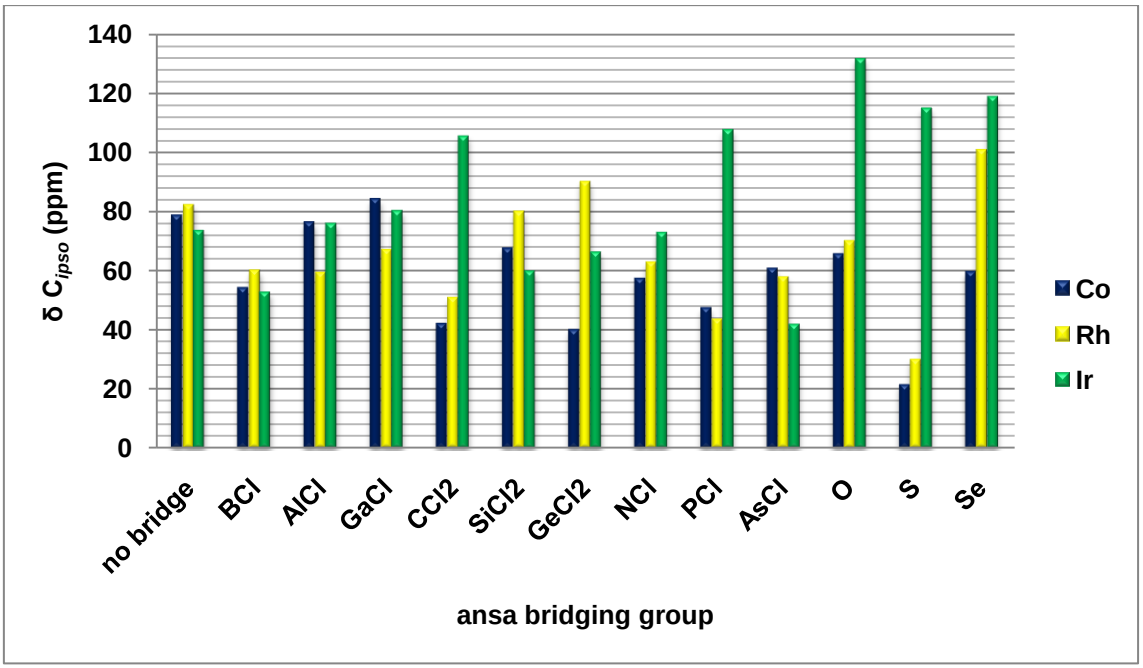

Figure 81. C_{ipso} ^{13}C NMR δ values of group 9 [1]metallocenophanes with different *ansa* bridges

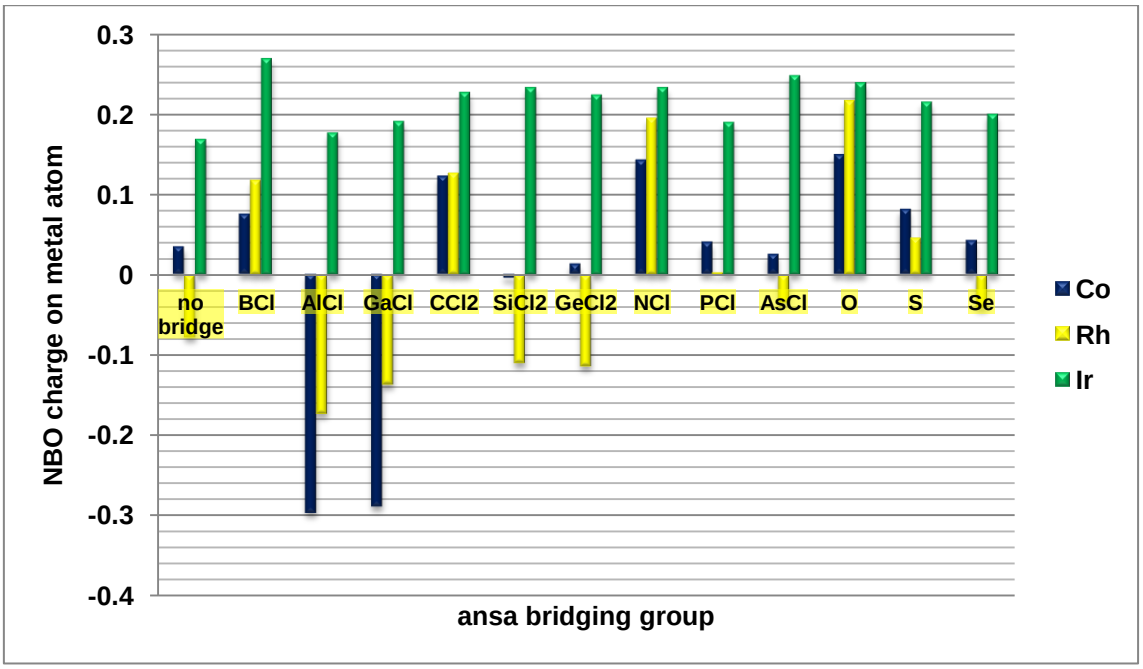

Figure 82. NBO charges on metal atom of group 9 [1]metallocenophanes with different *ansa* bridges

In Co, Rh and Ir complexes, generally an increase in charge on metal center is observed via *ansa* bridge formation, except for Al, Ga, Si, and Ge bridged complexes of Co and Ir, and As bridged complex of Co.

3.2.6.2.2. Dipole Moments

The zero dipole moments of parent metallocenes are increased via *ansa* bridge formation in Group 9.

3.2.6.2.3. Frontier Molecular Orbitals

As seen in Figure 83, HOMO-LUMO gaps are not changed in significant amounts via *ansa* formation in Group 9 *ansa* metallocenes.

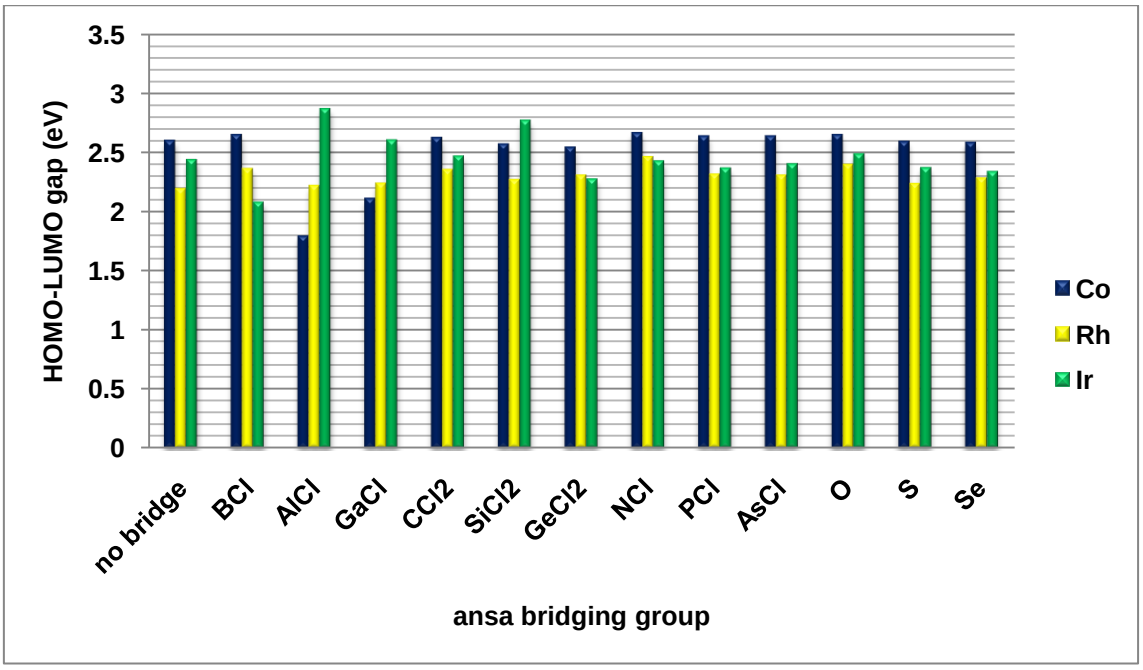

Figure 83. HOMO-LUMO gaps of group 9 [1]metallocenophanes with different *ansa* bridges

3.2.6.2.4. Absolute Hardness (η)

Hardness values of *ansa* metallocenes are slightly decreased with respect to the parent metallocenes.

3.2.6.2.5. Chemical Potential (μ)

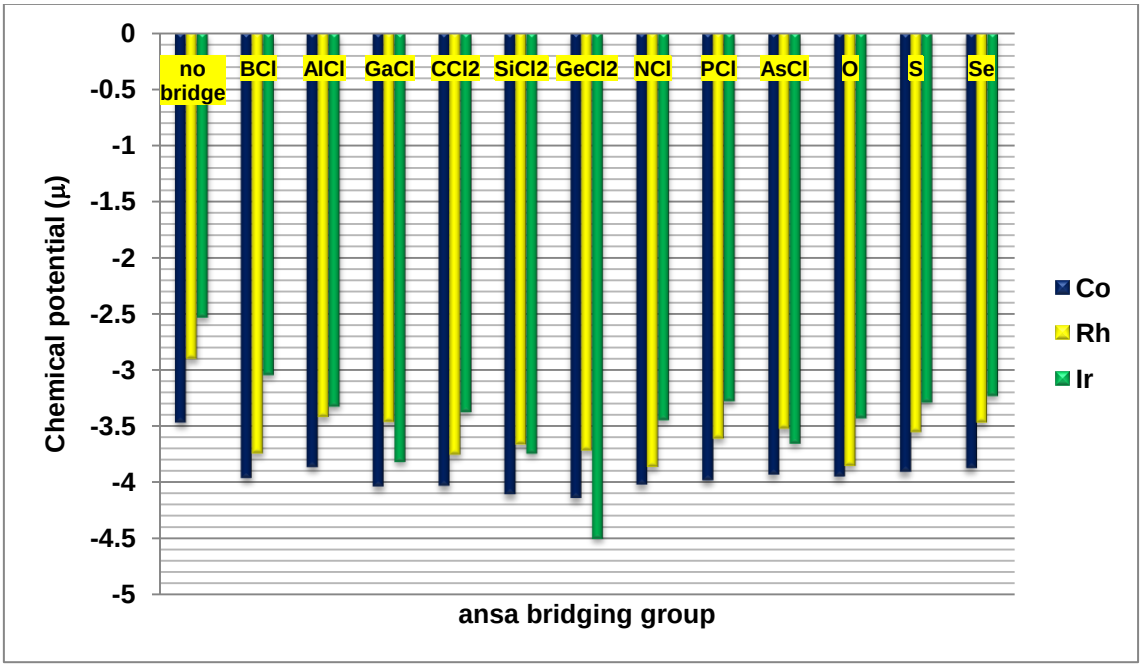

Figure 84. Chemical potential (μ) values of group 9 [1]metallocenophanes with different *ansa* bridges

Chemical potentials are decreased, and stability of molecules are increased via *ansa* ring formation.

3.2.6.2.6. Electronic Spectra

Computational electronic spectra of *ansa* titanocenes, *ansa* zirconocenes and *ansa* hafnocenes are given in Figures 85-87.

The highest energy absorbtion bands of parent mettallocenes, corresponding to the LMCT transitions between Cp and M orbitals were observed at 321, 350 and 270 nm for Co, Rh and Ir non-bridged metallocenes respectively.

Changes in absorbtion bands of parent metallocenes due to *ansa* bridge formation

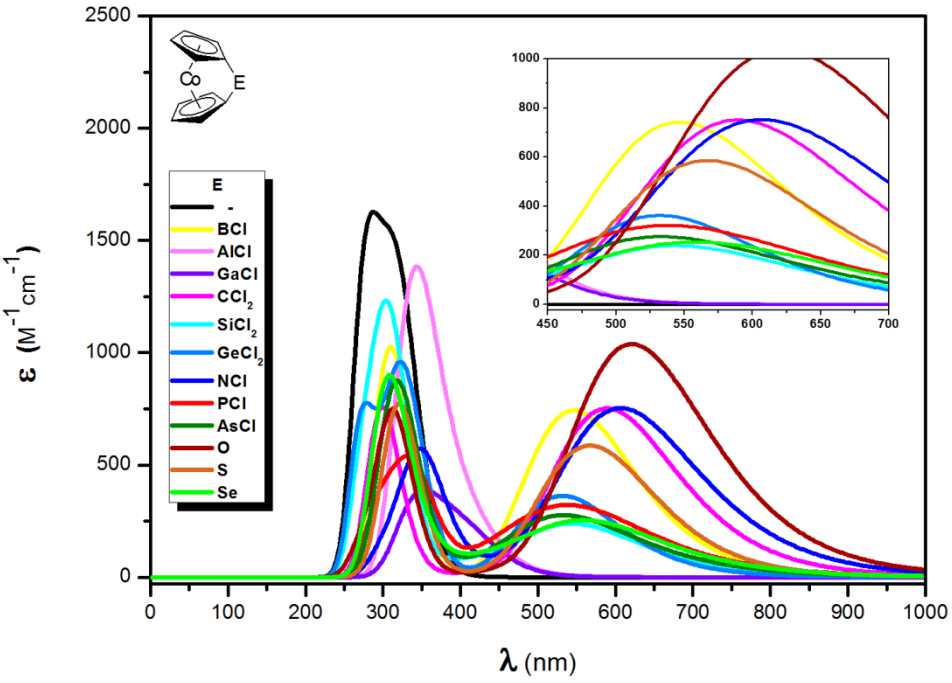

Figure 85. Change in electronic spectra of [1]cobaltocenophanes with changing *ansa* bridge

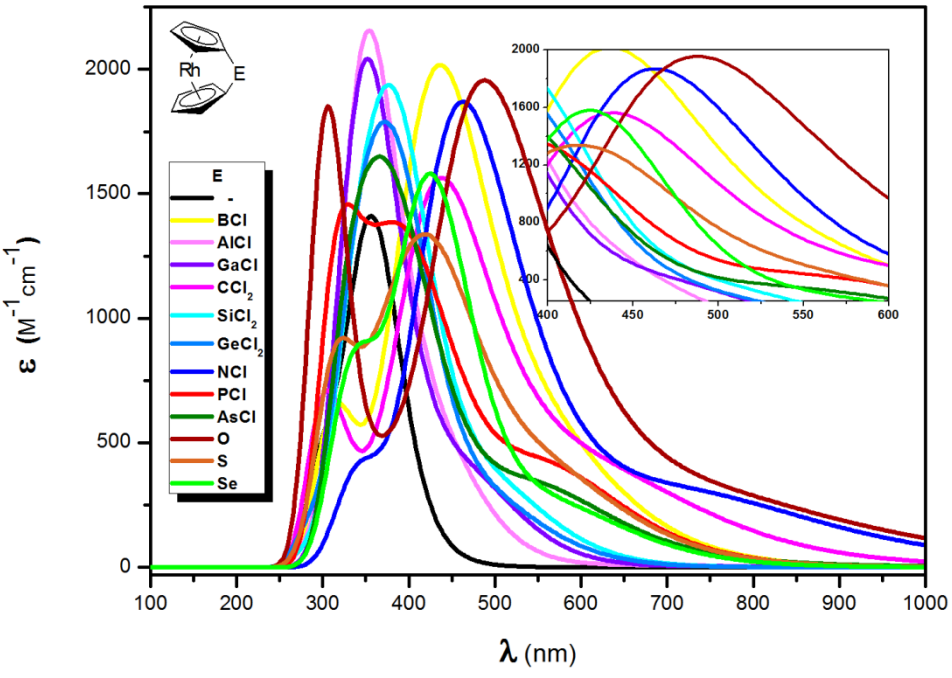

Figure 86. Change in electronic spectra of [1]rhodocenophanes with changing *ansa* bridge

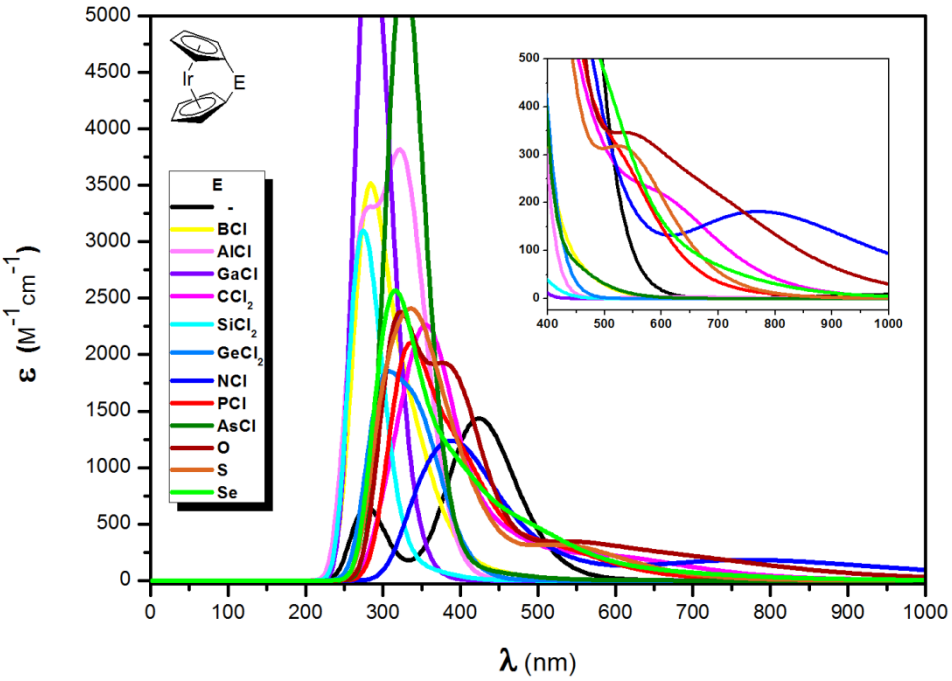

Figure 87. Change in electronic spectra of [1]iridocenophanes with changing *ansa* bridge

is similar in that of Group 8 *ansa* metallocenes as high tilt angles corresponds to high wavelengths.

4. CONCLUSIONS

In the first part of the work, bond lengths, bond angles, ^{13}C NMR chemical shifts and UV λ_{max} values for selected *ansa* metallocene structures from literature were computed at M06, B3LYP, B3PW91 and B3P86 levels of DFT and computational results were compared with corresponding experimental values. As a result, the overall performance of B3P86 functional was found to be better than the other three DFT functionals.

In the second part of the work, 216 model [1]metallocenophanes of Group 4-9 transition metals, having Group 13-16 elements in the *ansa* bridge, were constructed and their structural and electronic properties were determined computationally at B3P86/Def2-TZVP level of DFT.

According to the results of this study, for model *ansa* metallocenes of the same period transition metals, the tilt angle (α) decreases with increasing group number of the transition metal (M), except for Group 9 *ansa* metallocenes, which have greater relative α values than Group 8 elements. The decrerasing order of α is: Group 4> Group 5> Group 6> Group 7> Group 9> Group 8. When the bridging element (E) is considered, in the same group, α decreases with increasing atomic number of E, and in the same period α increases with increasing group number of E (Group 16> Group 15> Group 14> Group 13).

For Group 4-6 metallocenes, parent metallocenes are bent, and increasing the tilt angle from 50° up to about 70° does not cause an important increase in the relative energy of the molecules. Above 70° however, the rise in relative energy reaches greater values than 30 kcal/mol and in these groups, *ansa* metallocenes having greater tilt angles than 70° are expected to possess sufficient ring strain for ROP. To reach similar strain energies in Group 7 metallocenes, necessary tilt angle is about 60°, where in group 8 metallocenes the value is 30° and for group 9 metallocenes, 40° bending is needed.

Another parameter indicating the ring strain is weakening in Cp-M bonds, in other words, increasing Cp-M distances. In the same period, Cp-M decreases with the increasing group number of M, again except for Group 9 *ansa* metallocenes, which have greater Cp-M values than that of Group 8. When the bridging element (E) is

taken into the consideration, in the same group of E, in general, Cp-M increases with increasing atomic number .

The lowest Cp-M values belong to *ansa* metallocenes of 2nd period bridging elements (B, C, N,O), which have highest α values.

In general, a downfield shift on C_{ipso} carbon of Group 4-6 *ansa* metallocenes with respect to the high field ^{13}C NMR signal of the parent metallocene is observed, where in Groups 7-9 *ansa* metallocene formation leads upfield shifts.

Formation of *ansa* bridge causes a decrease in the dipole moments with respect to the parent metallocenes in Groups 4-7, where in Groups 8 and 9, since the parent metallocenes have zero dipole moments, an increase in the dipole moment was observed.

When the NBO charges of *ansa* metallocenes on the transition metal center (M) were compared, it was seen that in general, *ansa* metallocenes of 4th period transition metals possess the most negatively charged metal centers and that of 6th period transition metals have the most positively charged metal centers, which are potentially sensitive metal centers against nucleophilic attacks.

In general, *ansa* bridge formation cause a decrease in the energies of both the HOMO, and the LUMO of the with respect to the parent metallocenes, which results in the end with a decrease in HOMO-LUMO gaps.

Computed λ_{max} values of *ansa* metallocenes were observed longer than their metallocene analogues. Among *ansa* metallocenes, those having higher α values, have also longer λ_{max} values.

REFERENCES

[1] Smith, J. A., Von Seyerl, J., Huttner, G., Brintzinger, H. H., *Ansa*-metallocene derivatives: Molecular structure and proton magnetic resonance spectra of methylene- and ethylene-bridged dicyclopentadienyltitanium compounds, *Journal of Organometallic Chemistry*, 173, 175-185, **1979**.

[2] Herbert, D., Mayer, U. F. J., Manners, I., Strained metallocenophanes and related organometallic rings containing π-hydrocarbon ligands and transition-metal centers, *Angewandte Chemie International Edition,* 46, 5060–5081, **2007**.

[3] Green, J. C., Bent metallocenes revisited, *Chemical Society Reviews*, 27, 263-271, **1998**.

[4] Herberhold, M., Dörfler, U., Wrackmeyer, B., The first 1,2-dibora-[2]ferrocenophane and its dynamic behaviour in solution, *Journal of Organometallic Chemistry*, 530, 117-120, **1997**.

[5] Shapiro, P. J., The evolution of the *ansa*-bridge and its effect on the scope of metallocene chemistry, *Coordination Chemistry Reviews*, 231, 67-81, **2002**.

[6] Bellas, V., Rehahn, M., Polyferrocenylsilane-based polymer systems, *Angewandte Chemie International Edition,* 46, 5082–5104, 2007.

[7] Tamm, M., Kunst, A., Bannenberg, T., Randoll, S., Jones, P. G., Synthesis and reactivity of silicon- and germanium-bridged *ansa*-cycloheptatrienyl-cyclopentadienyl titanium complexes, *Organometallics*, 27, 417-424, **2007**.

[8] Wölfler, H. G., Flock, M., Sassmannshausen, J., Khinast, J., Structure-function-performance relationship of bis(cyclopentadienyl)-based group 4 metallocenes: a dft study, *Organometallics*, 27, 5196-5202, **2008**.

[9] Karttunnen, V. A., Linnolahti, M., Turunen, A., Pakkanen, T. A., Severn, J., R., Maaranen, J., Kokko, E., Pitkanen, P., Journal of Organometallic Chemistry, 693, 155-163, **2008**.

[10] Braunschweig, H., Dirk, R., Müller, M., Nguyen, P., Resendes, R., Gates, D. P., Manners, I., Incorporation of a first row element into the bridge of a strained

metallocenophane: synthesis of a boron-bridged [l]ferrocenophane, *Angewandte Chemie International Edition*, 36, 2338-2340, **1997**.

[11] Berenbaum, A., Braunschweig, H., Dirk, R., Englert, U., Green, J. C., Jaekle, F, Lough, A. J., Manners, I., *Journal of American Chemical Society*, 122, 5765-5774, **2000**.

[12] Denney, R. C., *Visible and Ultraviolet Spectroscopy*, John Wiley & Sons, London, **1987**.

[13] Rulkens, R., Gates, D. P., Balaishis, D., Pudelski, J. K., McIntosh, D. F., Lough, A. J., Manners, I., Highly strained, ring-tilted [1]ferrocenophanes containing group 16 elements in the bridge: synthesis, structures, and ring-opening oligomerization and polymerization of [1]thia- and [1]selenaferrocenophanes, *Journal of American Chemical Society*, 119, 10976-10986, **1997**.

[14] Foucher, F. A., Tang, B. Z., Manners, I., Ring-opening polymerization of strained, ring-tilted ferrocenophanes: a route to high-molecular-weight poly(ferrocenylsilanes), *Journal of American Chemical Society*, 114, 6246-6248, **1992**.

[15] Manners, I., Ring-opening polymerization of metallocenophanes: a new route to transition metal-based polymers, *Advances in Organometallic Chemistry*, 37, 131-168, **1996**.

[16] Kulbaba, K., Manners, I., Polyferrocenylsilanes: metal-containing polymers for

materials science, self-assembly and nanostructure applications, *Macromolecular Rapid Communications*, 22, 711-724, **2001**.

[17] Rider, D. A., Manners, I., Synthesis, self-assembly, and applications of polyferrocenylsilane block copolymers, *Polymer Reviews*, 47, 165-195, **2007**.

[18] Korczagin, I., Lammertink, R. G. H., Hempenius, M. A., Golze, S., Vancso, G. J., Surface nano- and microstructuring with organometallic polymers, *Advances in Polymer Science*, 200, 91-117, **2006**.

[19] Manners, I., Poly(ferrocenylsilanes): novel organometallic plastics, *Chemical Communications*, 857-865, **1999**.

[20] Nelson, J. M., Lough, A. J., Manners, I., Synthesis and ring-opening polymerization of highly strained, ring-tilted [2]ruthenocenophanes, *Angewandte Chemie International Edition*, 33, 989-991, **1994**.

[21] Vogel, U., Lough, A. J., Manners, I., Isolation of [1]ruthenocenophanes: synthesis of polyruthenocenylstannanes by ring-opening polymerization, *Angewandte Chemie International Edition*, 43, 3321-3325, **2004**.

[22] Conway, S. L. J., Doerrer, L. H., Green, J. C., Green, M. L. H., Scottow, A., Stephens, A. H. H., Synthesis, structure and density functional study of the *ansa*-rhenocene complex [Re{(η-C5H4)CMe2(η-C5H4)}Cl], *Journal of Chemical Society Dalton Transactions*, 329-333, **2000**.

[23] Fox, S., Dunne, J. P., Tacke, M., Schmitz, D., Dronskowski, R., Synthesis and structural characterisation of a novel chiral *ansa*-cobaltocenium hexafluorophosphate, *European Journal of Inorganic Chemistry*, 3039-3046, **2002**.

[24] Drewitt, M. J., Barlow, S., O-Hare, D., Nelson, J. M., Nguyen, P., Manners, I., The first [2]cobaltocenophane and [2]metallocenophanium salts, *Chemical Communications*, 2153-2154, **1996**.

[25] Braunschweig, H., Breher, F., Kaupp, M., Gross, M., Kupfer, T., Nied, D., Radacki, K., Schinzel, S., Synthesis, crystal structure, epr and dft studies, and redox properties of [2]tetramethyldisilacobaltocenophane, *Organometallics*, 27, 6427-6433, **2008**.

[26] Mayer, U. F. J., Gilroy, J. B., O-Hare, D., Manners, I., Ring-opening polymerization of 19-electron [2]cobaltocenophanes: a route to high-molecular-weight, water-soluble polycobaltocenium polyelectrolytes, *Journal of American Chemical Society*, 131, 10382-10383, **2009**.

[27] Prashar, S., Antinolo, A., Otero, A., Insights into group 4 and 5 *ansa*-bis(cyclopentadienyl) complexes with a single-atom bridge, *Coordination Chemistry Reviews*, 250, 133–154, **2006**.

[28] Hoveyda, A.H., Morken, J.P., Enantioselective C-C and C-H bond formation mediated or catalyzed by chiral ebthi complexes of titanium and zirconium, *Angewandte Chemie International Edition*, 35, 1262-1284, **1996**.

[29] Imori, T., Tilley, T. D., The influence of catalyst structure on the dehydropolymerization of phenylsilane, *Polyhedron*, 13, 2231-2243, **1994**.

[30] V.K. Dioumaev, J.F. Harrod, *Organometallics* 13 (1994) 1548.

[31] Frisch, M. J., Trucks, G. W., Schlegel, H. B., Scuseria, G. E., Robb, M. A., Cheeseman, J. R., Scalmani, G., Barone, V., Mennucci, B., Petersson, G. A., Nakatsuji, H., Caricato, M., Li, X., Hratchian, H. P., Izmaylov, A. F., Bloino, J., Zheng, G., Sonnenberg, J. L., Hada, M., Ehara, M., Toyota, K., Fukuda, R., Hasegawa, J., Ishida, M., Nakajima, T., Honda, Y., Kitao, O., Nakai, H., Vreven, T., Montgomery, J. A., Jr., Peralta, J. E., Ogliaro, F., Bearpark, M., Heyd, J. J., Brothers, E., Kudin, K. N., Staroverov, V. N., Keith, T., Kobayashi, R., Normand, J., Raghavachari, K., Rendell, A., Burant, J. C., Iyengar, S. S., Tomasi, J., Cossi, M., Rega, N., Millam, J. M., Klene, M., Knox, J. E., Cross, J. B., Bakken, V., Adamo, C., Jaramillo, J., Gomperts, R., Stratmann, R. E., Yazyev, O., Austin, A. J., Cammi, R., Pomelli, C., Ochterski, J. W., Martin, R. L., Morokuma, K., Zakrzewski, V. G., Voth, G. A., Salvador, P., Dannenberg, J. J., Dapprich, S., Daniels, A. D., Farkas, O., Foresman, J. B., Ortiz, J. V., Cioslowski, J., Fox, D. J., Gaussian, Inc., Wallingford CT, **2010**.

[32] Hohenberg, P., Kohn, W., Inhomogeneous Electron Gas, *Physical Reviews*, 136, B864-B71, **1964**.

[33] W. Kohn and L. J. Sham, Self-Consistent Equations Including Exchange and Correlation Effects, *Physical Review*, 140, A1133-A38, **1965**.

[34] Parr, R. G., Yang, W., *Density-functional theory of atoms and molecules*, Oxford Univ. Press, Oxford, **1989**.

[35] Bühl, M., Reimann, C., Pantazis, D. A., Bredow, T., Neese, F., geometries of third-row transition-metal complexes from density-functional theory, *Journal of Chemical Theory and Computation*, 4, 1449-1459, **2008**.

[36] Becke, A. D., Density-functional exchange-energy approximation with correct asymptotic-behavior, *Physical Review A*, 38, 3098-100, **1988**.

[37] Perdew, J. P., Density-functional approximation for the correlation energy of the inhomogeneous electron gas, *Physical Review B*, 33, 8822-24, **1986**.

[38] Lee, C., Yang, W., Parr, R. G., Development of the Colle-Salvetti correlation-energy formula into a functional of the electron density, *Physical Review B*, 37, 785-89, **1988**.

[39] Perdew, J. P., In *Electronic Structure of Solids '91*, Ed. Ziesche, P., Eschrig, H., Akademie Verlag, Berlin, 11, **1991**.

[40] Zhao, Y., Truhlar, D. G., The M06 suite of density functionals for main group thermochemistry, thermochemical kinetics, noncovalent interactions, excited states, and transition elements: two new functionals and systematic testing of four M06-class functionals and 12 other functionals, *Theoretical Chemistry Accounts*, 120, 215-41, **2008**.

[41] Weigend, F., Ahlrichs, R., Balanced basis sets of split valence, triple zeta valence and quadruple zeta valence quality for H to Rn: Design and assessment of accuracy, *Physical Chemistry Chemical Physics*, 7, 3297-305, **2005**.

[42] (a) The ECPs were obtained from the Gaussian Basis Set Library EMSL at https://bse.pnl.gov/bse/portal. (b) Feller, D., The role of databases in support of computational chemistry calculations, *Journal of Computational Chemistry*, 17, 1571-1586, **1996**. (c) Schuchardt, K.L., Didier, B.T., Elsethagen, T., Sun, L., Gurumoorthi, V., Chase, J., Li, J., Windus, T.L., Basis Set Exchange: A Community Database for Computational Sciences, *Journal of Chemical Information and Modeling*, 47, 1045-1052, **2007**.

[43] Zhang, X., Schwarz, H., Bonding in cationic MCH_2^+ (M=K–La, Hf–Rn): A theoretical study on periodic trends, *Chemistry - A European Journal***,** 16, 5882-5888, **2010**.

[44] Zhang, X., Schwarz, H., Bonding in cationic MOH_n^+ (M = K − La, Hf − Rn; n = 0–2): DFT performances and periodic trends, *Theoretical Chemistry Accounts*, 129, 389-399, **2011**.

[45] Mulliken, R. S., Electronic Population Analysis on LCAO-MO Molecular Wave Functions, *Journal of Chemical Physics,* 23, 1833-40, **1955**.

[46] Hamilton, T. P., Pulay, P., UHF natural orbitals for defining and starting MC-SCF calculations, *Journal of Chemical Physics,* 88, 4926-33, **1988**.

[47] Bauernschmitt, R., Ahlrichs, R., Stability analysis for solutions of the closed shell Kohn-Sham equation, *Journal of Chemical Physics*,104, 9047-52, **1996**.

[48] Ruud, K., Helgaker, T., Bak, K. L., Jørgensen, P., Jensen, H. J. A., Hartree Fock limit magnetizabilities from london orbitals, *Journal of Chemical Physics*, 99, 3847-3859, **1993**.

[49] Ditchfield, R., Molecular orbital theory of magnetic shielding and magnetic susceptibility, *Journal of Chemical Physics*, *56*, 5688-5691, **1986**.

[50] Pearson, R. G., Absolute electronegativity and hardness correlated with molecular orbital theory, *Proceedings of the National Academy of Sciences USA*, 83, 8440-8441, **1986**.

[51] Koopmans, T., Über die zuordnung von wellenfunktionen und eigenwerten zu den einzelnen elektronen eines atoms, *Physica*, 1, 104-113, **1934**.

[52] Butler, I. R., Cullen, W. R., Einstein, F. W. B., Rettig, S. J., Willis, A. J., Synthesis of some ring-substituted [1]ferrocenophanes and the structure of four representative examples, *Organometallics*, 2, 129-135, **1983**.

[53] Zechel, D.L., Hultzsch, K. C., Rulkens, R., Balaishis, D., Ni, Y., Pudelski, J. K., Lough, A. J., Manners I., Foucher, D.A., Thermal and transition-metal-catalyzed ring-opening polymerization (rop) of [1]silaferrocenophanes with chlorine substituents at silicon: a route to tunable poly(ferrocenylsilanes), *Organometallics*, 15, 1972-1978, **1996**.

[54] Chan, W. Y., Lough, A. J., Manners, I., Methylchlorosila[1]ferrocenophane, *Acta Crystallographica Section E,* 61, m375-m376, **2005**.

[55] Fischer, A. B., Kinney, J. B., Staley, R. H., Wrighton, M. S., Derivatization of surfaces via reaction of strained silicon-carbon bonds. characterization by photoacoustic spectroscopy, *Journal of the American Chemical Society* ,101, 6501-6506, **1979**.

[56] Finckh, W., Tang, B-Z., Foucher, D. A., Zamble, D. B., Ziembinski, R., Lough, A., Manners, I., The polymerization behavior of [1]- and [2]ferrocenophanes containing silicon atoms in the bridge: comparison of the molecular structure of the strained, polymerizable cyclic ferrocenylsilane $Fe(\eta\text{-}C_5H_4)_2(SiMe_2)$ with that of the cyclic ferrocenyldisilane $Fe(\eta\text{-}C_5H_4)_2(SiMe_2)_2$, *Organometallics*, 12, 823-829, **1993**.

[57] Foucher, D., Ziembinski, R., Petersen, R., Pudelski, J., Edwards, M., Ni, Y., Massey, J., Jaeger, C. R., Vancso, G. J., Manners, I., Synthesis, characterization, and properties of high molecular weight unsymmetrically substituted poly(ferrocenylsilanes), *Macromolecules*, 27, 3992-3999, **1994**.

[58] Foucher, D. A., Lough, A. J., Manners, I., Rasburn, J., Vancso, J. G., The first unsymmetrically substituted ring-tilted-siliconibridged [1]ferrocenophane, *Acta Crystallographica Section C*, 51, 580-582, **1995**.

[59] Foucher, D. A., Ziembinski, R., Tang, B. Z., Macdonald, P. M., Massey, J. Jaeger, C. R., Vancso, G. J., Manners, I., Synthesis, characterization, glass transition behavior, and the electronic structure of high molecular weight, symmetrically substituted poly(ferrocenylsilanes) with alkyl or aryl side groups, *Macromolecules*, 26, 2878, **1993**.

[60] a) Foucher, D. A., Edwards, M., Burrow, R. A., Lough, A. J., Manners, I., Ring-Opening Polymerization of Strained, ring-tilted [1]ferrocenophanes with germanium in the bridge: structures of the [1]germaferrocenophane Fe(η-$C_5H_4)_2GeMe_2$ and the ferrocenylgermane Fe(η-$C_5H_4GeEt_2Cl$)(η-C_5H_4), *Organometallics*, 13, 4959-4966, **1993**. b) D. A. Foucher, Manners, I., Ring-opening polymerization as a route to new organometallic polymers: synthesis of the first poly(ferrocenylgermane), Makromolecular Chemistry Rapid Communications, 14, 63-66, **1993**. c) Zürcher, S., Gramlich, V., Togni, A., Germanium-containing ferrocenes and ferrocenophanes. Potential precursors for ring-opening polymerizations and 'germaferrocenes', *Inorganica Chimica Acta*, 291, 355-364, **1999**.

[61] Herbert, D. E., Gilroy, J. B., Staubitz, A., Haddow, M. F., Harvey, J. N., Manners, I., Strain-induced cleavage of carbon-carbon bonds: bridge rupture reactions of group 8 dicarba[2]metallocenophanes, *Journal of American Chemical Society*, 132, 1988-1998, **2010**.

[62] Mayer, U. F. J., Charmant, J. P. H., Rae, J., Manners, I., Synthesis and structures of strained, neutral [d^7] and cationic [d^6] hydrocarbon-bridged [n]cobaltocenophanes (n = 2, 3), *Organometallics*, 27, 1524-1533, **2008**.

[63] Perrotin, P., Shapiro, P. J., Williams, M., Twamley, B., In search of a versatile pathway to *ansa*-chromocene complexes. synthesis and characterization of the highly unstable *ansa*-chromocene carbonyl complex $Me_2C(C_5H_4)_2CrCO$, *Organometallics*, 26, 1823-1826, **2007**.

[64] Schwemlein, H., Zsolnai, L., Huntner, G., Brintzinger, H.H., *ansa*-metallocene derivatives: VI. Synthesis and molecular structure of a stable tetramethylethylene-bridged chromocene carbonyl complex, $(CH_3)_4C_2(C_5H_4)_2CR(CO)$, *Journal of Organometallic Chemistry*, 256, 285-289, **1983**.

[65] Buschel, S., Daniliuc, C., Jones, P.G., Tamm, M., The *ansa*-zirconocene [bis(η^5-cyclopentadienyl)phenylphosphine]-dichloridozirconium(IV), *Acta Crystallographica Section C*, 66, m86–m88, **2010**.

[66] Erben, M., Cisarova, I., Dusek, M., Vinklarek, J., Picka, M., Dibromido(η^5, η^5-propane-2,2-diyl-dicyclopentadienyl)titanium(IV), *Acta Crystallographica Section E*, 63, m2699, **2007**.

[67] Picka, M., Cisarova, I., Vinklarek, J., Erben, M., Difluoro(η^5, η^5-propane-2,2-diyl-dicyclopentadienyl)titanium(IV), *Acta Crystallographica Section E*, 61, m1266-m1268, **2005**.

[68] Erben, M., Dusek, M., Picka, M., Vinklarek, J., Dibromido[bis(η^5-cyclopentadienyl)-dimethylsilane]zirconium(IV), *Acta Crystallographica Section E*, 65, m92, **2009**.

[69] Burley, J. C., Motherwell, W. D. S., Maaranenc, J., Ringwald, M., Dichloro[(η^5-cyclopentadienyl)dimethyl-(η^5-3-phenylindenyl)silane]hafnium(IV): a powder study, *Acta Crystallographica Section E*, 63, m238–m240, **2007**.

[70] Honzicek, J., Palacova, H., Cisarova, I., Vinklarek, J., *Ansa*-vanadocene complexes with short interannular bridges, *Journal of Organometallic Chemistry,* 691, 202–207, **2006**.

[71] Chirik, P.J., Zubris, D. L., Ackerman, L. J., Henling, L. M., Day, M. W., Bercaw, J. E., Preparation of *ansa*-niobocene and *ansa*-tantalocene olefin hydride complexes as transition state analogues in metallocene-catalyzed olefin polymerization, *Organometallics*, 22, 172-187, **2003**.

[72] Bailey, N. J., Cooper, J. A., Gailus, H., Green, M. L. H., James, J. T., Leech, M. A., Mono(cyclopentadienyl) and *ansa*-bis(cyclopentadienyl)imido derivatives of Group 5 and 6 transition metals; crystal structures of [M{(η-C_5H_4)CMe_2(η-C_5H_4)}(NR)X] (M=Nb, R=$SiMe_3$, X=Cl; R=Bu^t, X=Cl, Br or I; M=Ta, R=Bu^t, X=Cl), *Journal of Chemical Society Dalton Transactions*, 3579–3584, **1997**.

[73] Conway, S. L. J., Dijkstra, T., Doerrer, L. H., Green, J. C., Green, M. L. H., Stephens, A. H. H., Studies of *ansa*-bis(cyclopentadienyl)tungsten derivatives, *Journal of Chemical Society Dalton Transactions*, 2689-2695, **1998**.

[74] Ahmed, T. J., Zakharov, L. N., Tyler, D.R., Organometallic catalysis in aqueous solution. the hydrolytic activity of a water-soluble *ansa*-molybdocene catalyst, *Organometallics*, 26, 5179-5187, **2007**.

APPENDIX

APPENDIX A

CALCULATED PARAMETERS AT B3P86/Def2-TZVP LEVEL OF DFT

Table A1. Tilt Angle α (°)

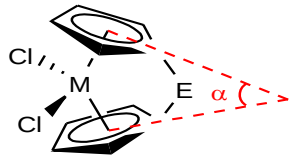

M = Ti, Zr, Hf, V, Nb, Ta, Cr, Mo, W

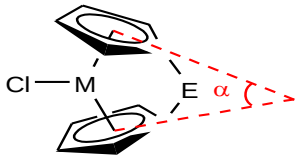

M = Mn, Tc, Re

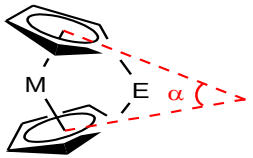

M = Fe, Ru, Os, Co, Rh, Ir

	M																	
E	**Ti**	**Zr**	**Hf**	**V**	**Nb**	**Ta**	**Cr**	**Mo**	**W**	**Mn**	**Tc**	**Re**	**Fe**	**Ru**	**Os**	**Co**	**Rh**	**Ir**
-	50.4	52.8	52.9	45.0	48.9	50.3	41.1	49.6	51.1	31.1	38.2	38.9	0.1	0.2	0.1	0	0.2	0.1
BCl	64.1	69.4	69.0	57.6	62.6	62.9	53.8	59.2	60.0	44.2	50.9	51.2	29.9	37.9	35.6	39.2	59.2	39.9
AlCl	53.4	57.4	57.1	47.1	51.5	52.3	41.3	48.9	50.3	32.7	40.2	41.0	13.7	18.8	17.3	18.5	29.5	22.1
GaCl	53.2	57.0	56.7	46.8	51.4	52.1	40.1	50.3	50.4	32.3	41.2	41.6	15.2	20.4	18.9	17.8	30.6	21.6
CCl_2	66.5	71.4	70.9	62.6	67.3	67.3	58.7	64.1	64.8	47.7	52.8	54.3	39.2	48.8	46.9	47.4	63.3	51.7
$SiCl_2$	55.4	59.6	59.4	50.1	55.6	56.1	45.1	52.6	53.6	35.7	42.1	43.7	20.2	25.7	22.7	27.4	36.3	29.5
$GeCl_2$	53.5	57.9	57.6	48.5	54.1	54.7	42.9	51.5	52.6	34.2	41.4	42.8	18.7	24.7	22.5	19.4	33.7	26.6
NCl	69.7	74.6	74.1	65.6	70.6	70.6	61.6	67.3	68.0	51.6	57.5	58.2	44.2	54.2	51.8	53.0	73.7	58.0
PCl	60.3	64.9	64.5	55.4	60.7	61.0	52.9	58.0	58.9	41.5	47.5	48.3	27.8	35.0	32.4	35.4	48.0	40.7
AsCl	57.8	62.2	61.9	52.7	58.4	58.7	49.6	56.0	57.1	39.1	45.1	46.0	24.0	30.2	27.1	26.9	42.2	31.2
O	72.2	77.0	76.4	68.3	73.3	73.1	64.4	70.1	70.8	54.7	59.7	60.4	48.2	58.7	55.8	57.9	80.6	59.3
S	62.1	66.7	66.4	58.5	63.0	63.1	55.5	60.4	61.2	43.7	48.0	49.5	32.3	41.0	39.4	40.2	53.1	44.6
Se	59.0	63.4	63.2	55.6	60.0	60.2	53.0	57.6	58.6	40.5	44.9	46.5	27.5	35.3	33.9	34.0	43.4	39.3

Table A2. Angle β (°)

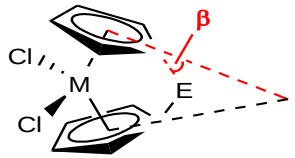

M = Ti, Zr, Hf, V, Nb, Ta, Cr, Mo, W

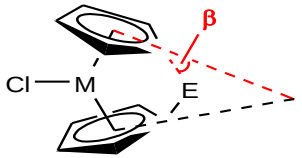

M = Mn, Tc, Re

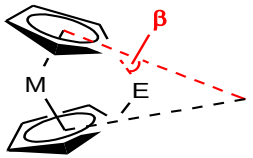

M = Fe, Ru, Os, Co, Rh, Ir

	M																	
E	**Ti**	**Zr**	**Hf**	**V**	**Nb**	**Ta**	**Cr**	**Mo**	**W**	**Mn**	**Tc**	**Re**	**Fe**	**Ru**	**Os**	**Co**	**Rh**	**Ir**
-	-	-	-	-	-	-	-	-	-	-	-	-	-	-	-	-	-	-
BCl	27.6	26.0	26.1	28.5	25.38	25.4	24.2	23.0	23.5	32.6	38.1	40.0	43.9	44.2	46.6	38.1	33.1	30.2
AlCl	26.5	23.7	23.6	28.7	22.96	22.5	30.2	22.7	22.2	30.4	41.6	42.0	43.1	45.5	47.8	33.5	41.0	35.2
GaCl	26.4	23.9	23.8	28.0	22.76	22.3	31.1	22.2	21.5	29.8	36.9	37.5	41.4	43.6	45.6	33.6	39.7	34.9
CCl_2	18.1	16.7	17.1	19.0	17.39	17.6	19.1	17.5	17.5	24.3	23.3	23.6	30.9	27.6	28.6	25.4	19.8	39.5
$SiCl_2$	21.9	20.0	20.1	23.2	20.72	20.5	23.5	20.8	20.6	28.0	28.1	28.9	39.3	39.6	42.8	37.3	36.7	30.6
$GeCl_2$	21.8	20.0	20.0	23.2	20.33	20.0	23.8	20.1	19.7	27.7	27.6	28.0	38.7	38.4	40.6	39.5	37.1	31.4
NCl	17.1	15.8	16.1	17.9	16.26	16.5	17.8	16.1	16.2	22.4	21.4	22.1	28.4	25.1	26.4	23.0	15.4	23.1
PCl	16.6	14.8	15.0	17.4	15.04	15.0	16.4	14.6	14.5	22.1	22.7	23.7	32.0	30.9	33.5	28.0	23.5	23.4
AsCl	16.0	14.1	14.3	17.4	14.29	14.2	15.9	13.7	13.5	21.5	22.4	23.5	32.5	32.1	35.4	31.4	25.6	27.3
O	14.6	13.2	13.6	15.3	13.34	13.5	14.9	12.8	12.7	18.8	17.6	18.2	24.3	20.5	21.9	18.2	8.96	37.9
S	13.3	12.3	12.5	14.1	12.75	12.8	13.6	12.3	12.2	19.6	19.1	19.5	27.8	25.1	26.1	22.3	18.6	36.6
Se	13.5	12.5	12.7	14.0	12.83	12.8	13.4	12.3	12.0	19.8	19.6	20.0	29.2	26.9	28.1	26.8	25.9	38.0

Table A3. Angle δ (°)

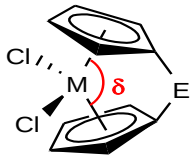

M = Ti, Zr, Hf, V, Nb, Ta, Cr, Mo, W

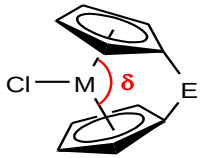

M = Mn, Tc, Re

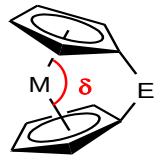

M = Fe, Ru, Os, Co, Rh, Ir

	M																	
E	**Ti**	**Zr**	**Hf**	**V**	**Nb**	**Ta**	**Cr**	**Mo**	**W**	**Mn**	**Tc**	**Re**	**Fe**	**Ru**	**Os**	**Co**	**Rh**	**Ir**
-	131.8	129.4	129.1	134.7	133.2	134.4	137.1	139.3	139.4	149.4	148.4	148.0	179.9	179.9	180.0	180.0	179.8	179.9
BCl	126.1	120.6	120.5	129.2	126.4	126.7	133.8	131.2	131.4	141.7	140.1	140.0	160.0	155.8	156.0	155.0	147.8	150.0
AlCl	131.6	127.6	127.5	134.1	134.7	134.9	135.7	139.9	140.2	148.8	145.7	145.6	170.0	166.9	167.1	165.1	161.2	163.0
GaCl	131.2	127.3	127.1	133.8	134.0	134.2	135.8	139.1	139.3	148.0	145.8	145.6	168.5	165.5	165.6	165.4	158.4	163.1
CCl_2	121.5	116.0	115.7	125.7	122.0	121.8	131.2	127.2	126.8	137.1	133.2	132.5	152.1	146.5	145.7	148.2	139.3	136.1
$SiCl_2$	129.8	125.6	125.5	133.0	131.8	131.9	137.1	120.5	129.8	146.3	144.0	143.5	166.0	162.8	163.9	159.3	152.4	158.4
$GeCl_2$	130.2	126.3	126.0	133.3	132.2	132.2	136.9	137.5	137.5	147.0	144.6	144.0	166.6	163.0	163.4	166.0	153.5	160.2
NCl	118.9	113.2	112.9	123.2	119.2	119.1	128.7	124.5	124.1	134.5	130.7	130.1	148.7	143.2	142.6	144.1	135.4	131.6
PCl	126.2	121.5	121.3	129.6	127.3	127.2	134.0	131.9	131.8	142.0	139.7	139.3	160.2	156.0	156.5	154.1	147.1	144.7
AsCl	127.4	123.1	122.9	130.5	128.8	128.8	134.8	133.4	133.3	134.9	141.3	140.9	162.5	158.9	159.9	159.8	149.4	156.8
O	116.6	110.6	110.4	120.9	116.6	116.5	126.6	122.1	121.6	132.0	127.8	127.2	145.7	140	139.4	141.5	132.6	130.8
S	124.6	119.7	119.5	128.5	125.4	125.4	133.5	130.2	130.0	140.4	137.4	136.8	157.2	152.1	151.5	153.9	145.4	142.3
Se	101.8	122.2	122.0	130.3	127.8	127.8	135.2	132.4	132.3	142.4	140.0	139.3	160.4	155.7	155.3	154.1	145.9	146.1

Table A4. Angle θ (°)

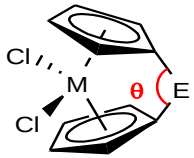

M = Ti, Zr, Hf, V, Nb, Ta, Cr, Mo, W

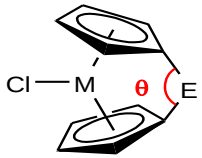

M = Mn, Tc, Re

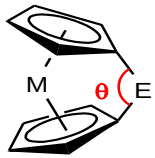

M = Fe, Ru, Os, Co, Rh, Ir

	M																	
E	**Ti**	**Zr**	**Hf**	**V**	**Nb**	**Ta**	**Cr**	**Mo**	**W**	**Mn**	**Tc**	**Re**	**Fe**	**Ru**	**Os**	**Co**	**Rh**	**Ir**
-	-	-	-	-	-	-	-	-	-	-	-	-	-	-	-	-	-	-
BCl	108.5	111.1	111.2	106.2	107.7	107.8	99.8	102.3	102.9	104.7	111.9	113.5	111.9	117.9	120.3	110.9	115.2	102.0
AlCl	96.3	98.7	98.7	94.9	95.8	95.5	93.6	92.0	91.8	92.8	101.7	101.8	100.2	107.5	109.6	96.2	108.0	93.4
GaCl	95.7	98.4	98.3	93.9	95.0	94.7	92.5	90.8	90.4	91.5	98.8	99.2	97.7	107.7	106.7	85.4	106.1	92.0
CCl_2	101.1	103.7	103.9	99.0	100.9	101.0	95.3	97.2	97.3	97.7	100.0	100.3	101.4	104.0	104.5	101.1	103.7	108.7
$SiCl_2$	95.2	98.2	98.2	93.2	95.5	95.3	90.0	91.8	91.9	92.4	95.6	96.4	99.0	105.3	108.9	100.4	106.1	91.9
$GeCl_2$	92.9	96.1	96.0	91.0	93.0	92.7	88.0	89.1	89.0	90.0	92.9	93.3	95.9	101.3	103.8	98.0	103.8	90.2
NCl	101.2	103.9	104.0	99.1	100.9	101.0	95.0	96.8	96.8	96.8	99.3	100.0	100.4	103.2	104.0	100.5	103.3	104.4
PCl	87.9	90.6	90.6	85.8	87.6	87.6	81.7	83.6	83.7	84.6	88.2	89.1	90.4	94.7	97.1	90.5	93.1	96.8
AsCl	84.5	87.3	87.3	82.7	84.3	84.2	78.5	80.3	90.2	81.4	85.1	86.0	87.7	92.5	95.5	90.6	91.2	86.8
O	100.0	102.4	102.6	97.8	99.1	99.1	93.3	94.5	94.4	94.1	96.4	96.9	97.7	100.0	100.5	97.4	100.0	107.3
S	87.2	90.3	90.4	95.01	87.4	87.4	81.0	83.2	83.4	84.0	86.9	87.2	88.4	91.27	92.1	88.0	91.3	95.6
Se	84.02	87.3	87.3	81.75	84.4	84.3	77.7	80.1	80.1	81.0	84.0	84.3	85.9	89.17	90.2	87.2	91.6	93.2

Table A5. Distance Cp-M (Å)

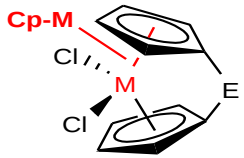

M = Ti, Zr, Hf, V, Nb, Ta, Cr, Mo, W

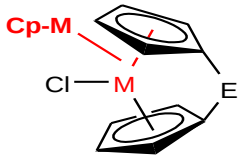

M = Mn, Tc, Re

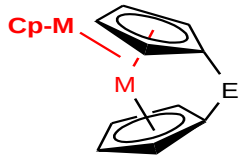

M = Fe, Ru, Os, Co, Rh, Ir

	M																	
E	**Ti**	**Zr**	**Hf**	**V**	**Nb**	**Ta**	**Cr**	**Mo**	**W**	**Mn**	**Tc**	**Re**	**Fe**	**Ru**	**Os**	**Co**	**Rh**	**Ir**
-	2.072	2.225	2.225	1.976	2.099	2.101	1.864	1.973	1.978	1.783	1.882	1.889	1.658	1.810	1.826	1.748	1.919	1.937
BCl	2.083	2.229	2.229	1.980	2.092	2.091	1.861	1.962	1.969	1.775	1.880	1.890	1.652	1.811	1.820	1.760	1.999	1.801
AlCl	2.088	2.237	2.237	1.991	2.112	2.111	1.923	1.988	1.992	1.800	1.897	1.908	1.657	1.812	1.829	1.639	1.930	1.806
GaCl	2.091	2.240	2.240	1.994	2.115	2.114	1.884	1.989	1.994	1.799	1.896	1.906	1.658	1.812	1.827	1.636	1.930	1.807
CCl_2	2.070	2.216	2.216	1.971	2.079	2.079	1.846	1.951	1.957	1.753	1.854	1.865	1.648	1.805	1.806	1.758	1.975	1.856
$SiCl_2$	2.088	2.237	2.237	1.991	2.103	2.103	1.879	1.978	1.983	1.786	1.879	1.887	1.653	1.806	1.821	1.744	1.915	1.805
$GeCl_2$	2.093	2.242	2.242	1.995	2.109	2.109	1.882	1.983	1.987	1.791	1.884	1.891	1.655	1.806	1.821	1.639	1.915	1.806
NCl	2.069	2.216	2.215	1.967	2.078	2.077	1.840	1.947	1.954	1.750	1.854	1.863	1.652	1.811	1.809	1.767	2.021	1.928
PCl	2.074	2.223	2.223	1.975	2.088	2.088	1.857	1.961	1.967	1.765	1.866	1.875	1.646	1.798	1.808	1.741	1.935	1.913
AsCl	2.075	2.225	2.225	1.976	2.092	2.092	1.861	1.964	1.970	1.769	1.869	1.879	1.646	1.798	1.811	1.636	1.923	1.802
O	2.066	2.214	2.213	1.965	2.077	2.076	1.835	1.944	1.951	1.745	1.850	1.857	1.654	1.816	1.810	1.775	2.065	1.939
S	2.075	2.221	2.221	1.975	2.086	2.086	1.849	1.955	1.962	1.760	1.860	1.868	1.645	1.799	1.804	1.753	1.945	1.857
Se	2.079	2.225	2.225	1.980	2.092	2.091	1.856	1.961	1.967	1.766	1.864	1.873	1.646	1.797	1.806	1.740	1.909	1.858

Table A6. Distance M-E (Å)

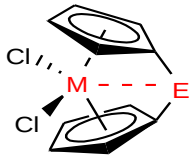

M = Ti, Zr, Hf, V, Nb, Ta, Cr, Mo, W

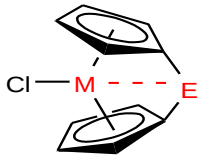

M = Mn, Tc, Re

M = Fe, Ru, Os, Co, Rh, Ir

	M																	
E	**Ti**	**Zr**	**Hf**	**V**	**Nb**	**Ta**	**Cr**	**Mo**	**W**	**Mn**	**Tc**	**Re**	**Fe**	**Ru**	**Os**	**Co**	**Rh**	**Ir**
-	-	-	-	-	-	-	-	-	-	-	-	-	-	-	-	-	-	-
BCl	2.800	2.904	2.912	2.769	2.869	2.867	2.806	2.845	2.837	2.618	2.468	2.431	2.312	2.297	2.273	2.373	2.414	2.696
AlCl	3.140	3.275	3.285	3.095	3.249	3.216	3.081	3.141	3.137	2.976	2.670	2.665	2.632	2.584	2.555	2.954	2.659	2.950
GaCl	3.168	3.293	3.304	3.137	3.250	2.248	3.079	3.177	3.177	3.017	2.800	2.795	2.693	2.649	2.625	2.979	2.752	2.988
CCl_2	2.983	3.092	3.098	2.910	2.977	2.981	2.827	2.891	2.898	2.727	2.788	2.797	2.520	2.597	2.620	2.545	2.661	2.755
$SiCl_2$	3.186	3.296	3.300	3.136	3.185	3.184	3.084	3.108	3.106	2.945	2.942	2.928	2.633	2.629	2.585	2.719	2.792	2.941
$GeCl_2$	3.258	3.363	3.374	3.207	3.262	3.264	3.158	3.185	3.185	3.018	3.012	3.009	2.712	2.726	2.703	2.655	2.855	2.999
NCl	2.947	3.058	3.066	2.875	2.945	2.947	2.792	2.861	2.869	2.699	2.747	2.753	2.507	2.574	2.593	2.539	2.635	2.742
PCl	3.270	3.383	3.391	3.221	3.293	3.296	3.177	3.226	3.229	3.050	3.036	3.028	2.779	2.913	2.792	2.853	2.947	3.010
AsCl	3.388	3.500	3.506	3.330	3.407	3.407	3.296	3.338	3.341	3.163	3.142	3.130	2.872	2.896	2.859	2.788	3.046	3.059
O	2.955	3.075	3.081	2.879	2.961	2.967	2.792	2.872	2.885	2.719	2.787	2.799	2.536	2.613	2.638	2.557	2.646	2.742
S	3.295	3.388	3.393	3.230	3.201	3.292	3.155	3.206	3.210	3.039	3.079	3.084	2.803	2.870	2.886	2.822	2.932	3.016
Se	3.414	3.495	3.500	3.352	3.391	3.391	3.280	3.321	3.325	3.153	3.181	3.187	2.896	2.954	2.965	2.968	3.087	3.099

Table A7. Distance C_{ipso}-M (Å)

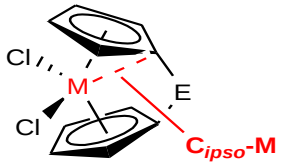

M = Ti, Zr, Hf, V, Nb, Ta, Cr, Mo, W

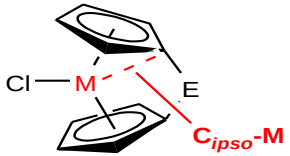

M = Mn, Tc, Re

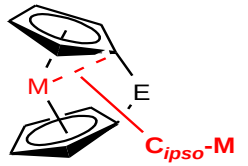

M = Fe, Ru, Os, Co, Rh, Ir

	M																	
E	**Ti**	**Zr**	**Hf**	**V**	**Nb**	**Ta**	**Cr**	**Mo**	**W**	**Mn**	**Tc**	**Re**	**Fe**	**Ru**	**Os**	**Co**	**Rh**	**Ir**
-	2.370	2.507	2.509	2.316	2.409	2.420	2.261	2.277	2.283	2.132	2.264	2.194	2.052	2.178	2.194	2.091	2.231	2.228
BCl	2.335	2.460	2.465	2.267	2.348	2.346	2.167	2.233	2.237	2.100	2.145	2.155	1.972	2.065	2.089	2.000	2.104	2.095
AlCl	2.390	2.519	2.523	2.330	2.399	2.392	2.297	2.275	2.268	2.163	2.208	2.217	2.037	2.146	2.172	2.020	2.204	2.148
GaCl	2.400	2.528	2.533	2.340	2.409	2.401	2.277	2.281	2.274	2.169	2.208	2.219	2.038	2.146	2.171	2.023	2.233	2.151
CCl_2	2.336	2.465	2.472	2.247	2.328	2.333	2.128	2.207	2.216	2.073	2.154	2.168	1.952	2.047	2.072	1.967	2.097	2.336
$SiCl_2$	2.381	2.509	2.514	2.308	2.375	2.372	2.212	2.254	2.254	2.134	2.190	2.197	2.008	2.112	2.141	2.093	2.241	2.114
$GeCl_2$	2.395	2.522	2.529	2.322	2.388	2.385	2.230	2.262	2.261	2.144	2.196	2.204	2.017	2.121	2.15	2.014	2.256	2.125
NCl	2.324	2.455	2.463	2.233	2.318	2.321	2.112	2.193	2.203	2.053	2.129	2.146	1.935	2.028	2.052	1.962	2.076	2.178
PCl	2.353	2.480	2.485	2.274	2.350	2.351	2.166	2.230	2.234	2.101	2.163	2.176	1.981	2.080	2.107	2.036	2.150	2.160
AsCl	2.367	2.494	2.499	2.290	2.362	2.361	2.181	2.238	2.240	2.114	2.175	2.188	1.996	2.100	2.131	2.065	2.183	2.108
O	2.320	2.455	2.463	2.226	2.314	2.318	2.097	2.181	2.192	2.039	2.126	2.142	1.924	2.016	2.042	1.940	2.054	2.098
S	2.351	2.475	2.481	2.262	2.340	2.342	2.139	2.215	2.221	2.085	2.161	2.173	1.963	2.059	2.083	1.973	2.110	2.353
Se	2.368	2.487	2.492	2.278	2.353	2.352	2.154	2.227	2.230	2.101	2.173	2.185	1.980	2.078	2.103	2.056	2.222	2.372

Table A8. Distance C_{ipso}-E (Å)

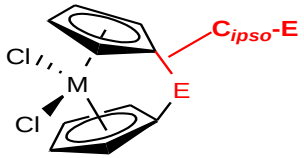

M = Ti, Zr, Hf, V, Nb, Ta, Cr, Mo, W

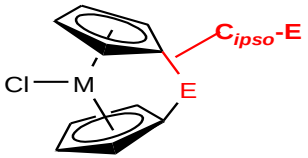

M = Mn, Tc, Re

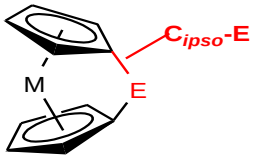

M = Fe, Ru, Os, Co, Rh, Ir

	M																	
E	**Ti**	**Zr**	**Hf**	**V**	**Nb**	**Ta**	**Cr**	**Mo**	**W**	**Mn**	**Tc**	**Re**	**Fe**	**Ru**	**Os**	**Co**	**Rh**	**Ir**
-	-	-	-	-	-	-	-	-	-	-	-	-	-	-	-	-	-	-
BCl	1.545	1.549	1.549	1.546	1.548	1.547	1.545	1.547	1.544	1.546	1.554	1.558	1.573	1.595	1.609	1.566	1.572	1.661
AlCl	1.931	1.936	1.936	1.933	1.929	1.928	1.940	1.922	1.92	1.925	1.943	1.943	1.953	1.978	1.991	2.068	1.970	2.109
GaCl	1.947	1.951	1.951	1.949	1.948	1.947	1.951	1.942	1.941	1.946	1.956	1.956	1.976	1.997	2.010	2.100	1.989	2.147
CCl_2	1.503	1.508	1.508	1.502	1.505	1.505	1.499	1.500	1.499	1.505	1.512	1.515	1.530	1.545	1.554	1.524	1.530	1.541
$SiCl_2$	1.848	1.851	1.852	1.849	1.849	1.847	1.846	1.844	1.842	1.846	1.856	1.857	1.871	1.893	1.907	1.871	1.885	2.006
$GeCl_2$	1.922	1.925	1.924	1.924	1.923	1.922	1.923	1.919	1.917	1.922	1.932	1.934	1.948	1.971	1.983	1.871	1.964	2.093
NCl	1.434	1.436	1.437	1.435	1.435	1.434	1.434	1.433	1.431	1.441	1.445	1.446	1.464	1.474	1.481	1.454	1.452	1.462
PCl	1.835	1.839	1.839	1.837	1.839	1.838	1.836	1.837	1.835	1.840	1.847	1.848	1.866	1.885	1.896	1.859	1.868	1.904
AsCl	1.951	1.955	1.955	1.953	1.955	1.954	1.951	1.952	1.951	1.956	1.963	1.964	1.984	2.007	2.020	1.844	1.990	2.066
O	1.392	1.393	1.393	1.392	1.395	1.395	1.392	1.394	1.395	1.405	1.409	1.412	1.429	1.439	1.447	1.419	1.418	1.426
S	1.785	1.789	1.789	1.786	1.789	1.788	1.784	1.786	1.784	1.793	1.800	1.803	1.820	1.837	1.845	1.814	1.822	1.821
Se	1.917	1.922	1.922	1.918	1.92	1.92	1.917	1.917	1.917	1.925	1.934	1.936	1.953	1.972	1.981	1.949	1.957	1.958

Table A9. ^{13}C NMR δC_{ipso} (ppm)

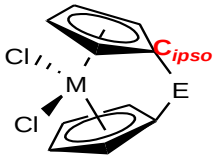

M = Ti, Zr, Hf, V, Nb, Ta, Cr, Mo, W

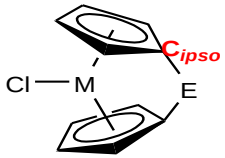

M = Mn, Tc, Re

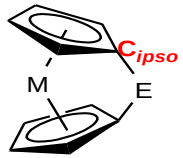

M = Fe, Ru, Os, Co, Rh, Ir

	M																	
E	**Ti**	**Zr**	**Hf**	**V**	**Nb**	**Ta**	**Cr**	**Mo**	**W**	**Mn**	**Tc**	**Re**	**Fe**	**Ru**	**Os**	**Co**	**Rh**	**Ir**
-	108.4	107.0	106.1	97.7	96.9	96.3	83.5	82.5	77.8	70.8	75.6	70.5	72.1	74.4	69.6	78.6	82.1	73.7
BCl	122.6	126.5	127.7	112.0	111.9	110.9	90.7	83.1	79.9	60.2	78.5	75.6	67.4	70.7	66.7	54.2	60.1	52.8
AlCl	118.2	119.5	121.2	105.9	111.6	110.8	87.7	96.3	92.6	65.9	81.5	76.6	56.6	56.9	53.7	76.3	59.4	76.1
GaCl	121.7	122.9	125.1	108.9	114.1	113.5	86.4	98.1	94.6	62.4	81.0	75.7	55.6	54.7	50.4	84.1	67.1	80.4
CCl_2	121.4	127.9	130.9	111.3	108.8	107.1	90.2	82.2	77.5	38.4	41.4	38.7	50.6	44.0	36.4	42.1	50.9	106
$SiCl_2$	110.6	115.2	117.8	100.9	101.4	99.96	85.8	81.9	77.3	46.3	49.5	45.4	43.2	39.5	35.6	67.5	80.0	60.0
$GeCl_2$	115.2	118.7	121.8	104.9	106.6	105.5	88.1	88.1	83.8	50.7	55.8	51.3	48.4	40.4	33.0	40.0	90.0	66.4
NCl	128.9	136.5	140.0	117.4	116.8	115.4	95.2	88.7	84.8	43.4	51.6	49.4	63.4	55.9	48.1	57.3	62.9	73.1
PCl	108.8	115.4	119.6	95.57	95.41	94.16	75.5	67.7	63.0	28.4	32.7	28.3	29.0	22.2	16.5	47.4	43.7	108
AsCl	110.7	116.6	120.9	96.31	96.93	95.63	77.9	69.8	65.0	32.0	34.7	30.0	29.5	22.2	16.8	60.7	57.9	42.0
O	136.0	144.2	147.9	124.5	123.6	122.1	102	94.7	90.6	46.4	52.6	50.4	71.7	62.3	53.3	65.5	70.0	132
S	106.5	111.3	115.9	95.68	91.27	89.84	74.7	65.2	60.9	17.8	18.1	15.8	27.5	16.8	9.46	21.6	30.1	115
Se	105.1	108.1	112.6	94.84	88.85	87.52	75.1	64.2	60.0	19.0	18.0	15.2	24.7	14.0	6.92	59.5	101.0	119

Table A10. Dipole Moment (debye)

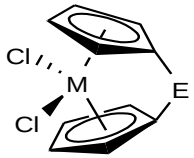

M = Ti, Zr, Hf, V, Nb, Ta, Cr, Mo, W

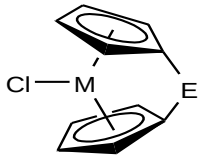

M = Mn, Tc, Re

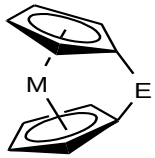

M = Fe, Ru, Os, Co, Rh, Ir

	M																	
E	**Ti**	**Zr**	**Hf**	**V**	**Nb**	**Ta**	**Cr**	**Mo**	**W**	**Mn**	**Tc**	**Re**	**Fe**	**Ru**	**Os**	**Co**	**Rh**	**Ir**
-	5.19	4.73	4.55	6.88	6.41	5.96	7.86	6.9	6.44	4.90	4.76	4.53	0	0.01	0	0	0.06	0.13
BCl	3.24	2.79	2.59	5.02	4.34	3.79	6.12	5.41	4.71	2.82	3.32	3.28	3.11	3.03	3.23	2.82	2.51	7.06
AlCl	3.90	3.21	3.01	5.63	4.51	4.11	7.03	5.39	4.82	3.00	4.59	4.26	2.91	3.09	3.27	8.34	2.77	7.85
GaCl	3.69	2.93	2.74	5.37	4.15	3.78	6.69	5.06	4.53	2.62	4.30	4.07	3.16	3.35	3.52	8.54	3.06	7.96
CCl_2	2.23	1.77	1.53	4.04	3.48	3.00	4.96	4.43	3.81	2.05	2.71	2.33	3.05	1.96	1.52	2.99	2.25	2.40
$SiCl_2$	2.37	1.57	1.36	4.16	3.24	2.82	5.25	4.16	3.58	1.69	2.13	2.03	3.89	3.63	3.88	3.98	3.70	8.71
$GeCl_2$	2.08	1.12	0.85	3.80	2.77	2.38	4.99	3.69	3.13	1.18	1.91	1.95	4.39	4.06	4.12	4.14	4.28	8.85
NCl	2.52	2.07	1.84	4.33	3.79	3.31	5.26	4.76	4.14	2.45	3.06	2.66	2.67	1.70	1.29	2.70	2.13	1.24
PCl	2.18	1.82	1.64	4.11	3.72	3.33	5.25	4.72	4.16	2.23	2.17	1.76	3.19	2.49	2.42	3.25	2.55	2.87
AsCl	2.50	2.39	2.22	4.30	4.26	3.89	5.57	5.20	4.70	2.78	2.31	1.78	3.12	2.55	2.57	3.22	2.61	9.96
O	2.92	2.49	2.26	4.65	4.21	3.79	5.58	5.19	4.63	3.10	3.77	3.30	1.97	1.06	0.61	2.01	1.58	1.52
S	2.93	2.47	2.25	4.70	4.16	3.78	5.63	5.14	4.62	2.81	3.30	3.15	2.31	1.50	1.17	2.25	1.67	2.12
Se	3.25	2.78	2.57	5.02	4.47	4.10	5.92	5.43	4.93	3.04	3.48	2.96	2.13	1.39	1.11	2.27	1.90	2.07

Table A11. Mulliken Charge on Metal

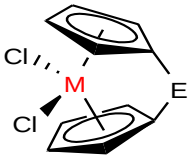

M = Ti, Zr, Hf, V, Nb, Ta, Cr, Mo, W

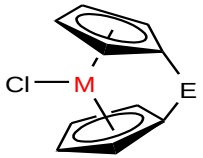

M = Mn, Tc, Re

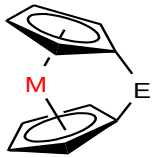

M = Fe, Ru, Os, Co, Rh, Ir

	M																	
E	**Ti**	**Zr**	**Hf**	**V**	**Nb**	**Ta**	**Cr**	**Mo**	**W**	**Mn**	**Tc**	**Re**	**Fe**	**Ru**	**Os**	**Co**	**Rh**	**Ir**
-	-0.131	0.037	0.022	-0.208	-0.234	-0.047	-0.597	-0.45	-0.112	-0.150	-0.232	0.058	-0.18	-0.027	0.207	-0.046	-0.049	0.121
BCl	-0.097	0.103	0.050	-0.198	-0.266	0.002	-0.576	-0.509	-0.061	-0.182	-0.372	0.064	-0.266	-0.251	-0.296	-0.045	-0.138	0.282
AlCl	-0.181	-0.002	-0.047	-0.249	-0.348	-0.129	-0.574	-0.552	-0.160	-0.172	-0.472	-0.101	-0.295	-0.294	0.165	-0.401	-0.266	0.173
GaCl	-0.182	0.006	-0.006	-0.250	-0.346	-0.100	-0.675	-0.558	-0.135	-0.182	-0.447	-0.039	-0.29	-0.285	0.193	-0.402	-0.251	0.188
CCl_2	-0.175	0.036	0.044	-0.283	-0.409	-0.003	-0.721	-0.72	-0.082	-0.301	-0.494	0.129	-0.297	-0.355	0.299	-0.085	-0.258	0.347
$SiCl_2$	-0.190	-0.050	-0.094	-0.269	-0.416	-0.168	-0.678	-0.648	-0.211	-0.252	-0.446	-0.032	-0.351	-0.347	0.150	-0.146	-0.316	0.185
$GeCl_2$	-0.156	-0.006	-0.050	-0.239	-0.365	-0.134	-0.647	-0.600	-0.189	-0.220	-0.415	-0.022	-0.329	-0.315	0.179	-0.117	-0.289	0.177
NCl	-0.058	0.150	0.096	-0.173	-0.240	0.019	-0.627	-0.533	-0.062	-0.208	-0.332	0.134	-0.182	-0.228	0.267	0.020	-0.085	-0.120
PCl	-0.134	0.009	-0.033	-0.217	-0.359	-0.130	-0.631	-0.586	-0.181	-0.201	-0.411	0.011	-0.266	-0.322	0.173	-0.061	-0.224	0.253
AsCl	-0.115	0.029	-0.014	-0.204	-0.316	-0.109	-0.604	-0.548	-0.171	-0.178	-0.374	0.026	-0.248	-0.281	0.174	-0.054	-0.202	0.189
O	-0.093	0.121	0.063	-0.197	-0.252	0.010	-0.659	-0.525	-0.072	-0.210	-0.306	0.146	-0.170	-0.223	0.245	0.035	-0.070	0.313
S	-0.121	-0.015	-0.092	-0.204	-0.384	-0.177	-0.647	-0.610	-0.210	-0.211	-0.426	-0.037	-0.251	-0.336	0.220	-0.025	-0.228	0.269
Se	-0,138	-0.041	-0.114	-0.213	-0.401	-0.186	-0.649	-0.621	-0.222	-0.214	-0.435	-0.034	-0.263	-0.326	0.210	-0.069	-0.287	0.255

Table A12. NBO Charge on Metal

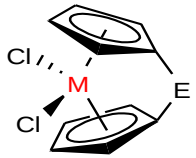

M = Ti, Zr, Hf, V, Nb, Ta, Cr, Mo, W

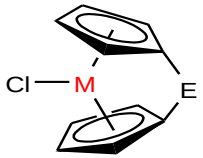

M = Mn, Tc, Re

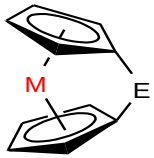

M = Fe, Ru, Os, Co, Rh, Ir

	M																	
E	**Ti**	**Zr**	**Hf**	**V**	**Nb**	**Ta**	**Cr**	**Mo**	**W**	**Mn**	**Tc**	**Re**	**Fe**	**Ru**	**Os**	**Co**	**Rh**	**Ir**
-	-0.416	0.756	0.923	-0.510	0.001	0.483	-1.015	-0.479	0.183	-0.451	-0.534	-0.047	-0.489	-0.457	-0.003	0.034	-0.078	0.169
BCl	-0.420	0.784	0.943	-0.531	0.028	0.518	-1.029	-0.446	0.232	-0.483	-0.529	-0.003	-0.511	-0.416	0.067	0.075	0.118	0.269
AlCl	-0.471	0.697	0.857	-0.554	-0.053	0.425	-0.947	-0.526	0.140	-0.454	-0.742	-0.239	-0.620	-0.649	-0.167	-0.297	-0.173	0.177
GaCl	-0.452	0.711	0.871	-0.531	-0.04	0.433	-1.049	-0.515	0.143	-0.446	-0.673	-0.177	-0.581	-0.607	-0.128	-0.289	-0.137	0.191
CCl_2	-0.409	0.804	0.960	-0.538	0.057	0.530	-1.057	-0.430	0.227	-0.528	-0.478	0.028	-0.439	-0.322	0.093	0.122	0.127	0.227
$SiCl_2$	-0.432	0.746	0.907	-0.523	-0.019	0.465	-1.031	-0.499	0.174	-0.470	-0.580	-0.072	-0.572	-0.548	-0.075	-0.005	-0.110	0.233
$GeCl_2$	-0.422	0.748	0.906	-0.514	-0.020	0.459	-1.022	-0.502	0.165	-0.459	-0.580	-0.076	-0.562	-0.542	-0.068	0.013	-0.114	0.224
NCl	-0.408	0.793	0.960	-0.549	0.061	0.531	-1.064	-0.424	0.223	-0.539	-0.459	0.041	-0.412	-0.286	0.120	0.142	0.195	0.233
PCl	-0.435	0.767	0.927	-0.547	0.007	0.486	-1.062	-0.481	0.182	-0.518	-0.549	-0.040	-0.519	-0.458	0.005	0.040	0.003	0.190
AsCl	-0.434	0.764	0.923	-0.543	-0.001	0.476	-1.059	-0.492	0.170	-0.511	-0.566	-0.061	-0.534	-0.496	-0.028	0.025	-0.035	0.248
O	-0.423	0.782	0.950	-0.560	0.052	0.520	-1.075	-0.429	0.218	-0.563	-0.462	0.036	-0.408	-0.278	0.116	0.149	0.217	0.239
S	-0.412	0.788	0.949	-0.537	0.030	0.508	-1.070	-0.463	0.205	-0.523	-0.521	-0.028	-0.486	-0.396	0.062	0.081	0.046	0.215
Se	-0.409	0.783	0.941	-0.526	0.019	0.495	-1.064	-0.477	0.191	-0.512	-0.541	-0.006	-0.508	-0.436	0.030	0.042	-0.041	0.200

Table A13. UV-vis Absorbtion λ_{max} (nm)

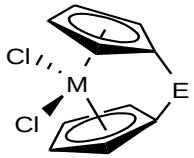

M = Ti, Zr, Hf, V, Nb, Ta, Cr, Mo, W

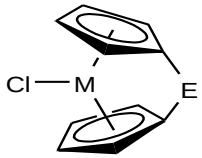

M = Mn, Tc, Re

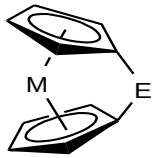

M = Fe, Ru, Os, Co, Rh, Ir

	M																	
E	**Ti**	**Zr**	**Hf**	**V**	**Nb**	**Ta**	**Cr**	**Mo**	**W**	**Mn**	**Tc**	**Re**	**Fe**	**Ru**	**Os**	**Co**	**Rh**	**Ir**
-	476	328	301	495	379	366	437	491	418	508	421	312	228	214	213	320	359	430
BCl	470	342	332	492	410	395	477	497	598	513	465	416	474	364	322	542	572	381
AlCl	472	331	308	496	405	400	462	515	357	513	459	411	461	329	328	409	448	336
GaCl	474	331	310	506	399	413	441	529	376	519	501	452	472	361	379	408	474	316
CCl_2	496	354	331	511	418	432	479	492	329	522	477	377	511	410	364	589	663	617
$SiCl_2$	479	346	323	514	407	386	466	523	303	519	427	288	470	341	293	561	500	301
$GeCl_2$	479	342	320	519	402	381	457	532	374	522	428	363	473	343	306	531	490	360
NCl	495	356	334	513	466	398	467	494	429	531	494	324	525	425	401	618	755	795
PCl	485	345	322	517	444	387	475	536	423	521	440	278	494	377	329	580	561	515
AsCl	485	343	320	518	404	382	470	546	484	520	431	298	489	367	384	575	563	333
O	494	353	327	516	413	391	457	491	429	537	530	334	536	437	390	621	798	703
S	494	347	323	531	407	386	488	538	477	530	465	258	500	390	352	567	588	535
Se	494	344	320	537	402	381	494	561	316	528	494	261	493	379	348	585	577	502

Table A14. HOMO Energy (eV)

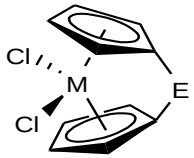

M = Ti, Zr, Hf, V, Nb, Ta, Cr, Mo, W

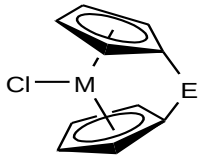

M = Mn, Tc, Re

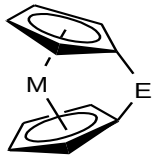

M = Fe, Ru, Os, Co, Rh, Ir

	M																	
E	**Ti**	**Zr**	**Hf**	**V**	**Nb**	**Ta**	**Cr**	**Mo**	**W**	**Mn**	**Tc**	**Re**	**Fe**	**Ru**	**Os**	**Co**	**Rh**	**Ir**
-	-7.12	-7.4	-7.37	-6.85	-5.58	-5.22	-6.37	-5.90	-5.68	-5.86	-5.63	-5.48	-6.03	-6.27	-6.11	-4.77	-3.99	-3.75
BCl	-7.36	-7.59	-7.54	-7.00	-5.80	-5.47	-6.55	-6.10	-5.91	-6.07	-6.00	-5.95	-6.51	-6.23	-6.14	-5.29	-4.92	-4.08
AlCl	-7.26	-7.51	-7.47	-6.96	-5.74	-5.37	-6.51	-5.98	-5.77	-6.05	-6.05	-5.91	-6.48	-6.55	-6.45	-4.77	-4.52	-4.75
GaCl	-7.30	-7.55	-7.51	-7.00	-5.77	-5.39	-6.50	-5.99	-5.78	-6.08	-5.98	-5.85	-6.46	-6.50	-6.39	-5.10	-4.57	-5.11
CCl_2	-7.38	-7.59	-7.56	-7.08	-5.92	-5.59	-6.73	-6.29	-6.10	-6.04	-5.57	-5.44	-6.37	-5.86	-6.12	-5.35	-4.92	-4.61
$SiCl_2$	-7.44	-7.70	-7.68	-7.13	-5.94	-5.59	-6.68	-6.22	-6.02	-6.24	-5.90	-5.81	-6.71	-6.61	-6.58	-5.39	-4.79	-5.12
$GeCl_2$	-7.49	-7.76	-7.73	-7.19	-5.98	-5.61	-6.72	-6.24	-6.04	-6.31	-5.98	-5.86	-6.75	-6.86	-6.54	-5.42	-4.86	-5.63
NCl	-7.34	-7.53	-7.49	-7.29	-5.89	-5.55	-6.70	-6.27	-6.07	-5.92	-5.52	-5.37	-6.19	-5.75	-5.54	-5.36	-5.08	-4.65
PCl	-7.38	-7.62	-7.59	-7.08	-5.88	-5.53	-6.66	-6.18	-5.98	-6.10	-5.78	-5.66	-6.44	-6.09	-5.82	-5.30	-4.76	-4.46
AsCl	-7.34	-7.59	-7.55	-7.05	-5.83	-5.47	-6.61	-6.12	-5.91	-6.08	-5.77	-5.65	-6.45	-6.13	-6.01	-5.25	-4.67	-4.85
O	-7.27	-7.45	-7.41	-6.97	-5.82	-5.47	-6.65	-6.22	-6.01	-5.75	-5.32	-5.17	-6.01	-5.58	-5.36	-5.28	-5.04	-4.67
S	-7.30	-7.56	-7.52	-7.02	-5.84	-5.49	-6.65	-6.17	-5.96	-5.97	-5.54	-5.43	-6.25	-5.94	-5.73	-5.20	-4.67	-4.47
Se	-7.28	-7.53	-7.50	-7.01	-5.81	-5.45	-6.61	-6.12	-5.90	-5.98	-5.57	-5.40	-6.27	-6.02	-5.82	-5.17	-4.60	-4.40

Table A15. LUMO Energy (eV)

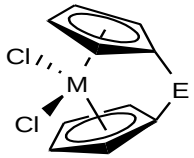

M = Ti, Zr, Hf, V, Nb, Ta, Cr, Mo, W

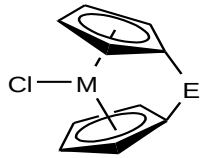

M = Mn, Tc, Re

M = Fe, Ru, Os, Co, Rh, Ir

	M																	
E	**Ti**	**Zr**	**Hf**	**V**	**Nb**	**Ta**	**Cr**	**Mo**	**W**	**Mn**	**Tc**	**Re**	**Fe**	**Ru**	**Os**	**Co**	**Rh**	**Ir**
-	-3.34	-2.62	-2.28	-3.16	-2.94	-2.86	-3.11	-2.32	-2.05	-2.55	-2.17	-1.75	-0.80	-0.40	0.19	-2.18	-1.81	-1.32
BCl	-3.76	-3.05	-2.94	-3.35	-3.47	-3.40	-3.28	-3.05	-2.93	-2.76	-2.51	-2.19	-1.62	-1.41	-1.30	-2.64	-2.56	-2.01
AlCl	-3.46	-2.78	-2.53	-3.30	-3.27	-3.15	-3.49	-2.58	-2.52	-2.80	-2.53	-2.20	-1.76	-1.80	-1.80	-2.97	-2.31	-1.89
GaCl	-3.51	-2.82	-2.69	-3.38	-3.26	-3.13	-3.37	-2.85	-2.79	-2.83	-2.64	-2.45	-2.06	-2.25	-2.30	-2.99	-2.34	-2.52
CCl_2	-3.75	-3.13	-2.89	-3.50	-3.58	-3.46	-3.44	-2.53	-2.30	-2.74	-2.12	-1.70	-1.42	-1.16	-1.00	-2.73	-2.58	-2.14
$SiCl_2$	-3.70	-3.16	-2.91	-3.58	-3.53	-3.41	-3.49	-2.60	-2.36	-2.95	-2.48	-2.08	-1.51	-1.22	-0.70	-2.83	-2.53	-2.36
$GeCl_2$	-3.75	-3.17	-2.93	-3.65	-3.53	-3.41	-3.57	-2.70	-2.42	-3.04	-2.63	-2.31	-1.56	-1.63	-1.70	-2.88	-2.56	-3.36
NCl	-3.70	-3.09	-2.87	-3.47	-3.55	-3.43	-3.37	-2.53	-2.42	-2.66	-2.30	-2.22	-1.57	-1.65	-1.70	-2.70	-2.63	-2.23
PCl	-3.67	-3.05	-2.80	-3.52	-3.47	-3.34	-3.40	-2.58	-2.36	-2.80	-2.29	-1.95	-1.92	-1.54	-1.10	-2.67	-2.46	-2.10
AsCl	-3.63	-2.99	-2.74	-3.49	-3.38	-3.24	-3.38	-2.78	-2.70	-2.78	-2.40	-2.34	-1.50	-1.96	-1.90	-2.62	-2.37	-2.46
O	-3.62	-2.94	-2.66	-3.43	-3.43	-3.27	-3.28	-2.38	-2.16	-2.53	-1.94	-1.51	-1.32	-1.18	-0.70	-2.63	-2.66	-2.19
S	-3.66	-3.01	-2.74	-3.52	-3.42	-3.29	-3.38	-2.55	-2.21	-2.71	-2.16	-1.91	-1.29	-1.10	-0.80	-2.62	-2.44	-2.11
Se	-3.63	-2.97	-2.69	-3.52	-3.36	-3.22	-3.37	-2.64	-2.31	-2.72	-2.21	-1.76	-1.33	-1.18	-1.10	-2.59	-2.33	-2.07

Table A16. HOMO-LUMO Gap (eV)

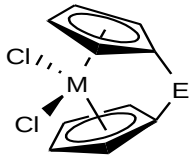

M = Ti, Zr, Hf, V, Nb, Ta, Cr, Mo, W

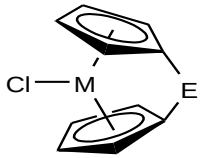

M = Mn, Tc, Re

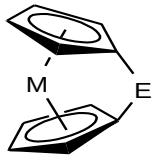

M = Fe, Ru, Os, Co, Rh, Ir

	M																	
E	**Ti**	**Zr**	**Hf**	**V**	**Nb**	**Ta**	**Cr**	**Mo**	**W**	**Mn**	**Tc**	**Re**	**Fe**	**Ru**	**Os**	**Co**	**Rh**	**Ir**
-	3.77	4.78	5.09	3.68	2.64	2.36	3.26	3.58	3.63	3.31	3.46	3.72	5.23	5.87	6.30	2.60	2.18	2.43
BCl	3.60	4.54	4.607	3.65	2.33	2.07	3.27	3.05	2.98	3.30	3.49	3.76	4.88	4.82	4.83	2.64	2.35	2.07
AlCl	3.8	4.72	4.937	3.65	2.46	2.22	3.02	3.40	3.25	3.25	3.51	3.70	4.72	4.74	4.64	1.79	2.21	2.86
GaCl	3.79	4.73	4.825	3.62	2.51	2.26	3.14	3.14	2.99	3.25	3.34	3.40	4.40	4.25	4.08	2.11	2.23	2.59
CCl_2	3.63	4.46	4.662	3.58	2.34	2.13	3.29	3.76	3.80	3.29	3.44	3.74	4.95	4.71	5.14	2.62	2.34	2.46
$SiCl_2$	3.74	4.55	4.763	3.56	2.41	2.17	3.19	3.62	3.66	3.29	3.43	3.73	5.19	5.39	5.85	2.57	2.26	2.76
$GeCl_2$	3.74	4.59	4.804	3.54	2.45	2.21	3.15	3.54	3.61	3.27	3.35	3.55	5.19	5.23	4.86	2.54	2.30	2.27
NCl	3.64	4.44	4.627	3.82	2.33	2.11	3.33	3.73	3.65	3.26	3.22	3.15	4.62	4.10	3.85	2.66	2.45	2.42
PCl	3.71	4.57	4.784	3.56	2.42	2.19	3.26	3.6	3.62	3.30	3.49	3.70	4.52	4.55	4.75	2.63	2.31	2.36
AsCl	3.71	4.59	4.807	3.56	2.46	2.23	3.23	3.34	3.21	3.29	3.37	3.31	4.95	4.18	4.09	2.63	2.30	2.40
O	3.65	4.51	4.757	3.54	2.39	2.20	3.38	3.84	3.86	3.22	3.38	3.67	4.69	4.40	4.68	2.64	2.39	2.48
S	3.65	4.55	4.784	3.51	2.42	2.20	3.27	3.62	3.75	3.26	3.38	3.52	4.96	4.84	4.94	2.59	2.23	2.36
Se	3.65	4.56	4.807	3.49	2.45	2.23	3.24	3.48	3.59	3.26	3.36	3.65	4.94	4.83	4.75	2.58	2.27	2.33

Table A17. Chemical Potential (μ)

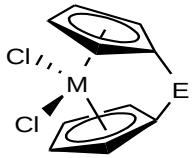

M = Ti, Zr, Hf, V, Nb, Ta, Cr, Mo, W

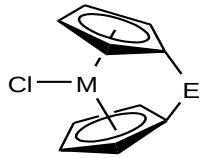

M = Mn, Tc, Re

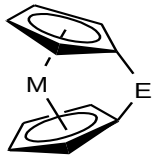

M = Fe, Ru, Os, Co, Rh, Ir

	M																	
E	**Ti**	**Zr**	**Hf**	**V**	**Nb**	**Ta**	**Cr**	**Mo**	**W**	**Mn**	**Tc**	**Re**	**Fe**	**Ru**	**Os**	**Co**	**Rh**	**Ir**
-	-5.23	-5.01	-4.83	-5.01	-4.26	-4.04	-4.74	-4.11	-3.86	-4.21	-3.90	-3.61	-3.42	-3.33	-2.96	-3.48	-2.9	-2.53
BCl	-5.56	-5.32	-5.24	-5.17	-4.64	-4.44	-4.92	-4.58	-4.42	-4.41	-4.25	-4.07	-4.06	-3.82	-3.72	-3.97	-3.74	-3.04
AlCl	-5.36	-5.14	-5.00	-5.13	-4.50	-4.26	-5.00	-4.28	-4.15	-4.42	-4.29	-4.06	-4.12	-4.17	-4.12	-3.87	-3.42	-3.32
GaCl	-5.40	-5.19	-5.10	-5.19	-4.51	-4.26	-4.93	-4.42	-4.28	-4.45	-4.31	-4.15	-4.26	-4.37	-4.35	-4.04	-3.46	-3.82
CCl_2	-5.56	-5.36	-5.23	-5.29	-4.75	-4.52	-5.09	-4.41	-4.20	-4.39	-3.85	-3.57	-3.89	-3.51	-3.55	-4.04	-3.75	-3.37
$SiCl_2$	-5.57	-5.43	-5.29	-5.36	-4.73	-4.50	-5.08	-4.41	-4.19	-4.60	-4.19	-3.95	-4.11	-3.91	-3.66	-4.11	-3.66	-3.74
$GeCl_2$	-5.62	-5.47	-5.33	-5.42	-4.76	-4.51	-5.15	-4.47	-4.23	-4.67	-4.30	-4.09	-4.15	-4.24	-4.12	-4.15	-3.71	-4.50
NCl	-5.52	-5.31	-5.18	-5.38	-4.72	-4.49	-5.03	-4.40	-4.25	-4.29	-3.91	-3.79	-3.88	-3.70	-3.62	-4.03	-3.86	-3.44
PCl	-5.53	-5.34	-5.20	-5.30	-4.67	-4.43	-5.03	-4.38	-4.17	-4.45	-4.03	-3.80	-4.18	-3.82	-3.44	-3.99	-3.61	-3.28
AsCl	-5.48	-5.29	-5.15	-5.27	-4.60	-4.36	-4.99	-4.45	-4.31	-4.43	-4.08	-3.99	-3.98	-4.05	-3.97	-3.94	-3.52	-3.65
O	-5.45	-5.20	-5.03	-5.20	-4.62	-4.37	-4.97	-4.30	-4.09	-4.14	-3.63	-3.34	-3.67	-3.38	-3.02	-3.95	-3.85	-3.43
S	-5.48	-5.28	-5.13	-5.27	-4.63	-4.39	-5.02	-4.36	-4.09	-4.34	-3.85	-3.67	-3.77	-3.52	-3.26	-3.91	-3.55	-3.29
Se	-5.45	-5.25	-5.10	-5.26	-4.58	-4.33	-4.99	-4.38	-4.11	-4.35	-3.89	-3.58	-3.80	-3.60	-3.44	-3.88	-3.47	-3.23

Table A18. Hardness (η)

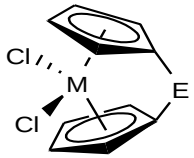

M = Ti, Zr, Hf, V, Nb, Ta, Cr, Mo, W

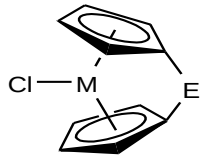

M = Mn, Tc, Re

M = Fe, Ru, Os, Co, Rh, Ir

	M																	
E	**Ti**	**Zr**	**Hf**	**V**	**Nb**	**Ta**	**Cr**	**Mo**	**W**	**Mn**	**Tc**	**Re**	**Fe**	**Ru**	**Os**	**Co**	**Rh**	**Ir**
-	1.89	2.39	2.55	1.84	1.32	1.18	1.63	1.79	1.82	1.65	1.73	1.86	2.62	2.93	3.15	1.3	1.09	1.22
BCl	1.80	2.27	2.30	1.83	1.17	1.03	1.63	1.52	1.49	1.65	1.74	1.88	2.44	2.41	2.42	1.32	1.18	1.04
AlCl	1.90	2.36	2.47	1.83	1.23	1.11	1.51	1.70	1.63	1.63	1.76	1.85	2.36	2.37	2.32	0.9	1.11	1.43
GaCl	1.89	2.36	2.41	1.81	1.25	1.13	1.57	1.57	1.49	1.62	1.67	1.70	2.20	2.13	2.04	1.05	1.11	1.30
CCl_2	1.82	2.23	2.33	1.79	1.17	1.06	1.65	1.88	1.90	1.65	1.72	1.87	2.47	2.35	2.57	1.31	1.17	1.23
$SiCl_2$	1.87	2.27	2.38	1.78	1.21	1.09	1.60	1.81	1.83	1.65	1.71	1.87	2.60	2.70	2.92	1.28	1.13	1.38
$GeCl_2$	1.87	2.30	2.40	1.77	1.22	1.10	1.57	1.77	1.81	1.63	1.68	1.77	2.60	2.61	2.43	1.27	1.15	1.13
NCl	1.82	2.22	2.31	1.91	1.17	1.06	1.67	1.87	1.82	1.63	1.61	1.58	2.31	2.05	1.92	1.33	1.23	1.21
PCl	1.86	2.29	2.39	1.78	1.21	1.09	1.63	1.8	1.81	1.65	1.75	1.85	2.26	2.28	2.37	1.32	1.15	1.18
AsCl	1.86	2.30	2.40	1.78	1.23	1.11	1.62	1.67	1.60	1.65	1.68	1.65	2.47	2.09	2.04	1.32	1.15	1.20
O	1.82	2.25	2.38	1.77	1.20	1.10	1.69	1.92	1.93	1.61	1.69	1.83	2.35	2.20	2.34	1.32	1.19	1.24
S	1.82	2.28	2.39	1.75	1.21	1.10	1.63	1.81	1.87	1.63	1.69	1.76	2.48	2.42	2.47	1.29	1.11	1.18
Se	1.83	2.28	2.40	1.75	1.23	1.12	1.62	1.74	1.79	1.63	1.68	1.82	2.47	2.42	2.37	1.29	1.14	1.16

Table A19. Sum of electronic and zero-point Energies of the Model Structures of Group 4-6 (hartree/particle)

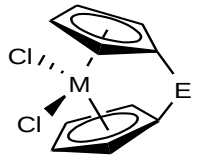

M = Ti, Zr, Hf, V, Nb, Ta, Cr, Mo, W

	M								
E	**Ti**	**Zr**	**Hf**	**V**	**Nb**	**Ta**	**Cr**	**Mo**	**W**
-	-2159.482003	-1356.959841	-1357.92913	-2253.996536	-1366.853703	-1366.897165	-2354.4213	-1378.05831	-1376.955586
BCl	-2643.792996	-1841.269102	-1842.237998	-2738.305043	-1851.16279	-1851.207574	-2838.730171	-1862.369719	-1861.267416
AlCl	-2861.561515	-2059.040138	-2060.009094	-2956.074499	-2068.933943	-2068.978376	-3056.496772	-2080.137875	-2079.035622
GaCl	-4544.450484	-3741.929385	-3742.898371	-4638.963106	-3751.822297	-3751.866401	-4739.385705	-3763.025363	-3761.922551
CCl_2	-3117.564812	-2315.03874	-2316.007892	-3212.078238	-2324.93495	-2324.979646	-3312.506361	-2336.144045	-2335.041643
$SiCl_2$	-3369.239003	-2566.718003	-2567.687152	-3463.750974	-2576.611989	-2576.656795	-3564.174279	-2587.816602	-2586.714631
$GeCl_2$	-5157.21751	-4354.697009	-4355.666182	-5251.729214	-4364.590215	-4364.634691	-5352.152002	-4375.79384	-4374.691432
NCl	-2673.635169	-1871.108415	-1872.077622	-2768.148892	-1881.004419	-1881.049095	-2868.577769	-1892.214077	-1891.111547
PCl	-2960.481512	-2157.957844	-2158.927037	-3054.994536	-2167.852615	-2167.897247	-3155.420683	-2179.059434	-2177.956997
AsCl	-4855.502173	-4052.978992	-4053.948213	-4950.015333	-4062.873582	-4062.918005	-5050.441001	-4074.07982	-4072.977162
O	-2233.617174	-1431.089521	-1432.058842	-2328.131429	-1440.985638	-1441.029924	-2428.561259	-1452.196166	-1451.093148
S	-2556.767797	-1754.243688	-1755.213022	-2651.280877	-1764.13877	-1764.183486	-2751.708055	-1775.346358	-1774.244065
Se	-4560.618865	-3758.09589	-3759.065228	-4655.13173	-3767.990517	-3768.035094	-4755.558007	-3779.197049	-3778.094586

Table A20. Sum of electronic and zero-point Energies of the Model Structures of Group 7-9 (hartree/particle)

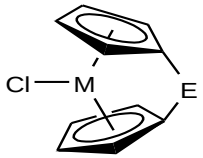

M = Mn, Tc, Re

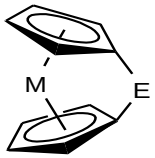

M = Fe, Ru, Os, Co, Rh, Ir

	M								
E	**Mn**	**Tc**	**Re**	**Fe**	**Ru**	**Os**	**Co**	**Rh**	**Ir**
-	-2000.400682	-930.097069	-927.579152	-1652.634312	-483.66792	-479.452247	-1771.713022	-499.300117	-493.080547
BCl	-2484.703609	-1414.398741	-1411.88225	-2136.903233	-967.922493	-963.701269	-2255.982909	-983.56014	-977.329247
AlCl	-2702.474845	-1632.17864	-1629.66257	-2354.697533	-1185.726954	-1181.51011	-2473.752898	-1201.35686	-1195.15776
GaCl	-4385.363141	-3315.063698	-3312.5464	-4037.583906	-2868.611742	-2864.3934	-4156.64799	-2884.24341	-2878.05322
CCl_2	-2958.476457	-1888.162894	-1885.64221	-2610.666591	-1441.677656	-1437.45075	-2729.748581	-1457.32105	-1451.08733
$SiCl_2$	-3210.154788	-2139.848767	-2137.33081	-2862.369454	-1693.392672	-1689.17324	-2981.445809	-1709.02434	-1702.78713
$GeCl_2$	-4998.132913	-3927.827591	-3925.30937	-4650.350371	-3481.374497	-3477.15457	-4769.427215	-3497.00717	-3490.79568
NCl	-2514.543524	-1444.228649	-1441.70804	-2166.72763	-997.737673	-993.509739	-2285.812585	-1013.38677	-1007.15073
PCl	-2801.395782	-1731.086911	-1728.56814	-2453.598911	-1284.616086	-1280.39316	-2572.67839	-1300.25367	-1294.02527
AsCl	-4696.416873	-3626.109452	-3623.59084	-4348.624241	-3179.643913	-3175.4223	-4467.703006	-3195.27952	-3189.06025
O	-2074.521924	-1004.205304	-1001.68371	-1726.701256	-557.71059	-553.481826	-1845.787521	-573.362017	-567.123235
S	-2397.68067	-1327.36915	-3328.70363	-2049.879379	-880.895289	-876.671238	-2168.959631	-896.534401	-890.306646
Se	-4401.532936	-3331.22305	-1324.84931	-4053.737334	-2884.755835	-2880.53314	-4172.816067	-2900.39258	-2894.16731

APPENDIX B: Electrostatic Potential Maps, Frontier Molecular Orbitals And Orbital Energies of the Model Molecules

Ti Complexes

MOLECULE	ESP	HOMO-2 (hartrees)	HOMO-1 (hartrees)	HOMO (hartrees)	LUMO (hartrees)	LUMO+1 (hartrees)	LUMO+2 (hartrees)
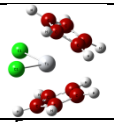	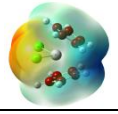	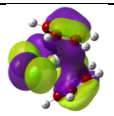	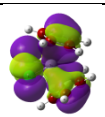	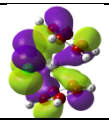		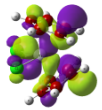	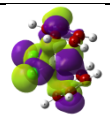
$[Ti(\eta^5\text{-}C_5H_5)_2Cl_2]$		-0.28019	-0.27255	-0.26148	-0.12284	-0.08698	-0.08547
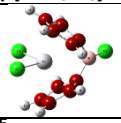	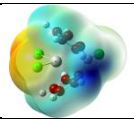	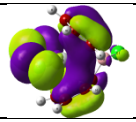	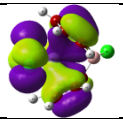	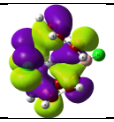	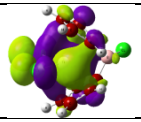	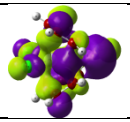	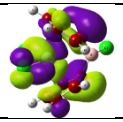
$[Ti\{(\eta^5\text{-}C_5H_4)_2BCl\}Cl_2]$		-0.29132	-0.28082	-0.27052	-0.13083	-0.10386	-0.09533
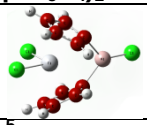	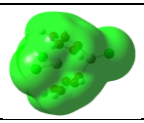	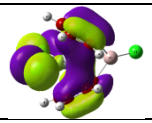	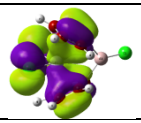	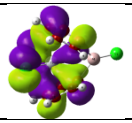	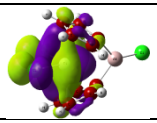	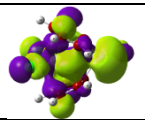	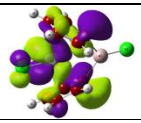
$[Ti\{(\eta^5\text{-}C_5H_4)_2AlCl\}Cl_2]$		-0.28566	-0.27680	-0.26684	-0.12704	-0.09821	-0.09218
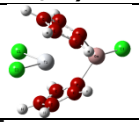	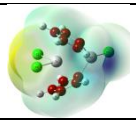	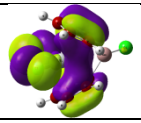	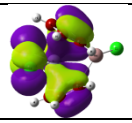	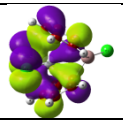	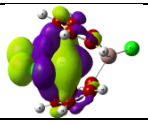	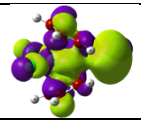	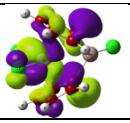
$[Ti\{(\eta^5\text{-}C_5H_4)_2GaCl\}Cl_2]$		-0.28700	-0.27855	-0.26820	-0.12899	-0.10137	-0.09493
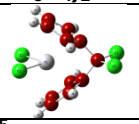	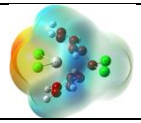	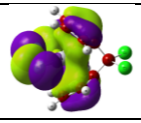	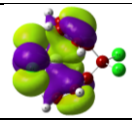	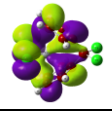	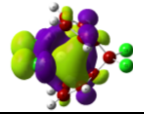	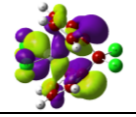	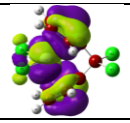
$[Ti\{(\eta^5\text{-}C_5H_4)_2CCl_2\}Cl_2]$		-0.29522	-0.28460	-0.27119	-0.13773	-0.10077	-0.09095
$[Ti\{(\eta^5\text{-}C_5H_4)_2SiCl_2\}Cl_2]$		-0.29284	-0.28412	-0.27348	-0.13605	-0.10308	-0.09860

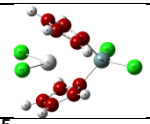	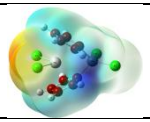	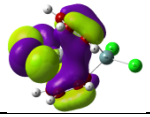	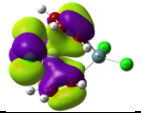	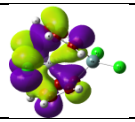	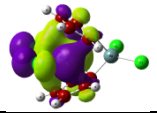	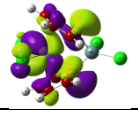	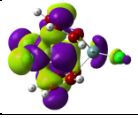
$[Ti\{(\eta^5\text{-}C_5H_4)_2GeCl_2\}Cl_2]$		-0.29447	-0.28591	-0.27536	-0.13782	-0.10591	-0.10083
	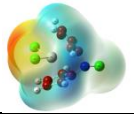	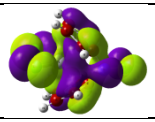	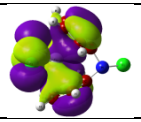	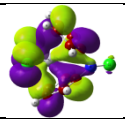	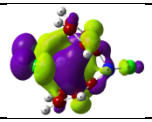	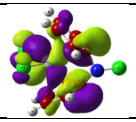	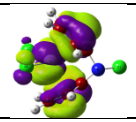
$[Ti\{(\eta^5\text{-}C_5H_4)_2NCl\}Cl_2]$		-0.29368	-0.28342	-0.26966	-0.13604	-0.09998	-0.09039
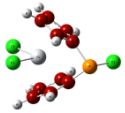	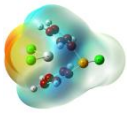	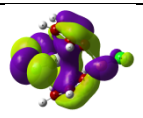	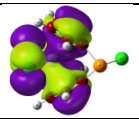	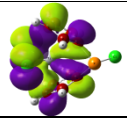	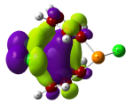	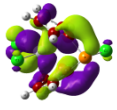	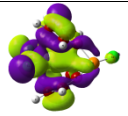
$[Ti\{(\eta^5\text{-}C_5H_4)_2PCl\}Cl_2]$		-0.29241	-0.28347	-0.27133	-0.13488	-0.10164	-0.09470
	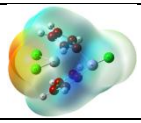	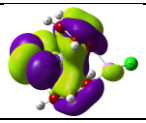	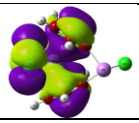	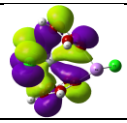	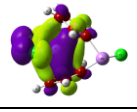	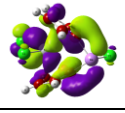	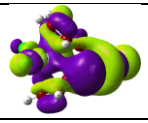
$[Ti\{(\eta^5\text{-}C_5H_4)_2AsCl\}Cl_2]$		-0.29090	-0.28193	-0.26977	-0.13325	-0.10075	-0.09221
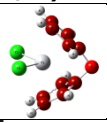	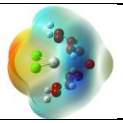	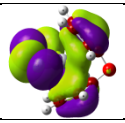		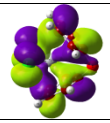	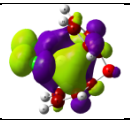	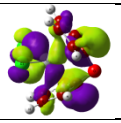	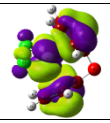
$[Ti\{(\eta^5\text{-}C_5H_4)_2O\}Cl_2]$		-0.29355	-0.28163	-0.26712	-0.13311	-0.09803	-0.08874
$[Ti\{(\eta^5\text{-}C_5H_4)_2S\}Cl_2]$		-0.29037	-0.28150	-0.26840	-0.13437	-0.10185	-0.08850
$[Ti\{(\eta^5\text{-}C_5H_4)_2Se\}Cl_2]$		-0.28032	-0.27874	-0.26751	-0.13334	-0.10265	-0.08803

Zr Complexes

MOLECULE	ESP MAP	HOMO-2 (hartrees)	HOMO-1 (hartrees)	HOMO (hartrees)	LUMO (hartrees)	LUMO+1 (hartrees)	LUMO+2 (hartrees)
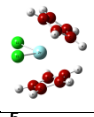	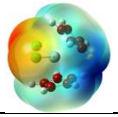			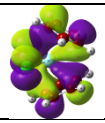	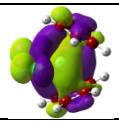	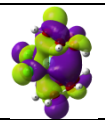	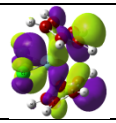
$[Zr(\eta^5\text{-}C_5H_5)_2Cl_2]$		-0.28788	-0.28275	-0.27204	-0.09623	-0.06068	-0.04957
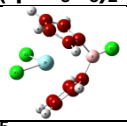	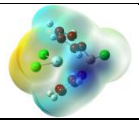	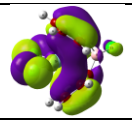	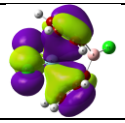	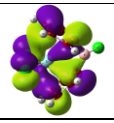	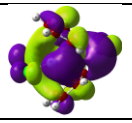	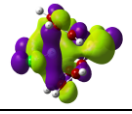	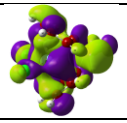
$[Zr\{(\eta^5\text{-}C_5H_4)_2BCl\}Cl_2]$		-0.30011	-0.29110	-0.27872	-0.11200	-0.09485	-0.05904
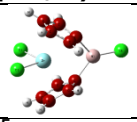	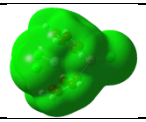	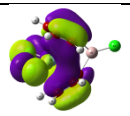	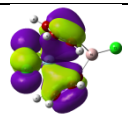	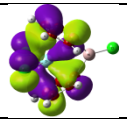	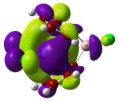	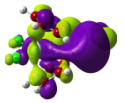	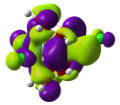
$[Zr\{(\eta^5\text{-}C_5H_4)_2AlCl\}Cl_2]$		-0.29321	-0.28664	-0.27587	-0.10227	-0.09126	-0.06748
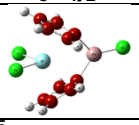	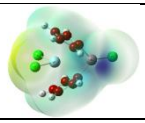	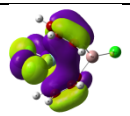	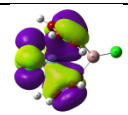	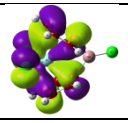	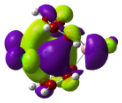	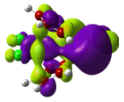	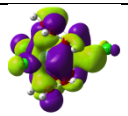
$[Zr\{(\eta^5\text{-}C_5H_4)_2GaCl\}Cl_2]$		-0.29494	-0.28849	-0.27747	-0.10366	-0.09906	-0.06798
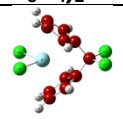	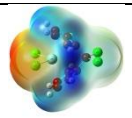	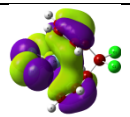	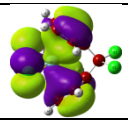	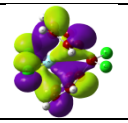	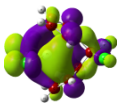	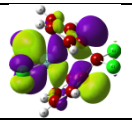	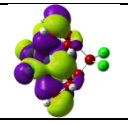
$[Zr\{(\eta^5\text{-}C_5H_4)_2CCl_2\}Cl_2]$		-0.30450	-0.29487	-0.27904	-0.11509	-0.06391	-0.06271
$[Zr\{(\eta^5\text{-}C_5H_4)_2SiCl_2\}Cl_2]$		-0.30091	-0.29462	-0.28313	-0.11600	-0.06792	-0.06719

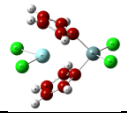	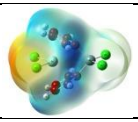	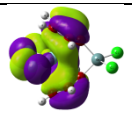	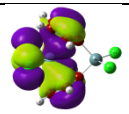	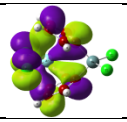	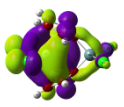	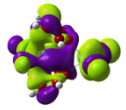	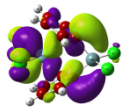
$[Zr\{(\eta^5\text{-}C_5H_4)_2GeCl_2\}Cl_2]$		-0.30274	-0.29629	-0.28529	-0.11649	-0.07262	-0.06942
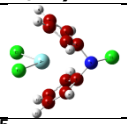	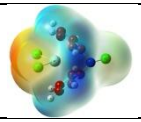	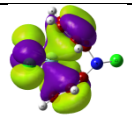	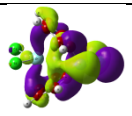	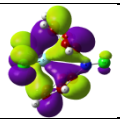	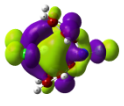	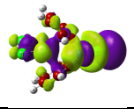	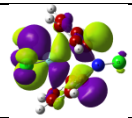
$[Zr\{(\eta^5\text{-}C_5H_4)_2NCl\}Cl_2]$		-0.29345	-0.29153	-0.27681	-0.11370	-0.0814	-0.06368
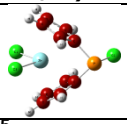	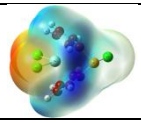	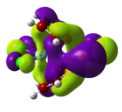	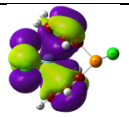		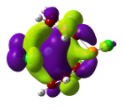	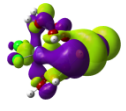	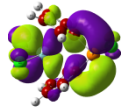
$[Zr\{(\eta^5\text{-}C_5H_4)_2PCl\}Cl_2]$		-0.29805	-0.29367	-0.28013	-0.11210	-0.08009	-0.06775
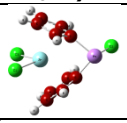	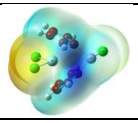	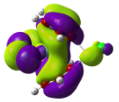	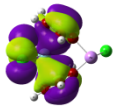	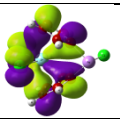	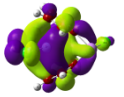	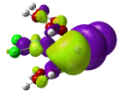	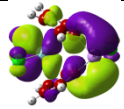
$[Zr\{(\eta^5\text{-}C_5H_4)_2AsCl\}Cl_2]$		-0.29887	-0.29202	-0.27875	-0.11000	-0.09264	-0.06827
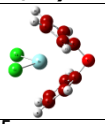	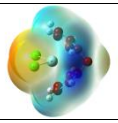	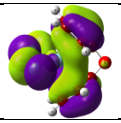		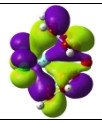	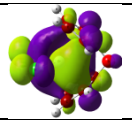		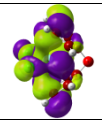
$[Zr\{(\eta^5\text{-}C_5H_4)_2O\}Cl_2]$		-0.30313	-0.29131	-0.27375	-0.10813	-0.06309	-0.05714
$[Zr\{(\eta^5\text{-}C_5H_4)_2S\}Cl_2]$		-0.29208	-0.28921	-0.27780	-0.11059	-0.06853	-0.06062
$[Zr\{(\eta^5\text{-}C_5H_4)_2Se\}Cl_2]$		-0.29096	-0.27760	-0.27675	-0.10917	-0.07178	-0.06052

Hf Complexes

MOLECULE	ESP MAP	HOMO-2 (hartrees)	HOMO-1 (hartrees)	HOMO (hartrees)	LUMO (hartrees)	LUMO+1 (hartrees)	LUMO+2 (hartrees)
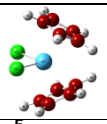	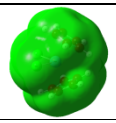	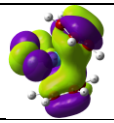	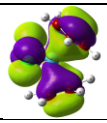	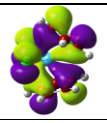	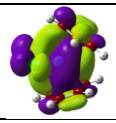	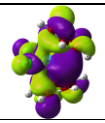	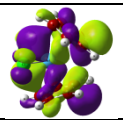
$[Hf(\eta^5\text{-}C_5H_5)_2Cl_2]$		-0.28834	-0.28213	-0.27085	-0.08379	-0.05284	-0.03389
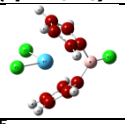	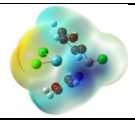	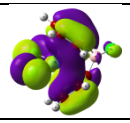	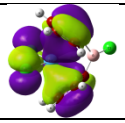		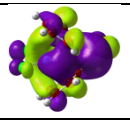	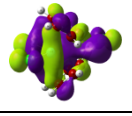	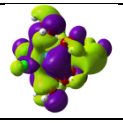
$[Hf\{(\eta^5\text{-}C_5H_4)_2BCl\}Cl_2]$		-0.30058	-0.29046	-0.27727	-0.10798	-0.08557	-0.05197
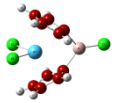	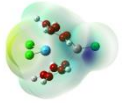	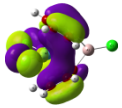	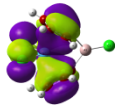	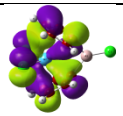	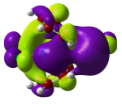	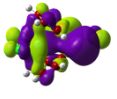	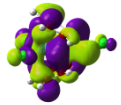
$[Hf\{(\eta^5\text{-}C_5H_4)_2AlCl\}Cl_2]$		-0.29361	-0.28601	-0.27452	-0.09309	-0.08862	-0.06016
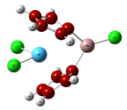	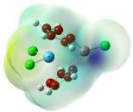	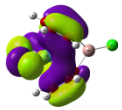	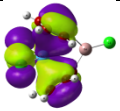	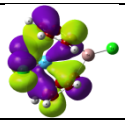	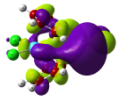	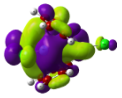	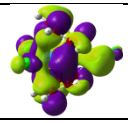
$[Hf\{(\eta^5\text{-}C_5H_4)_2GaCl\}Cl_2]$		-0.29537	-0.28784	-0.27610	-0.09878	-0.09180	-0.06050
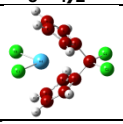	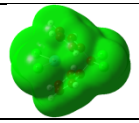	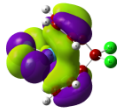	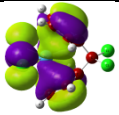	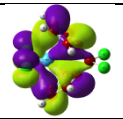	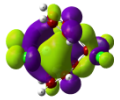	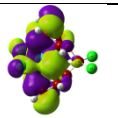	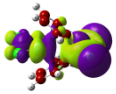
$[Hf\{(\eta^5\text{-}C_5H_4)_2CCl_2\}Cl_2]$		-0.30526	-0.29407	-0.27770	-0.10638	-0.05502	-0.05009
$[Hf\{(\eta^5\text{-}C_5H_4)_2SiCl_2\}Cl_2]$		-0.30155	-0.29398	-0.28209	-0.10705	-0.05985	-0.05201

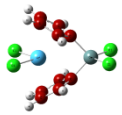	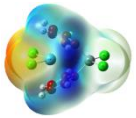	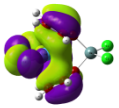	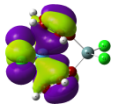	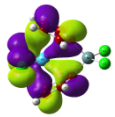	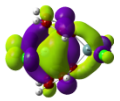	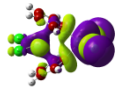	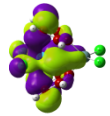
$[Hf\{(\eta^5\text{-}C_5H_4)_2GeCl_2\}Cl_2]$		-0.30340	-0.29569	-0.28413	-0.10760	-0.06762	-0.06181
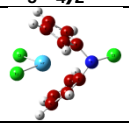	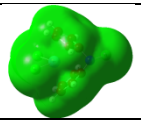	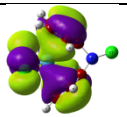	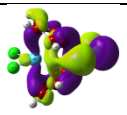	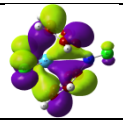	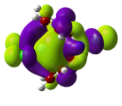	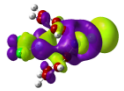	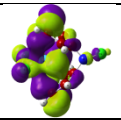
$[Hf\{(\eta^5\text{-}C_5H_4)_2NCl\}Cl_2]$		-0.29254	-0.29022	-0.27534	-0.10531	-0.07663	-0.05222
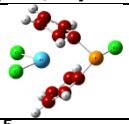	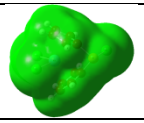	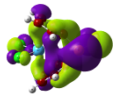	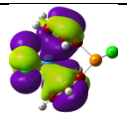		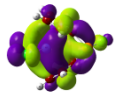	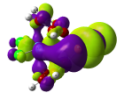	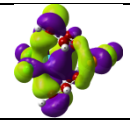
$[Hf\{(\eta^5\text{-}C_5H_4)_2PCl\}Cl_2]$		-0.29741	-0.29296	-0.27882	-0.10301	-0.07726	-0.05533
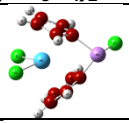	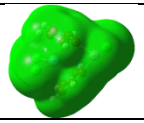	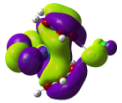	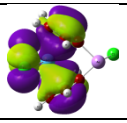	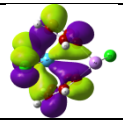	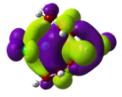	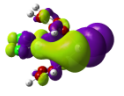	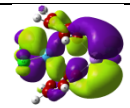
$[Hf\{(\eta^5\text{-}C_5H_4)_2AsCl\}Cl_2]$		-0.29940	-0.29129	-0.27749	-0.10085	-0.09036	-0.05629
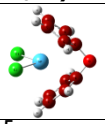	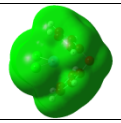	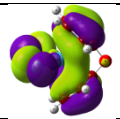		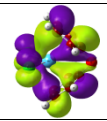	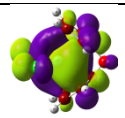	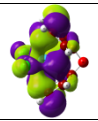	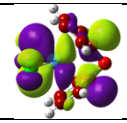
$[Hf\{(\eta^5\text{-}C_5H_4)_2O\}Cl_2]$		-0.30385	-0.29032	-0.27242	-0.09761	-0.04933	-0.04576
$[Hf\{(\eta^5\text{-}C_5H_4)_2S\}Cl_2]$		-0.29129	-0.28804	-0.27651	-0.10069	-0.05499	-0.05236
$[Hf\{(\eta^5\text{-}C_5H_4)_2Se\}Cl_2]$		-0.29020	-0.27639	-0.27569	-0.09903	-0.06166	-0.05217

V Complexes*

MOLECULE	ESP MAP	HOMO-2 (hartrees)	HOMO-1 (hartrees)	HOMO (hartrees)	LUMO (hartrees)	LUMO+1 (hartrees)	LUMO+2 (hartrees)
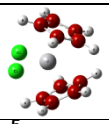	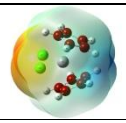	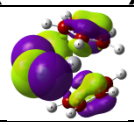	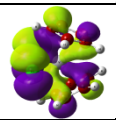	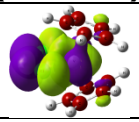	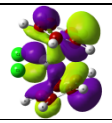	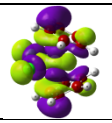	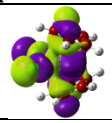
$[V(\eta^5\text{-}C_5H_5)_2Cl_2]$		-0.26704	-0.25981	-0.25164	-0.11625	-0.10385	-0.09903
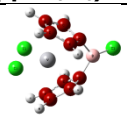	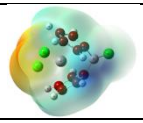	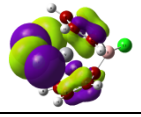	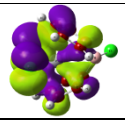	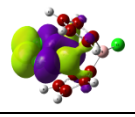	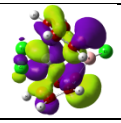	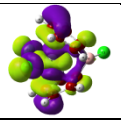	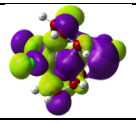
$[V\{(\eta^5\text{-}C_5H_4)_2BCl\}Cl_2]$		-0.27592	-0.26811	-0.25715	-0.12299	-0.11546	-0.10962
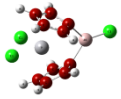	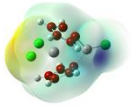	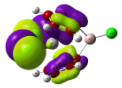	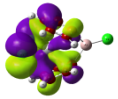	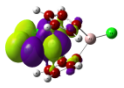	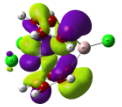	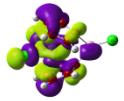	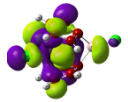
$[V\{(\eta^5\text{-}C_5H_4)_2AlCl\}Cl_2]$		-0.27295	-0.26526	-0.25562	-0.12131	-0.11037	-0.10721
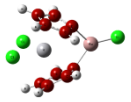	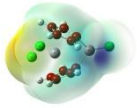	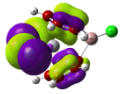	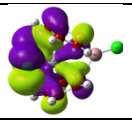	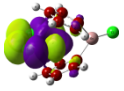	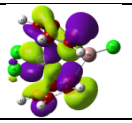	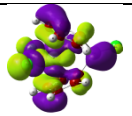	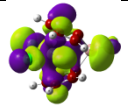
$[V\{(\eta^5\text{-}C_5H_4)_2GaCl\}Cl_2]$		-0.27384	-0.26614	-0.25721	-0.12425	-0.11268	-0.10786
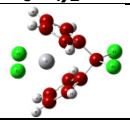	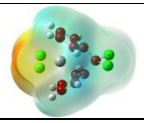	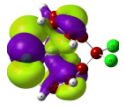	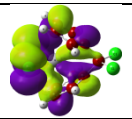	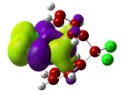	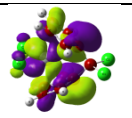	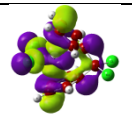	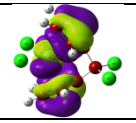
$[V\{(\eta^5\text{-}C_5H_4)_2CCl_2\}Cl_2]$		-0.27940	-0.26916	-0.26001	-0.12850	-0.12153	-0.10702
$[V\{(\eta^5\text{-}C_5H_4)_2SiCl_2\}Cl_2]$		-0.27857	-0.27041	-0.26213	-0.13146	-0.12061	-0.11051

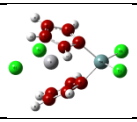	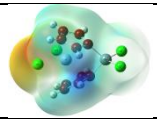	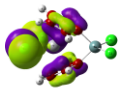	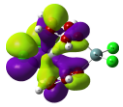	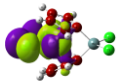	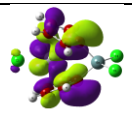	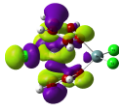	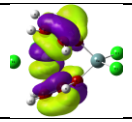
$[V\{(\eta^5\text{-}C_5H_4)_2GeCl_2\}Cl_2]$		-0.28017	-0.27215	-0.26413	-0.13421	-0.12236	-0.11321
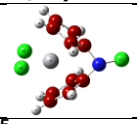	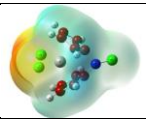	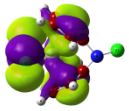	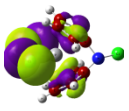	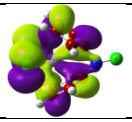	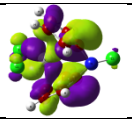	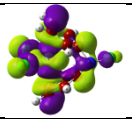	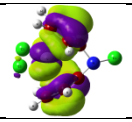
$[V\{(\eta^5\text{-}C_5H_4)_2NCl\}Cl_2]$		-0.27713	-0.27398	-0.26786	-0.12755	-0.11941	-0.10652
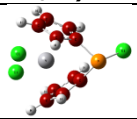	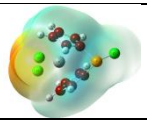	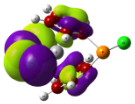	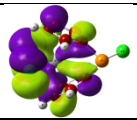	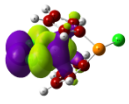	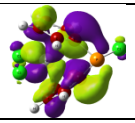	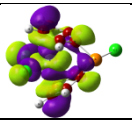	
$[V\{(\eta^5\text{-}C_5H_4)_2PCl\}Cl_2]$		-0.27797	-0.26879	-0.26004	-0.12927	-0.11855	-0.10751
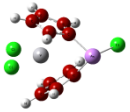	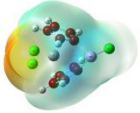	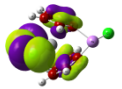	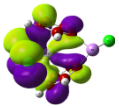	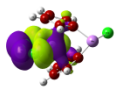	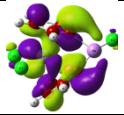	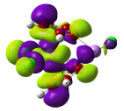	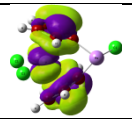
$[V\{(\eta^5\text{-}C_5H_4)_2AsCl\}Cl_2]$		-0.27661	-0.26771	-0.25900	-0.12831	-0.11587	-0.10656
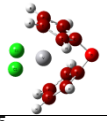	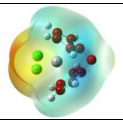	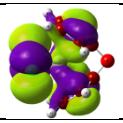	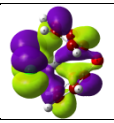	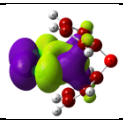	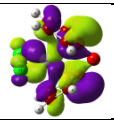	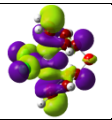	
$[V\{(\eta^5\text{-}C_5H_4)_2O\}Cl_2]$		-0.27703	-0.26646	-0.25620	-0.12605	-0.11629	-0.10521
$[V\{(\eta^5\text{-}C_5H_4)_2S\}Cl_2]$		-0.27648	-0.26576	-0.25807	-0.12922	-0.11945	-0.10433
$[V\{(\eta^5\text{-}C_5H_4)_2Se\}Cl_2]$		-0.27525	-0.26438	-0.25762	-0.12934	-0.11904	-0.10340

*HOMO orbitals are singly occupied.

Nb Complexes*

MOLECULE	ESP MAP	HOMO-2 (hartrees)	HOMO-1 (hartrees)	HOMO (hartrees)	LUMO (hartrees)	LUMO+1 (hartrees)	LUMO+2 (hartrees)
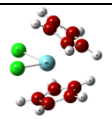	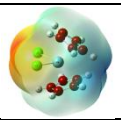	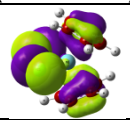	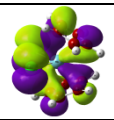	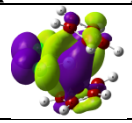	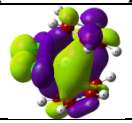		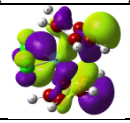
$[Nb(\eta^5\text{-}C_5H_5)_2Cl_2]$		-0.27933	-0.27093	-0.20496	-0.10812	-0.06858	-0.06217
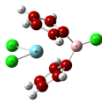	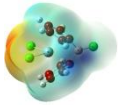	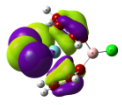	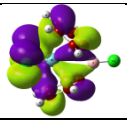	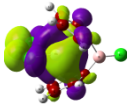	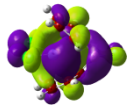	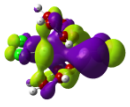	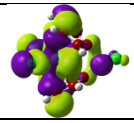
$[Nb\{(\eta^5\text{-}C_5H_4)_2BCl\}Cl_2]$		-0.28899	-0.27894	-0.21331	-0.12758	-0.09957	-0.07321
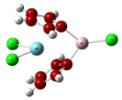	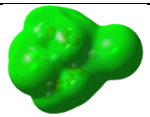	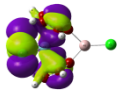	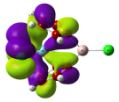	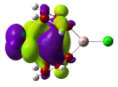	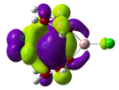	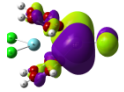	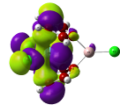
$[Nb\{(\eta^5\text{-}C_5H_4)_2AlCl\}Cl_2]$		-0.28405	-0.27374	-0.21076	-0.12030	-0.09319	-0.07093
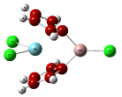	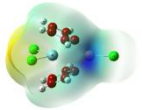	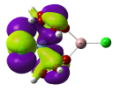	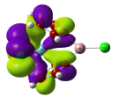	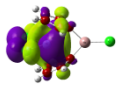	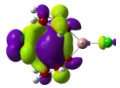	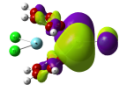	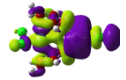
$[Nb\{(\eta^5\text{-}C_5H_4)_2GaCl\}Cl_2]$		-0.28562	-0.27492	-0.21186	-0.11969	-0.10266	-0.07323
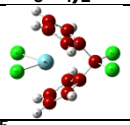	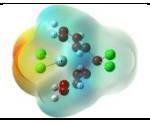	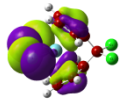	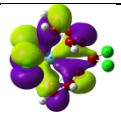	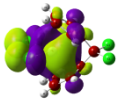	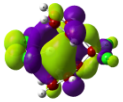	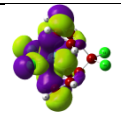	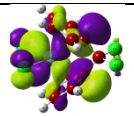
$[Nb\{(\eta^5\text{-}C_5H_4)_2CCl_2\}Cl_2]$		-0.29301	-0.28197	-0.21769	-0.13165	-0.07403	-0.07224
$[Nb\{(\eta^5\text{-}C_5H_4)_2SiCl_2\}Cl_2]$		-0.29167	-0.28241	-0.21822	-0.12962	-0.07796	-0.07555

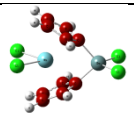	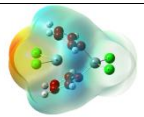	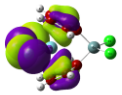	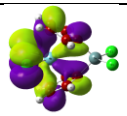	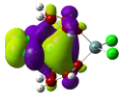	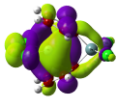	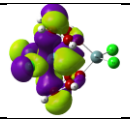	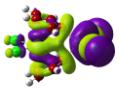
[Nb{(η^5-C_5H_4)$_2$GeCl$_2$}Cl$_2$]		-0.29312	-0.28381	-0.21973	-0.12980	-0.07954	-0.07852
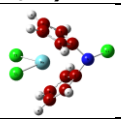	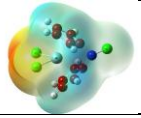	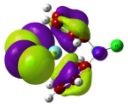	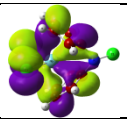	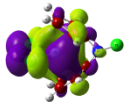	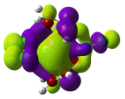	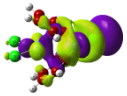	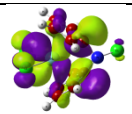
[Nb{(η^5-C_5H_4)$_2$NCl}Cl$_2$]		-0.29236	-0.28066	-0.21628	-0.13056	-0.08615	-0.07204
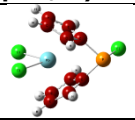	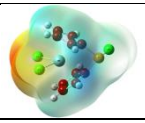	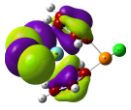	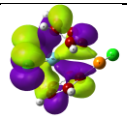	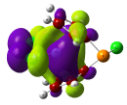	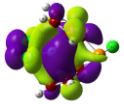	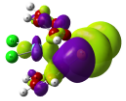	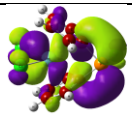
[Nb{(η^5-C_5H_4)$_2$PCl}Cl$_2$]		-0.29052	-0.28025	-0.21610	-0.12735	-0.08399	-0.07790
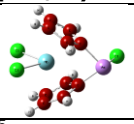	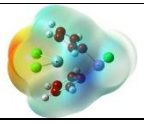	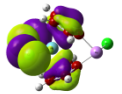	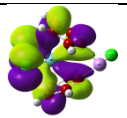	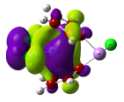	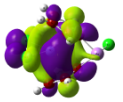	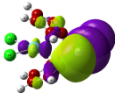	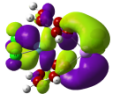
[Nb{(η^5-C_5H_4)$_2$AsCl}Cl$_2$]		-0.28876	-0.27828	-0.21435	-0.12410	-0.09807	-0.07864
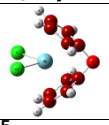	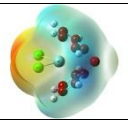	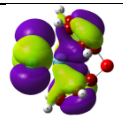	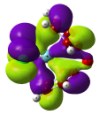	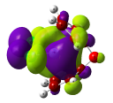	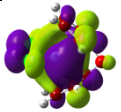	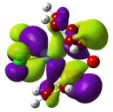	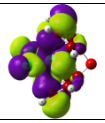
[Nb{(η^5-C_5H_4)$_2$O}Cl$_2$]		-0.29082	-0.27820	-0.21379	-0.12588	-0.07105	-0.06888
[Nb{(η^5-C_5H_4)$_2$S}Cl$_2$]		-.28939	-0.27901	-0.21465	-0.12585	-0.07861	-0.07193
[Nb{(η^5-C_5H_4)$_2$Se}Cl$_2$]		-0.28370	-0.27803	-0.21352	-0.12340	-0.08258	-0.07147

*HOMO orbitals are singly occupied.

Ta Complexes*

MOLECULE	ESP MAP	HOMO-2 (hartrees)	HOMO-1 (hartrees)	HOMO (hartrees)	LUMO (hartrees)	LUMO+1 (hartrees)	LUMO+2 (hartrees)
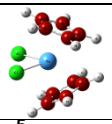	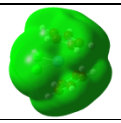	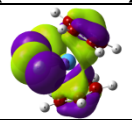	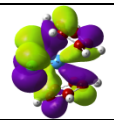	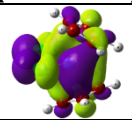	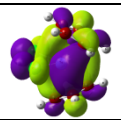	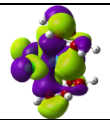	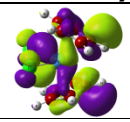
$[Ta(\eta^5\text{-}C_5H_5)_2Cl_2]$		-0.28180	-0.27151	-0.19174	-0.10513	-0.05859	-0.04058
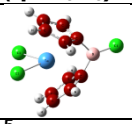	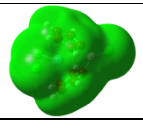	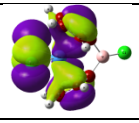	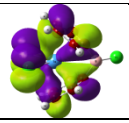	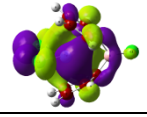	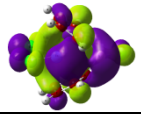	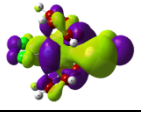	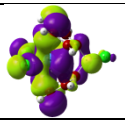
$[Ta\{(\eta^5\text{-}C_5H_4)_2BCl\}Cl_2]$		-0.29153	-0.28053	-0.20108	-0.012503	-0.09514	-0.06519
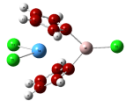	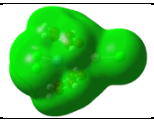	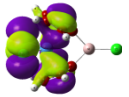	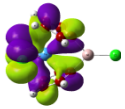	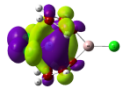	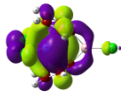	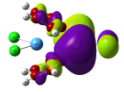	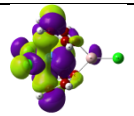
$[Ta\{(\eta^5\text{-}C_5H_4)_2AlCl\}Cl_2]$		-0.28583	-0.27502	-0.19731	-0.11590	-0.09158	-0.06228
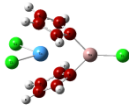	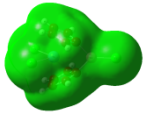	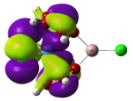	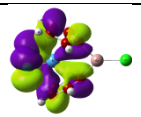	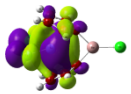	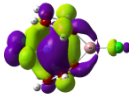	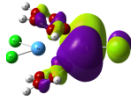	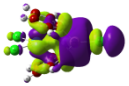
$[Ta\{(\eta^5\text{-}C_5H_4)_2GaCl\}Cl_2]$		-0.28733	-0.27611	-0.19807	-0.11490	-0.10121	-0.06966
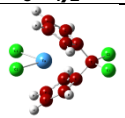	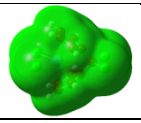	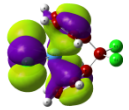	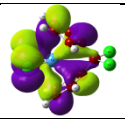	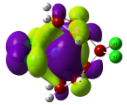	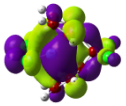	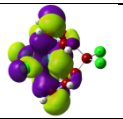	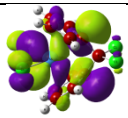
$[Ta\{(\eta^5\text{-}C_5H_4)_2CCl_2\}Cl_2]$		-0.29559	-0.28321	-0.20530	-0.12718	-0.06675	-0.05467
$[Ta\{(\eta^5\text{-}C_5H_4)_2SiCl_2\}Cl_2]$		-0.29390	-0.2895	-0.20536	-0.12545	-0.07011	-0.05871

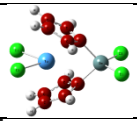	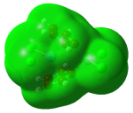	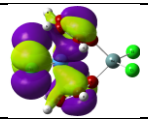	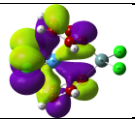	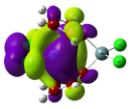	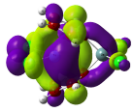	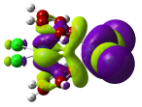	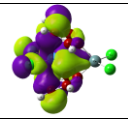
$[Ta\{(\eta^5\text{-}C_5H_4)_2GeCl_2\}Cl_2]$		-0.29527	-0.28524	-0.20624	-0.12519	-0.07590	-0.07153
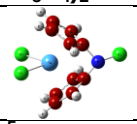	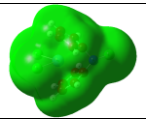	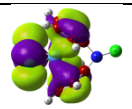	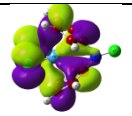	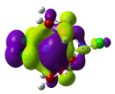	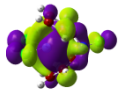	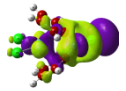	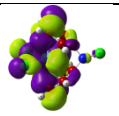
$[Ta\{(\eta^5\text{-}C_5H_4)_2NCl\}Cl_2]$		-0.29472	-0.28182	-0.2037	-0.12608	-0.08308	-0.06479
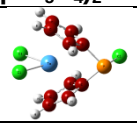	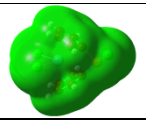	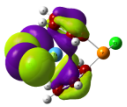	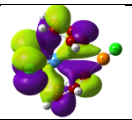	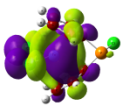	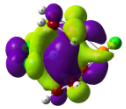	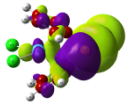	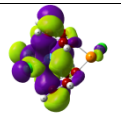
$[Ta\{(\eta^5\text{-}C_5H_4)_2PCl\}Cl_2]$		-0.29300	-0.28145	-0.20313	-0.12269	-0.08155	-0.06656
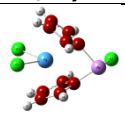	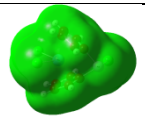	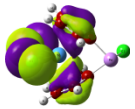	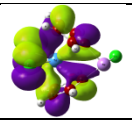	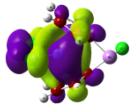	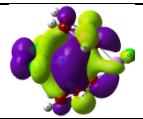	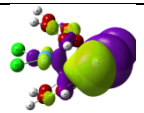	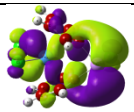
$[Ta\{(\eta^5\text{-}C_5H_4)_2AsCl\}Cl_2]$		-0.29103	-0.27949	-0.20112	-0.11922	-0.09616	-0.06641
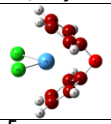	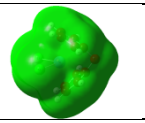	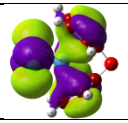	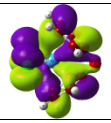	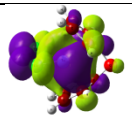	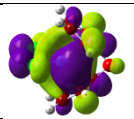	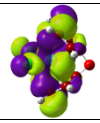	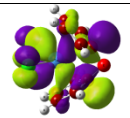
$[Ta\{(\eta^5\text{-}C_5H_4)_2O\}Cl_2]$		-0.29283	-0.27901	-0.20093	-0.120020	-0.06180	-0.05268
$[Ta\{(\eta^5\text{-}C_5H_4)_2S\}Cl_2]$		-0.29168	-0.28017	-0.20163	-0.12078	-0.06476	-0.06407
$[Ta\{(\eta^5\text{-}C_5H_4)_2Se\}Cl_2]$		-0.28187	-0.27915	-0.20023	-0.011823	-0.07239	-0.06345

*HOMO orbitals are singly occupied.

Cr Complexes

MOLECULE	ESP MAP	HOMO-2 (hartrees)	HOMO-1 (hartrees)	HOMO (hartrees)	LUMO (hartrees)	LUMO+1 (hartrees)	LUMO+2 (hartrees)
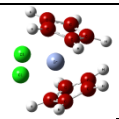	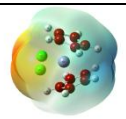	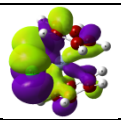	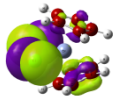	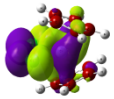	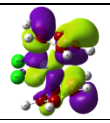	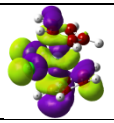	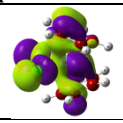
$[Cr(\eta^5\text{-}C_5H_5)_2Cl_2]$		-0.25580	-0.25318	-0.23489	-0.11398	-0.10934	-0.09667
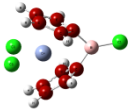	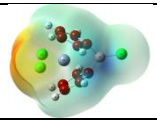	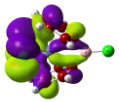	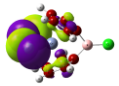	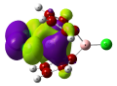	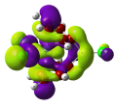	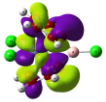	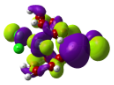
$[Cr\{(\eta^5\text{-}C_5H_4)_2BCl\}Cl_2]$		-0.25944	-0.25791	-0.24074	-0.12065	-0.11764	-0.11661
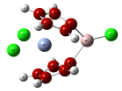	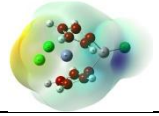	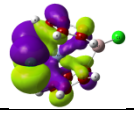	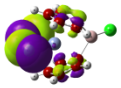	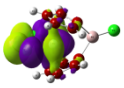	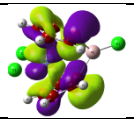	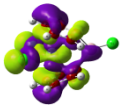	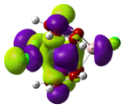
$[Cr\{(\eta^5\text{-}C_5H_4)_2AlCl\}Cl_2]$		-0.26227	-0.25819	-0.23917	-0.12834	-0.11876	-0.10911
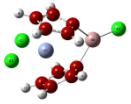	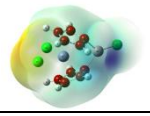	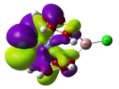	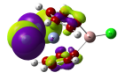	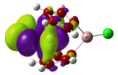	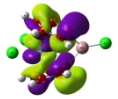	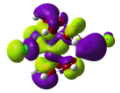	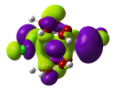
$[Cr\{(\eta^5\text{-}C_5H_4)_2GaCl\}Cl_2]$		-0.26274	-0.25849	-0.23891	-0.12367	-0.11370	-0.10704
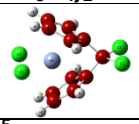	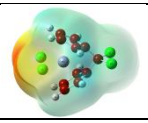	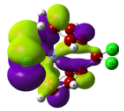	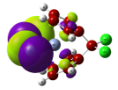	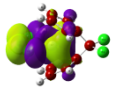	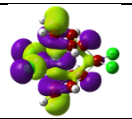	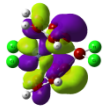	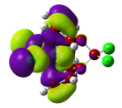
$[Cr\{(\eta^5\text{-}C_5H_4)_2CCl_2\}Cl_2]$		-0.26468	-0.26128	-0.24748	-0.12642	-0.12230	-0.10594
$[Cr\{(\eta^5\text{-}C_5H_4)_2SiCl_2\}Cl_2]$		-0.26556	-0.26262	-0.24542	-0.12818	-0.12457	-0.10911

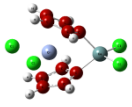	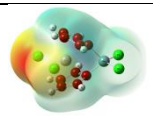	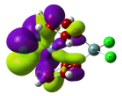	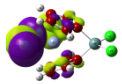	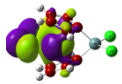	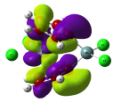	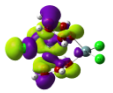	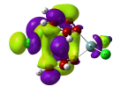
$[Cr\{(\eta^5\text{-}C_5H_4)_2GeCl_2\}Cl_2]$		-0.26765	-0.26398	-0.24689	-0.13130	-0.12491	-0.11123
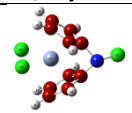	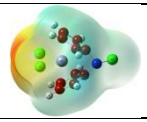	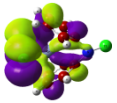	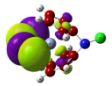	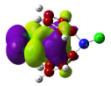	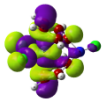		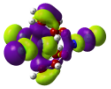
$[Cr\{(\eta^5\text{-}C_5H_4)_2NCl\}Cl_2]$		-0.26409	-0.25999	-0.24621	-0.12373	-0.12105	-0.10451
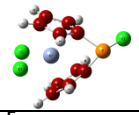	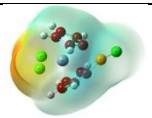	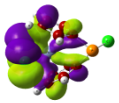	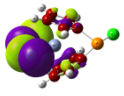	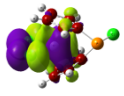	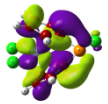	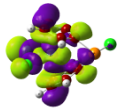	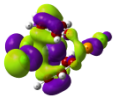
$[Cr\{(\eta^5\text{-}C_5H_4)_2PCl\}Cl_2]$		-0.26314	-0.26091	-0.24467	-0.12481	-0.12347	-0.10588
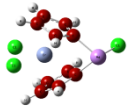	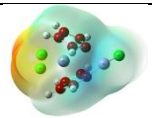	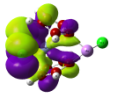	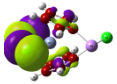	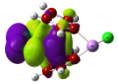	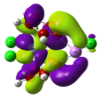	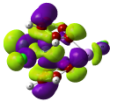	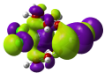
$[Cr\{(\eta^5\text{-}C_5H_4)_2AsCl\}Cl_2]$		-0.26179	-0.25986	-0.24294	-0.12416	-0.12125	-0.10676
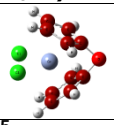	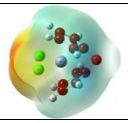	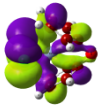	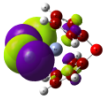	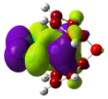		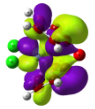	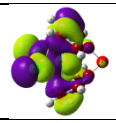
$[Cr\{(\eta^5\text{-}C_5H_4)_2O\}Cl_2]$		-0.26235	-0.25788	-0.24455	-0.12038	-0.11846	-0.10048
$[Cr\{(\eta^5\text{-}C_5H_4)_2S\}Cl_2]$		-0.26113	-0.25918	-0.24443	-0.12426	-0.12280	-0.10311
$[Cr\{(\eta^5\text{-}C_5H_4)_2Se\}Cl_2]$		-0.25972	-0.25882	-0.24306	-0.12398	-0.12338	-0.10222

Mo Complexes

MOLECULE	ESP MAP	HOMO-2 (hartrees)	HOMO-1 (hartrees)	HOMO (hartrees)	LUMO (hartrees)	LUMO+1 (hartrees)	LUMO+2 (hartrees)
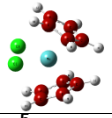	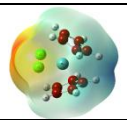	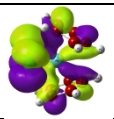	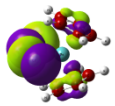	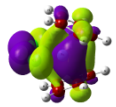	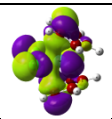	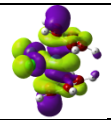	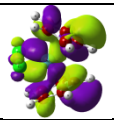
$[Mo(\eta^5\text{-}C_5H_5)_2Cl_2]$		-0.26492	-0.26204	-0.21670	-0.08508	-0.08111	-0.07232
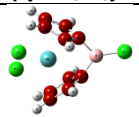	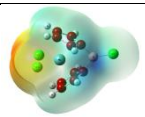	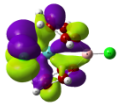	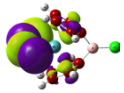	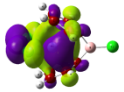	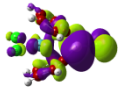	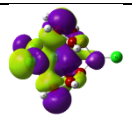	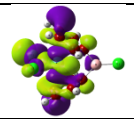
$[Mo\{(\eta^5\text{-}C_5H_4)_2BCl\}Cl_2]$		-0.27260	-0.26746	-0.22414	-0.11220	-0.08869	-0.08211
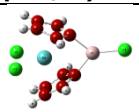	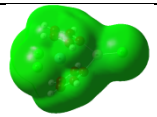	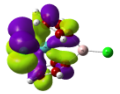	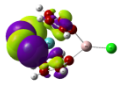	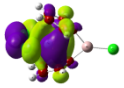	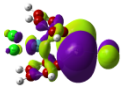	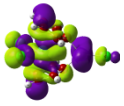	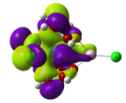
$[Mo\{(\eta^5\text{-}C_5H_4)_2AlCl\}Cl_2]$		-0.26807	-0.26613	-0.21975	-0.09488	-0.09115	-0.08869
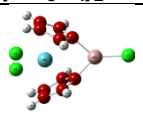	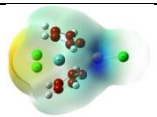	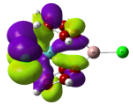	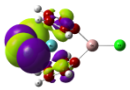	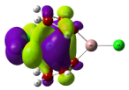	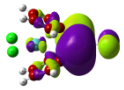	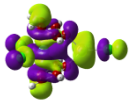	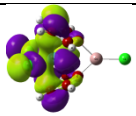
$[Mo\{(\eta^5\text{-}C_5H_4)_2GaCl\}Cl_2]$		-0.26912	-0.26726	-0.22027	-0.10472	-0.09411	-0.08955
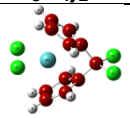	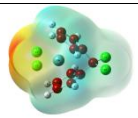	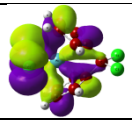	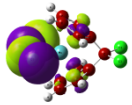	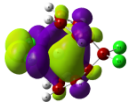	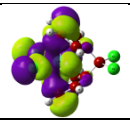	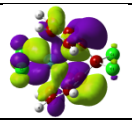	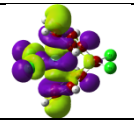
$[Mo\{(\eta^5\text{-}C_5H_4)_2CCl_2\}Cl_2]$		-0.27801	-0.27128	-0.23113	-0.09281	-0.08824	-0.08607
$[Mo\{(\eta^5\text{-}C_5H_4)_2SiCl_2\}Cl_2]$		-0.27666	-0.27184	-0.22862	-0.09570	-0.09369	-0.09093

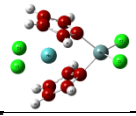	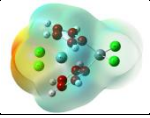	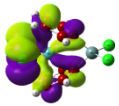	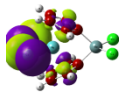	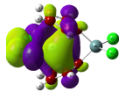	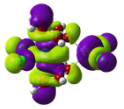	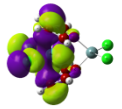	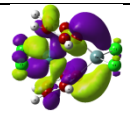
[Mo{(η^5-C_5H_4)$_2$GeCl$_2$}Cl$_2$]		-0.27783	-0.27340	-0.22942	-0.09921	-0.09723	-0.09285
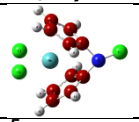	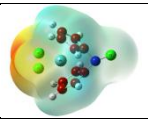	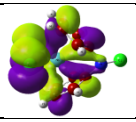	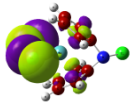	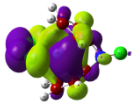	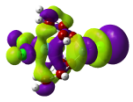	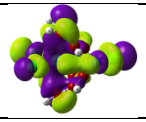	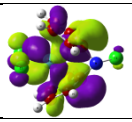
[Mo{(η^5-C_5H_4)$_2$NCl}Cl$_2$]		-0.27707	-0.27028	-0.23025	-0.09309	-0.09016	-0.08786
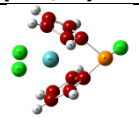	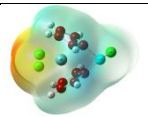	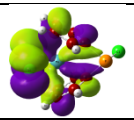	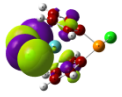	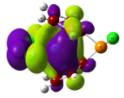	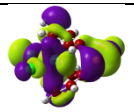	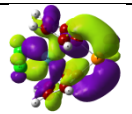	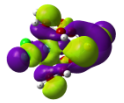
[Mo{(η^5-C_5H_4)$_2$PCl}Cl$_2$]		-0.27489	-0.26974	-0.22722	-0.09476	-0.09332	-0,08786
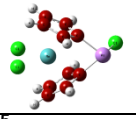	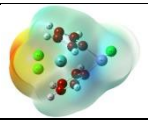	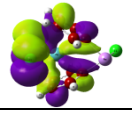	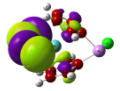	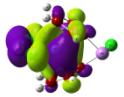	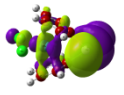	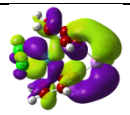	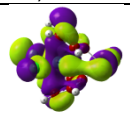
[Mo{(η^5-C_5H_4)$_2$AsCl}Cl$_2$]		-0.27284	-0.26827	-0.22494	-0.10233	-0.09326	-0.09072
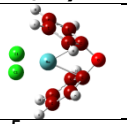	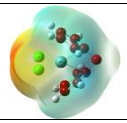	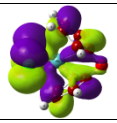	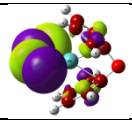	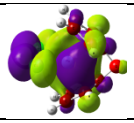	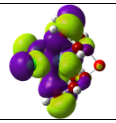	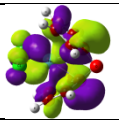	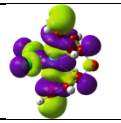
[Mo{(η^5-C_5H_4)$_2$O}Cl$_2$]		-0.27486	-0.26858	-0.22858	-0.08750	-0.08583	-0.08031
[Mo{(η^5-C_5H_4)$_2$S}Cl$_2$]		-0.27409	-0.26826	-0.22679	-0.09364	-0.09018	-0.08618
[Mo{(η^5-C_5H_4)$_2$Se}Cl$_2$]		-0.27268	-0.26735	-0.22474	-0.09695	-0.08965	-0.08700

W Complexes

MOLECULE	ESP MAP	HOMO-2 (hartrees)	HOMO-1 (hartrees)	HOMO (hartrees)	LUMO (hartrees)	LUMO+1 (hartrees)	LUMO+2 (hartrees)
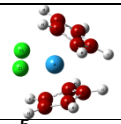	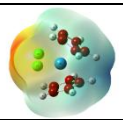	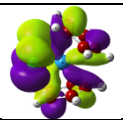	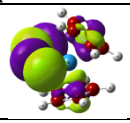		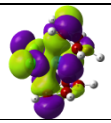		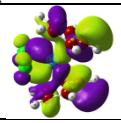
$[W(\eta^5\text{-}C_5H_5)_2Cl_2]$		-0.26749	-0.26542	-0.20871	-0.07530	-0.06371	-0.05106
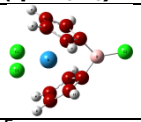	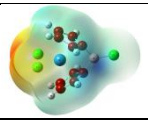	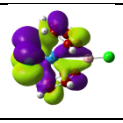	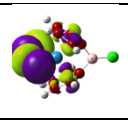	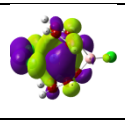	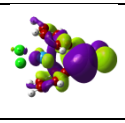	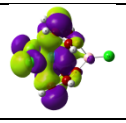	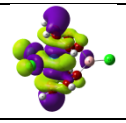
$[W\{(\eta^5\text{-}C_5H_4)_2BCl\}Cl_2]$		-0.27618	-0.27212	-0.21735	-0.10782	-0.08081	-0.06289
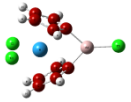	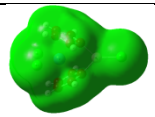	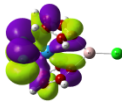	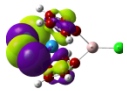	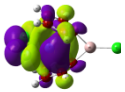	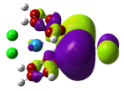	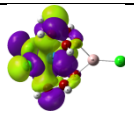	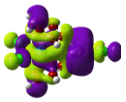
$[W\{(\eta^5\text{-}C_5H_4)_2AlCl\}Cl_2]$		-0.27084	-0.26972	-0.21219	-0.09260	-0.07959	-0.07934
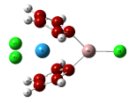	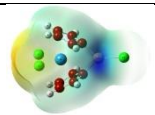	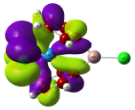	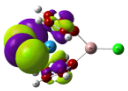	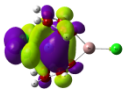	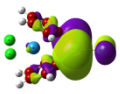	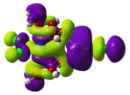	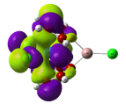
$[W\{(\eta^5\text{-}C_5H_4)_2GaCl\}Cl_2]$		-0.27174	-0.27071	-0.21229	-0.10261	-0.08450	-0.08042
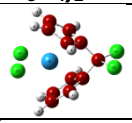	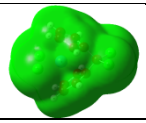	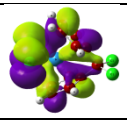	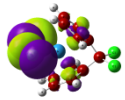	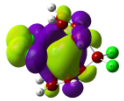	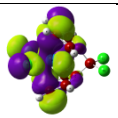	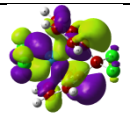	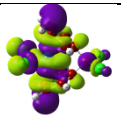
$[W\{(\eta^5\text{-}C_5H_4)_2CCl_2\}Cl_2]$		-0.28124	-0.27602	-0.22402	-0.08447	-0.06960	-0.06473
$[W\{(\eta^5\text{-}C_5H_4)_2SiCl_2\}Cl_2]$		-0.27989	-0.27575	-0.22141	-0.08683	-0.07596	-0.07213

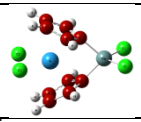	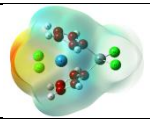	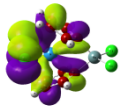	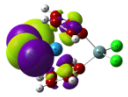	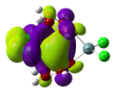	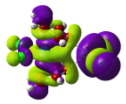	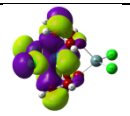	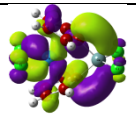
$[W\{(\eta^5\text{-}C_5H_4)_2GeCl_2\}Cl_2]$		-28095	-0.27729	-0.22180	-0.08898	-0.08821	-0.07375
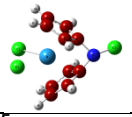	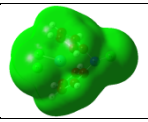	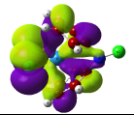	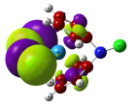	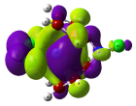	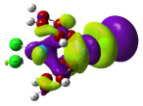	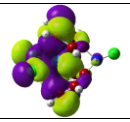	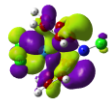
$[W\{(\eta^5\text{-}C_5H_4)_2NCl\}Cl_2]$		-0.28024	-0.27514	-0.22301	-0.08904	-0.08247	-0.06925
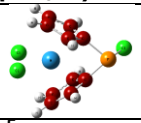	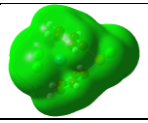	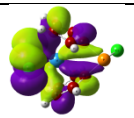	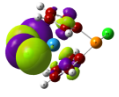	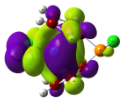	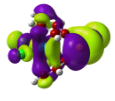	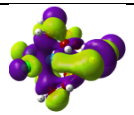	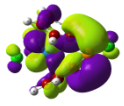
$[W\{(\eta^5\text{-}C_5H_4)_2PCl\}Cl_2]$		-0.27789	-0.27375	-0.21975	-0.08689	-0.08219	-0.07761
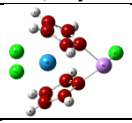	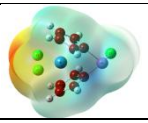	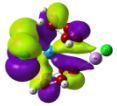	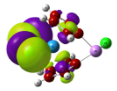	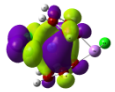	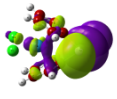	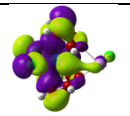	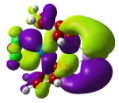
$[W\{(\eta^5\text{-}C_5H_4)_2AsCl\}Cl_2]$		-0.27562	-0.27206	-0.21715	-0.09933	-0.08199	-0.07913
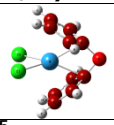	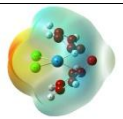	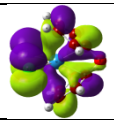	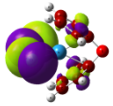	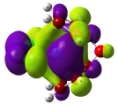	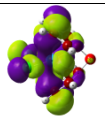	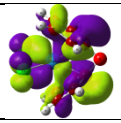	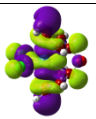
$[W\{(\eta^5\text{-}C_5H_4)_2O\}Cl_2]$		-0.27764	-0.27331	-0.22102	-0.07928	-0.06708	-0.05906
$[W\{(\eta^5\text{-}C_5H_4)_2S\}Cl_2]$		-0.27701	-0.27234	-0.21914	-0.08138	-0.07844	-0.06622
$[W\{(\eta^5\text{-}C_5H_4)_2Se\}Cl_2]$		-0.27548	-0.27109	-0.21697	-0.08504	-0.8084	-0.06799

Mn Complexes

MOLECULE	ESP MAP	HOMO-2 (hartrees)	HOMO-1 (hartrees)	HOMO (hartrees)	LUMO (hartrees)	LUMO+1 (hartrees)	LUMO+2 (hartrees)
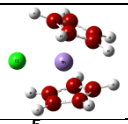	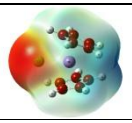		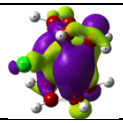	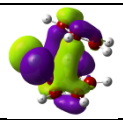	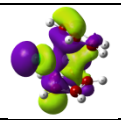		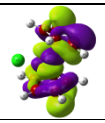
[Mn(η^5-C_5H_5)$_2$Cl]		-0.25133	-0.22950	-0.21706	-0.09585	-0.07826	-0.04898
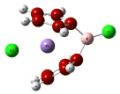	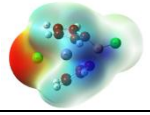	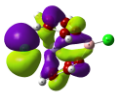	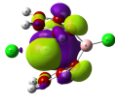	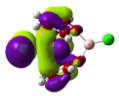	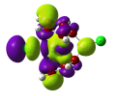	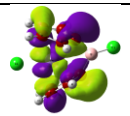	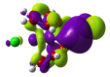
[Mn{(η^5-C_5H_4)$_2$BCl}Cl]		-0.26013	-0.24450	-0.22289	-0.10152	-0.09103	-0.08945
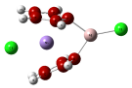	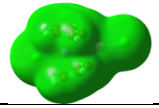	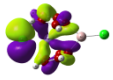	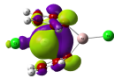	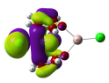	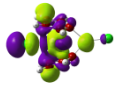	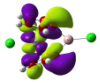	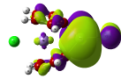
[Mn{(η^5-C_5H_4)$_2$AlCl}Cl]		-0.25626	-0.23681	-0.22239	-0.10283	-0.08926	-0.08334
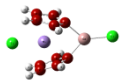	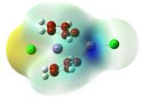	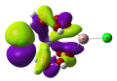	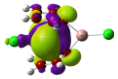	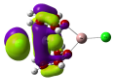	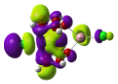	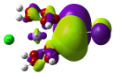	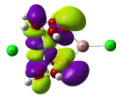
[Mn{(η^5-C_5H_4)$_2$GaCl}Cl]		-0.25723	-0.23821	-0.22332	-0.10394	-0.09315	-0.09137
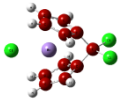	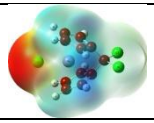	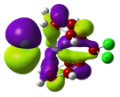	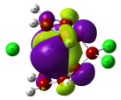	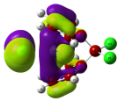	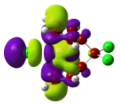	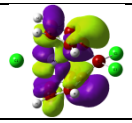	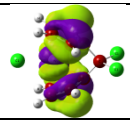
[Mn{(η^5-C_5H_4)$_2$CCl$_2$}Cl]		-0.26220	-0.25036	-0.22193	-0.10085	-0.09478	-0.06680
[Mn{(η^5-C_5H_4)$_2$SiCl$_2$}Cl]		-0.26499	-0.24840	-0.22942	-0.10837	-0.09867	-0.06679

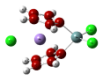	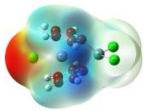	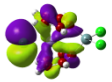	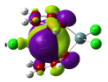	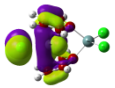	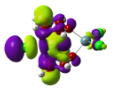	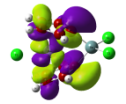	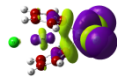
[Mn{(η^5-C_5H_4)$_2$$GeCl_2$}Cl]		-0.26664	-0.24984	-0.23178	-0.11165	-0.10109	-0.06922
	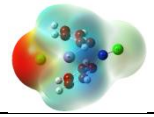	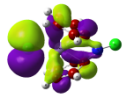	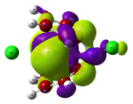	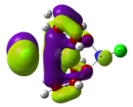	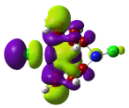	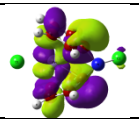	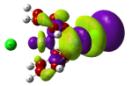
[Mn{(η^5-C_5H_4)$_2$NCl}Cl]		-0.26004	-0.24818	-0.21771	-0.09792	-0.09260	-0.07971
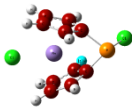	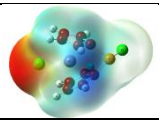	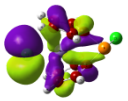	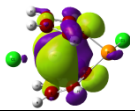	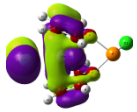	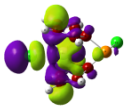	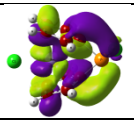	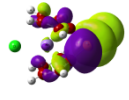
[Mn{(η^5-C_5H_4)$_2$PCl}Cl]		-0.26160	-0.24699	-0.22415	-0.10291	-0.09676	-0.07497
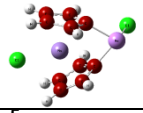	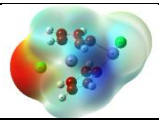	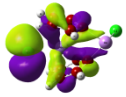	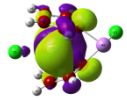	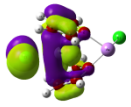	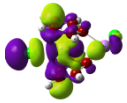	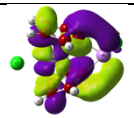	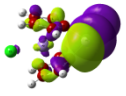
[Mn{(η^5-C_5H_4)$_2$AsCl}Cl]		-0.26018	-0.24442	-0.22328	-0.10227	-0.09575	-0.08920
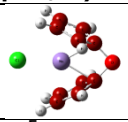	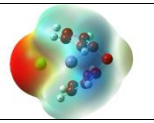	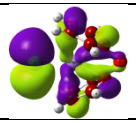	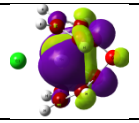	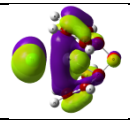	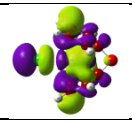	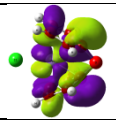	
[Mn{(η^5-C_5H_4)$_2$O}Cl]		-0.25580	-0.24492	-0.21137	-0.09296	-0.08884	-0.06406
[Mn{(η^5-C_5H_4)$_2$S}Cl]		-0.25940	-0.24517	-0.21930	-0.09951	-0.09481	-0.06222
[Mn{(η^5-C_5H_4)$_2$Se}Cl]		-0.25905	-0.24330	-0.21987	-0.10011	-0.09579	-0.06070

Tc Complexes

MOLECULE	ESP MAP	HOMO-2 (hartrees)	HOMO-1 (hartrees)	HOMO (hartrees)	LUMO (hartrees)	LUMO+1 (hartrees)	LUMO+2 (hartrees)
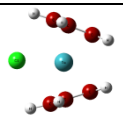	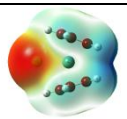	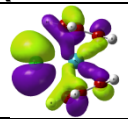	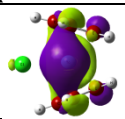	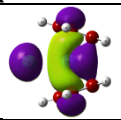	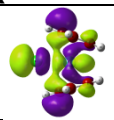	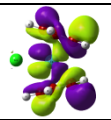	
$[Tc(\eta^5\text{-}C_5H_5)_2Cl]$		-0.26028	-0.22068	-0.20690	-0.07992	-0.05126	-0.02839
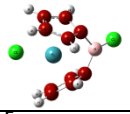	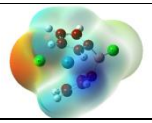	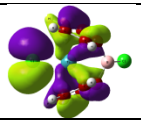	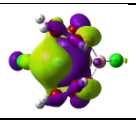	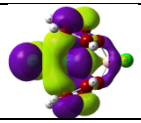	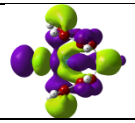	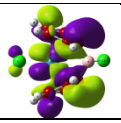	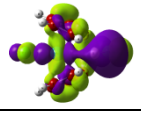
$[Tc\{(\eta^5\text{-}C_5H_4)_2BCl\}Cl]$		-0.27709	-0.24547	-0.22036	-0.09220	-0.06949	-0.06498
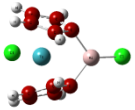	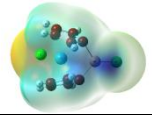	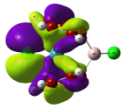	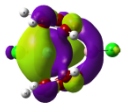	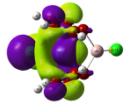	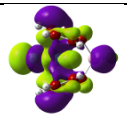	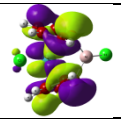	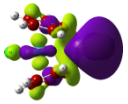
$[Tc\{(\eta^5\text{-}C_5H_4)_2AlCl\}Cl]$		-0.27265	-0.24631	-0.22221	-0.09315	-0.06898	-0.05814
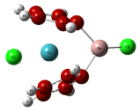	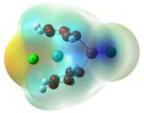	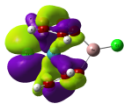	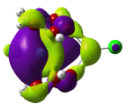	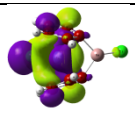	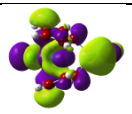	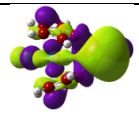	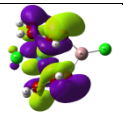
$[Tc\{(\eta^5\text{-}C_5H_4)_2GaCl\}Cl]$		-0.27220	-0.24017	-0.21992	-0.09709	-0.07697	-0.06797
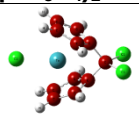	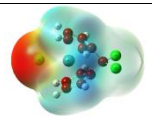	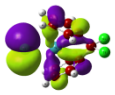	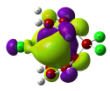	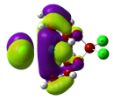	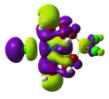	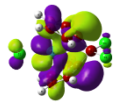	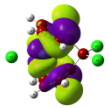
$[Tc\{(\eta^5\text{-}C_5H_4)_2CCl_2\}Cl]$		-0.26918	-0.24955	-0.20454	-0.07809	-0.07350	-0.05484
$[Tc\{(\eta^5\text{-}C_5H_4)_2SiCl_2\}Cl]$		-0.27409	-0.24275	-0.21699	-0.09105	-0.07312	-0.05001

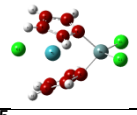	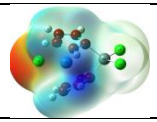	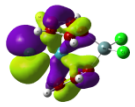	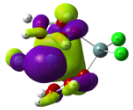	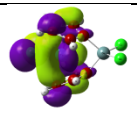	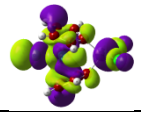	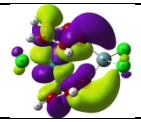	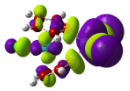
[Tc{(η^5-C_5H_4)$_2$$GeCl_2$}Cl]		-0.27579	-0.24370	-0.21977	-0.09649	-0.07475	-0.06539
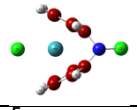	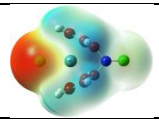	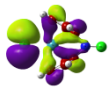	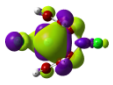	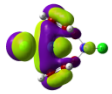	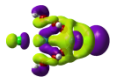	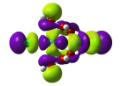	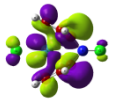
[Tc{(η^5-C_5H_4)$_2$NCl}Cl]		-0.26914	-0.24820	-0.20279	-0.08447	-0.07240	-0.07156
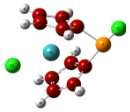	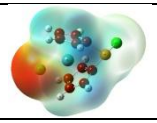	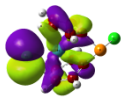	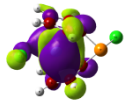	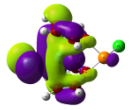	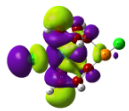	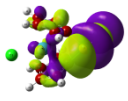	
[Tc{(η^5-C_5H_4)$_2$PCl}Cl]		-0.27213	-0.24349	-0.21238	-0.08402	-0.07297	-0.07392
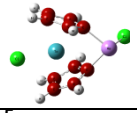	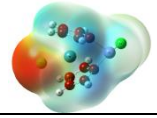	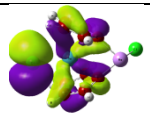	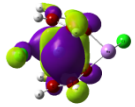	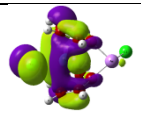	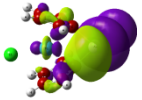	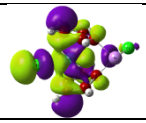	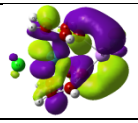
[Tc{(η^5-C_5H_4)$_2$AsCl}Cl]		-0.27054	-0.24053	-0.21194	-0.08822	-0.08417	-0.07326
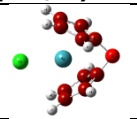	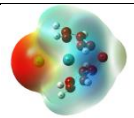	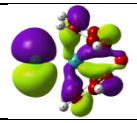	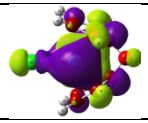	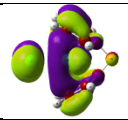	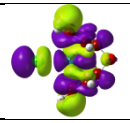	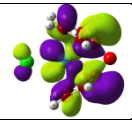	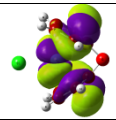
[Tc{(η^5-C_5H_4)$_2$O}Cl]		-0.26351	-0.24638	-0.19554	-0.07146	-0.07107	-0.05607
[Tc{(η^5-C_5H_4)$_2$S}Cl]		-0.26726	-0.24281	-0.20349	-0.07936	-0.07713	-0.04967
[Tc{(η^5-C_5H_4)$_2$Se}Cl]		-0.26704	-0.23971	-0.20483	-0.08125	-0.07961	-0.04683

Re Complexes

MOLECULE	ESP MAP	HOMO-2 (hartrees)	HOMO-1 (hartrees)	HOMO (hartrees)	LUMO (hartrees)	LUMO+1 (hartrees)	LUMO+2 (hartrees)
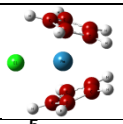	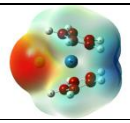	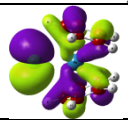	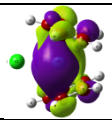	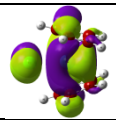	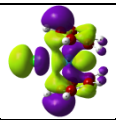	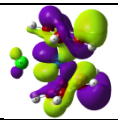	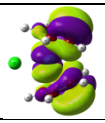
$[Re(\eta^5\text{-}C_5H_5)_2Cl]$		-0.26403	-0.21271	-0.20122	-0.06434	-0.03236	-0.00866
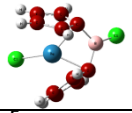	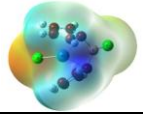	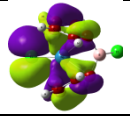	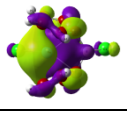	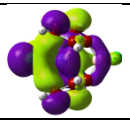	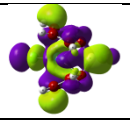	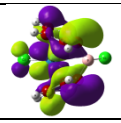	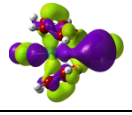
$[Re\{(\eta^5\text{-}C_5H_4)_2BCl\}Cl]$		-0.28418	-0.24045	-0.21857	-0.08043	-0.05340	-0.05034
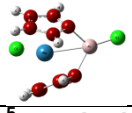	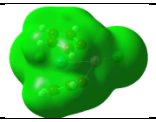	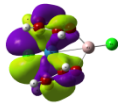	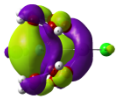	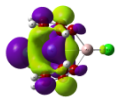	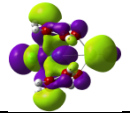	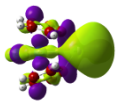	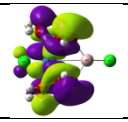
$[Re\{(\eta^5\text{-}C_5H_4)_2AlCl\}Cl]$		-0.27764	-0.24127	-0.21714	-0.08102	-0.05125	-0.05125
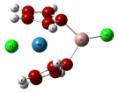	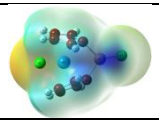	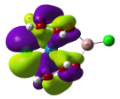	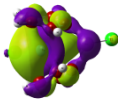	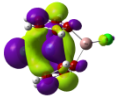	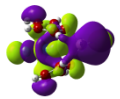	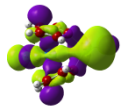	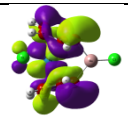
$[Re\{(\eta^5\text{-}C_5H_4)_2GaCl\}Cl]$		-0.27731	-0.23451	-0.21494	-0.09015	-0.06678	-0.05023
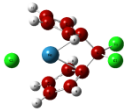	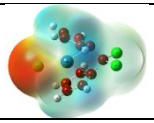	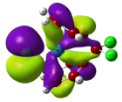	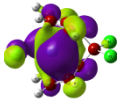	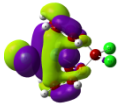	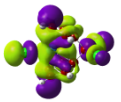	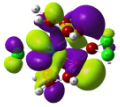	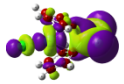
$[Re\{(\eta^5\text{-}C_5H_4)_2CCl_2\}Cl]$		-0.27618	-0.24318	-0.19991	-0.06250	-0.05756	-0.04741
$[Re\{(\eta^5\text{-}C_5H_4)_2SiCl_2\}Cl]$		-0.2965	-0.23572	-0.21369	-0.07659	-0.05643	-0.03134

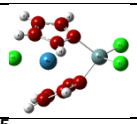	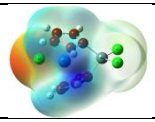	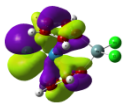	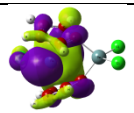	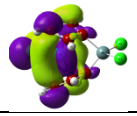	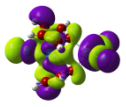	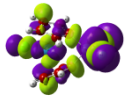	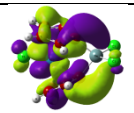
[Re{(η^5-C$_5$H$_4$)$_2$GeCl$_2$}Cl]		-0.28078	-0.23665	-0.21545	-0.08499	-0.05983	-0.05759
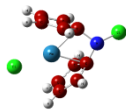	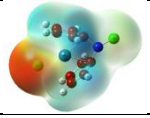	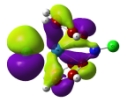	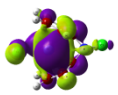	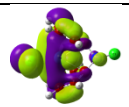	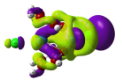	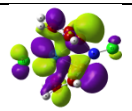	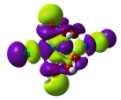
[Re{(η^5-C$_5$H$_4$)$_2$NCl}Cl]		-0.27578	-0.24238	-0.19724	-0.08142	-0.05568	-0.05536
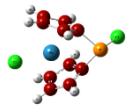	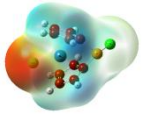	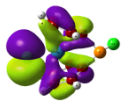	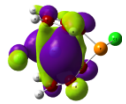		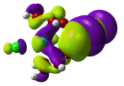	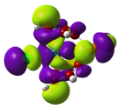	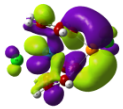
[Re{(η^5-C$_5$H$_4$)$_2$PCl}Cl]		-0.27785	-0.23688	-0.20782	-0.07178	-0.06732	-0.05940
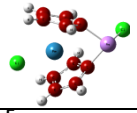	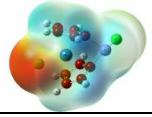	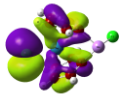	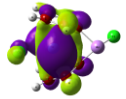		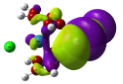	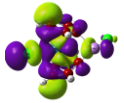	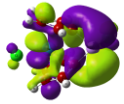
[Re{(η^5-C$_5$H$_4$)$_2$AsCl}Cl]		-0.27604	-0.23382	-0.20750	-0.08586	-0.06827	-0.05969
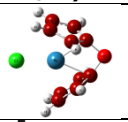	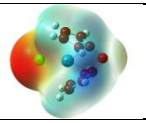	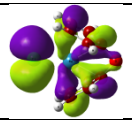	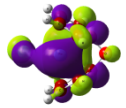	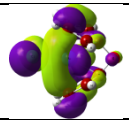	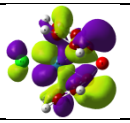	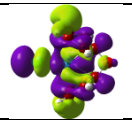	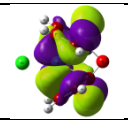
[Re{(η^5-C$_5$H$_4$)$_2$O}Cl]		-0.27103	-0.24071	-0.19017	-0.05547	-0.05445	-0.03961
[Re{(η^5-C$_5$H$_4$)$_2$S}Cl]		-0.27315	-0.23608	-0.19857	-0.06451	-0.06387	-0.03225
[Re{(η^5-C$_5$H$_4$)$_2$Se}Cl]		-0.27221	-0.23280	-0.19957	-0.07024	-0.06633	-0.03028

Fe Complexes

MOLECULE	ESP MAP	HOMO-2 (hartrees)	HOMO-1 (hartrees)	HOMO (hartrees)	LUMO (hartrees)	LUMO+1 (hartrees)	LUMO+2 (hartrees)
	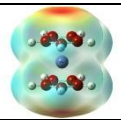	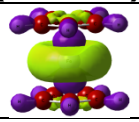	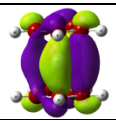	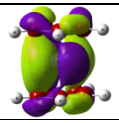	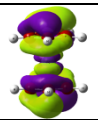	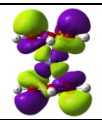	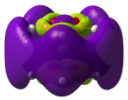
$[Fe(\eta^5\text{-}C_5H_5)_2]$		-0.25128	-0.22169	-0.22167	-0.02936	-0.02934	-0.01896
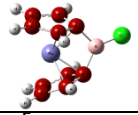	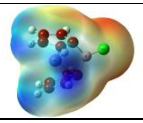	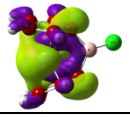	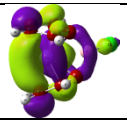	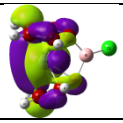	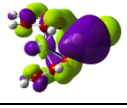	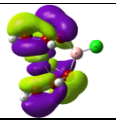	
$[Fe\{(\eta^5\text{-}C_5H_4)_2BCl\}]$		-0.26325	-0.24176	-0.23907	-0.05967	-0.05342	-0.04916
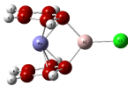	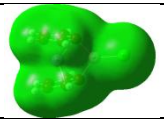	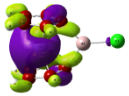	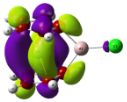	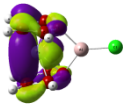	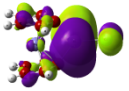	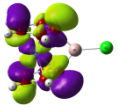	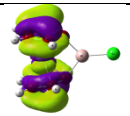
$[Fe\{(\eta^5\text{-}C_5H_4)_2AlCl\}]$		-0.26089	-0.24029	-0.23818	-0.06485	-0.04603	-0.04408
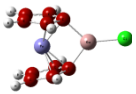	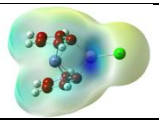	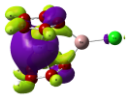	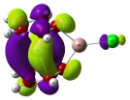	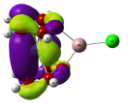	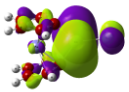	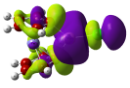	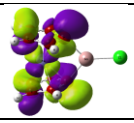
$[Fe\{(\eta^5\text{-}C_5H_4)_2GaCl\}]$		-0.26138	-0.23898	-0.23735	-0.07534	-0.04962	-0.04620
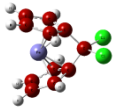	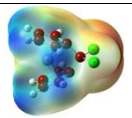	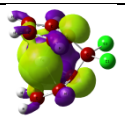	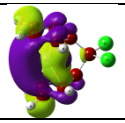	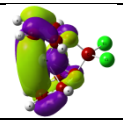		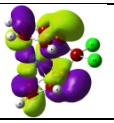	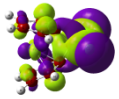
$[Fe\{(\eta^5\text{-}C_5H_4)_2CCl_2\}]$		-0.26235	-0.23468	-0.23396	-0.05211	-0.04969	-0.03187
$[Fe\{(\eta^5\text{-}C_5H_4)_2SiCl_2\}]$		-0.26978	-0.24851	-0.24651	-0.05563	-0.05395	-0.01892

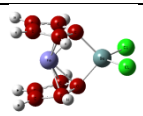	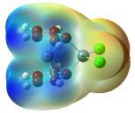	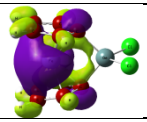	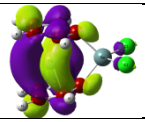	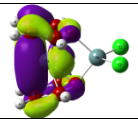	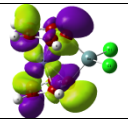	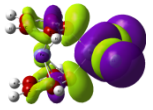	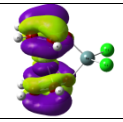
[Fe{(η^5-C_5H_4)$_2$$GeCl_2$}]		-0.27207	-0.25009	-0.24806	-0.05726	-0.05676	-0.05552
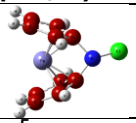	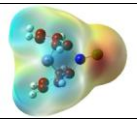	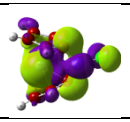	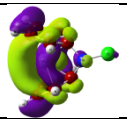	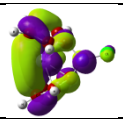	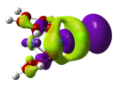	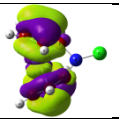	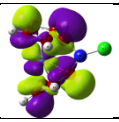
[Fe{(η^5-C_5H_4)$_2$NCl}]		-0.25696	-0.22951	-0.22741	-0.0572	-0.05212	-0.04771
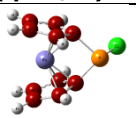	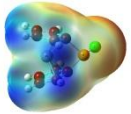	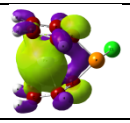	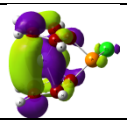	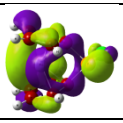	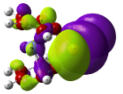		
[Fe{(η^5-C_5H_4)$_2$PCl}]		-0.26311	-0.23759	-0.23704	-0.05522	-0.05075	-0.04907
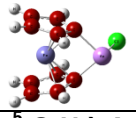	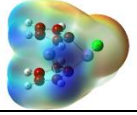			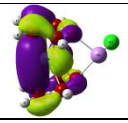	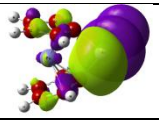	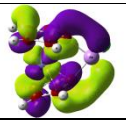	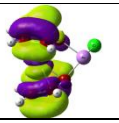
[Fe{(η^5-C_5H_4)$_2$AsCl}]		-0.26127	-0.23683	-0.23668	-0.07069	-0.04884	-0.04663
	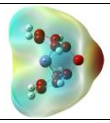	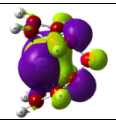					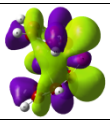
[Fe{(η^5-C_5H_4)$_2$O}]		-0.25385	-0.22302	-0.22101	-0.04865	-0.04452	-0.01857
[Fe{(η^5-C_5H_4)$_2$S}]		-0.25873	-0.23383	-0.22963	-0.04751	-0.04627	-0.02677
[Fe{(η^5-C_5H_4)$_2$Se}]		-0.25641	-0.23454	-0.23042	-0.04877	-0.04430	-0.03186

Ru Complexes

MOLECULE	ESP MAP	HOMO-2 (hartrees)	HOMO-1 (hartrees)	HOMO (hartrees)	LUMO (hartrees)	LUMO+1 (hartrees)	LUMO+2 (hartrees)
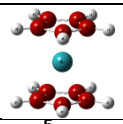	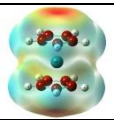	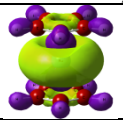	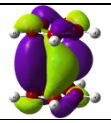		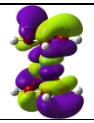		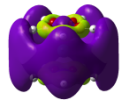
$[Ru(\eta^5\text{-}C_5H_5)_2]$		-0.23354	-0.3045	-0.23037	-0.01468	-0.01466	0.01786
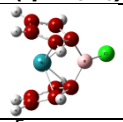	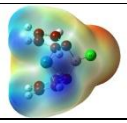		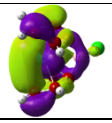		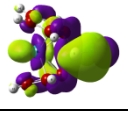	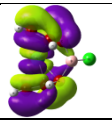	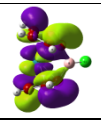
$[Ru\{(\eta^5\text{-}C_5H_4)_2BCl\}]$		-0.26461	-0.24700	-0.22900	-0.05183	-0.04599	-0.04298
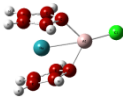	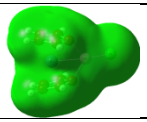	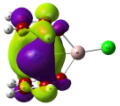	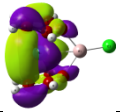	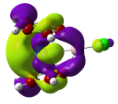	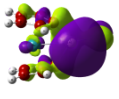	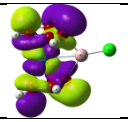	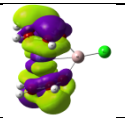
$[Ru\{(\eta^5\text{-}C_5H_4)_2AlCl\}]$		-0.25804	-0.25005	-0.24054	-0.06620	-0.03686	-0.03456
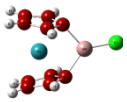	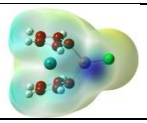	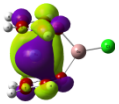	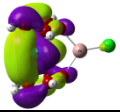	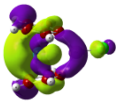	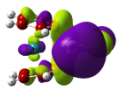	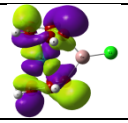	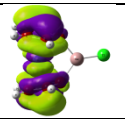
$[Ru\{(\eta^5\text{-}C_5H_4)_2GaCl\}]$		-0.25793	-0.24824	-0.23891	-0.08262	-0.03772	-0.03521
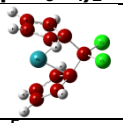	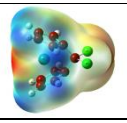		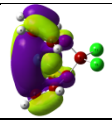	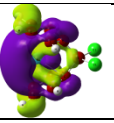	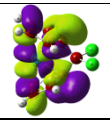		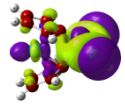
$[Ru\{(\eta^5\text{-}C_5H_4)_2CCl_2\}]$		-0.26510	-0.22869	-0.21543	-0.04252	-0.04228	-0.003455
$[Ru\{(\eta^5\text{-}C_5H_4)_2SiCl_2\}]$		-0.26690	-0.25131	-0.24292	-0.04468	-0.04235	-0.01738

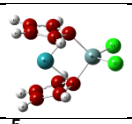	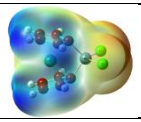	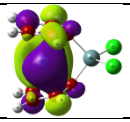	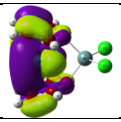	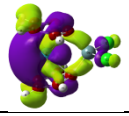	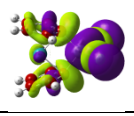	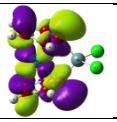	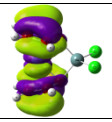
[Ru{(η^5-C$_5$H$_4$)$_2$GeCl$_2$}]		-0.26731	-0.25200	-0.24427	-0.05997	-0.04562	-0.04273
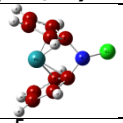	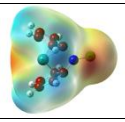	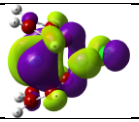	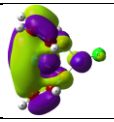	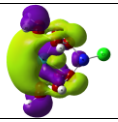	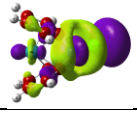	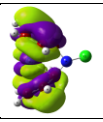	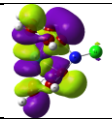
[Ru{(η^5-C$_5$H$_4$)$_2$NCl}]		-0.26240	-0.22279	-0.21126	-0.06047	-0.04496	-0.04260
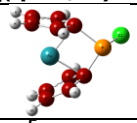	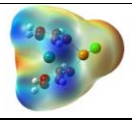	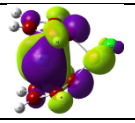		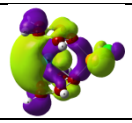	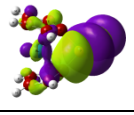	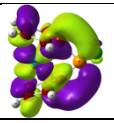	
[Ru{(η^5-C$_5$H$_4$)$_2$PCl}]		-0.26122	-0.23745	-0.22396	-0.05659	-0.04049	-0.03752
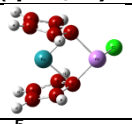	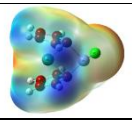	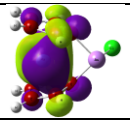	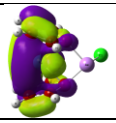	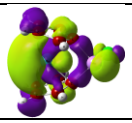	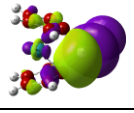	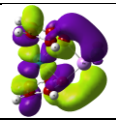	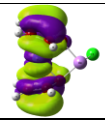
[Ru{(η^5-C$_5$H$_4$)$_2$AsCl}]		-0.25873	-0.23861	-0.22545	-0.07200	-0.03799	-0.03413
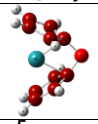	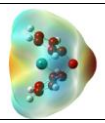	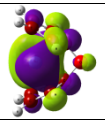				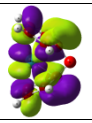	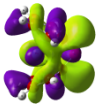
[Ru{(η^5-C$_5$H$_4$)$_2$O}]		-0.26118	-0.21620	-0.20501	-0.04340	-0.04173	-0.01441
[Ru{(η^5-C$_5$H$_4$)$_2$S}]		-0.25870	-0.22766	-0.21832	-0.04054	-0.03503	-0.02565
[Ru{(η^5-C$_5$H$_4$)$_2$Se}]		-0.25620	-0.23007	-0.22114	-0.04349	-0.03414	-0.03173

Os Complexes

MOLECULE	ESP MAP	HOMO-2 (hartrees)	HOMO-1 (hartrees)	HOMO (hartrees)	LUMO (hartrees)	LUMO+1 (hartrees)	LUMO+2 (hartrees)
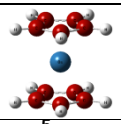	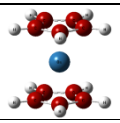	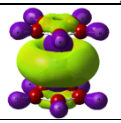		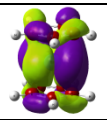		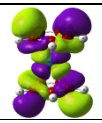	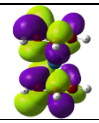
$[Os(\eta^5\text{-}C_5H_5)_2]$		-0.22606	-0.22447	-0.22443	0.00694	0.00696	0.01837
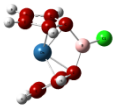	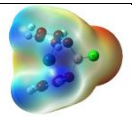	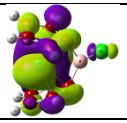	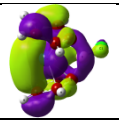	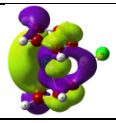	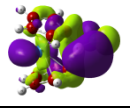	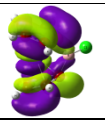	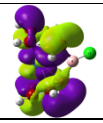
$[Os\{(\eta^5\text{-}C_5H_4)_2BCl\}]$		-0.26168	-0.24816	-0.22566	-0.04805	-0.024870	-0.02487
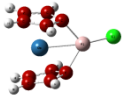	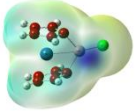	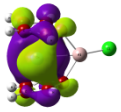	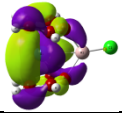	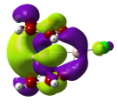	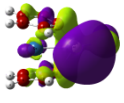	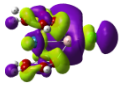	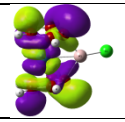
$[Os\{(\eta^5\text{-}C_5H_4)_2AlCl\}]$		-0.25405	-0.24952	-0.23688	-0.06622	-0.01855	-.01743
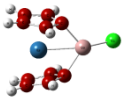	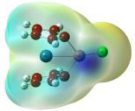	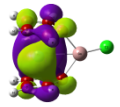	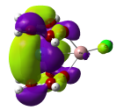	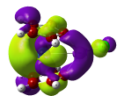	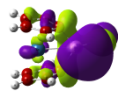	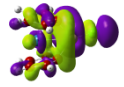	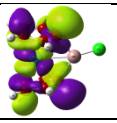
$[Os\{(\eta^5\text{-}C_5H_4)_2GaCl\}]$		-0.25375	-0.24700	-0.23471	-0.08482	-0.02635	-0.01855
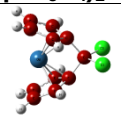	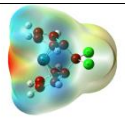	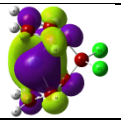	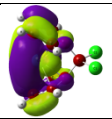	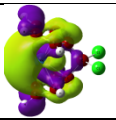	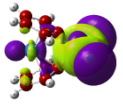	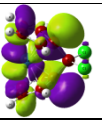	
$[Os\{(\eta^5\text{-}C_5H_4)_2CCl_2\}]$		-0.26210	-0.22505	-0.20735	-0.03603	-0.02506	-0.02076
$[Os\{(\eta^5\text{-}C_5H_4)_2SiCl_2\}]$		-0.26357	-0.25144	-0.24194	-0.02714	-0.02248	-0.01787

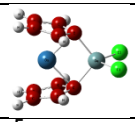	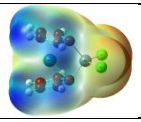	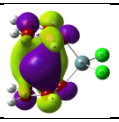	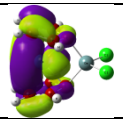	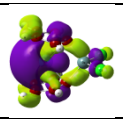		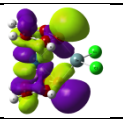	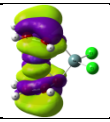
[Os{(η^5-C$_5$H$_4$)$_2$GeCl$_2$}]		-0.26298	-0.25014	-0.24044	-0.06202	-0.02745	-0.02170
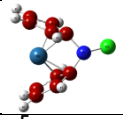	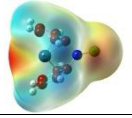	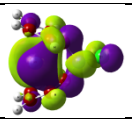	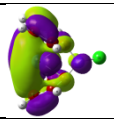	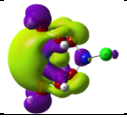	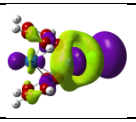	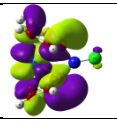	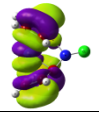
[Os{(η^5-C$_5$H$_4$)$_2$NCl}]		-0.26011	-0.21998	-0.20361	-0.06227	-0.02563	-0.02326
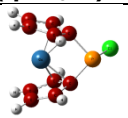	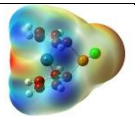	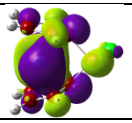		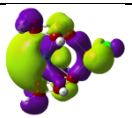	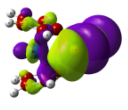	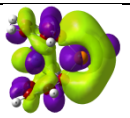	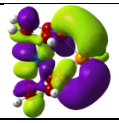
[Os{(η^5-C$_5$H$_4$)$_2$PCl}]		-0.25734	-0.23604	-0.21866	-0.05585	-0.02503	-0.02366
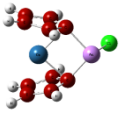	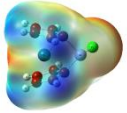		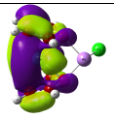	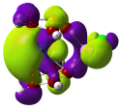	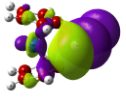	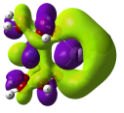	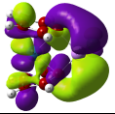
[Os{(η^5-C$_5$H$_4$)$_2$AsCl}]		-0.25483	-0.23806	-0.22101	-0.07087	-0.03338	-0.02121
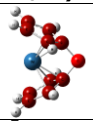	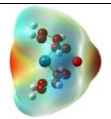	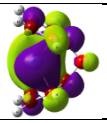	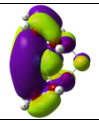	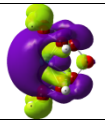	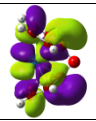		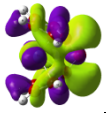
[Os{(η^5-C$_5$H$_4$)$_2$O}]		-0.25947	-0.21371	-0.19709	-0.02508	-0.02247	-0.01742
[Os{(η^5-C$_5$H$_4$)$_2$S}]		-0.25506	-0.22413	-0.21066	-0.02930	-0.02720	-0.01338
[Os{(η^5-C$_5$H$_4$)$_2$Se}]		-0.25195	-0.22653	-0.21370	-0.03929	-0.03710	-0.00989

Co Complexes*

MOLECULE	ESP MAP	HOMO-2 (hartrees)	HOMO-1 (hartrees)	HOMO (hartrees)	LUMO (hartrees)	LUMO+1 (hartrees)	LUMO+2 (hartrees)
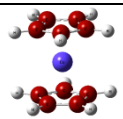	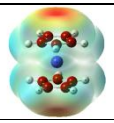	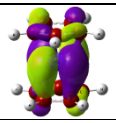	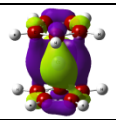	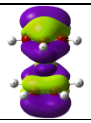	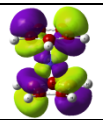	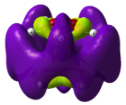	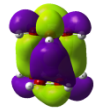
$[Co(\eta^5\text{-}C_5H_5)_2]$		-0.25918	-0.25513	-0.17540	-0.08002	-0.01950	-0.02607
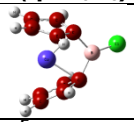	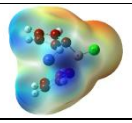	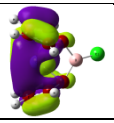		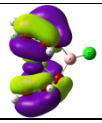	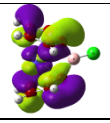	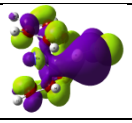	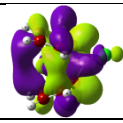
$[Co\{(\eta^5\text{-}C_5H_4)_2BCl\}]$		-0.26823	-0.26201	-0.19438	-0.09720	-0.06712	-0.01409
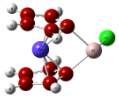		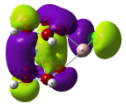	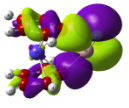	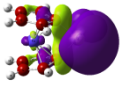	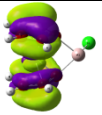	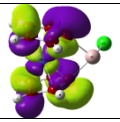	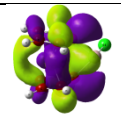
$[Co\{(\eta^5\text{-}C_5H_4)_2AlCl\}]$		-0.29938	-0.28872	-0.17511	-0.10929	-0.10692	-0.01699
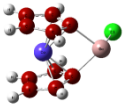	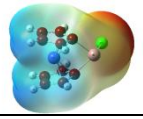	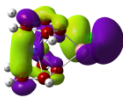	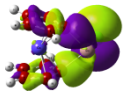	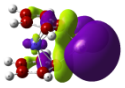	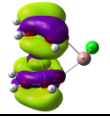	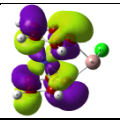	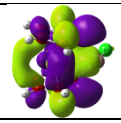
$[Co\{(\eta^5\text{-}C_5H_4)_2GaCl\}]$		-0.29429	-0.28094	-0.18726	-0.10977	-0.10764	-0.01893
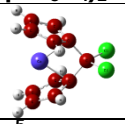	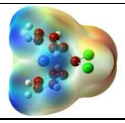	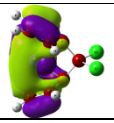	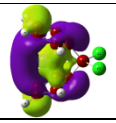	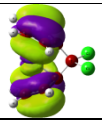	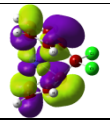	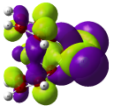	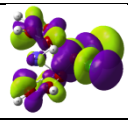
$[Co\{(\eta^5\text{-}C_5H_4)_2CCl_2\}]$		-0.26574	-0.25677	-0.19645	-0.10014	-0.03896	-0.01828
$[Co\{(\eta^5\text{-}C_5H_4)_2SiCl_2\}]$		-0.27612	-0.26835	-0.19818	-0.10391	-0.03352	-0.01036

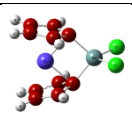	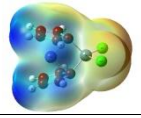	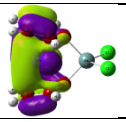	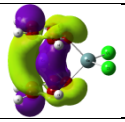	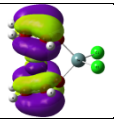	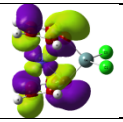	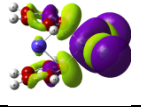	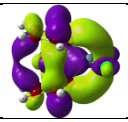
[Co{(η^5-C_5H_4)$_2$$GeCl_2$}]		-0.28065	-0.27567	-0.19900	-0.10569	-0.05617	-0.02891
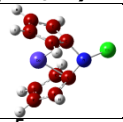	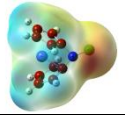	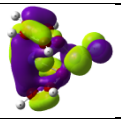	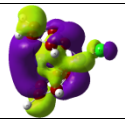	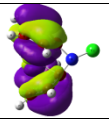	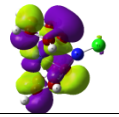	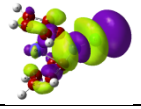	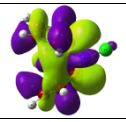
[Co{(η^5-C_5H_4)$_2$NCl}]		-0.25711	-0.24945	-0.19687	-0.09904	-0.06168	-0.02243
	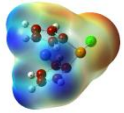	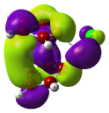	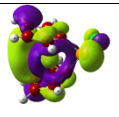	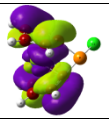		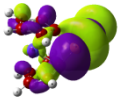	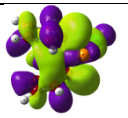
[Co{(η^5-C_5H_4)$_2$PCl}]		-0.26708	-0.26011	-0.19492	-0.09816	-0.05664	-0.03216
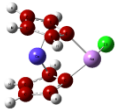	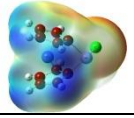	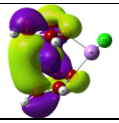	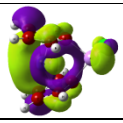	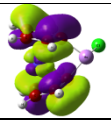	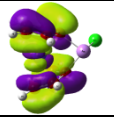	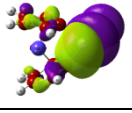	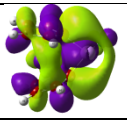
[Co{(η^5-C_5H_4)$_2$AsCl}]		-0.26767	-0.25925	-0.19303	-0.09621	-0.07097	-0.03569
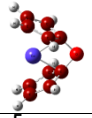	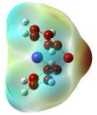		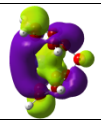		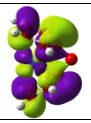		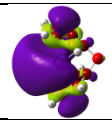
[Co{(η^5-C_5H_4)$_2$O}]		-0.25425	-0.24154	-0.19393	-0.09673	-0.01545	-0.00303
[Co{(η^5-C_5H_4)$_2$S}]		-0.25868	-0.25764	-0.19124	-0.09609	-0.02808	-0.00265
[Co{(η^5-C_5H_4)$_2$Se}]		-0.25905	-0.24722	0.18989	-0.09513	-0.03893	-0.02233

*HOMO orbitals are singly occupied.

Rh Complexes*

MOLECULE	ESP MAP	HOMO-2 (hartrees)	HOMO-1 (hartrees)	HOMO (hartrees)	LUMO (hartrees)	LUMO+1 (hartrees)	LUMO+2 (hartrees)
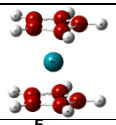	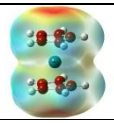		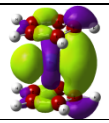	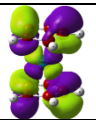		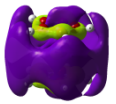	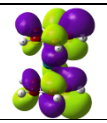
$[Rh(\eta^5\text{-}C_5H_5)_2]$		-0.25921	-0.25612	-0.14671	-0.06642	0.01232	0.02260
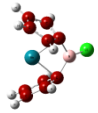	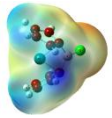	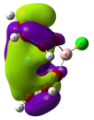	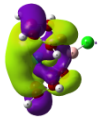	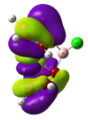	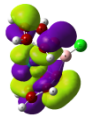	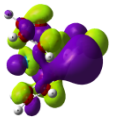	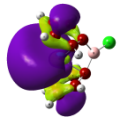
$[Rh\{(\eta^5\text{-}C_5H_4)_2BCl\}]$		-0.25660	-0.24470	-0.18064	-0.09417	-0.06564	-0.02319
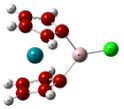	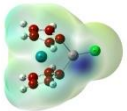	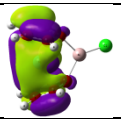	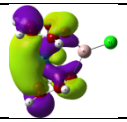			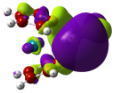	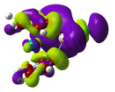
$[Rh\{(\eta^5\text{-}C_5H_4)_2AlCl\}]$		-0.26438	-0.25623	-0.16619	-0.08495	-0.06686	-0.02590
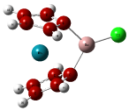	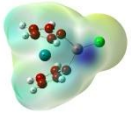	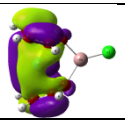	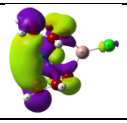		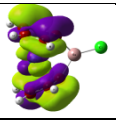	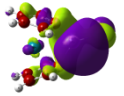	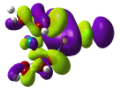
$[Rh\{(\eta^5\text{-}C_5H_4)_2GaCl\}]$		-0.26066	-0.25350	-0.16808	-0.08614	-0.07903	-0.04039
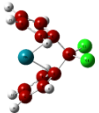	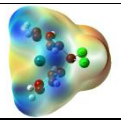	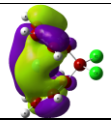	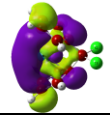		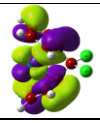	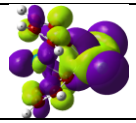	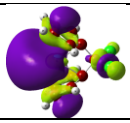
$[Rh\{(\eta^5\text{-}C_5H_4)_2CCl_2\}]$		-0.24961	-0.23395	-0.18094	-0.09481	-0.04139	-0.02225
$[Rh\{(\eta^5\text{-}C_5H_4)_2SiCl_2\}]$		-0.26022	-0.25276	-0.17595	-0.09291	-0.03475	-0.01088

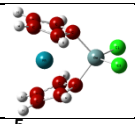	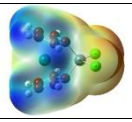	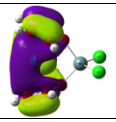	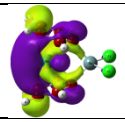	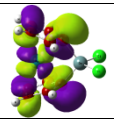	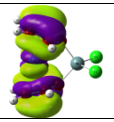	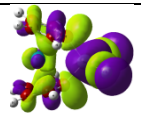	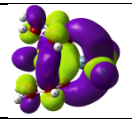
[Rh{(η^5-C_5H_4)$_2$$GeCl_2$}]		-0.26326	-0.25677	-0.17866	-0.09426	-0.05750	-0.02989
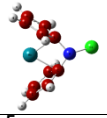	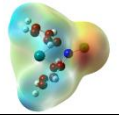	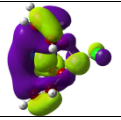	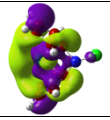	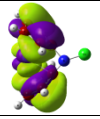	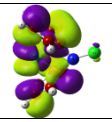	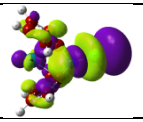	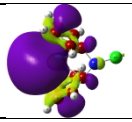
[Rh{(η^5-C_5H_4)$_2$NCl}]		-.24371	-0.23233	-0.18687	-0.09678	-0.06545	-0.03563
	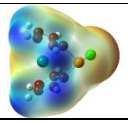	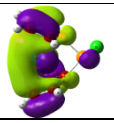	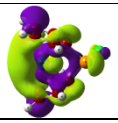	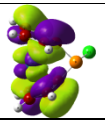	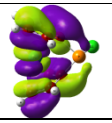	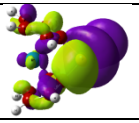	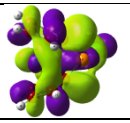
[Rh{(η^5-C_5H_4)$_2$PCl}]		-0.25334	-0.23964	-0.17498	-0.09023	-0.05998	-0.02833
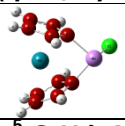	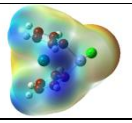	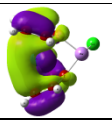	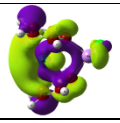	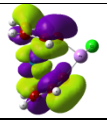	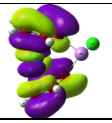	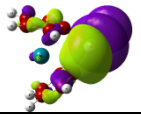	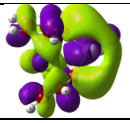
[Rh{(η^5-C_5H_4)$_2$AsCl}]		-0.25330	-0.23992	-0.17154	-0.08711	-0.07389	-0.03493
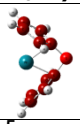	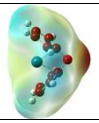		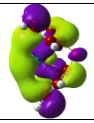		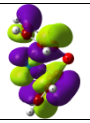	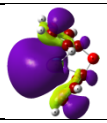	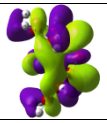
[Rh{(η^5-C_5H_4)$_2$O}]		-0.24101	-0.22609	-0.18531	-0.09762	-0.04103	-0.00031
[Rh{(η^5-C_5H_4)$_2$S}]		-0.24907	-0.23513	-0.17149	-0.08959	-0.02741	-0.01030
[Rh{(η^5-C_5H_4)$_2$Se}]		-0.24067	-0.23595	-0.16914	-0.08558	-0.04508	-0.01980

*HOMO orbitals are singly occupied.

Ir Complexes*

MOLECULE	ESP MAP	HOMO-2 (hartrees)	HOMO-1 (hartrees)	HOMO (hartrees)	LUMO (hartrees)	LUMO+1 (hartrees)	LUMO+2 (hartrees)
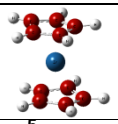	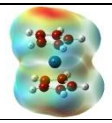			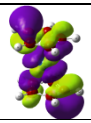		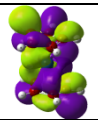	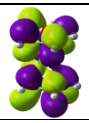
$[Ir(\eta^5\text{-}C_5H_5)_2]$		-0.25699	-0.25032	-0.13780	-0.04480	-0.01070	-0.01596
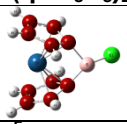	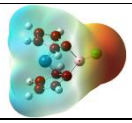	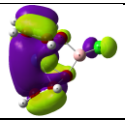	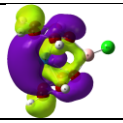	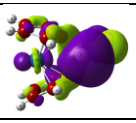			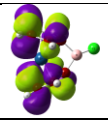
$[Ir\{(\eta^5\text{-}C_5H_4)_2BCl\}]$		-0.28207	-0.26165	-0.14998	-0.07379	-0.07048	-0.01689
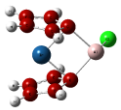	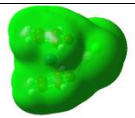	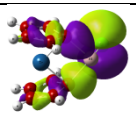	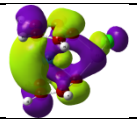	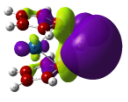	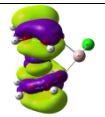	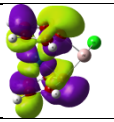	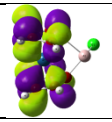
$[Ir\{(\eta^5\text{-}C_5H_4)_2AlCl\}]$		-0.29240	-0.28399	-0.17470	-0.06962	-0.06853	-0.01778
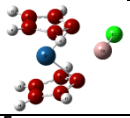	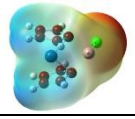	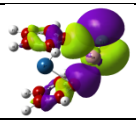	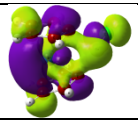	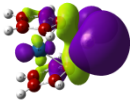	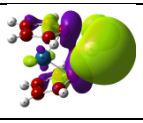		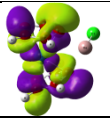
$[Ir\{(\eta^5\text{-}C_5H_4)_2GaCl\}]$		-0.28481	-0.28455	-0.18789	-0.09253	-0.06913	-0.06756
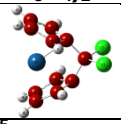	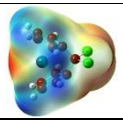		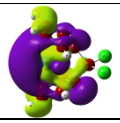	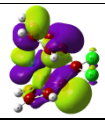	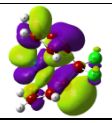	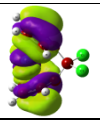	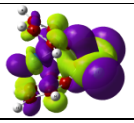
$[Ir\{(\eta^5\text{-}C_5H_4)_2CCl_2\}]$		-0.24245	-0.22528	-0.16924	-0.07881	-0.06192	-0.03692
$[Ir\{(\eta^5\text{-}C_5H_4)_2SiCl_2\}]$		-0.30076	-0.28567	-0.18822	-0.08678	-0.08360	-008229

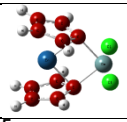	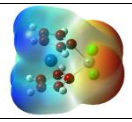	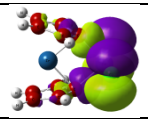	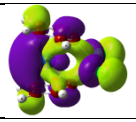	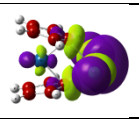	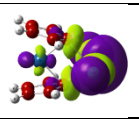	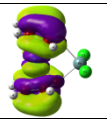	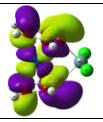
$[Ir\{(\eta^5\text{-}C_5H_4)_2GeCl_2\}]$		-0.29936	-0.28920	-0.20700	-0.12364	-0.08351	-0.08243
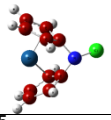	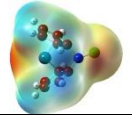	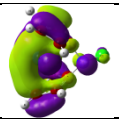	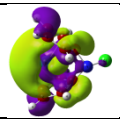	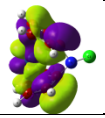	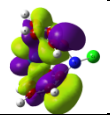	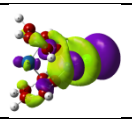	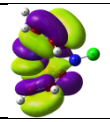
$[Ir\{(\eta^5\text{-}C_5H_4)_2NCl\}]$		-0.23430	-0.21186	-0.17105	-0.08210	-0.06610	-0.06383
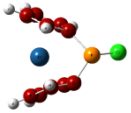	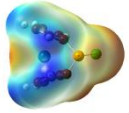	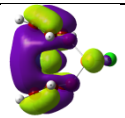	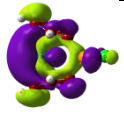	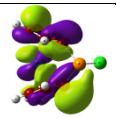	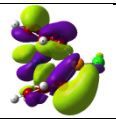		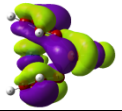
$[Ir\{(\eta^5\text{-}C_5H_4)_2PCl\}]$		-0.24897	-023383	-0.16382	-0.07712	-0.05899	-0.05503
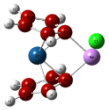	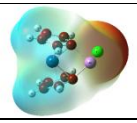	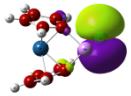	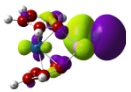	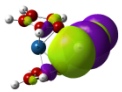	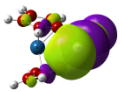		
$[Ir\{(\eta^5\text{-}C_5H_4)_2AsCl\}]$		-0.25145	-0.24955	-0.17837	-0.09030	-0.08308	-0.08242
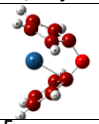	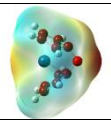		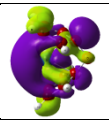	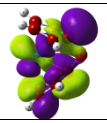	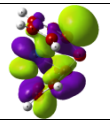		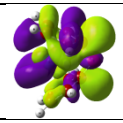
$[Ir\{(\eta^5\text{-}C_5H_4)_2O\}]$		-0.23163	-0.21791	-0.17156	-0.08048	-0.06202	-0.02534
$[Ir\{(\eta^5\text{-}C_5H_4)_2S\}]$		-0.24020	-0.23060	-0.16423	-0.07738	-0.05451	-0.03253
$[Ir\{(\eta^5\text{-}C_5H_4)_2Se\}]$		-0.24076	-0.23447	-0.16155	-0.07594	-0.05107	-0.03779

*HOMO orbitals are singly occupied.

CURRICULUM VITAE

Personal Information

Name Surname : Dilek YÜKSEL

Place of Birth : Ankara

Marital Status : Single

e-mail : dilexita@hacettepe.edu.tr

Adress : Hacettepe University, Department of Chemistry,

06800 Beytepe, Ankara, TURKEY

Education

High School : 1991-1998, Çankaya Anadolu Lisesi, Ankara, TURKEY

B.Sc. : 1998-2003, Hacettepe University, Department of Chemistry, Ankara, TURKEY

M.Sc. : 2004-2007, Hacettepe University, Department of Chemistry, Ankara, TURKEY

Ph.D. : 2007-2013, Hacettepe University, Department of Chemistry, Ankara, TURKEY

Foreign Languages

English, German (advanced), Spanish (intermediate)

Professional Experience

2005-2013: Research Assistant at Hacettepe University, Department of Chemistry, Organic Chemistry Section

Research Interests

Computational Chemistry, Organic Chemistry, Organometallic Chemistry, Carbon Arc Reactions, Metal Carbenes, Olefin Metathesis, *ansa*-Metallocenes